Thermo Electron Engineering Corporation, 85 First Avenue, Waltham, Massachusetts 02154

Report No. TE 12-67

N67 13216

FACILITY FORM 602

(ACCESSION NUMBER)	(THRU)
264	1
(PAGES)	(CODE)
CR 80525	03
(NASA CR OR TMX OR AD NUMBER)	(CATEGORY)

FINAL REPORT

THERMIONIC RESEARCH PROGRAM

Contract 951262

August 1966

by

S. Kitrilakis

D. Lieb

F. Rufeh

L. van Someren

GPO PRICE $ _____

CFSTI PRICE(S) $ _____

Hard copy (HC) 5.00

Microfiche (MF) 1.25

ff 653 July 65

Prepared for

Jet Propulsion Laboratory

Pasadena, California

Thermo Electron Engineering Corporation, 85 First Avenue, Waltham, Massachusetts 02154

Report No. TE 12-67

This work was performed for the Jet Propulsion Laboratory, California Institute of Technology, sponsored by the National Aeronautics and Space Administration under Contract NAS7-100.

FINAL REPORT

THERMIONIC RESEARCH PROGRAM

Contract 951262

August 1966

by

S. Kitrilakis

D. Lieb

F. Rufeh

L. van Someren

Prepared for

Jet Propulsion Laboratory

Pasadena, California

Approved by: S. Kitrilakis

S. Kitrilakis
Research Manager

TABLE OF CONTENTS

Chapter		Page
I	INTRODUCTION	I-1
II	SUMMARY	II-1
III	TEST VEHICLE AND INSTRUMENTATION	III-1
	A. General	III-1
	B. Converter	III-1
	1. Spacing	III-1
	2. Reservoir	III-1
	3. Collectors	III-2
	4. Dial Indicators	III-2
	C. Base Plate	III-11
	D. Top Plate	III-11
	E. Instrumentation	III-12
	1. Temperature Control	III-12
	2. Data Collection Equipment	III-13
	F. Experimental Procedure	III-14
	1. Parallelization	III-17
	2. Emitter Work Function	III-18
	3. Collector Work Function	III-18
	4. Parametric Data	III-20
	a. Variable-Cs-Reservoir-Temperature Families	III-20
	b. Variable-Spacing Families	III-21

TABLE OF CONTENTS (continued)

Chapter			Page
IV	EMITTER PREPARATION		IV-1
	A.	Tungsten	IV-1
		1. Materials	IV-1
		2. Surface Preparation	IV-1
		3. Heat Treatment	IV-4
		4. Examination of Emitter Surfaces	IV-4
		5. Conclusions	IV-9
	B.	Rhenium	IV-9
		1. Materials	IV-9
		2. Surface Preparation	IV-11
		3. Heat Treatment	IV-11
		4. Examination of Emitter Surface	IV-11
		5. Conclusions	IV-16
	C.	Discussion — Electroetched Rhenium Emitters	IV-16
V	ADDITIVE STUDIES		V-1
	A.	Introduction	V-1
	B.	Theoretical Analysis	V-4
		1. The Interdependence of Cs and Additive Effects	V-5
		2. The Rate Equilibrium and Coverage Relations for Adsorbed Additives	V-8
		3. Desorption Energy	V-11

TABLE OF CONTENTS (continued)

Chapter		Page
C.	Cesium Fluoride Investigations	V-15
	1. Contaminant Control	V-15
	2. Surface Studies with Purified CsF	V-18
	a. Test Vehicle Design and Assembly	V-18
	b. Filaments	V-20
	c. Outgassing	V-20
	d. Work Function Experiments	V-24
	e. Steady-State Results	V-34
	f. Desorption Energy	V-36
	g. Coverage Relations	V-36
	3. Converter Studies	V-42
	a. Experimental Procedure	V-42
	b. Experimental Results	V-44
	4. Glass Tube Studies	V-59
	a. Experimental Procedure	V-60
	b. Experimental Results	V-60
D.	Oxygen Surface Additive	V-68
	1. General	V-68
	2. Oxygen Adsorption Constants	V-68
	3. Chemical Equilibrium	V-70
	4. Critical Experiment	V-74
	5. Oxygen-Additive Test Vehicle	V-77

TABLE OF CONTENTS (continued)

Chapter		Page
	E. Conclusions	V-95
	1. Cesium Fluoride	V-95
	2. Oxygen	V-95
	References	V-97
VI	THE OUTPUT CHARACTERISTICS OF AN ELECTROETCHED RHENIUM SURFACE	VI-1
	A. Introduction	VI-1
	B. Bare Work Function	VI-1
	C. Cesiated Work Function	VI-4
	D. Parametric Performance Data	VI-9
	Reference	VI-19
VII	INERT GAS STUDIES	VII-1
	A. Introduction	VII-1
	B. Selection of Plasma Additives	VII-3
	C. Experimental Apparatus	VII-6
	D. The Ignited Mode in Presence of Inert Gases	VII-10
	1. Introduction	VII-10
	2. Theory	VII-10
	3. Experimental Approach	VII-15
	4. Experimental Results and Conclusions	VII-16

TABLE OF CONTENTS (continued)

Chapter		Page
	E. The Overall Effect of the Inert Gases on the Output Characteristics	VII-24
	1. Introduction	VII-24
	2. Experimental Procedure	VII-25
	3. Experimental Results and Conclusions	VII-26
	References	VII-57
VIII	ELECTRON SCATTERING IN THE BOLTZMANN REGION	VIII-1
	A. Introduction	VIII-1
	B. Theoretical Analysis	VIII-2
	1. Long-Mean-Free-Path Solution, $d/\lambda << 1$	VIII-5
	2. Short-Mean-Free-Path Solution, $d/\lambda >> 1$	VIII-6
	C. Experimental Technique and Results	VIII-9
	D. Comparison of Experimental Results with Theory	VIII-11
	E. Conclusions	VIII-21
	References	VIII-23

LIST OF ILLUSTRATIONS

Figure		Page
III-1	Test Converter and Base Plate	III-3
III-2	Cross Section of Test Converter	III-5
III-3	Emitter Temperature Correction	III-15
III-4	Schematic of Guard Balance Control	III-16
III-5	Ideal Emission	III-19
IV-1	Emitter W9 after Electropolishing, 310x	IV-2
IV-2	Emitter W10 after Electropolishing, 310x	IV-3
IV-3	Emitter W9 after Heat Treatment, 310x	IV-5
IV-4	Emitter W10 after Heat Treatment, 310x	IV-6
IV-5	Interference Fringe Pattern from W9 after Heat Treatment, Showing Edge, 74x	IV-7
IV-6	Interference Fringe Pattern from W10 after Heat Treatment, Showing Edge, 152x	IV-8
IV-7	Interference Fringe Pattern from W10, Showing Polishing Defect, 152x	IV-10
IV-8	Emitter Re31 after Electroetching, 310x	IV-12
IV-9	Another Area of Re31, 310x	IV-13
IV-10	Re31 after Heat Treatment, 310x	IV-14
IV-11	Another area of Re31, 310x	IV-15
V-1	Experimental and Theoretical Cesiated-Surface Work Work Functions with Electronegative Additive	V-9
V-2	Bare-Work-Function Shift Produced by Oxygen Additive	V-13
V-3	Oxygen Pressure Required for Substantial Coverage as a Function of Surface Temperature	V-14
V-4	Mass Spectrometer Analysis of CsF Outgassing	V-17

LIST OF ILLUSTRATIONS (continued)

Figure		Page
V-5	Drawing of Surface Studies Device	V-19
V-6	Filament Temperature as a Function of Heating Current and Influence of End Connections on Temperature Uniformity	V-21
V-7	Outgassing Set-up for Surface-Studies Device	V-22
V-8	Circuit Diagram for Emission Measurements	V-25
V-9	Left Filament Work Function, No Liquid Nitrogen Cooling	V-26
V-10	Right Filament Work Function with Liquid Nitrogen Cooling	V-29
V-11	Typical J-V Characteristic Showing Ion Currents	V-30
V-12	Emission Current Transient for Step Change in Filament Heating Current, No CsF	V-31
V-13	Emission Current Transient for Step Change in Filament Heating Current, Constant CsF Arrival Rate	V-32
V-14	Emission-Current Transient for Constant Filament Heating Current, Quenched CsF Reservoir	V-33
V-15	Surface Work Function of a Tungsten Filament in the Presence of CsF Vapor	V-35
V-16	Characteristic Decay of CsF Coverage for Several Filament Temperatures	V-37
V-17	Decay-Time Constant for CsF Coverage as a Function of Filament Temperature	V-38
V-18	Surface Work Function Change Produced by CsF Coverage	V-39
V-19	CsF Arrival Rate Required to Maintain Half a Monolayer Coverage at a Given Surface Temperatre	V-41
V-20	Saturation Current vs Reciprocal Emitter Temperature for Bare Surface	V-45
V-21	Variable-Spacing, Current-Voltage Family	V-46
V-22	Time and Temperature History of CsF Converter (500)	V-47

LIST OF ILLUSTRATIONS (continued)

Figure		Page
V-23	Time and Temperature History of CsF Converter (500) . . .	V-48
V-24	CsF-Only Work Functions in Converter 5000	V-51
V-25	CsF Arrival Rate as A function of Temperature, Low Pressure Range	V-52
V-26	CsF Arrival Rate as a Function of Temperature, High Pressure Range	V-53
V-27	Cs^+ Ion Current, Showing Space-Charge Limiting	V-54
V-28	Electron Current Peaks Due to Cs Coverage Changes with Heating and Cooling of the Emitter	V-55
V-29	Comparison of Cesiated ϕ for Various CsF Converters . . .	V-57
V-30	Typical Glass-Tube Press with Electrodes	V-61
V-31	Typical Glass-Tube J-V Characteristic	V-62
V-32	Work Function Change Produced in CsF Glass Tube	V-63
V-33A	Micro-Photograph of Tungsten Filament Eroded in a Glass Tube	V-65
V-33B	Micro-Photograph of Tungsten Filament Eroded in a Glass Tube	V-65
V-33C	Micro-Photograph of Tungsten Filament Operated at High Temperature in Vacuum	V-65
V-34	Oxygen Pressure in Equilibrium with Various Metal Oxides as a Function of Temperature	V-75
V-35	Cesiated-Surface Work Function vs T/T_R in the Presence of Cs_2O and Cu_2O	V-76
V-36	Performance Envelope with Cs_2O and Cesium	V-79
V-37	Schematic of Parametric Converter Showing Additive Reservoir	V-80
V-38	Cesiated Collector Work Function Comparison With and Without Oxygen	V-83

LIST OF ILLUSTRATIONS (continued)

Figure		Page
V-39	J-V Family with Cu_2O Additive, T_E 1760°K	V-84
V-40	J-V Family with Cu_2O Additive, T_E 1760°K	V-85
V-41	J-V Family with Cesium Only, T_E 1750°K	V-86
V-42	J-V Family with Cesium Only, T_E 1750°K	V-87
V-43	Performance Envelope Comparison Cs Only and Cs plus Cu_2O, T_E 1960°K	V-88
V-44	Performance Envelope Comparison Cs Only and Cs plus Cu_2O, T_E 1850°K	V-89
V-45	Performance Envelope Comparison Cs Only and Cs plus Cu_2O, T_E 1750°K	V-90
V-46	Power-Density Comparison of Cs Only and Cs plus Cu_2O, T_E 1960°K	V-91
V-47	Power-Density Comparison of Cs Only and Cs plus Cu_2O, T_E 1850°K	V-92
V-48	Power-Density Comparison of Cs Only and Cs plus Cu_2O, T_E 1750°K	V-93
VI-1	Typical J-V Characteristic used for "Bare" Work Function Determination	VI-2
VI-2	Typical J-V Characteristic used for "Bare" Work Function Determination	VI-3
VI-3	Plot of Richardson Equation	VI-5
VI-4	Typical J-V Characteristic used for Cesiated Work Function Determination	VI-6
VI-5	Typical J-V Characteristic used for Cesiated Work Function Determination	VI-7
VI-6	Work Function vs Surface-to-Reservoir Temperature Ratio Plot of Cesiated Work Function Measurements	VI-8

LIST OF ILLUSTRATIONS (continued)

Figure		Page
VI-7	Comparison of the Work Functions of Electroetched and Electropolished Rhenium	VI-10
VI-8	Summary of J-V Families at 1560°K	VI-12
VI-9	Summary of J-V Families at 1650°K	VI-13
VI-10	Summary of J-V Families at 1740°K	VI-14
VI-11	Summary of J-V Families at 1860°K	VI-15
VI-12	Summary of J-V Families at 1960°K	VI-16
VI-13	Fully Optimized Performance Map	VI-17
VI-14	Fully Optimized Electrode Power Output Map	VI-18
VII-1	The Modified Cesium Reservoir	VII-7
VII-2	Schematic of the Standard Gas Injection System	VII-8
VII-3	Modes of Discharge	VII-11
VII-4	Typical Variable-Spacing Electrical Output Characteristic	VII-14
VII-5	Plot of Variable-Spacing Families According to Equation (15).	VII-17
VII-6	Variable-Spacing Families According to Equation (15)	VII-18
VII-7	Plot of Variable-Spacing Families According to Equation (15).	VII-19
VII-8	Plot of the Focal Points According to Equation (18)	VII-20
VII-9	Collision Probability of Electrons with Argon	VII-22
VII-10	Effective Collision Probability of Electrons with Argon	VII-23
VII-11	Variable-Reservoir-Temperature Envelopes at T_E = 1863°K and d = 20 mils	VII-27
VII-12	Variable-Reservoir-Temperature Envelopes at T_E = 1863°K and d = 10 mils	VII-28
VII-13	Variable-Reservoir-Temperature Envelopes at T_E = 1863°K and d = 2 mils	VII-29

LIST OF ILLUSTRATIONS (continued)

Figure		Page
VII-14	Variable-Reservoir-Temperature Envelopes at T_E = 1740°K and d = 20 mils	VII-30
VII-15	Variable-Reservoir-Temperature Envelopes at T_E = 1740°K and d = 10 mils	VII-31
VII-16	Variable-Reservoir-Temperature Envelopes at T_E = 1740°K and d = 2 mils	VII-32
VII-17	Variable-Reservoir-Temperature Envelopes at T_E = 1645°K and d = 20 mils	VII-33
VII-18	Variable-Reservoir-Temperature Envelopes at T_E = 1645°K and d = 10 mils	VII-34
VII-19	Variable-Reservoir-Temperature Envelopes at T_E = 1645°K and d = 2 mils	VII-35
VII-20	Cross Plot Corresponding to Figure VII-11	VII-36
VII-21	Cross Plot Corresponding to Figure VII-12	VII-37
VII-22	Cross Plot Corresponding to Figure VII-13	VII-38
VII-23	Cross Plot Corresponding to Figure VII-14	VII-39
VII-24	Cross Plot Corresponding to Figure VII-15	VII-40
VII-25	Cross Plot Corresponding to Figure VII-16	VII-41
VII-26	Cross Plot Corresponding to Figure VII-17	VII-42
VII-27	Cross Plot Corresponding to Figure VII-18	VII-43
VII-28	Cross Plot Corresponding to Figure VII-19	VII-44
VII-29	Fractional Current Attenuation by Argon for Cesium Pressure of 1 Torr and Several Interelectrode Spacings	VII-48
VII-30	Fractional Current Attenuation by Argon for Cesium Pressure of 2 Torr and Several Interelectrode Spacings	VII-49

LIST OF ILLUSTRATIONS (continued)

Figure		Page
VII-31	Fractional Current Attenuation by Argon for Cesium Pressure of 4 Torr and Several Interelectrode Spacings . .	VII-50
VII-32	Fractional Current Attenuation by Krypton for Cesium Pressure of 1 Torr and Several Interelectrode Spacings . .	VII-51
VII-33	Fractional Current Attenuation by Krypton for Cesium Pressure of 2 Torr and Several Interelectrode Spacings . .	VII-52
VII-34	Fractional Current Attenuation by Krypton for Cesium Pressure of 4 Torr and Several Interelectrode Spacings . .	VII-53
VII-35	Fractional Current Attenuation by Xenon for Cesium Pressure of 1 Torr and Several Interelectrode Spacings . .	VII-54
VII-36	Fractional Current Attenuation by Xenon for Cesium Pressure of 2 Torr and Several Interelectrode Spacings . .	VII-55
VII-37	Fractional Current Attenuation by Xenon for Cesium Pressure of 4 Torr and Several Interelectrode Spacings . .	VII-56
VIII-1	Boltzmann Region	VIII-3
VIII-2	Schematic of the Cesium Diode	VIII-10
VIII-3	Variation in Collector Work Function with Spacing. T_E = 1314°K, T_C = 609°K, T_R = 543°K	VIII-12
VIII-4	Variation in Collector Work Function with Spacing. T_E = 1313°K, T_C = 611°K, T_R = 554°K	VIII-13
VIII-5	Variation in Collector Work Function with Spacing. T_E = 1298°K, T_C = 618°K, T_R = 572°K	VIII-14
VIII-6	Variation in Collector Work Function with Spacing. T_E = 1308°K, T_C = 621°K, T_R = 593°K	VIII-15
VIII-7	Variation in Collector Work Function with Spacing. (a) T_C = 628°K, (b) T_C = 628°K, (c) T_C = 627°K (d) T_C = 827°K, (e) T_C = 623°K.	VIII-16
VIII-8	Plot for Obtaining Electron Mean Free Path	VIII-17

LIST OF ILLUSTRATIONS (continued)

Figure		Page
VIII-9	Plot for Obtaining Electron Mean Free Path	VIII-18
VIII-10	Electron Mean Free Path in Cesium Vapor	VIII-19
VIII-11	Recommended Correction for Collector Work Function Measured by Retarding Technique	VIII-22

LIST OF TABLES

Table		Page
V-1	GLASS TUBE EXPERIMENTS AT TEECO.	V-67
V-2	SUMMARY OF DATA ON OXYGEN ADSORPTION	V-71
VII-1	EFFECT OF ADDITION OF 1 TORR OF INERT GAS IN A 10-MIL WIDE PLASMA AT 1000°K	VII-9
VIII-1	COLLISION CROSS SECTION OF ELECTRONS WITH Cs ATOMS	VIII-20

CHAPTER I

INTRODUCTION

This report covers work performed by Thermo Electron for NASA/JPL under contract 951262/NAS7-100 during the one-year period ending in June 1966. The program is a continuation of a research program which has been in progress for several years. It consists of applied research in thermionic energy conversion and includes experimental and analytical tasks.

The basic objectives of this effort have been to generate knowledge and to devise techniques for improving the performance of thermionic converters. These objectives can only be attained through a combination of analysis and experiment. Using the evidence at hand, hypotheses are formulated, tested experimentally, improved on the basis of new evidence, tested again, and so on. What is reported here is a step in just such an iterative process.

At the time this contract was initiated the capabilities of cesium-vapor diodes were well defined, and it was obvious that any step increases in performance could only come from significant changes in the nature of the conversion process. As a result, this program undertook the study of two new regimes of operation.

The first is the use of CsF vapor in addition to metallic cesium in the converter. The presence of CsF causes the Cs vapor to be more tightly bound to the emitter surface, so that the cesium pressure required to maintain a given coverage is greatly reduced. This reduction of Cs pressure results in less scattering of electrons in the plasma, and therefore improved performance. Evidence of these effects had been obtained in the previous year, and an analytical framework forming the basis for further investigation was devised. Questions of stability, however,

still remained to be answered before these improvements could be put to effective use. Chapter V of this report gives experimental results which lead to the conclusion that water vapor contamination of the CsF had been responsible for the effects previously observed. Two additional phases of experimental work determined the true behavior of the CsF additive and demonstrated that oxygen can be used as a surface additive in a stable fashion and under steady-state conditions.

The second main task of the program was a study of the effects of inert gases on the characteristics of the converter. There were three reasons for undertaking this study. Because of the very low cross section of inert gas atoms for low-energy electron collisions, it was hypothesized that inert gases could act as diffusion barriers to Cs ions, thus conserving them, while they remained transparent to electrons. It was reasoned that, if Cs ions were indeed conserved, fewer would be required and the internal voltage loss necessary for ion production in the converter would be reduced.

The second reason for undertaking this study was that the presence of an additional gas in the interelectrode space can be used as a tool in the study of the converter plasma. Experimental and analytical work of this nature proved very useful in furthering the understanding of the diffusion processes taking place in the converter.

The third reason for this study was the fact that inert gases are major constituents of the fission products of thermionic reactor systems. As such, they may be vented, intentionally or unintentionally, into the interelectrode space. It is therefore desirable to know their effects on converter performance. Studies of this kind have been made in the past, but the results were inconclusive because of oxygen contamination. In Chapter VII the results of very extensive experimental studies are presented, and fairly conclusive answers to these questions are given.

The test converter and associated equipment, as well as experimental techniques, are discussed in detail in Chapter III.

Metallurgical data on the preparation and the definition of the emitter surfaces employed are given in Chapter IV.

In the inert gas studies an etched rhenium emitter was used. This emitter, when tested with Cs only, to provide a performance reference prior to the introduction of inert gas, showed exceptionally high output. A detailed parametric study was performed, which demonstrated that this type of surface was indeed superior to rhenium surfaces previously tested. The results are presented in Chapter VI.

Chapter VIII presents in a completed form the analysis of converter characteristics in the Boltzmann region.

Significant results and conclusions of the program are presented in summary form in Chapter II.

CHAPTER II

SUMMARY

This program depends to a great extent on extensive and accurate experimental results for the attainment of its objectives. A great deal of effort has therefore been expended in the design, construction and improvement of the converters and other devices and instrumentations used for gathering experimental data. All parametric-type data have been generated using variable-parameter converters. These converters employ planar electrodes and an active collector guard ring and allow variation of all important parameters over wide ranges. The devices and associated electronic equipment are described in detail in Chapter III. In addition to these converters it became necessary, in the case of the additive studies, to develop and construct tubes capable of attaining the extremely high vacuums necessary for the experiments. Filament-type metal-ceramic tubes were constructed which were able to maintain, in operation, vacuums of the order of 10^{-10} torr. These tubes are described in Chapter V of this report. Carefully controlled metallurgical procedures were used in the preparation of emitter surfaces. These are described in Chapter IV, and the results of metallurgical and chemical examinations of emitter surfaces are also reported there. It is expected that this information will allow a precise definition of the surfaces and will also make possible their reproduction by this and other laboratories.

Several significant conclusions regarding surface additive have been reached in the course of this year's work. Additive effects which previously had been attributed to cesium fluoride were shown to be the result of water present as a contaminant in the cesium fluoride charge used in the converters. A specially designed filament metal-ceramic tube capable of extremely high vacuums was constructed, and this tube permitted the determination of the true effects of cesium

fluoride. At complete coverage of fluoride only about 0.36 eV of work function change was observed. In addition, the energy of desorption of fluorine on tungsten was measured at 3.3 eV. As a result of this rather small change in work function and low energy for desorption, it appears that fluorine holds little promise of improving the performance of converters. To provide conclusive evidence that the exceptional performance previously observed was indeed due to oxygen, and furthermore, to allow use of oxygen in operating converters, a study was conducted using oxygen as an additive. It was possible to employ oxygen in the form of copper oxide for periods exceeding 300 hours with no significant changes in the operation of the device. The use of the continuous oxygen source appears to be a feasible method of introducing the beneficial effects of oxygen. The results with oxygen are considered preliminary at this point, and several areas for future work are now apparent. While oxygen can be used satisfactorily as an additive, additional data are desirable to define the mechanism of operation and enable the selection of other materials which might possibly be more effective and more easily controlled. The effect of oxygen on the tungsten collector has not yet been explored, and it is possible that some other material might produce a better collector under other conditions.

The results of parametric tasks conducted with an electroetched rhenium surface are presented in Chapter VI. This surface exhibits a bare work function value of 4.88 eV, which is about 0.13 eV higher than the typical values obtained before with electropolished or mechanically polished rhenium surfaces. The parametric performance data, representing a total of 1000 volt-ampere characteristics, clearly demonstrate that the performance of this device is significantly higher than that of other rhenium emitters. In particular, it appears that the same performance can be obtained at roughly twice the spacing, and that the power output can be increased by a factor of 2 at the same spacing. The method employed in preparation of this surface is outlined in Chapter IV.

The effects of argon on converter output were documented by recording approximately 1200 volt-ampere characteristics. These data conclusively show that there is no enhancement of performance under any conditions in the presence of argon. A gradual decrease in output was observed with increasing inert gas pressure. However, argon appears to have little effect on the characteristics at pressures below 20 torr. This result is of particular interest to nuclear thermionics, since inert gas fission products may enter the interelectrode space of converters located in a reactor core. Typically, 10 torr of argon would result in a 10% reduction in the output of the converter. Two torr of krypton or one torr of xenon would have the same effect.

Chapter VIII presents in completed form an analysis and experimental correlation of the Boltzmann region of the converter characteristic. This portion of the characteristic is of practical importance when collector work function measurements are made.

CHAPTER III

TEST CONVERTER AND EQUIPMENT

A. General

The test converters used in this program are variable-parameter research-type devices. An active collector guard ring and planar geometry are used. Parameters whose values can be varied and accurately controlled include the emitter temperature, the interelectrode spacing, the collector and reservoir temperatures, and, of course, the output. The active collector guard ring is a very desirable feature, since it renders the conversion process free from any radial geometric dependence, and precisely defines the active area of the device. Elimination of edge effects is possible because the voltage and temperature of the guard ring can be adjusted to be equal to those of the collector at all times.

B. Converter

1. Spacing. The variation of spacing is accomplished by flexing a bellows joining the emitter and collector structures by means of a mechanism operated externally to the bell jar. Figure III-1 shows how this is accomplished. Three micrometer spindles (61) are driven by shafts (98) which are geared together above the top plate. The interelectrode spacing is measured directly on three dial indicators (1) which are set to measure changes in the relative position of the emitter and collector structures.

2. Reservoir. A tubulation (18) leads from the emitter support structure to the cesium reservoir (62). A similar reservoir is used for the cesium fluoride. The only difference between the two is that the entrance to the tubulation leading to the cesium reservoir is restricted by a 10-mil orifice. This orifice prevents

cesium fluoride vapor from condensing in the cesium reservoir at a rapid rate. In the case of the plasma-additive converter, inert gas is introduced by means of a tubulation (144) leading from the cesium reservoir to the exterior of the vacuum envelope of the converter and to the inert-gas injection system.

In the devices constructed in the second half of the program, the cesium reservoir was modified slightly. The reservoir tubulation was brought out to the side of the device through the space between the top plate support ring (17) and the top plate (15). The reservoir was then suspended below the tubulation which entered from the top. It was located at about the level of the bellows (29). This arrangement provided better control in the presence of the additive gases and is described more fully in the section on gas injection in Chapter VI.

3. Collectors. The gap between collector and guard ring, shown in Figure III-2, is kept to a value close to 1 mil. The height of the step between the collector and guard ring is kept at approximately 1/2 mil, with the collector protruding beyond the guard ring surface.

4. Dial Indicators. The dial indicators (1) were relocated well above the emitter cooling plate through the use of an extension tube (138). This change was made because, on some occasions in previous work, the dial indicators were overheated by radiation from the emitter cavity. Overheating caused them to jam and necessitated their replacement.

For a description of the individual components of this device more detailed than the summary given above, the reader is referred to Ref. 19. The changes made in the test vehicles used in the present program will now be outlined in detail.

Figure III-1

Test Converter and Base Plate

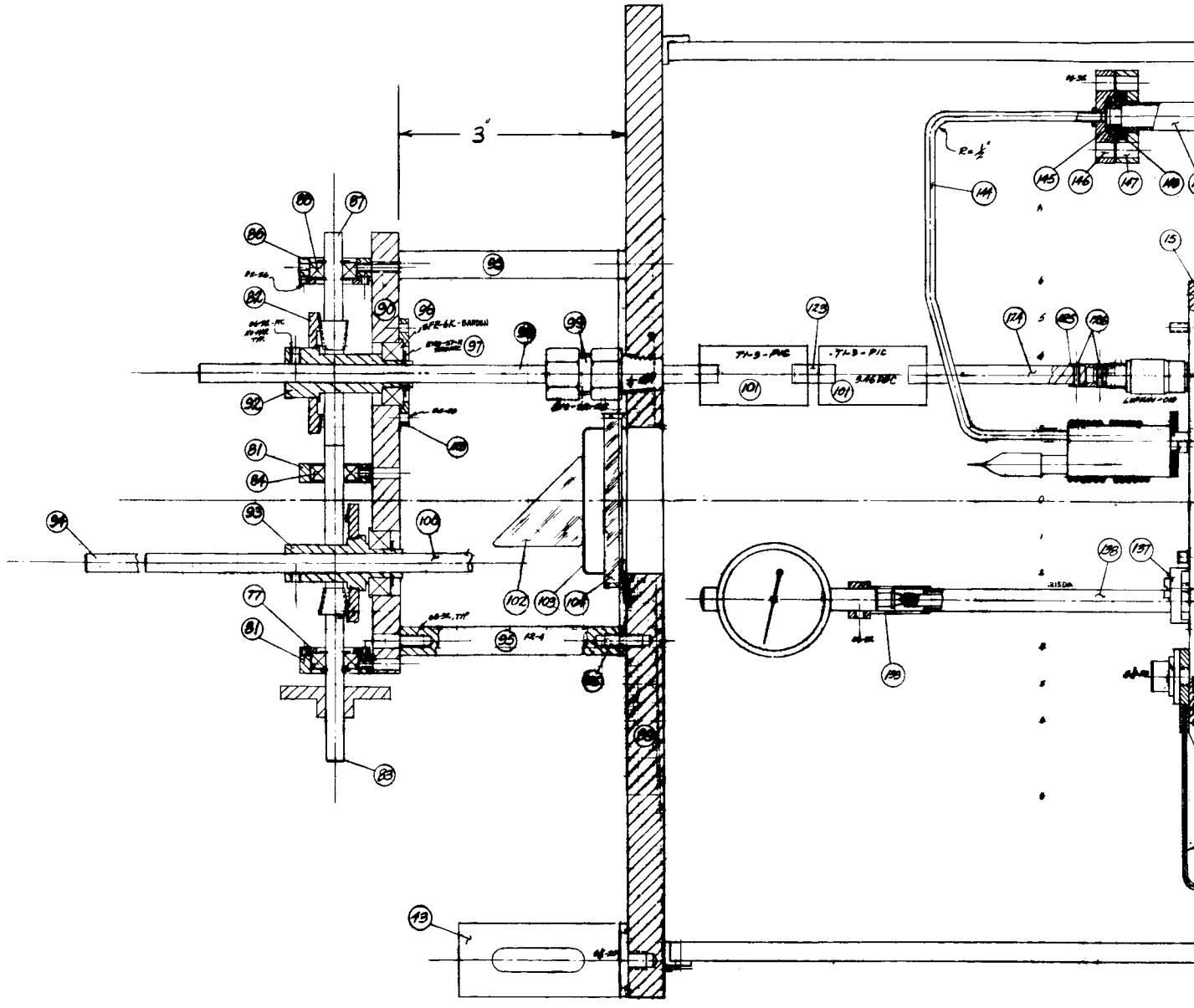
3"
TI-9-PNC
TI-9-P/C
R=½"

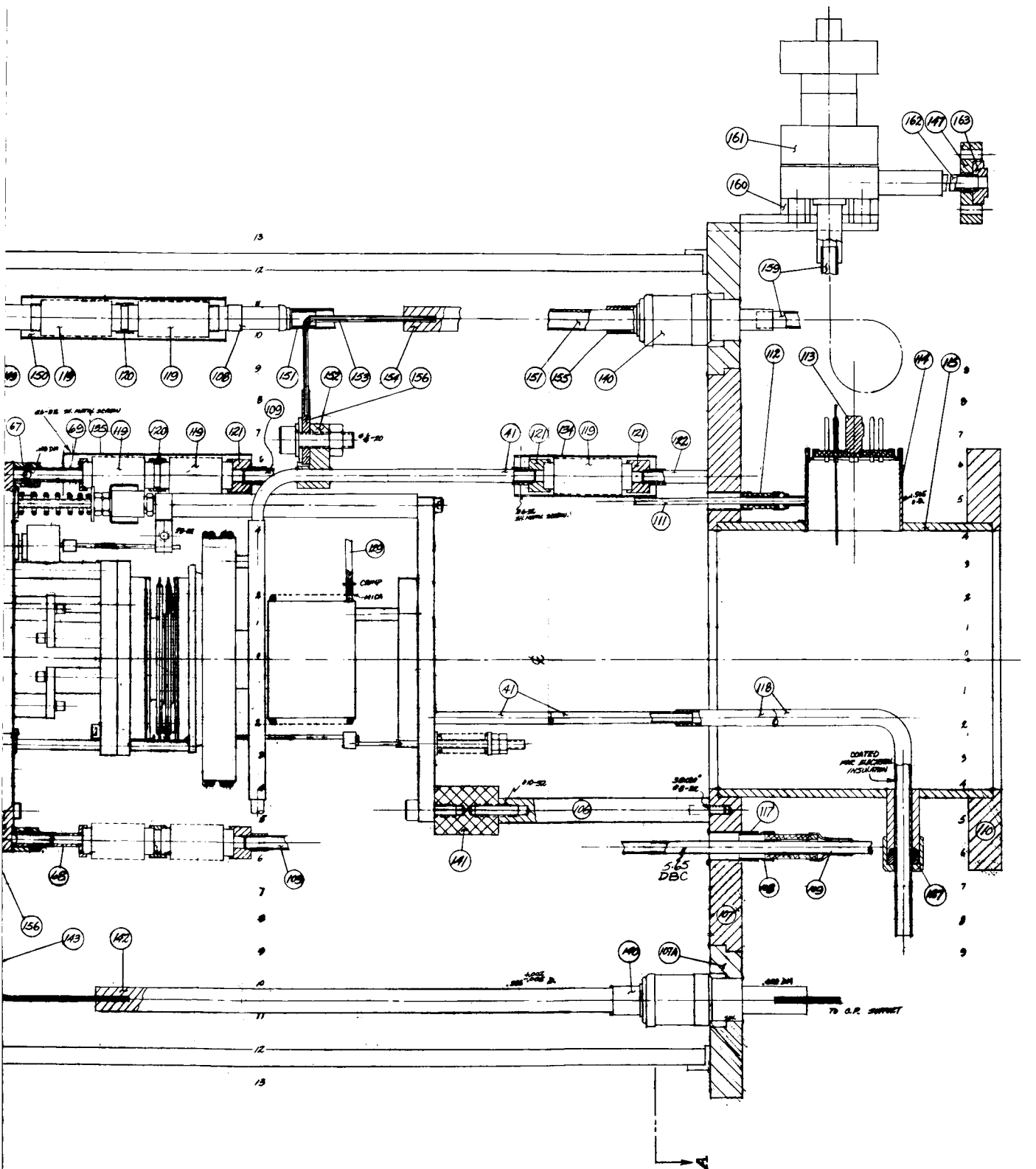
161
160
162
147
163
159
112
113
114
115
111
41
118
106
117
110
141
107
107A
140
148
149
108
109
156
143
142
150
119
120
151
152
153
154
155
140
67
60
135
121
122
139
COMP
MICA
COATED
FIRE BLOCKING
INSULATION
5-65
DBC
TO O.P. SWITCH

2

Figure III-2

Cross Section of Test Converter

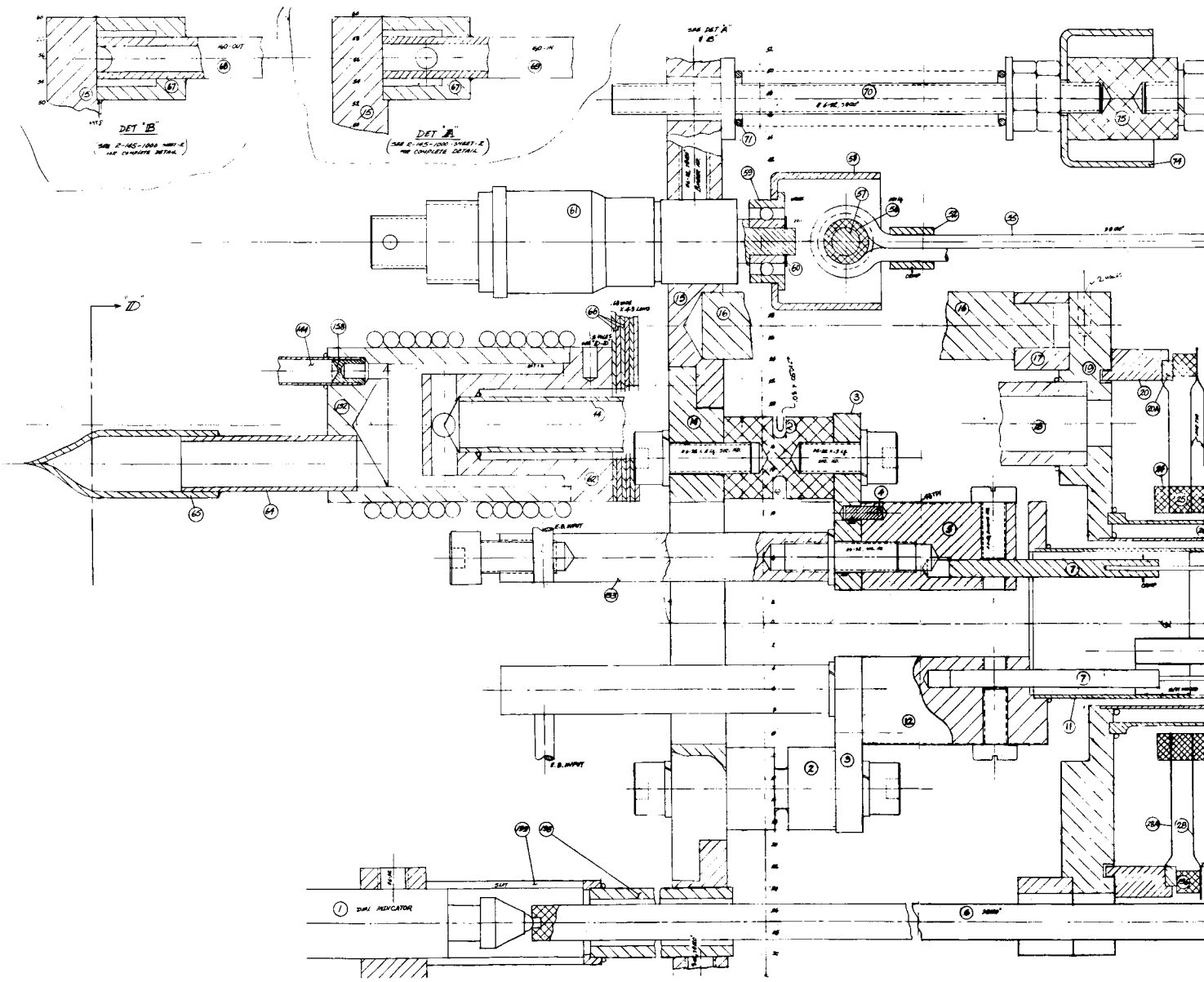

III-C-1

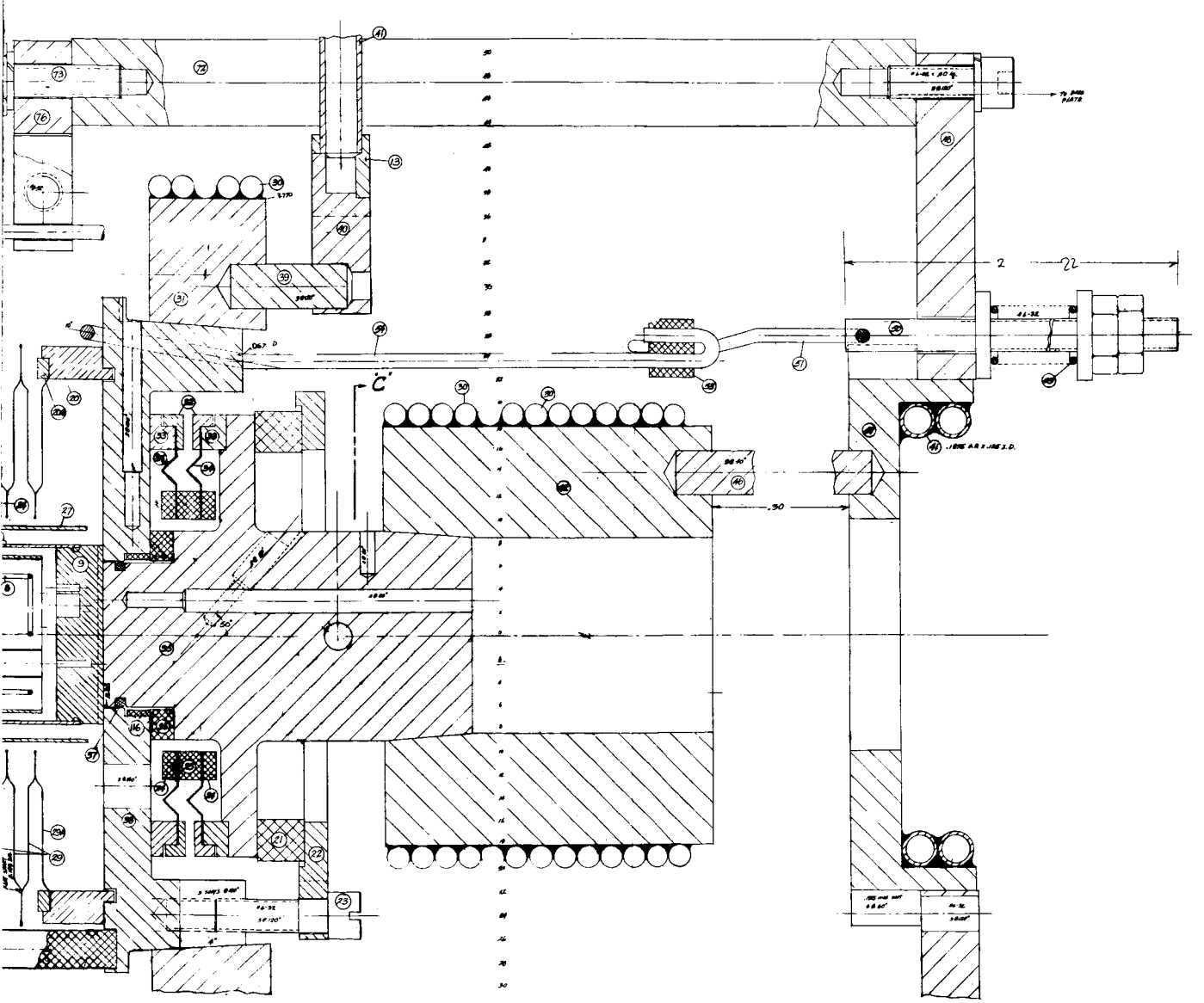

III-6-2

TABLE OF NOMENCLATURE

for Figures III-1 and III-2

1.	Dial Indicator	26.	Emitter Sleeve
2.	Insulator	27.	Emitter Shield
3.	Gun Holder	28.	Bellows Flanges
4.	Pin	28A.	
5.	Filament Support	29.	
6.	Sapphire Rod	29A.	
7.	Filament Lead	30.	Guard Ring Heater
8.	Filament	31.	Guard Ring Heater Block
9.	Emitter	32.	Flexible Flange Retainer
10.	Sight Pipe	33.	Flexible Flange Adapter
11.	Filament Shield	34.	Flexible Flange
12.	Shield Support	35.	Collector
13.	Guard Ring Cooler Adapter	36.	Collector - Guard Ring Spacer
14.	Gun Base	37.	Sapphire Balls
15.	Top Plate	38.	Guard Ring
16.	Top Plate Support Rod	39.	Guard Ring Heater Support Rod
17.	Top Plate Support Ring	40.	Guard Ring Cooler
18.	Cesium Reservoir Tubulation	41.	Water Tube
19.	Emitter Support Plate	42.	Collector Heater
20.	Bellows Adapter	43.	Pyrometer Support
20A.	Bellows Adapter Reinforcement	44.	Cesium Tubulation
21.	Insulator	45.	Thermocouple Wire
22.	Collector to Guard Compression Ring	46.	Collector Heater Support Rod
23.	Compression Screws	47.	Collector Cooling Plate
24.	Seal	48.	Support Plate
25.		49.	Spring

TABLE OF NOMENCLATURE

for Figures III-1 and III-2 (continued)

50. Tension Rod
51. Tension Wire
52. Wire Retainer
53. Insulator
54. Tension Wire
55. Tension Wire
56. Tension Wire Insulator
57. Rod
58. Micrometer Adapter
59. Ball Bearing
60. Ball Bearing Retaining Washer
61. Micrometer
62. Cesium Reservoir
63. Cesium Reservoir Heater
64. Evacuation Tubulation Adapter
65. Evacuation Tubulation
66. Cooling Strap
67. Water Cooling Ring
68. Cooling Water Outlet
69. Cooling Water Inlet
70. Guide Rod
71. Compression Spring
72. Guide Rod Base
73. Stud
74. Insulator Shade
75. Insulator
76. Tension Wire Clamp
77. Anti-Backlash Plate
78. Gear
79. Shaft
80. Gear
81. Plate
82. Bevel Gear
83. Pinion
84. Bearing
85. Spring Retaining Washer
86. Bearing Housing
87. Pinion
88. Bearing
89. Top Plate
90. Mechanism Support Plate
91. Shaft Adapter
92. Gear Adapter
93. Gear Adapter
94. Shaft
95. Support Rod
96. Bearing
97. Bearing Retainer Washer
98. Shaft
99. Gland
100. Shaft
101. Bellows

TABLE OF NOMENCLATURE

for Figures III-1 and III-2 (continued)

102. Prism
103. Prism Support Plate
104. Pyrex Window
105. Stud
106. Support Plate Rod
107. Base Plate
107A Base Plate Adapter
108. Water Feedthrough
109. Water Tube
110. Base Plate Lower Ring
111. Lead Wire
112. Lead Wire Feedthrough
113. Octal Plug
114. Octal Plug Adapter
115. Base Plate Neck
116. Sapphire Spacer
117. Leadthrough Adapter
118. Water Tube
119. Bellows
120. Bellows Adapter
121. Water Tube Adapter
122. Water Tube
123. Bellows Connector
124. Shaft
125. Micrometer Adapter
126. Roll Pins
127. Water Tube Coupling
128. Bearing Retainer
129. Heater Connectors
130. Gear
131. Shaft
132. Cesium Reservoir Heater
133. E.B. Filament Arms.
134. Bellows Retainer
135. Bellows Retainer
136. Ceramic Insulator
137. E.B. Gun Retainer
138. Dial Indicator Extension
139. Dial Indicator Holder
140. Emitter Output Leadthrough
141. Standoff
142. Emitter Output Lead
143. Output Strips
144. Inner Gas Inlet Tube
145. Copper Gasket
146. Vacuum Flange
147. Vacuum Flange
148. Flange Adapter
149. Flange Adapter Pipe
150. Bellows Retainer
151. Gas Inlet Pipe

TABLE OF NOMENCLATURE

for Figures III-1 and III-2 (continued)

152. Guard Output Adapter
153. Output Strips
154. Guard Output Lead
155. Gas Pipe Adapter
156. Output Strip Adapter
157. Cesium Strip Connector
158. Cesium Restriction Plug
159. Flexible Tube
160. Valve Adapter
161. Inner Gas Inlet Valve
162. Valve Adapter Tube
163. Vacuum Flange Adapter

C. Base Plate

To provide room for the inert-gas injection tubulation, the size of the glass bell jar around the converter was increased from 8 to 12 inches. This change required that the base plate diameter also be increased. A new ring (107A) was added to the old base plate (107). The two were welded as shown in Figure III-1. In this new ring, large feedthroughs (140) were placed to allow for the passage of the inert-gas injection tube (151) and the emitter current lead (142). The guard-current lead (154) was also brought out of the bell jar in the same manner. An all-metal diaphragm valve (161) was added to the base plate to allow for the isolation of the interior of the converter from the gas injection system.

D. Top Plate

The top plate diameter had to be increased to allow the use of the larger bell jar. In this case new top plates were fabricated. An opening was provided in the center of the top plate to accommodate a Pyrex window (104); the emitter temperature observation prism (102) is located above this window. In the previous design this prism was located immediately above the emitter cooling ring (15). With that arrangement the emitter black-body cavity had to be sighted through the Pyrex bell jar walls, and, since these walls have a certain amount of ripple, distortion of the black-body hole image always occurred to some extent. The present system eliminates any distortion whatsoever of the black-body hole image, since it is viewed through a ripple-free window. Support for the pyrometer was also provided on the top plate by a bracket (43), and in this manner the pyrometer is fixed on the top plate permanently.

E. Instrumentation

The instrumentation used for the converter studies part of this program provides for the virtual elimination of edge effects in the device through temperature and electrical potential control of the active guard ring. This equipment, with a minimum of operator attention, maintains the guard and collector electrodes as a single equipotential and uniform-temperature surface. Because of this guarding action, leakage currents are eliminated.

The actual equipment for these experiments was developed under the previous program* and will be discussed only briefly in this section.

1. Temperature Control. Precise adjustment and control of electrode temperatures is necessary, if accurate, useful data is to be obtained from the converter. A multipoint strip-chart recorder connected to thermocouples located in significant portions of the device (except the emitter) serves as the primary means of temperature indication for the experiments and at the same time furnishes a time and temperature history of them.

The emitter is heated by electron bombardment from a hot filament. A servo system regulates the bombardment current to maintain constant input power. Manual adjustment, based on the optical pyrometer measurements, is required to establish the desired temperatures under the various conditions of the experiments.

The lens system of the standard Leeds & Northrop pyrometer was modified so that the image of the 0.032" black-body cavity on the emitter was larger than five times the filament width. This change was aimed at improving the

* Final Report for the Thermionic Research Program, Task IV, Contract 950671, Thermo Electron Report No. TE 7-66, 2 August 1965.

emitter temperature measurement accuracy. One modified pyrometer was calibrated by Leeds & Northrop, and a second instrument was calibrated by the Bureau of Standards against a primary standard. This unit was later used as a reference. Figure III-3 shows the temperature corrections and includes a factor for the optical system and the thermal conductivity of rhenium.

Collector, guard, and cesium reservoir temperatures are controlled by balancing the heat input from a resistance heater on the element against the losses to a water-cooled sink. A time-proportioning, on-off type of controller connected to a thermocouple mounted near the heater, controls the power input and thus regulates the temperatures. Some manual adjustment of the set point is required to compensate for the varying heat loads during testing.

2. Data Collection Equipment. The two main types of experiments performed under this program were quasi-static, low-power work function and dynamic, high power performance tests. In each of these, the output was obtained in the form of current density-voltage plots on an X-Y recorder. Valid data required that there be no electrode temperature variation during a particular run.

The work function tests are performed at low power densities, where electron heating or cooling effects are negligible. For this reason, manually adjusted dc power supplies may be used to sweep over the J-V characteristics of the converter without causing significant temperature variations. To avoid leakage effects at the very low current levels necessary, there must be a high degree of balance between the collector and guard voltages. A separate dc supply functioning as an operational amplifier provides this balancing action. Resistive loading and bucking batteries make smooth sweeping possible over the entire characteristics in both power-absorbing and power-producing regions. Precision

shunts in series with the collector current lead supply the current signal to the recorder. Voltage taps, connected directly to the emitter, collector and guard electrodes, eliminate any voltage drops in the leads and furnish the voltage input to the X-Y plotter.

In the high power regions the electron-cooling load is significant, and any variations in converter load current will be reflected in electrode temperature changes. High-current tests must therefore be performed under dynamic conditions; that is, the entire J-V characteristic must be swept at a rate greater than the thermal time constants of the electrodes. This was accomplished by using a transformer-isolated, half-wave rectified line frequency sweeping source, so that the characteristics were swept in a series of 60-Hz pulses. A solid-state follower consisting of an operational amplifier driving a set of series-pass transistors provides the required balancing action between the collector and guard. The stability and range of the follower were further improved during this program, and the modified schematic is shown in Figure III-4. Because of the limited response time of the X-Y recorder, the effective sweeping of the tube characteristics must be slowed to about a one-per-second rate. A sample-and-hold circuit driven at a rate differing only slightly from 60 Hz samples the current and voltage pulses from the converter and slows their effective rate of change. Precision water-cooled shunts provide the current signal for the sampler, and voltage taps at the electrodes provide the voltage signal. An oscilloscope continually monitors the actual characteristics and provides the operator with a continuous display of the behavior of the device.

F. Experimental Procedure

This section will briefly describe the general procedure for the converter experiments. A more complete description can be found in the report of the

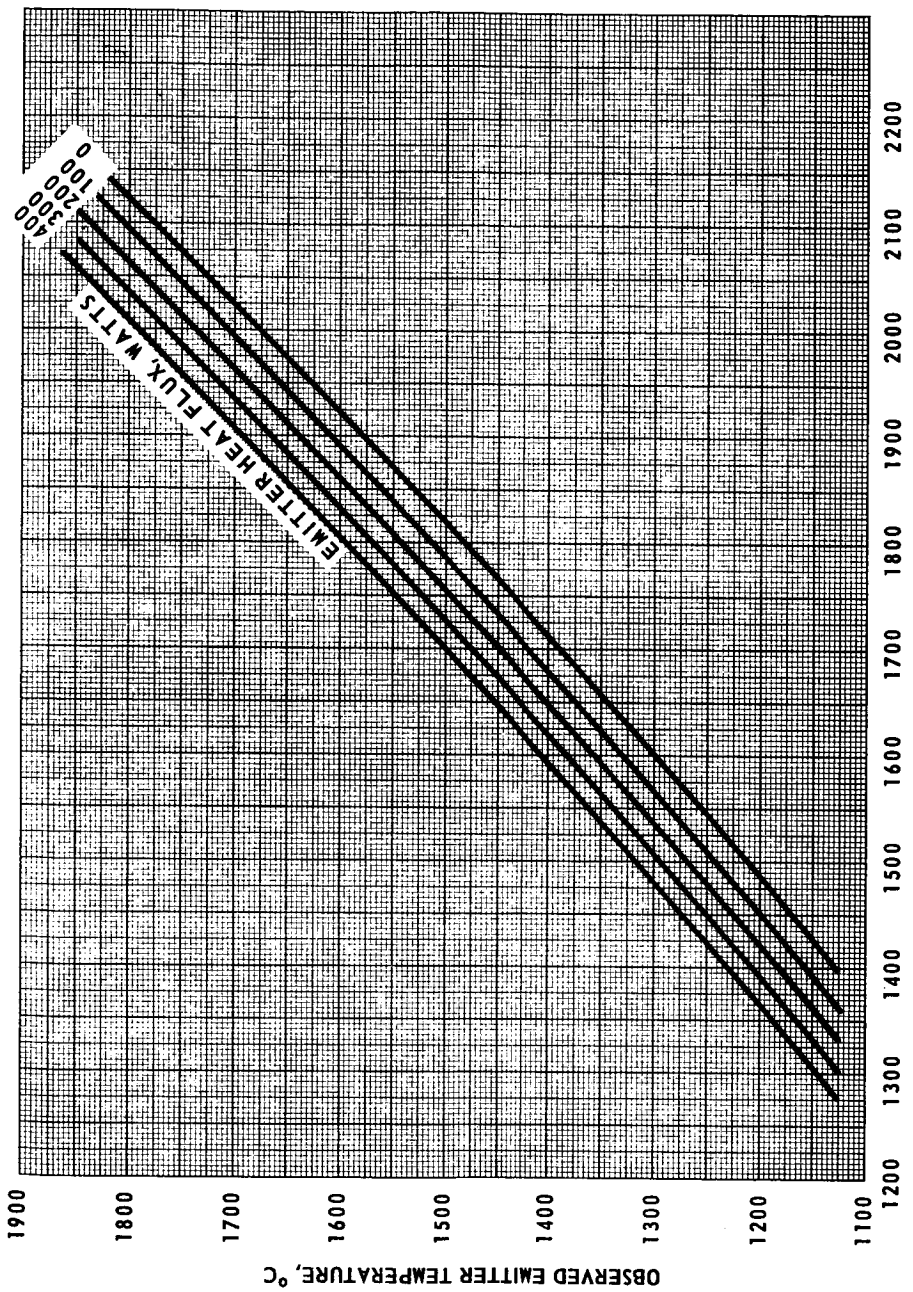

Figure III-3. Emitter Temperature Correction

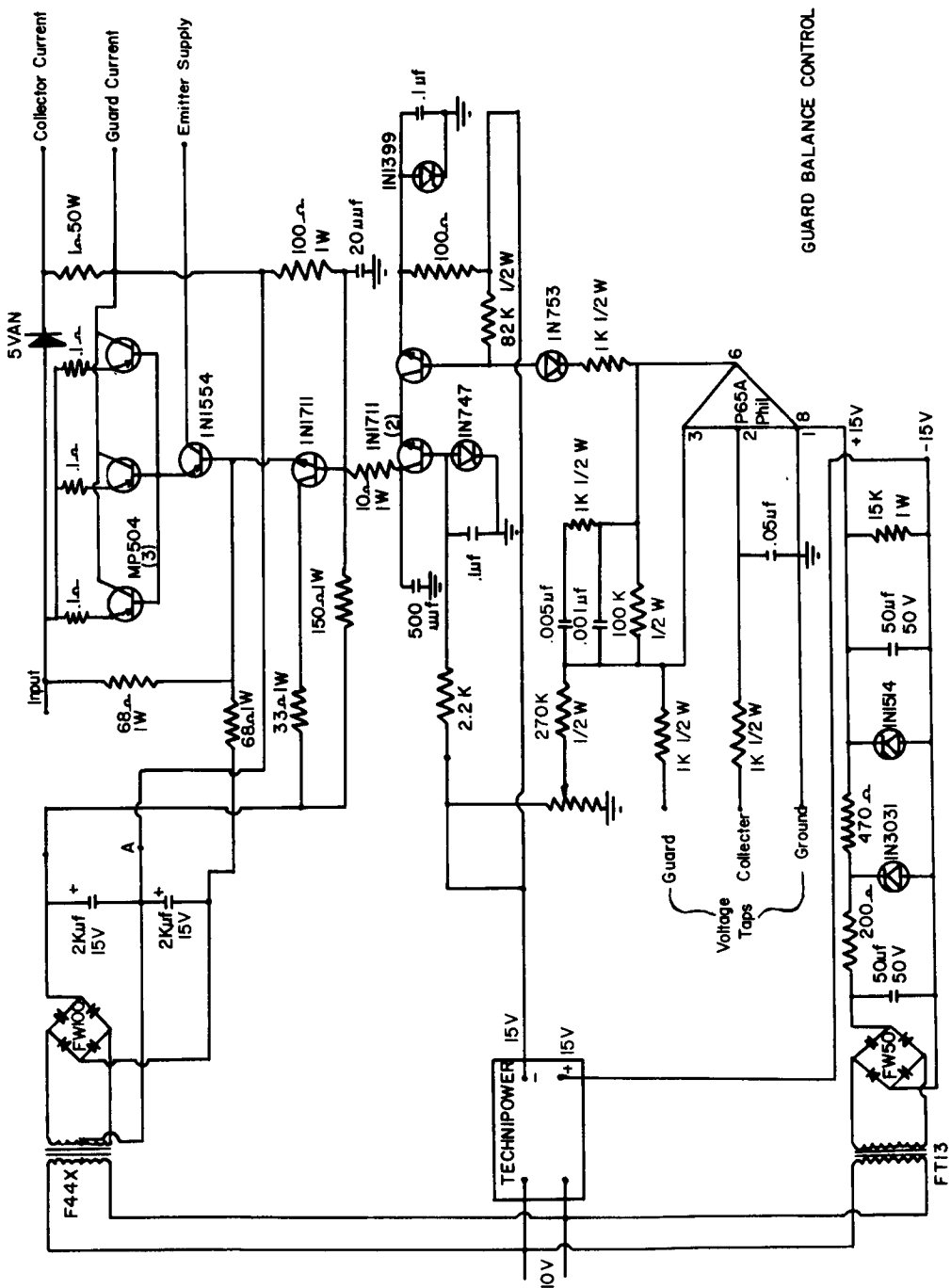

Figure III-4. Schematic of Guard Balance Control

previous program. Any special techniques specific to a particular task will be discussed in the appropriate individual sections.

The two main types of measurements used are the quasi-static, low-power work function and the dynamic, high-power performance tests. The electrical instrumentation has already been discussed, and therefore this section will describe the necessary steps for actual operation of the converter.

1. Parallelization. All measurements assume a value for emitter-collector spacing, and for this value to be meaningful their surfaces must be flat and parallel. During fabrication of the test vehicle the surfaces are carefully polished and ground to produce as flat a surface as possible. Parallelizing of emitter and collector is then the first step in any of the testing procedures.

Electrode and cesium temperatures are adjusted to establish electron-rich conditions at a relatively low emitter temperature. The output current is therefore space-charge-limited and very sensitive to changes in spacing. By trial-and-error manipulation of the three spacing micrometers, the shape of the J-V characteristic is made to approach the ideal form as closely as possible without shorting the emitter to either the collector or the guard. The dynamic-testing oscilloscope display monitors this process. When the optimum characteristics are obtained, the emitter will short to the collector before shorting to the guard. It is now assumed that while the actual spacing may change with temperature, all micrometers will be affected equally, and parallelism will be maintained. The zero reference for spacing is established with each set of electrode temperatures by momentarily shorting the emitter to the collector. This operation must be performed rapidly and carefully to avoid welding of the two surfaces at small spots, with the subsequent growth of a projection or "pimple" from the collector surface.

2. Emitter Work Function. The emitter work function, ϕ_E, is determined from the emitter saturation current, J_s, obtained at a given emitter temperature, T_E, by substituting these values in the Richardson equation,

$$\phi_E = -kT_E \ln [J_s/AT_E^2]$$

where k is the Boltzmann constant and A is the Richardson constant.

The validity of the results is strongly dependent upon the measurement of the true value of saturation current density. A sufficiently large electron-accelerating voltage must be employed to ensure that the emitter work function is the only barrier controlling the current. Ion-rich temperature conditions must be established to eliminate any space-charge barrier formation. A further requirement introduced by back-scattering of electrons in the plasma is that spacing be held to small values.

For the range of work functions greater than about 2.9 eV, the current levels are small and the above conditions are easily fulfilled. The quasi-static low-current instrumentation is used in these tests.

In the lower range of work function values, the currents are too great for quasi-static testing, and the saturation currents are determined from the dynamic J-V plots. In the ignited mode the ions generated in the plasma provide space-charge neutralization; however, the increased scattering in this mode limits the usefulness of the technique to relatively small values of current.

3. Collector Work Function. The most useful method of measuring collector work function is the retarding plot. The J-V characteristic for an idealized diode, shown in Figure III-5, is made up of two curves; the first is given by:

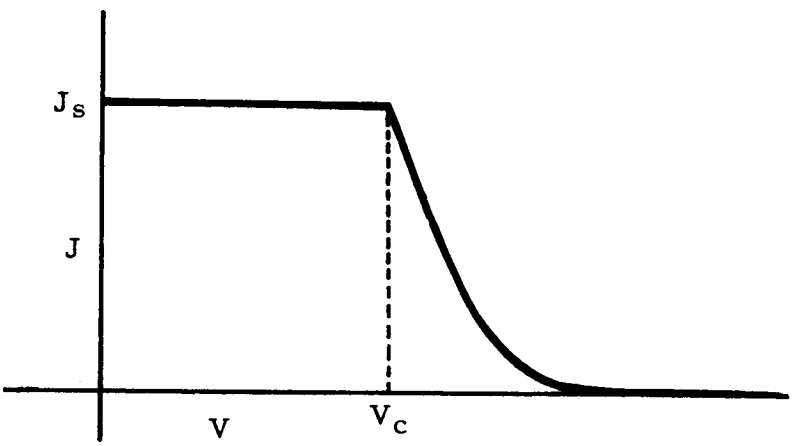

Figure III-5. Ideal Emission.

$$J = J_s \qquad \text{for } V < V_c$$

and the second by:

$$J = AT_E^2 \exp\left[-(\phi_c + V/kT_E)\right] \text{ for } V > V_c$$

Any point on the exponential part of the characteristic can be used to compute collector work function by substituting J, V and T_E in the second equation.

Satisfactory testing with this technique requires low collector temperature (for low back emission), low emitter temperature (for low ion currents), and small spacing (because of scattering effects). The low current levels associated with these measurements allow the use of the quasi-static equipment which at the same time provides the accurate guard potential control necessary to eliminate leakage effects.

4. Parametric Data. The term "parametric data" describes sets or families of current-voltage characteristics generated through the systematic variation of parameters. Such families may be generated by using, as the variable parameter, emitter temperature, spacing, collector temperature, or cesium reservoir temperature, all other parameters being held constant.

In general, the range of variation covered included the region of interest for power production. Therefore the emitter temperature range extends from 1600 to 2050°K, the spacing from 0.2 to 60 mils, and the Cs reservoir temperature from 540 to 700°K. Since this is the high-current region of the characteristics, the dynamic test equipment must be used.

a. Variable-Cs-Reservoir-Temperature Families. The variable-T_R family is especially useful for hardware design. The Cs reservoir temperature,

T_R, is usually the only variable about which the hardware designer has complete freedom of choice. It is, therefore, very convenient for him to have design data available in this form.

The experimental procedure used consisted of selecting emitter temperature, spacing and collector temperature values and then recording J-V curves at 10 - 15°K intervals of Cs reservoir temperature. The first recorded curve is at a T_R resulting in current levels considered to be at the lower limit of interest. The last recorded curve is almost vertical and at the upper limit of interest. The envelope tangent to all curves in the family is the locus of the maximum current obtainable at any given voltage for the condition under which the family was generated. This envelope (solid line) may be corrected for the voltage drop along the emitter sleeve to represent the output at the electrodes. The correction necessary is 3 mV/ampere, and the resultant curve is shown as a dashed line on the family. Envelopes for all spacings at each emitter temperature may be superimposed to form summary plots of J-V characteristics. Figures VI-8 to VI-12 show such plots. Further, the envelopes of the envelopes may be drawn and superimposed to present the maximum performance map for a given emitter material. Figure VI-13 is a map for the etched rhenium emitter.

b. Variable-Spacing Families. This type of experimental result is particularly suited to analytical work and has, in fact, formed the foundation of that work in this program. The analytical value of the variable-spacing family derives from the fact that, when spacing is changed, all other parameters remain constant.

The experimental procedure used to generate these families was to set all parameters at selected values and reach equilibrium at some small value of spacing (approximately 1-2 mils). The spacing was reduced until the

emitter shorted to the collector, and was then increased by an amount just enough to avoid shorting. The interelectrode spacing under these circumstances is estimated to be between 0.2 and 0.5 mil. At that point the first J-V curve was recorded. The spacing was then varied in a geometric progression and a J-V curve recorded at each value of spacing.

CHAPTER IV

EMITTER PREPARATION

The experimental work using cesium fluoride additive was conducted in a tungsten-emitter converter. The inert-gas additive converter used a rhenium emitter. This chapter describes the composition, preparation and definition of the emitter surfaces.

A. Tungsten

Two polycrystalline tungsten emitters have been prepared with electropolished and heat-treated surfaces. These have TEECO designations W9 and W10.

1. Materials

Wrought sheet stock was used for the tungsten emitters. The manufacturer, General Electric Co., Refractory Metals Plant, supplied, and certified, the following spectroscopic analysis: (all units ppm).

Al < 6	Fe 13	Mn < 6	Mo 30
Ca < 3	Ni 8	Mg < 3	Co 29
Si 50	Cu < 3	Sn < 6	Zr < 3

2. Surface Preparation

The stock had a good ground surface. The emitters were first electrical-discharge machined to shape, then cleaned, and electropolished in a 5% aqueous sodium hydroxide solution at a potential of 10 volts for about 30 seconds. The resulting surfaces were photographed, and typical areas are shown in Figures IV-1 and IV-2. Slightly different polishing rates on adjacent grains make some boundaries prominent, and small pits are also visible.

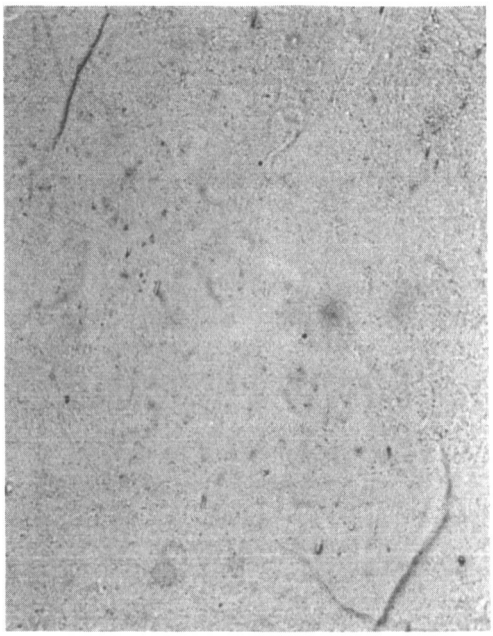

Figure IV-1. Emitter W9 after Electropolishing, 310x.

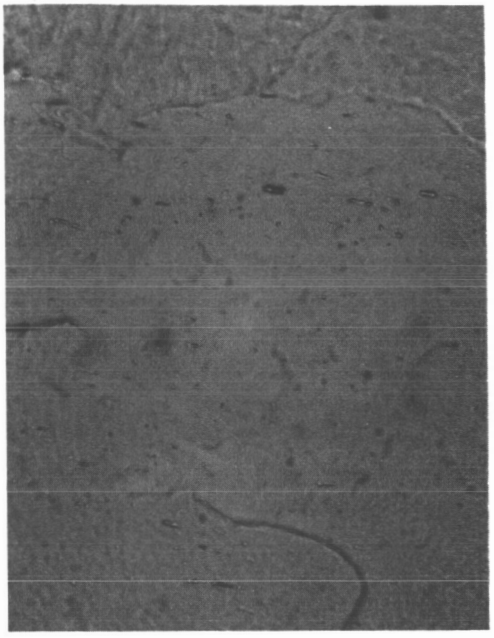

Figure IV-2. Emitter W10 after Electropolishing, 310x.

3. Heat Treatment

Each emitter was heated by electron bombardment in a cold-walled vacuum furnace for 1 hour and 5 minutes at 2300°C. The temperature was read with an optical pyrometer (0.65μ) and was corrected for the emissivity of tungsten. The pressure was determined from the current in the Vac Ion pump used to evacuate the system, and was found to be less than 1×10^{-6} torr while the specimen was at temperature. The heat treatment was chosen to duplicate that used on earlier tungsten emitters in Task IV of this contract.

4. Examination of Emitter Surfaces

After heat treatment the surfaces were again photomicrographed, and typical areas are shown in Figures IV-3 and IV-4. Grain growth and grain-boundary grooving have occurred, as expected. The new grain structure is clearly delineated by the grain-boundary grooves, and faint traces of the old grain structure are visible, especially on Figure IV-4.

Electropolishing tends to produce "roll-off," or rounding at the edge of a specimen. In order to study this, interference fringe patterns were made at the edge of each emitter using sodium yellow light. Figures IV-5 and IV-6 are composite photographs of typical areas at the edge of emitters W9 and W10 at 74x and 150x. The roll-off is visible as rows of increasingly close-spaced fringes parallel with and close to the edge of the emitter. Measurements on these, taking the magnification into account, show that the roll-off is completely confined within 0.04" of the edge of the emitter. This area faces the guard ring in the converter, and therefore it will not in any way affect the converter performance. More detailed visual examination showed:

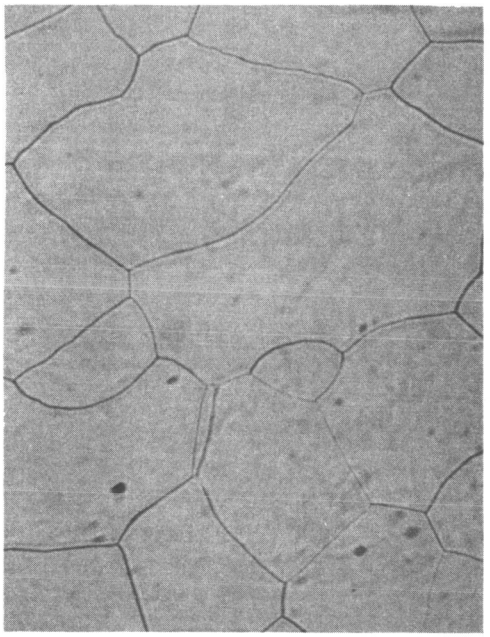

Figure IV-3. Emitter W9 after Heat Treatment, 310x.

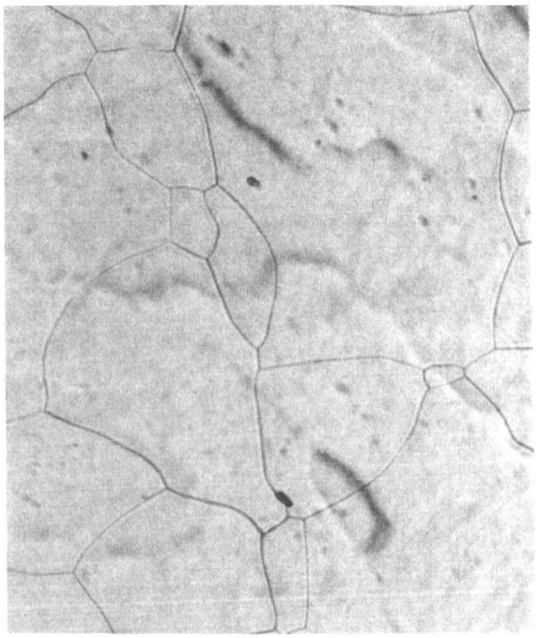

Figure IV-4. Emitter W10 after Heat Treatment, 310x.

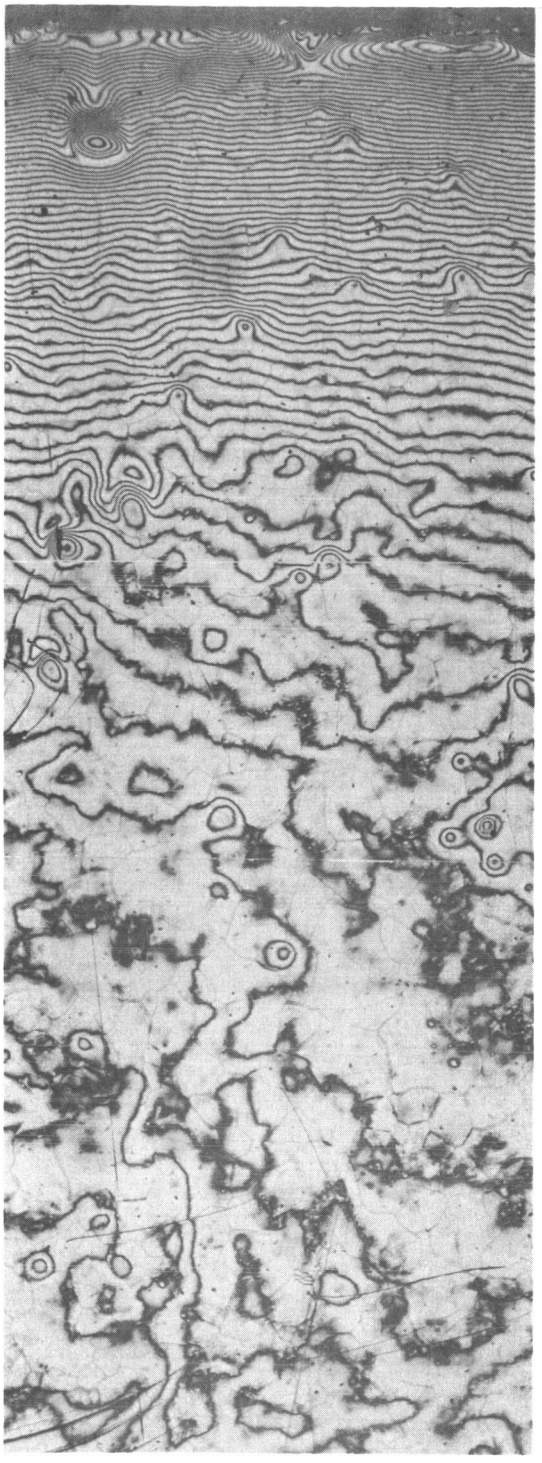

Figure IV-5. Interference Fringe Pattern from W9 after Heat Treatment, Showing Edge, 74x.

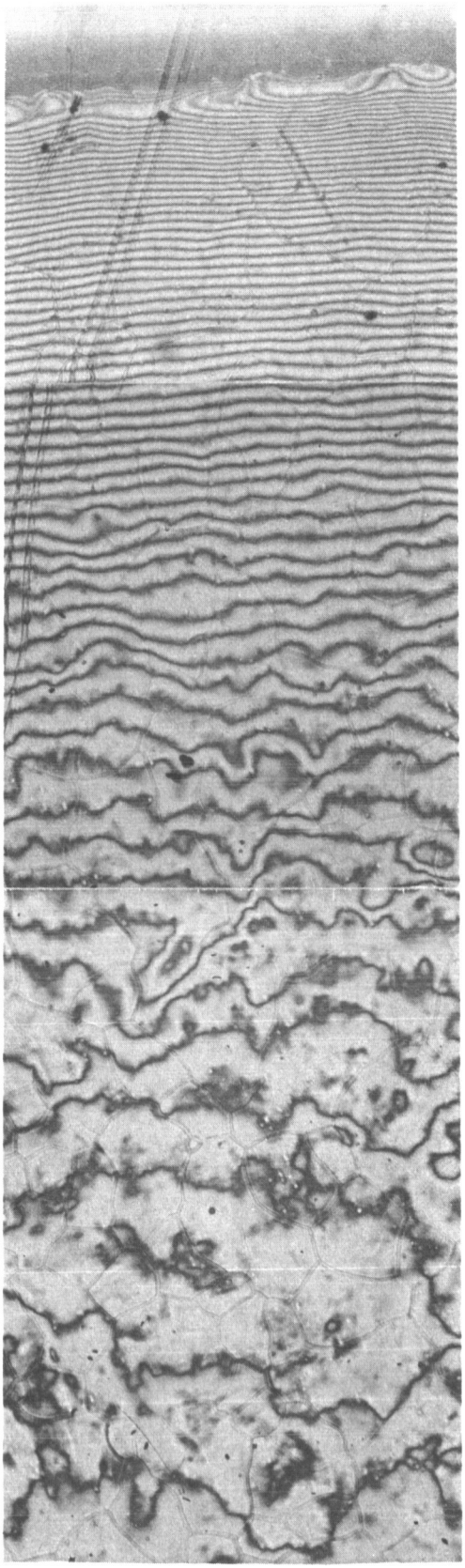

Figure IV-6. Interference Fringe Pattern from W10 after Heat Treatment, Showing Edge, 152x.

1. that the photographed areas were typical, and that in no area was the roll-off width likely to approach the guard ring width; and

2. that the inner areas of each composite photograph are typical of the central parts of the emitters, which show no steep gradients (except at a few polishing defects, such as that in Figure IV-7, which is about 7 mils across and 1/4 mil deep) and are flat to within a micron or so.

5. Conclusions

The changes on the emitter surface which were observed to occur during preparation were grain growth and grain-boundary grooving. Each of these changes was expected on the basis of prior experience. Since the emitter is exposed to much lower temperatures during diode operation, and the rate of surface change decreases with time, no further changes are expected to occur during testing.

B. Rhenium

One polycrystalline rhenium emitter has been prepared with an electro-etched and heat-treated surface. This has the TEECO designation Re 31.

1. Materials

Wrought sheet stock was used for the rhenium emitter. The manufacturer supplied and certified the following spectroscopic analysis (all units ppm):

Al <1 Cu <1 Fe 43 Mg <1 Si <1

Ag B Be Mn Mo Na Nb Pb Sn Th Ta V Zr W sought but not detected.

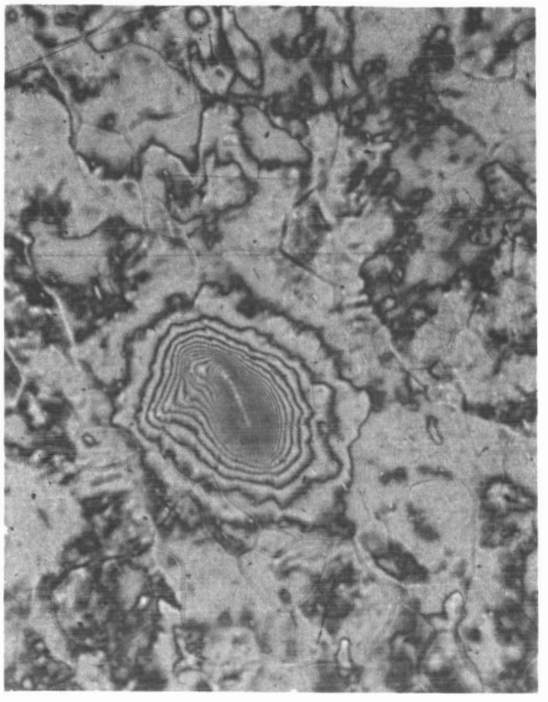

Figure IV-7. Interference Fringe Pattern from W10, Showing Polishing Defect, 152x.

2. Surface Preparation

The surfaces were ground flat and parallel, and the slug was annealed for 2.8 hours at 2350°C in a cold-walled furnace. It was then shaped by electrical-discharge machining, and electropolished in the usual perchloric acid/alcohol mixture at 22 volts (9 amps) for about 20 seconds. It was next electroetched in the same electrolyte at 5 volts (1.6 amps) for 80 secs. The resulting surface was photographed, and typical areas are shown in Figures IV-8 and IV-9. The differential etching rate removes some grains much faster than others, so that they are not all in focus on the photomicrograph.

3. Heat Treatment

The emitter was heated in the cold-walled furnace for 3 hours at 2420°C. The temperature was read with an optical pyrometer, and is corrected for the emissivity of rhenium. The pressure at the Vac Ion pump was found to be less than 1×10^{-6} torr while the specimen was at temperature. The heat treatment was designed to duplicate that used on earlier rhenium emitters in Task IV of this contract.

4. Examination of Emitter Surface

After this heat treatment the surface was again photomicrographed, and typical areas are shown in Figures IV-10 and IV-11. Only slight traces of grain boundary movement are visible, because the specimen was annealed prior to surface preparation and heat treatment. The etched grain boundaries, which have well defined sharp edges in Figures IV-8 and IV-9, have, as expected, become rounded by the heat treatment. Two small thermally etched flat surfaces are visible on Figure IV-10 — one at the center and one near a corner. These are commonly observed following heat treatment of an etched surface. The smoothing effect has extended to the surfaces of the grains that had a textured appearance in Figures IV-8 and IV-9.

Figure IV-8. Emitter Re31 after Electroetching, 310x.

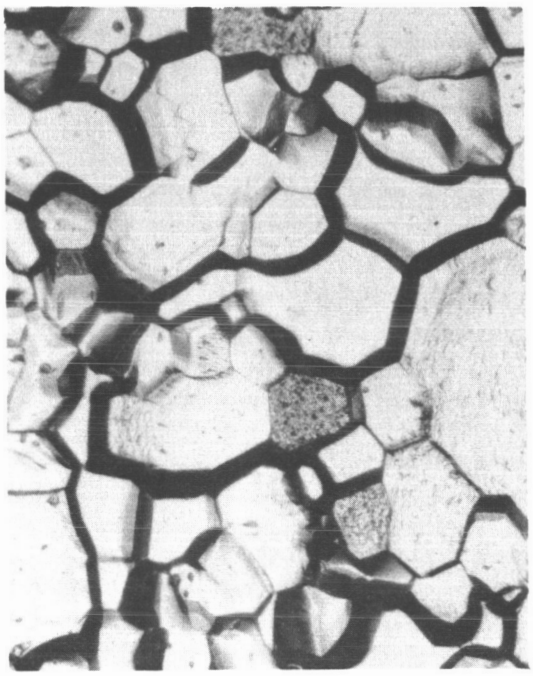

Figure IV-9. Another Area of Re31, 310x.

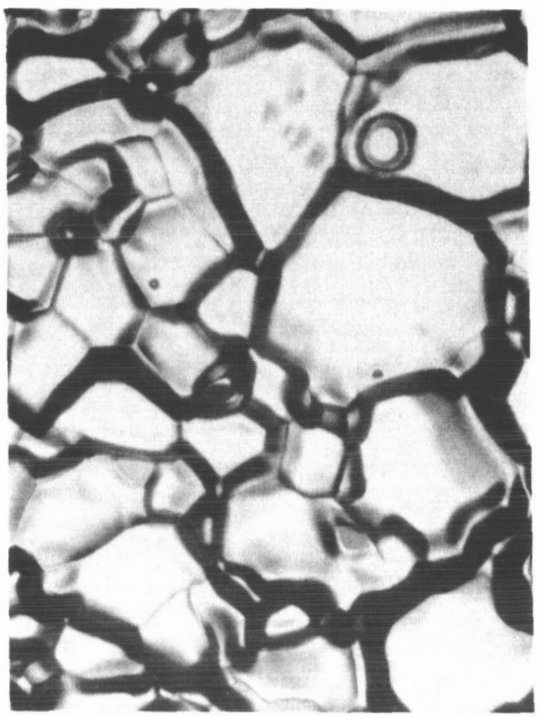

Figure IV-10. Re31 after Heat Treatment, 310x.

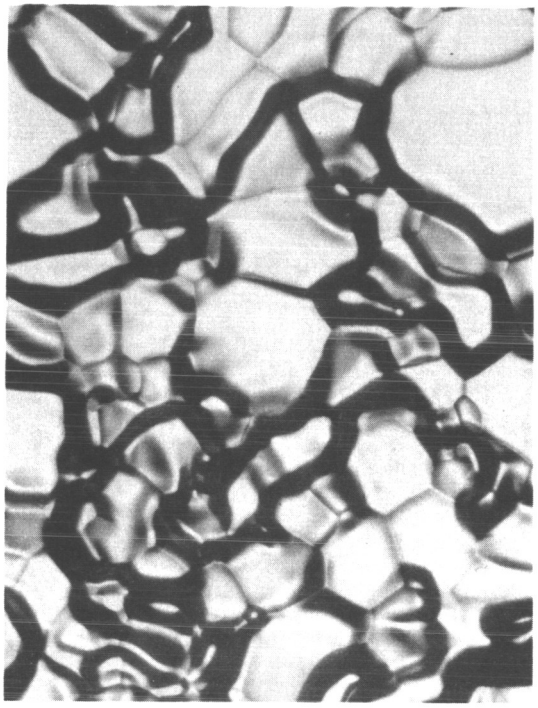

Figure IV-11. Another Area of Re31, 310x.

The surfaces of this emitter are too rough to produce meaningful interference fringe patterns, and so no detailed study of "roll-off" is possible. However, there is every reason to believe that it is confined to a narrow band at the edge, just as it is in tungsten. In any case the "roughness," or depression of some grains below their neighbors, is probably greater than any roll-off.

5. Conclusions

This emitter surface showed rounding and smoothing of the etched surface, and faint traces of grain movement exactly as predicted from our considerable experience with rhenium surfaces. As with the tungsten emitter, this is expected to be completely stable during diode operation.

C. Discussion – Electroetched Rhenium Emitters

As mentioned in the Third Quarterly Report on this program, the etched rhenium emitter represented a substantial improvement over the electropolished rhenium emitter studied during the previous year. In particular, it was found to have a bare work function of 4.88 eV, as compared with 4.75 eV for the polished emitter. In terms of performance, this meant that the etched emitter would produce the same power at twice the spacing used with the polished emitter.

Since the raw material for each emitter was polycrystalline rhenium prepared by powder metallurgy and rolling, supplied by Chase Brass and Copper Co., we can account for the difference in performance of the two emitters only in terms of their surface preparation. Their preparation was substantially the same except that, after being polished, the earlier emitter was heat-treated for 3 hours at 2380°C, while the later emitter was electroetched and heat-treated for 3 hours at 2420°C.

The difference in annealing temperature is probably not significant in producing the superior performance. On the other hand, the effect of electroetching is to remove material selectively from the surface. The fast-etching grains are those with a high specific surface free energy, and their removal tends to increase the proportion of slow-etching, low-surface-energy grains on the emitter surface. These latter grains, having surfaces composed of basal or (00.1) planes, also have a high bare work function; therefore, they bind cesium well, and their presence enhances the performance of the emitter. So we attribute the superior performance of the emitter to the fact that its surface is composed not of the random crystal surfaces exposed by polishing, but of the non-random, preferentially basal-plane surfaces exposed by etching. Atoms are removed from the emitter surface in both electropolishing and electroetching, but the rate-determining steps in the two techniques are different, and so the limiting forms of the surfaces are different. High-temperature heat treatment allows the surface atoms to rearrange themselves in a minimum-energy configuration, and therefore it is of interest to examine the limiting form of the surface under this treatment. The factor determining the form of the surface after vacuum annealing is the specific surface free energy, and the limiting form is that having the minimum integrated free energy. That form will therefore have the maximum possible area of low-energy basal plane. As mentioned above, such planes are favorable for emitters, and so heat treatment will tend to improve the thermionic performance of an emitter.

From our observation that emitters with different electrochemical treatments and similar heat treatments differ in performance, we conclude that the heat treatment used does not have an overriding or determining effect on the form of the surface, and that the electrochemical treatment is important. The varying thermionic emission properties of an etched emitter during the course of heat

treatment have not been studied in this work because it has been of more value to know that the emitter surface was stable, and to eliminate possible emitter changes as variables in the analysis of the diode.

We conclude that combined electrochemical and thermal treatment to develop high-work-function planes can be important in the preparation of rhenium thermionic emitters.

CHAPTER V

ADDITIVE STUDIES

A. Introduction

The performance of cesium thermionic converters has been well documented over a wide temperature range and with many different combinations of emitter and collector materials. It is now possible to evaluate the influence of electrode material and geometry variations on the power output, and it is apparent that further improvements in performance will require the introduction of additional components into the converter system. Electronegative elements form a suitable group of additives and will act primarily on the electrode surfaces. These substances establish an additional degree of freedom for the hardware designer and enable him to produce an improved device by providing an independent means for varying the surface conditions.

The Rasor-Warner[1] theory of cesiated surface work function shows that high work functions in the uncesiated or bare condition are associated with low work functions at any given cesium arrival rate. Electronegative ions adsorbed on an electrode surface form a negative dipole layer, inhibiting the emission of electrons; that is, raising the bare work function of the surface. From the theory, it is expected that such a covered surface would require lower cesium pressures to produce a given work function than would the bare emitter material.

Part of the preceding program[2] was devoted to defining the relation between spacing and cesium pressure. In this study, the influence of the spacing-pressure product on power output was described, and an optimum value for a wide range of conditions was shown to exist. As the spacing is increased beyond this optimum, increased scattering losses in the plasma cause a reduction in

output power. Thus, if the cesium pressure could be reduced while holding the emitter work function at a low enough value to establish the required current density, spacing could be increased, greatly simplifying the hardware design. The electronegative additives offer this possibility.

Langmuir and Villars[3], in 1931, were probably the first to conduct controlled experiments with electronegative elements and cesium. They studied the effects of oxygen adsorbed on tungsten filaments, both with and without cesium vapor, and showed increased uncesiated work function values and significantly lowered cesiated ones in the presence of oxygen. These results did not arouse much further interest until the advent of practical cesium thermionic converters, when the possibilities of fluorine compound additives were investigated by Aamodt,[4] Ranken,[5] and Langpape.[6] Actual converter performance studies had also been undertaken by Thermo Electron[2,7,8] and Jester.[9] Even though the validity of these results may be doubtful as far as the role of fluorine as an additive is concerned, they have shown that the effects of electronegative additives are in accord with the predictions. These experiments are discussed in more detail later in this report. The literature of the field is also surveyed briefly in Appendix A.

While CsF is an attractive additive because of the high electronegativity of fluorine and the compatibility of Cs with present devices, investigations with CsF have shown consistently poor reproducibility and given unreliable results. The initial effort in this program was therefore to develop a correlation between the work function of a surface and the fluoride coverage on this surface. Experiments designed to check the reproducibility and stability of the results were performed under controlled equilibrium conditions in the research parametric converter described in Chapter III. The experiments were only partially

successful, and finally the additive became inactive as it had in many previous cases. At this time the CsF additive techniques were reviewed, and a series of simple glass-tube filament-emitter experiments was initiated. Glass tubes provided a convenient vehicle for a number of short-term, low-cost experiments which could determine the effects of various additives, outgassing techniques, and reservoir temperatures, and at the same time eliminate additive transport problems. The difficulties associated with the previous additive studies were traced to water contamination in the fluoride and it is believed that this water was responsible for the additive effects obtained previously — the fluoride itself being relatively ineffective in the devices.

The surface-additive work was then subdivided into two tasks.

The first task was to purify CsF enough to permit the determination of its effect on the work function of tungsten at thermionic temperatures. To accomplish this, the background pressure over the CsF crystals and in the test vehicle must be reduced below 10^{-10} torr. A special metal-ceramic tube capable of fulfilling this requirement was designed and fabricated. Experiments were performed which documented the effects of CsF, including measurements of its desorption energy. This work determined the true effects of fluorine and furnishes data to develop a theory explaining the unexpectedly small changes in comparison with oxygen.

The second task was to utilize the beneficial effects of oxygen. The thermodynamic equilibrium of oxygen in the converter environment was analyzed, and the conclusion was reached that the O_2 pressure required for coverage was chemically compatible with the environment in the vicinity of the collector. Some formation of oxides of Mo may occur but no loss of collector material is expected at these temperatures. A critical experiment was conducted using Cs_2O as the O_2 source. In this experiment, O_2 was used

in a converter under steady-state conditions for the first time. The emitter work function and power output of the device closely resembled those of the CsF-charged devices. This converter was then tested for stability. A second converter, specifically designed for oxygen additive using a Cu_2O source, was then fabricated, and it produced consistent and reproducible data. This system can exploit, simply and directly, the beneficial effects of oxygen under steady-state equilibrium.

B. Theoretical Analysis

In this program and in previous work, a considerable volume of data has been accumulated pertaining to the tungsten-electronegative additive system. The task of analyzing and correlating these data has progressed concurrently with the experimental task. As a result of these efforts, a framework has emerged which allows a phenomenological description of this system. In this section, the framework is presented and compared with experimental results. These hypotheses will be used later to analyze the experimental data.

The ultimate objective of the surface additive studies is to formulate a detailed model of the tungsten surface covered with fluorine, or any other element, and cesium. As an interim approach, the possibility of considering the tungsten surface with a fixed additive coverage as a metal with higher bare work function and then using the Rasor-Warner theory to predict the cesiated work function was investigated and proved successful. This result, apart from helping to correlate experimental observations, is significant because it implies that the effects of electropositive and electronegative adsorbates, acting concurrently, are separable in terms of their individual effects. The dynamics of additive desorption have been considered, and a relation between coverage, surface temperature, and arrival rate is presented. Finally, using

a simple electrostatic model, the arrival rate required for a given work function changes with low coverages is derived.

1. The Interdependence of Cs and Additive Effects. The Rasor-Warner analysis considers the system composed of two components, cesium and emitter surface. It postulates a physical model for the surface and develops certain relationships among the properties of the system. The present analysis proposes to apply the conclusions of the Rasor-Warner theory to the three-component system composed of cesium, electronegative element, and emitter surface. To do this, the hypothesis is made that at constant additive coverage, the additive-emitter portion of the system is equivalent to an emitter with a bare (non-cesiated) work function value equal to that obtained when the additive is the only adsorbate.

Rasor and Warner give the following expression for $\Delta\phi$, the change in work function of a metal surface when covered with an adsorbate:

$$\Delta\phi = \frac{1}{1-f}\left(\phi_o + \phi_{io} - I - T/T_R\, h - kT\ell nB/C\right) \qquad (1)$$

where:

- f is a fraction of the dipole layer potential drop penetrated by the ion core of the adatom.
- ϕ_o is the normal bare electrode work function.
- ϕ_{io} is the image force binding the adatom to the bare surface.
- I is the ionization potential of the adatom.
- T/T_R is the ratio of surface temperature, T, to cesium reservoir temperature, T_R.
- h is an activation energy for the evaporation of cesium from the reservoir.

B, C are the constants describing the desorption from the surface and evaporation from the reservoir, respectively.

In this relation, all the terms except the last two are practically independent of temperature in the region of most interest in thermionic converters. Therefore the equation may be simplified to:

$$\Delta\phi = A(\phi_o + D - hT/T_R - kT\ell n B/C) \tag{2}$$

Furthermore, the last term may be neglected since the constants B and C are practically equal, so that $\ell nB/C \approx 0$. For two materials differing in bare work function by a given amount it is possible to relate the T/T_R values required to produce a given work function change, $\Delta\phi$. Let the bare work function of the reference material be ϕ_o and the change in work function be $\Delta\phi$ for a surface-to-reservoir temperature ratio, T/T_R. Now, consider a material with bare work function equal to $\phi_o + \delta\phi_o$ and assume that it exhibits a change of work function equal to the reference $\Delta\phi$ at a new ratio, $(T/T_R)'$. It follows from equation (2) that

$$\phi_o + \delta\phi_o - h(T/T_R)' = \phi_o - h(T/T_R) \tag{3}$$

or the ratio of surface-to-reservoir temperature required to produce the same work function change in the new material as in the reference material is given by:

$$\left(\frac{T}{T_R}\right)' = T/T_R + \frac{\delta\phi_o}{h} \tag{4}$$

where h for cesium is 0.76 eV. Substituting this value in equation (4),

$$\left(\frac{T}{T_R}\right)' = \frac{T}{T_R} + 1.32\,\delta\phi_o \tag{5}$$

The effective work function value, ϕ', corresponding to $(T/T_R)'$ is given in terms of the properties of the reference material by

$$\phi' = \phi + \delta\phi_o = (\phi_o + \Delta\phi) + \delta\phi_o \qquad (6)$$

By use of these relations and a ϕ versus T/T_R plot for tungsten and cesium, a new plot of the straight-line portion can be constructed for an additive-covered surface, knowing the $\delta\phi_o$ for a given additive coverage.

Measurements taken during this program have shown that the additive increases the bare-tungsten-surface work function by 0.4 to 0.7 eV, depending on coverage, the most stable value being about 0.4, and the maximum 0.7 eV. Figure V-1 shows the ϕ versus T/T_R curve for ϕ_o of 4.62 eV, corresponding to tungsten. The two dotted lines show the shift expected for a $\delta\phi_o$ of 0.4 and 0.7 eV and were determined by the procedure outlined above. Experimentally determined work function values for tungsten in the presence of additive and cesium are shown as points in this figure, each group corresponding to a different emitter temperature.

These points give excellent agreement with the calculated curves in the higher T/T_R region, showing that at low Cs coverages the additive modifies the surface to produce a behavior equivalent to that of a pure surface of the same bare work function. At higher coverages, however, the curves do not bend so rapidly but continue toward lower work function values.

This deviation is probably a limitation of the Rasor theory rather than an indication of additive behavior, since it has been observed in non-additive systems as well.

2. The Rate Equilibrium and Coverage Relations for Adsorbed Additives

The temperature dependence of reactions such as adsorption or desorption on a surface may in many cases be described by the Arrhenius equation. This relation associates with the reaction an activation energy which has been interpreted as the energy required for the reaction to take place. A knowledge of this quantity will aid the understanding of the binding between the adsorbed atoms and the substrate. Furthermore, this relation can provide a basis for calculations of the arrival rate, and therefore the additive vapor pressure necessary to maintain a given coverage on the emitter surface.

The rate of desorption, from the Arrhenius equation, will be

$$\frac{dn}{dt} = A\,n e^{-E^*/kT_E} \tag{7}$$

where

- n is the concentration of the adsorbed layer
- $\frac{dn}{dt}$ is its time rate of change
- A is a frequency factor which is dependent on temperature
- E^* is the activation energy for the process
- k is the Boltzmann constant
- T_E is the emitter temperature.

To maintain a constant concentration, n, it is necessary to provide an arrival rate, μ, equal to $\frac{dn}{dt}$. The coverage, θ, is then given by

$$\theta = \frac{n}{N} = \frac{\mu}{AN} e^{E^*/kT_E} \tag{8}$$

where n is the total number of available sites. This relation may be used

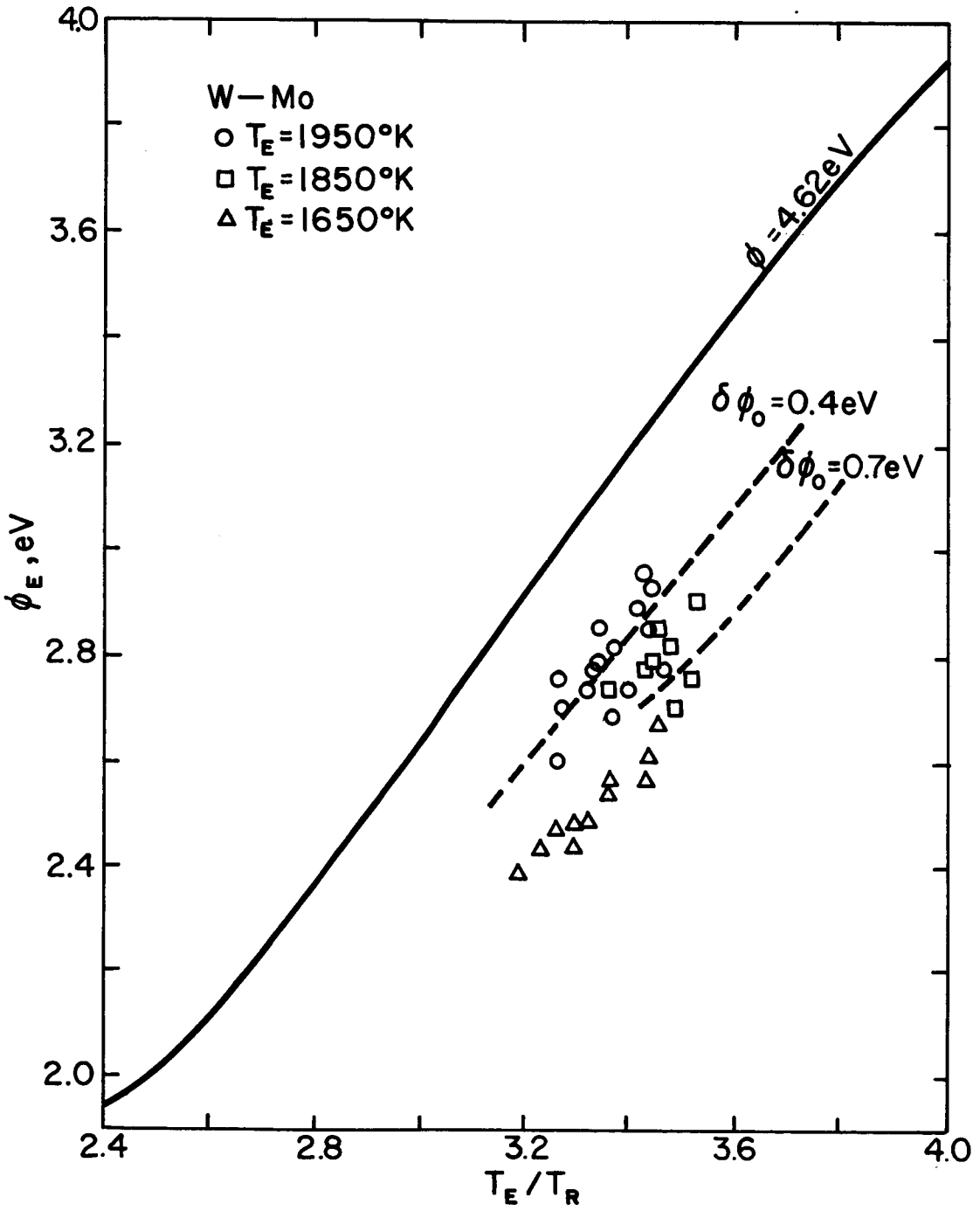

Figure V-1. Experimental and Theoretical Cesiated-Surface Work Functions with Electronegative Additive.

to determine the arrival rates required for a given coverage at different temperatures. Once the quantity E has been evaluated, arrival rate for any given coverage can be calculated. To maintain a given θ at temperatures T_1 and T_2, the arrival rates μ_1 and μ_2 must be related by

$$\frac{\mu_1}{\mu_2} = \frac{T_1}{T_2} e^{E^*\left(\frac{1}{kT_2} - \frac{1}{kT_1}\right)} \tag{9}$$

Equation (9) includes the temperature dependence of A.

Assuming that the surface work function is modified by the formation of the dipole layer of adsorbed ions and substrate, the work function will increase by the potential drop across this layer. If depolarization of adjacent dipoles is neglected, the potential may be estimated as

$$\chi = 4\pi\sigma r_1 q \quad \text{(esu)} \tag{10}$$

where:

- σ is the surface charge density per unit area
- r_1 is the effective distance (in this case, the covalent radius)
- q is the electronic charge (in cgs units, 4.77×10^{-10}.

The covalent radii of both fluorine and oxygen are given in Ref. 10 as about 0.7×10^{-8} cm. If we assume that at full coverage, one additive atom contributing one charge is adsorbed for every tungsten atom, σ will be set equal to the value of N for $\langle 110 \rangle$ tungsten (1.4×10^{15} atoms/cm^2). Actually, from the formula for the oxide (WO_3) and the relative size of the substrate and adsorbate atoms, the density could be three times this value. Substituting these values in equation (9) gives a χ of about 21 volts. Taking $\delta\phi_{max}$ (the change

in work function that would result from a monolayer of additive in the absence of depolarization) equal to the dipole layer potential, the change in work function at low coverages is then:

$$\delta\phi_o = \delta\phi_{max}\ \theta = \frac{\chi M}{AN} \exp[E^*/kT_E] \qquad (11)$$

Equation (11) relates the work function changes resulting from the adsorbed layer to the coverage and arrival rates. By comparing experimental data with this expression, the validity of the hypotheses can be verified.

Using the desorption energy data for oxygen currently available[11,12,13] (135 - 160 K cal/g-atom), the arrival rate required to maintain a given coverage or the equivalent, $\delta\phi_\alpha$, for various emitter temperatures was calculated from equation (11). An average E* of 145 K cal/g-atom and an A equal to kT_E/h, as derived from statistical theory, were used for the plot of Figure V-2. Note that θ is of the order of 0.1, and the assumption of no depolarization is probably valid. Figure V-3 is a similar plot, but shows pressure as well as arrival rate.

3. Desorption Energy. One of the objectives of this program has been the measurement of the energy, E*, associated with desorption for the fluorine-tungsten system. The theoretical relations necessary to evaluate this energy from transient experiments will now be developed. A typical experiment starts with a heated emitter surface in equilibrium coverage with an arriving stream of fluoride particles. By measuring the changes in electron emission with time, when the arriving stream is suddenly interrupted, the approach to bare surface conditions may be related to E* through equations (7) and (11) and the Richardson equation.

Rearranging equation (7) and substituting from equation (8) gives:

$$\frac{\frac{dn}{dt}}{n} = \frac{d[\ell n\,\theta]}{dt} = Ae^{-E^*/kT_E} \qquad (12)$$

A time constant, τ, may be defined as the slope of $\ell n\,\theta$ versus t. From equation (11) and the Richardson equation, it is evident that

$$\theta_t \alpha\ \delta\phi_t \alpha\ \ell n \frac{i_t}{i_o} \tag{13}$$

where the subscript t refers to the value at time t, and o refers to the value in the bare state. To simplify the time measurement, any time during the delay may be chosen as an initial state. This is true because the relations are exponential. Then normalizing with respect to the final values gives:

$$\frac{\theta_t}{\theta_{t_o}} = \frac{\ell n \frac{i_t}{i_o}}{\ell n \frac{i_i}{i_o}} \tag{14}$$

with the subscript i referring to the initial state. Measurements obtained over a range of temperatures give a set of values for τ which can then be used with equation (12) to give a value of E* from the slope of $1/kT_E$ versus τ plot. Thus,

$$\ell n\,\tau = \ell n A - E^*/kT_E \tag{15}$$

and

$$\frac{d\,\ell n\,\tau}{d\,\frac{1}{kT_E}} = -E^* \tag{16}$$

These techniques were used with the surface studies device to determine the desorption energy of fluorine additive on tungsten.

Those same experiments make it possible to approximate the initial coverage if the initial arrival rate is known. A plot similar to that of Figure V-2

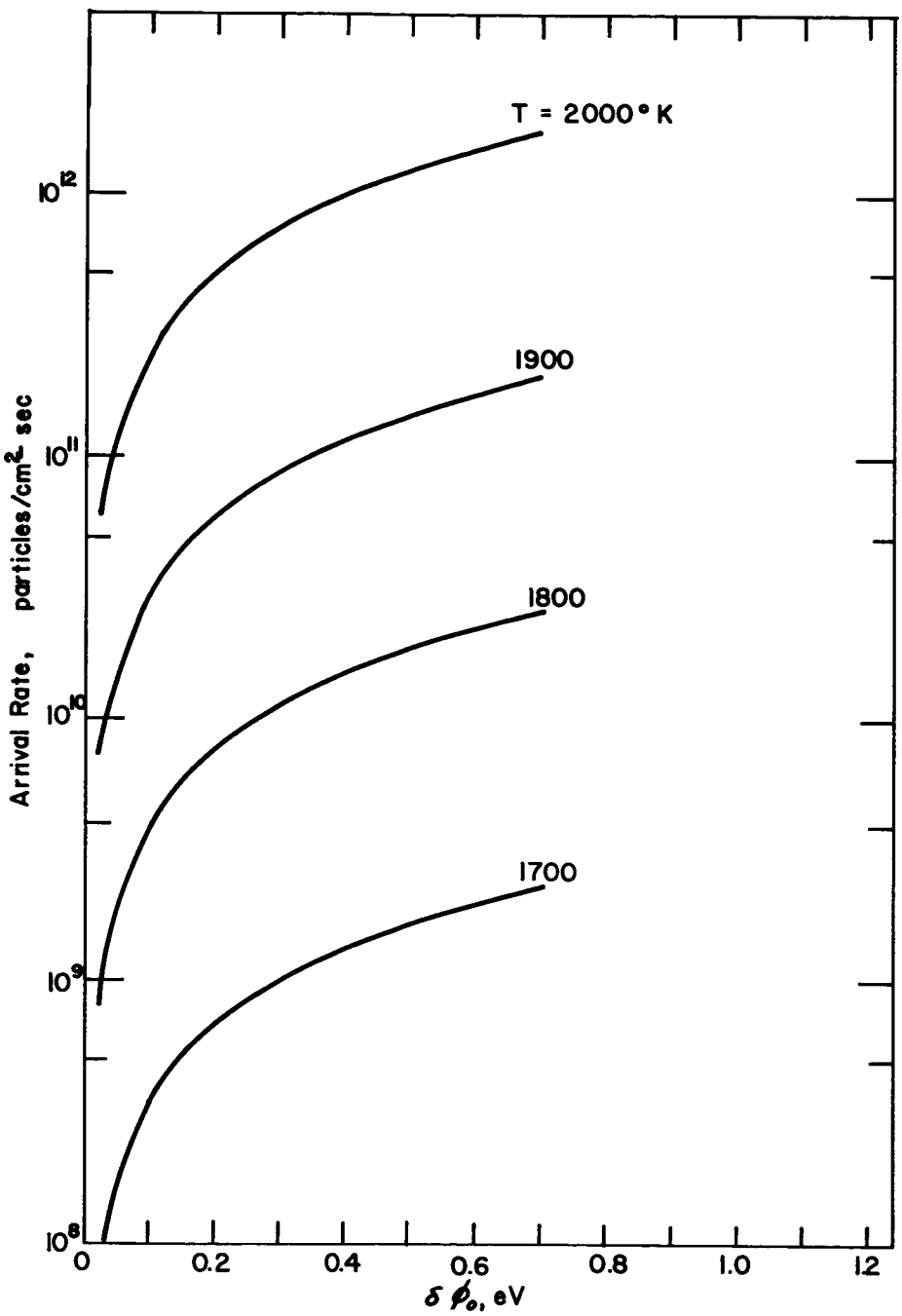

Figure V-2. Bare-Work-Function Shift Produced by Oxygen Additive.

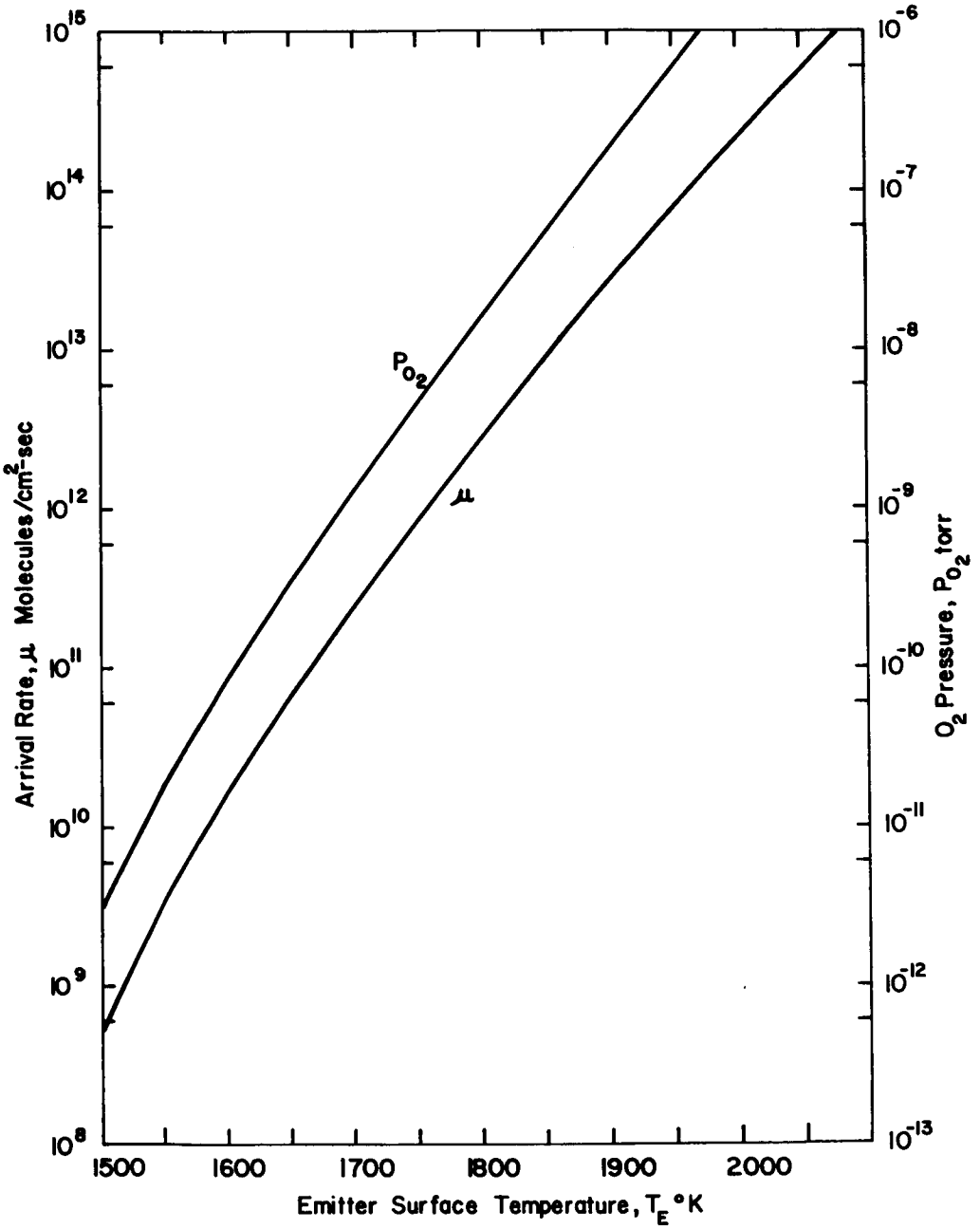

Figure V-3. Oxygen Pressure Required for Substantial Coverage as a Function of Surface Temperature.

may be constructed for fluorine using the observed values of $\delta\phi$. Assuming an exponential decay, the initial rate of decay of the number of atoms adsorbed, dn_o/dt, must be equal to the original arrival rate, μ_o. Then, with n_o the original adsorbed layer density,

$$\frac{dn_o}{dt} = \mu_o = \frac{n_o}{\tau} \tag{17}$$

Since τ has been determined as described above, the initial coverage is simply

$$\theta_o = \frac{n_o}{N} = \tau\mu_o \tag{18}$$

This series of experiments assumes that the coverage is always small and depolarization negligible.

C. Cesium Fluoride Investigations

The original objective of this program was to develop and characterize the use of CsF as an electronegative additive. As in the past, the behavior of this additive in the converter was found to be erratic, and finally the effect was lost. Rather than detail in chronological order the experiments performed, this section will discuss the results of a careful study of CsF behavior and interpret its earlier performance in the light of these studies.

1. Contaminant Control. Langmuir's work[3] on oxygen and water vapor has shown that extremely small amounts of these substances are enough to modify the surface work function of a tungsten emitter. Engelmaier and Stickney[12] have also shown that at O_2 pressures as low as 10^{-8} torr there is an observable effect on work function below 1900°K. It follows then that surface studies require great care to ensure a clean, oxygen-free environment for the tests. In cesium-filled

devices these effects are not usually observed, since the cesium quickly getters the limited amounts of oxygen present. Two dominant sources of oxygen must be considered in additive investigations: the additive and the test vehicle itself.

With the CsF additive, experiments were performed to evaluate the time and temperature characteristics and the type of contaminant appearing during outgassing. As a start, a getter ion pump was connected to a pinched-off copper tube containing a charge of CsF. As the charge was heated the pressure, time, and temperature characteristics of evolved gases were recorded. It was found that, on heating to 400°C, there was a large pressure rise which, after a period of a few hours, finally decayed. However, twenty-four hours later when the temperature was further increased to 500°C, additional gas was still given off. A second, more definitive test was next performed with a mass spectrometric analysis of the gases.

The sample of CsF was placed in a vacuum-fired, low carbon-nickel tube, one end of which was closed while the other was connected to a mass spectrometer system. A heater was placed around the CsF container and the entire system exhausted. The temperature of the sample was raised, and again rapid gas evolution was observed. After an overnight bake at 100°C, the pressure was found to be steady and finally became low enough to analyze. In Figure V-4, the partial pressures of the gases detected are plotted versus time. The left-hand scale corresponds to the partial pressure of each gas in the CsF container. After each increase in baking temperature the pressures gradually decayed, but even after fifteen hours at 450°C to 550°C an increase in the temperature resulted in 10^{-5} torr of CO and 10^{-6} torr of H_2. This agrees with the results of the first experiment and shows that particular care in the fluoride outgassing is required. Up to this time, none of the fluoride used in

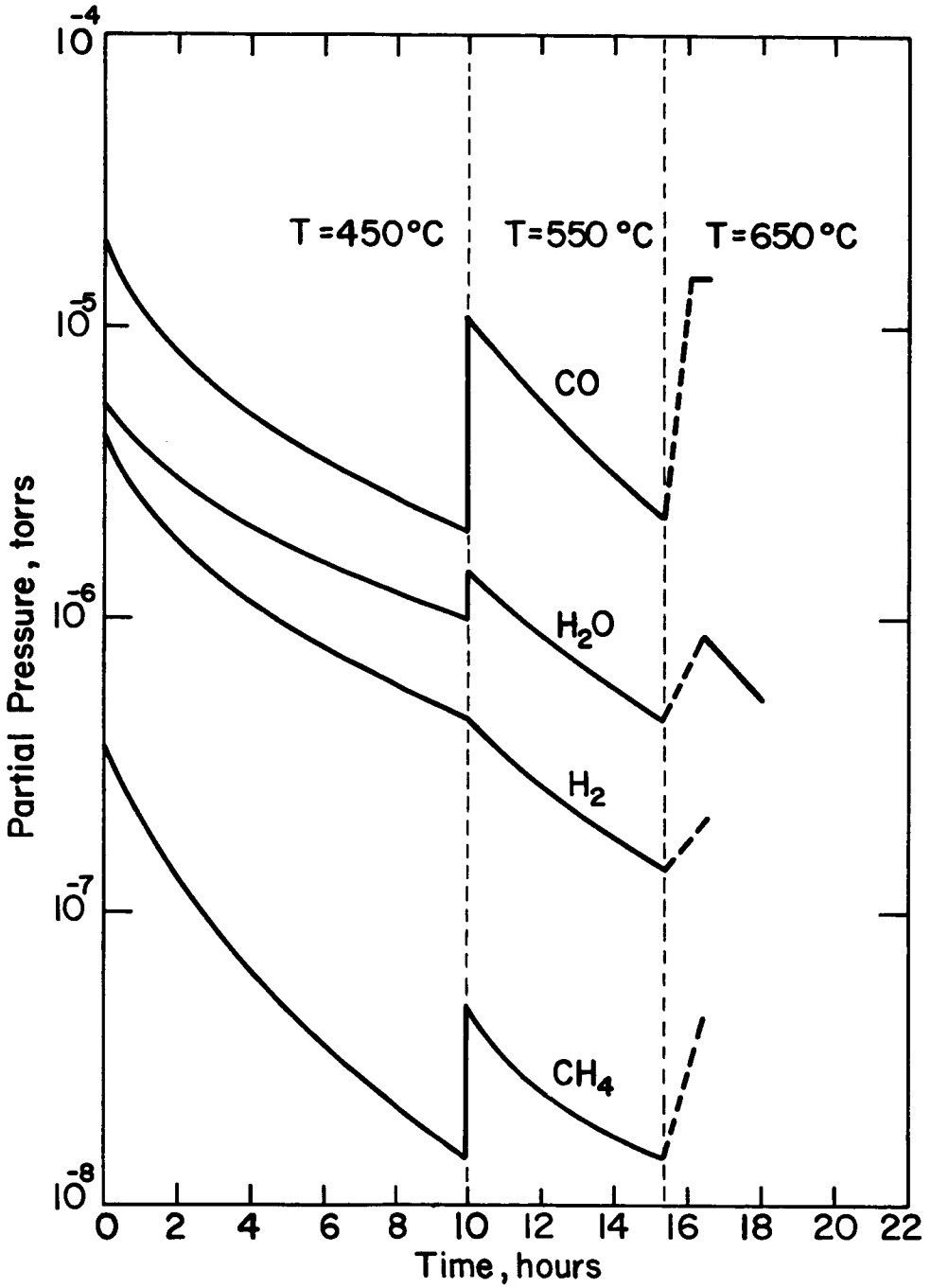

Figure V-4. Mass Spectrometer Analysis of CsF Outgassing.

additive investigations had been particularly carefully outgassed and therefore contained large enough amounts of water vapor to cause work function shifts and invalidate the tests.

2. Surface Studies with Purified CsF. The experiments discussed above make it clear that much more elaborate control of the test vehicle atmosphere is necessary in order to isolate and measure the effects of CsF on the emitter surface. A new test vehicle was therefore constructed for such experiments. The new vehicle employed fabrication and testing techniques capable of reducing residual gas pressure to extremely low values, i.e., 10^{-11} torr. This section gives a detailed description of the device and experimental procedure.

a. Test Vehicle Design and Assembly. The test vehicle shown in Figure V-5 incorporates two tungsten filaments mounted with springs which maintain tension on the wire to avoid sagging. Feedthroughs provide connections for heating current and emission measurements. Guard rings, isolated by ceramic insulators from the active collector, provide for electrical guarding action. The entire shell can be immersed in liquid nitrogen to aid in minimizing gas evolution during tests. A getter ion pump connected to the upper flange provides continuous pumping. The CsF dispenser is heated electrically by passing a current through its shell. Its orifice is arranged to form a beam of CsF molecules which will deposit on the filaments in the region of the collector.

Assembly of the tube was accomplished by first brazing together the guard rings, ceramics, flange, and upper feedthroughs. The filaments with their attached springs were then spot-welded to the feedthroughs. The additive dispenser with the attached tubulation was next welded into place at its outer edge and remained connected to a separate ion pump until after outgassing.

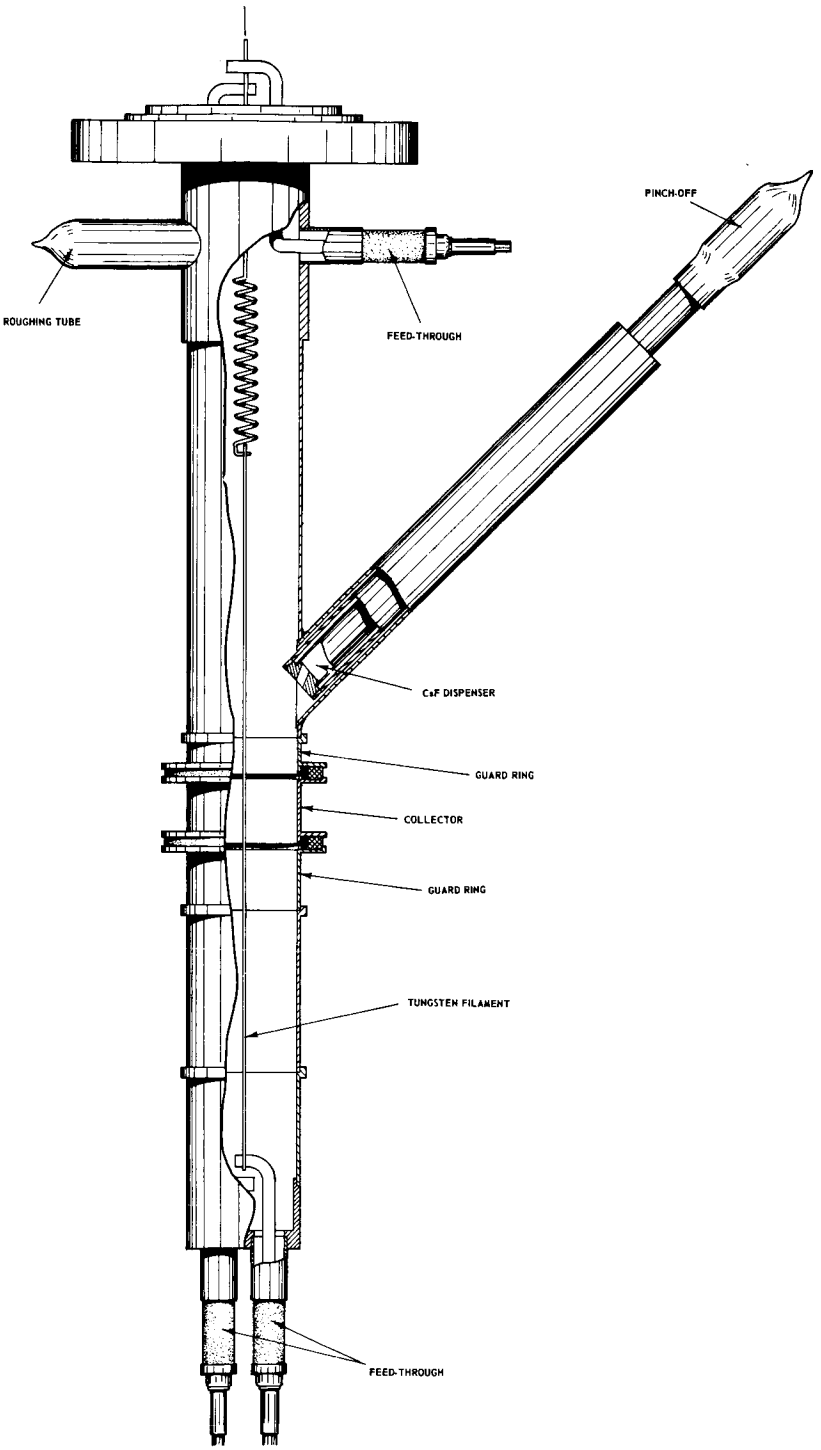

Figure V-5. Drawing of Surface Studies Device

b. Filaments. The filaments were constructed of 0.005"-diameter tungsten wire about 6 inches in length. Since the filaments were not visible in operation. their temperature was inferred from the heating power input. Using the Langmuir-Jones[14] relations for a tungsten filament 0.005" in diameter, Figure V-6 was plotted giving filament temperature as a function of heating current. This relation assumes no gas cooling and an accurate knowledge of the wire diameter. A check on the calculation was performed using a dummy filament in a glass bell jar. The results agreed with an optical pyrometer reading to within 20° at 1800°K

Non-uniformity in the temperature may arise because of end-cooling effects. From the calculations of Langmuir, MacLane and Blodgett[15], a plot was made of distance from the end connection for 99.9% of maximum temperature versus temperature. This plot is also shown in Figure V-6 and assumes that the lead connection is at room temperature. It is seen that lead influence extends less than 0.5 cm from the connection for all temperatures. Clearly, the temperature will be uniform in the collector region.

c. Outgassing. The entire tube assembly with its ion pumps was mounted in a vacuum enclosure during this process to avoid oxidation of the envelope. Figure V-7 is a schematic of the outgassing arrangement. The CsF is contained in the trap formed by the "U" bend in its tubulation and may be heated and pumped separately from the test vehicle body. Most of the gases given off were, therefore, rapidly exhausted without entering and contaminating the actual test vehicle or its pump. Since cesium fluoride normally contains large quantities of water, the baked fluoride samples obtained from the outgassing and mass-spectrometer experiments described above were used to charge the test vehicle. A glove-bag with a dry nitrogen ambient reduced water pickup during this charging procedure. Dry nitrogen was also

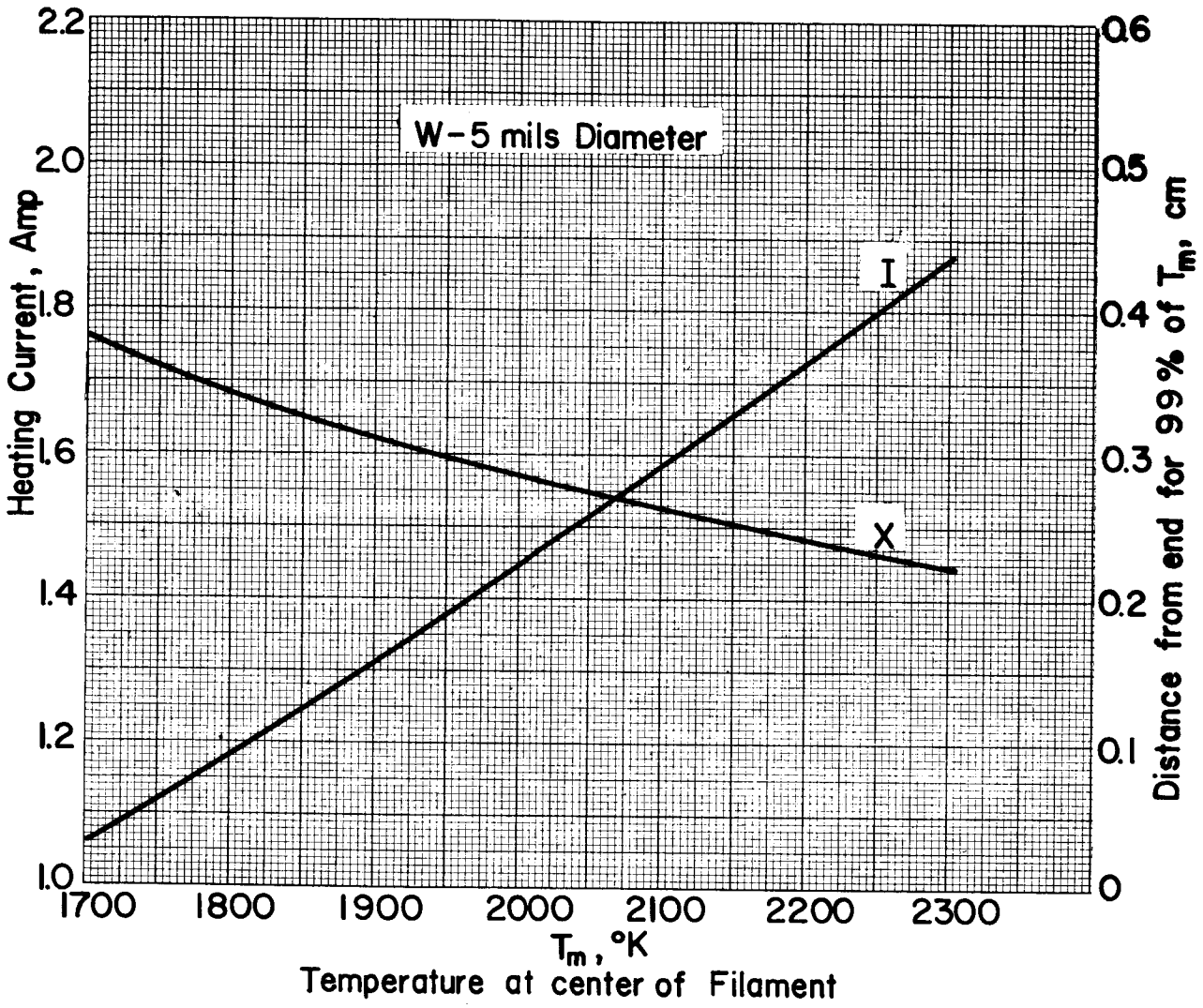

Figure V-6. Filament Temperature as a Function of Heating Current and Influence of End Connections on Temperature Uniformity.

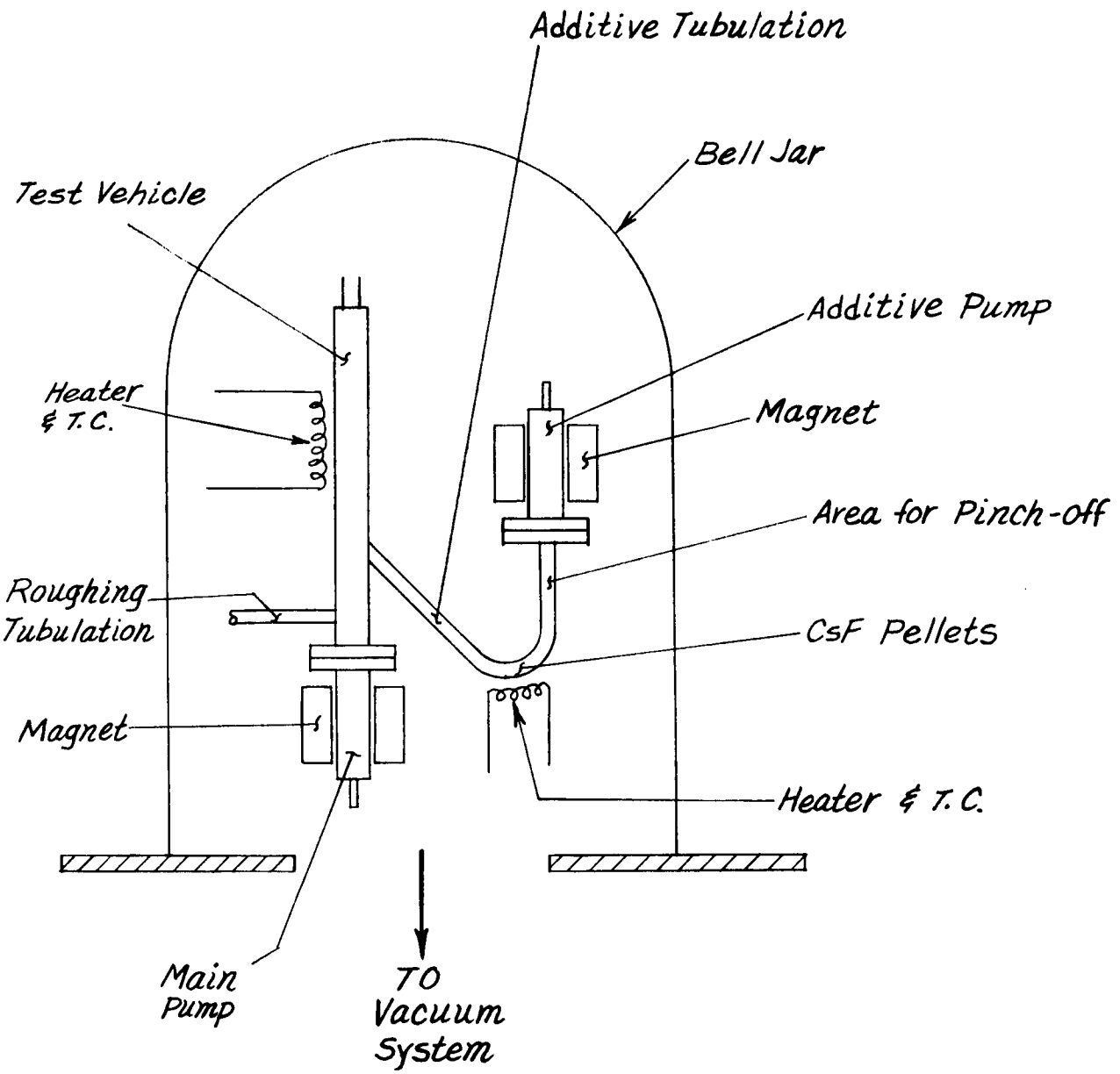

Figure V-7. Outgassing Set-up for Surface-Studies Device.

forced through the test vehicle until the additive ion pump was attached, again minimizing possible water and carbon dioxide absorption.

The device was then pumped through the roughing tubulation. When the pressure was low enough to start the ion pumps and their operation appeared stable, this tubulation was pinched off. Pumping was continued with the device at room temperature until a pressure of the order of 10^{-7} torr was reached. The enclosure was then evacuated, and heat was applied to the test vehicle to raise its temperature until a pressure of 3×10^{-6} torr was reached at about 200°C. When the pressure rise had leveled off, the additive tubulation was heated but maintained at a lower temperature. A slowly rising pressure only remotely responsive to the test vehicle temperature appeared after a short time. This was traced to heating of the ion pumps by direct conduction through the flanges in the absence of convective cooling with the vacuum environment. Water cooling was provided for both pumps and heating was continued. The tube itself was finally maintained at 500°C for 18 hours and the fluoride at 300°C for 17 hours. The fluoride was raised to 500°C for 1/2 hour preceding the final bake. Since at this level the evaporation rate becomes significant, the temperature was reduced to avoid excessive loss. The pressure in the hot tube was 10^{-7} torr, which dropped to 5×10^{-10} torr after cooling. This was considered a satisfactory value, so the additive pump was pinched off and the test vehicle removed from the vacuum enclosure.

During testing, pressure in the tube was monitored by recording the ion pump current. Because of the close coupling of the pump to the tube, the readings were an accurate representation of the actual tube pressure. This measurement was limited by the pump leadthrough leakage current, which was estimated under actual vacuum conditions by removing the pump magnet and

determining the residual current. The pressure corresponding to this leakage was less than 10^{-13} torr and was considered negligible.

d. Work Function Experiments. Surface work function was calculated, using the Richardson equation, from measurements of emitted current at specific surface temperatures. Since the accuracy of the result is dependent on the current density, both area and emitted current must be well defined. The guard structure used in the device eliminates leakage currents and at the same time provides a precise active filament length for use in the calculation of area. Since direct observation was not possible, filament temperature was determined from the Langmuir-Jones tables using the filament heating current. A diagram of the electrical circuit used in these tests is shown in Figure V-8. The precision voltmeter was necessary because of the strong dependence of temperature on current. The electrometer ammeter, as well as measuring collector current, provided a low-impedance guarding circuit and furnished the required following action for the guard electrodes. The output I-V curves were plotted on the X-Y recorder, providing a complete graph of the characteristics from which saturation currents could be determined.

The completed test vehicle, after outgassing, was inverted in such a manner that the CsF pellets fell into the pinch-off rather than down into the tube itself. The objective was to evaluate the bare work function values of the filament before admitting additives to furnish a control. First, the filaments were cycled several times to about 2000°K and soaked at this temperature for about an hour. This treatment further outgassed the device by cleaning the filaments. The preliminary runs without liquid nitrogen, showing approximately the expected tungsten values of about 4.7 eV, are plotted in Figure V-9. Note that the plot is parallel to the work function lines, indicating that there is

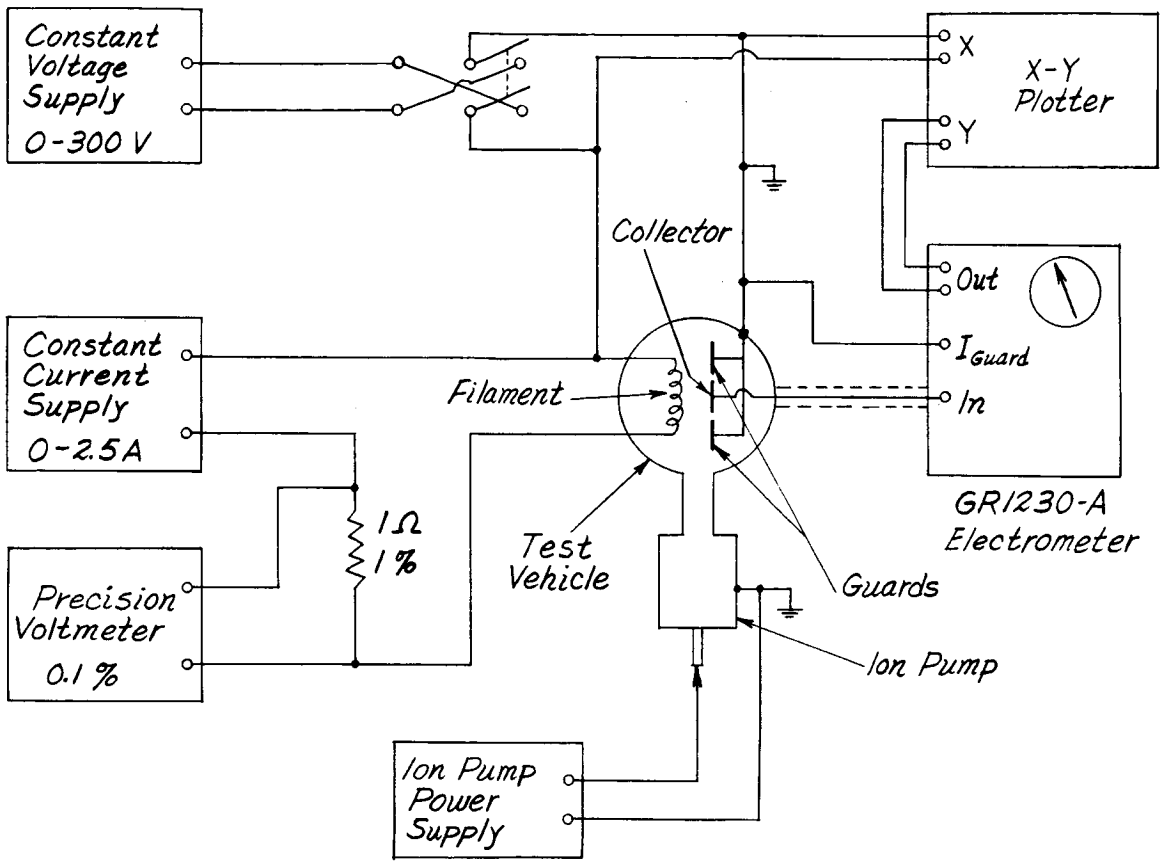

Figure V-8. Circuit Diagram for Emission Measurements.

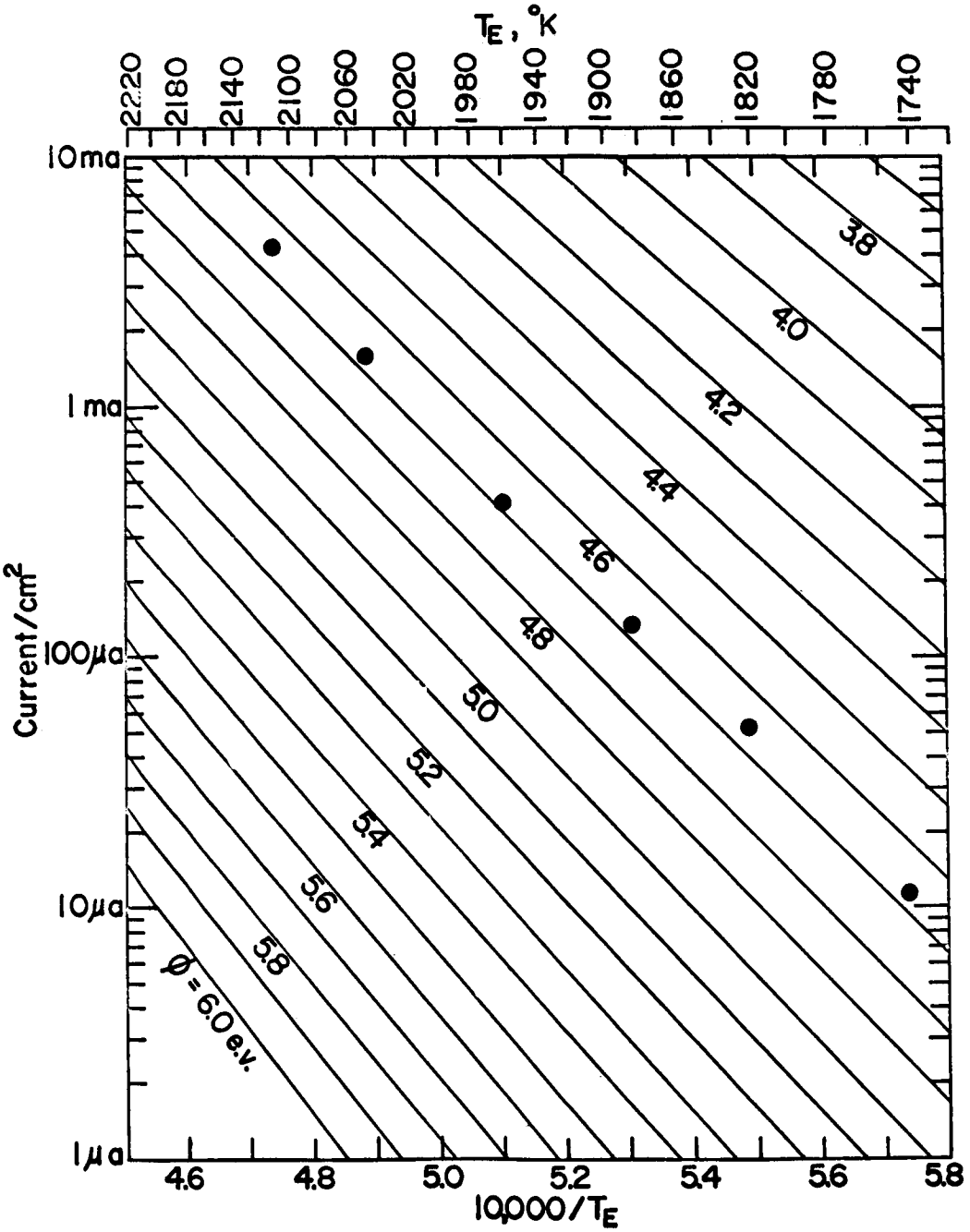

Figure V-9. Left Filament Work Function, No Liquid Nitrogen Cooling.

no temperature dependence. These results validated the assumption that the surfaces were clean and that nothing significant was being evaporated from the filament at the higher temperatures. Near the saturation knee an unusual bump appeared in the curves. With different filament polarity the character changed and became a smooth decrease. This effect is unexplained, but may be connected with the magnetic field of the pump.

The test vehicle was then immersed in liquid nitrogen for further testing. Figure V-10 shows the plots of these results. Only a small change was produced by flashing the filament 2600°K for five minutes between runs. The pressure during the flashing rose to 5×10^{-8} torr and then fell to about 10^{-9} torr during the run. A control run using both a hot and a cold filament was made by heating the additive reservoir but not the tubulation. No change was observed in the characteristics of either filament indicating that heating the empty CsF reservoir had no effect on the emission. These experiments completed the control evaluation of the test vehicle.

The test vehicle was prepared for additive tests by dismounting and tipping it so that the CsF pellets fell from their trap in the tubulation bend, down into the reservoir. Since the pellets could be heard dropping into place, their presence was verified.

Before each day's run, the filaments in the test vehicle were held at about 1900°K for one-half to one hour. The resultant heating of the test vehicle removed adsorbed gases from the walls and filaments. A burst of gas to about 10^{-7} torr was observed initially, followed by a recovery to 10^{-9} torr. The pressure then rose slowly to 10^{-8} as the walls became heated, and recovered to 10^{-9} near the end of the heating time. After cooling to liquid nitrogen temperature, a final pressure of 10^{-11} torr was obtained. A final flash to 2600°K

for three minutes stripped the filament of any adsorbed layers prior to testing. Throughout the testing the maximum pressure observed was 5×10^{-10} torr, but the pressure was below 5×10^{-11} most of the time. Since these pressures were two orders of magnitude below that required for oxygen effects, the device was considered clean.

In steady-state experiments, the reservoir was heated to the desired temperature, and the J-V characteristics at each of several filament temperatures were determined. The presence and arrival rate of CsF were evaluated from the current in the ion-accelerating portion of the characteristic. Figure V-11 shows typical curves for two different filament temperatures. The ion current change is due to a drift in reservoir temperature and not to the filament temperature change.

Transient behavior was examined in two different groups of experiments. In the first, a step function current change was applied to the unheated filament, and the emission current was plotted as a function of time. Plots were made both with and without the CsF beam, and samples are shown in Figures V-12 and V-13. A variable delay, dependent on the time since the filament was last heated, appeared in the bare runs. By following a specific cold, preheat, and final current time schedule for each run, the variations were held to about 0.1 sec. In the second group, equilibrium was first established between the additive arrival rate and the heated filament. The CsF dispenser was then quenched, abruptly terminating the arrival of CsF onto the filament. Again current was recorded as a function of time. In this case, since the filament temperature is constant during the desorption, it is easier to evaluate the desorption energies. A typical run is shown in Figure V-14. Initially, steady-state conditions prevailed under a fixed CsF arrival rate, as is indicated

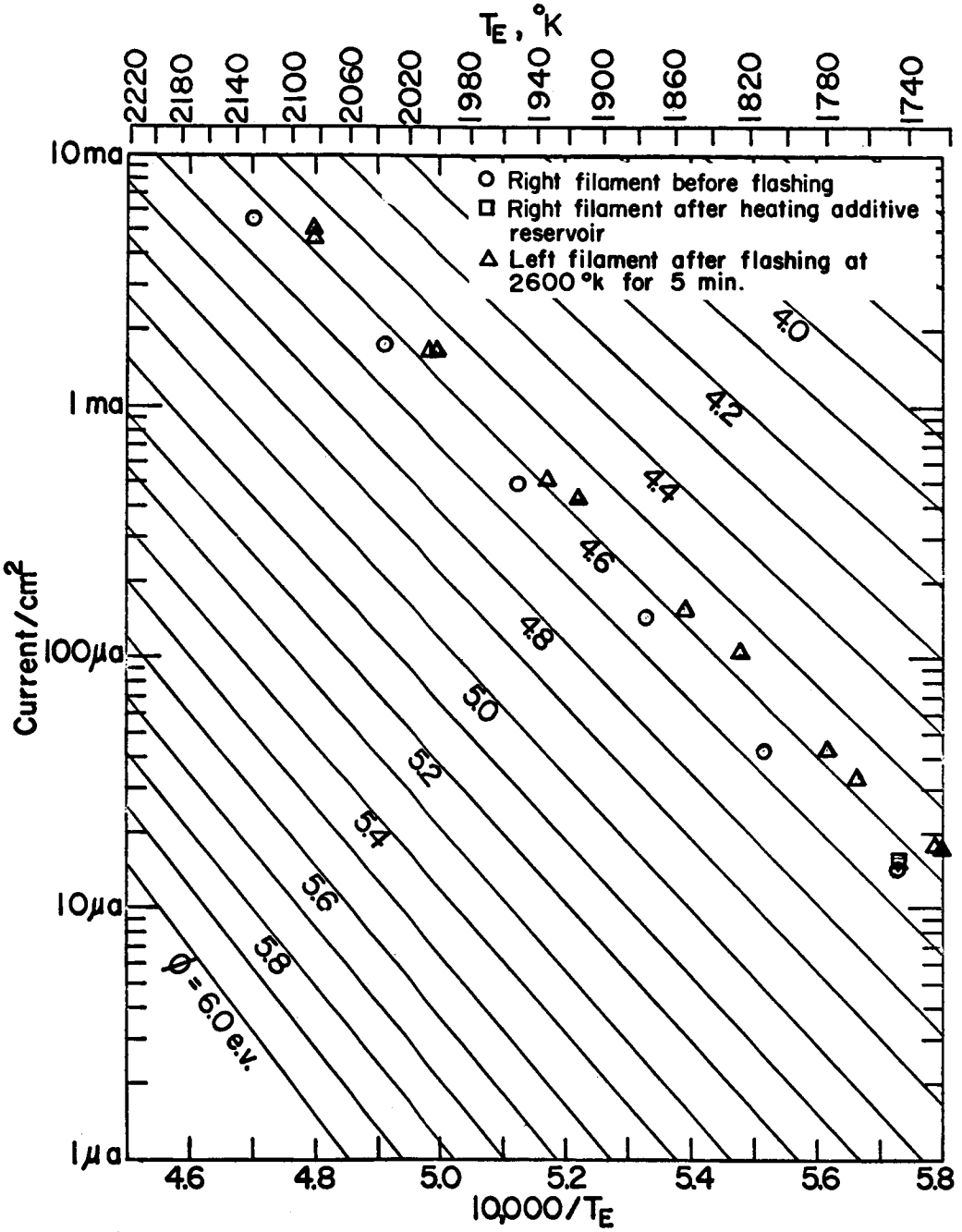

Figure V-10. Right Filament Work Function with Liquid Nitrogen Cooling.

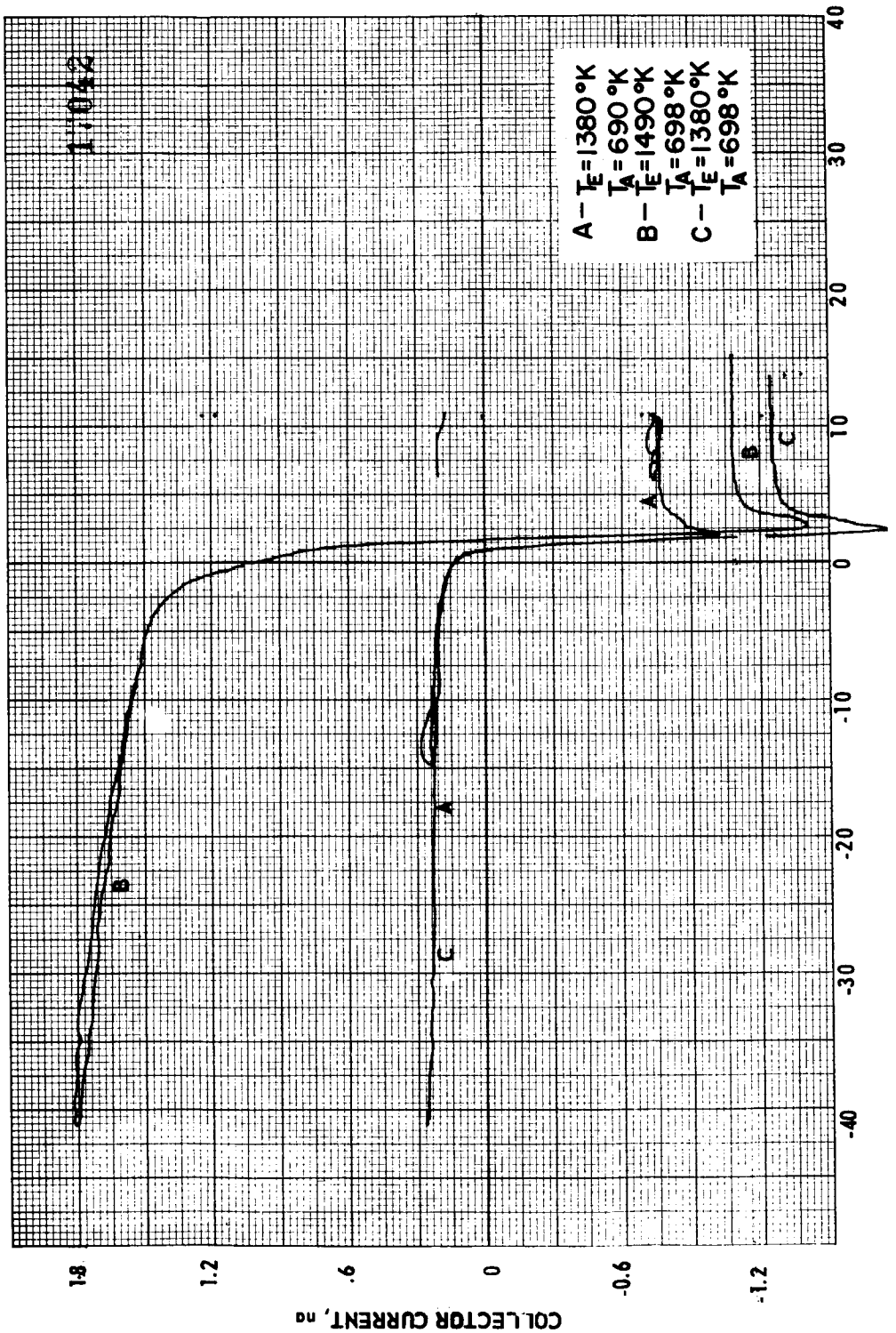

Figure V-11. Typical J-V Characteristic Showing Ion Currents.

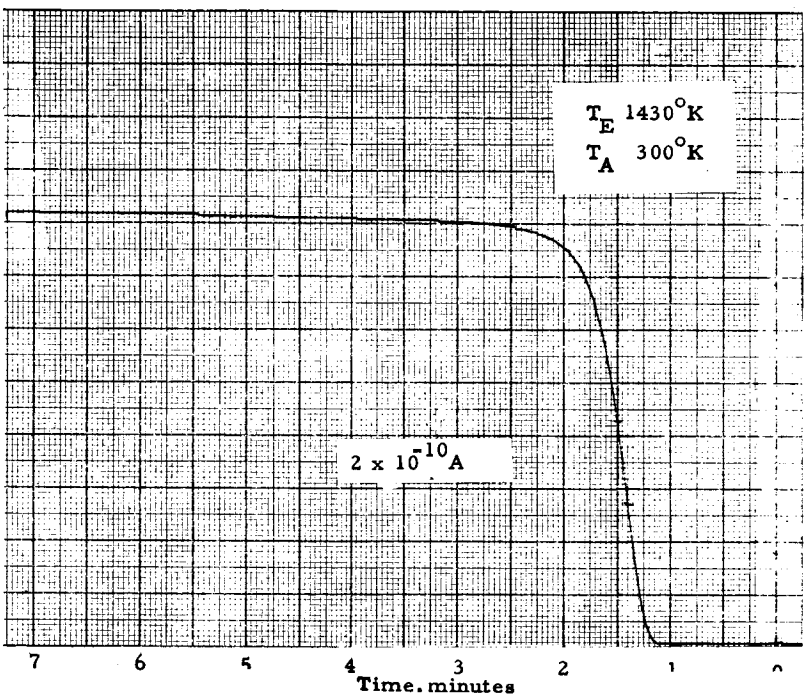

Figure V-12. Emission Current Transient for Step Change in Filament Heating Current, No CsF.

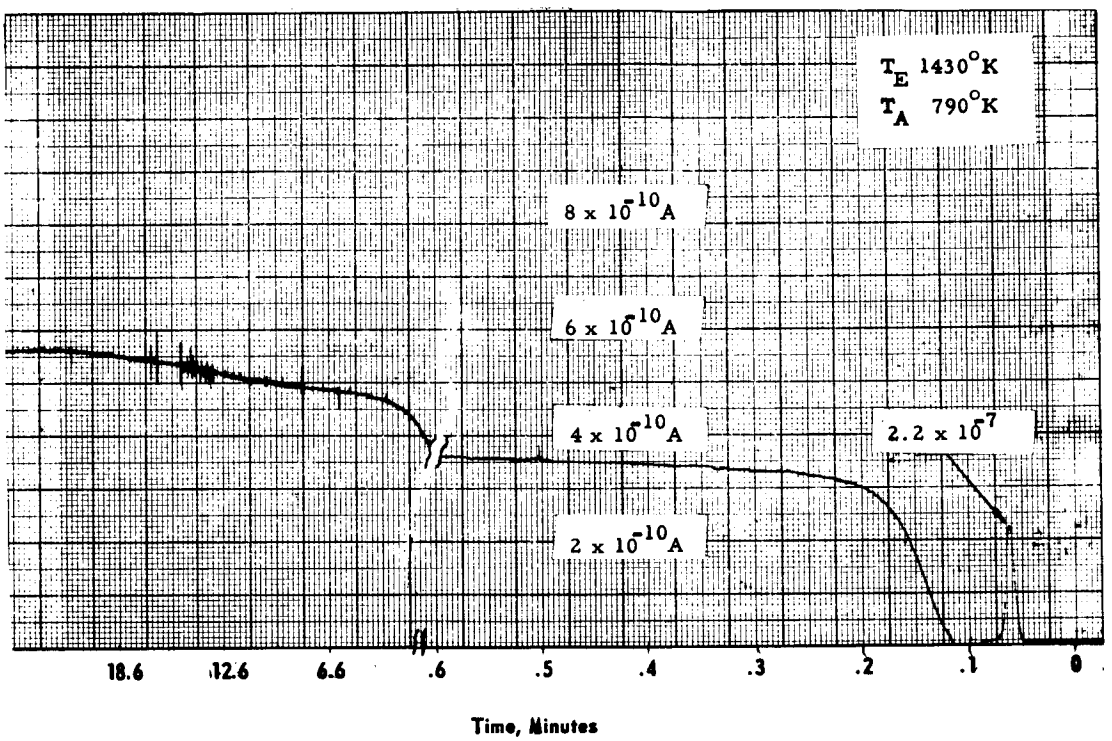

Figure V-13. Emission Current Transient for Step Change in Filament Heating Current, Constant CsF Arrival Rate.

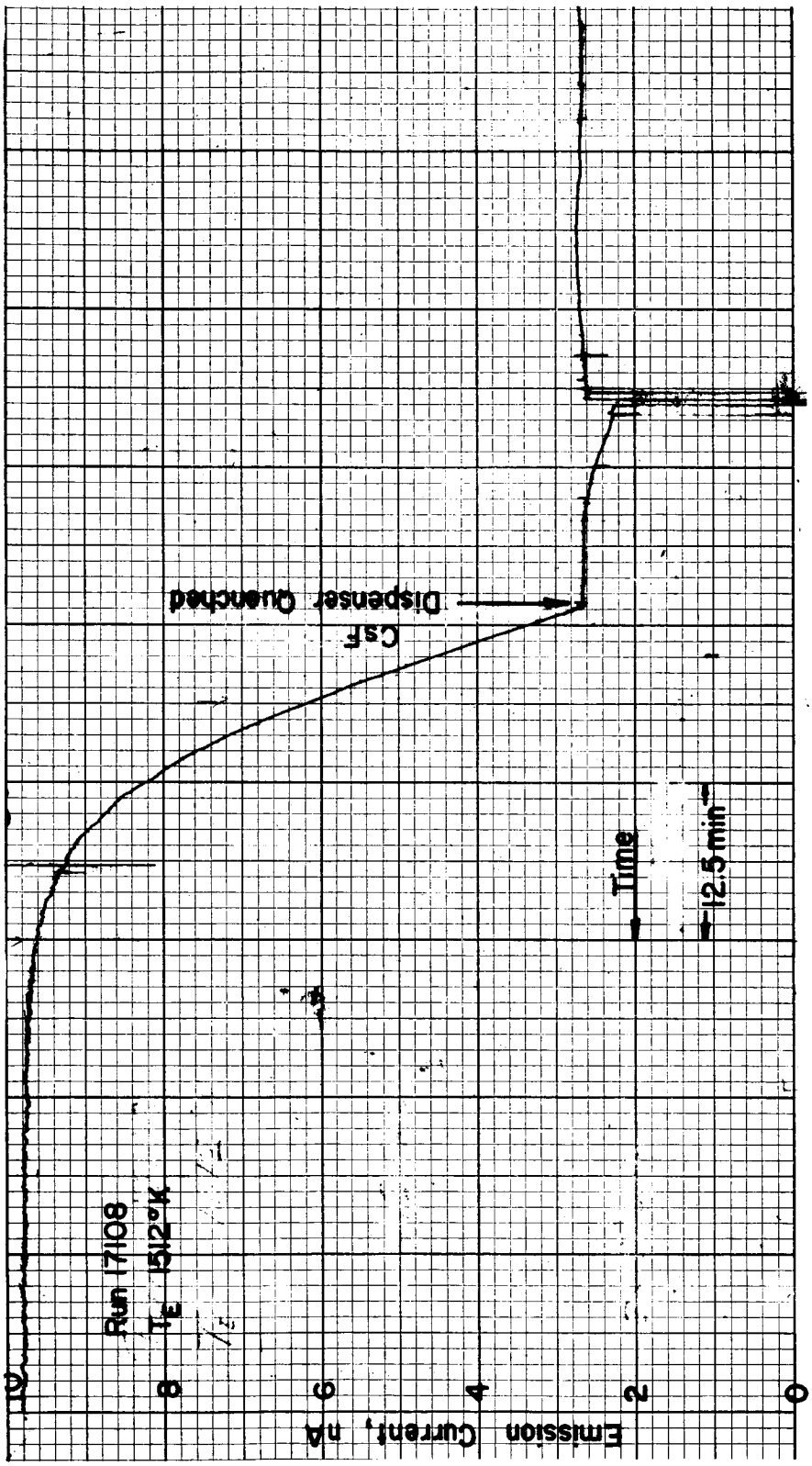

Figure V-14. Emission-Current Transient for Constant Filament Heating Current, Quenched CsF Reservoir.

by the constant value of the emitted current. When the CsF dispenser was quenched, the current increased exponentially, and eventually it reached a final value corresponding to "bare" tungsten emission. Runs were taken over a range of surface temperature from 1380°K to 1650°K, these limits being imposed by the restrictions in available arrival rates and current-measuring techniques. At the lower temperatures the signal-to-noise ratio deteriorated, while at the higher limit coverage became so small that the work function changes were not detectable.

e. Steady-State Results. Data from these experiments was analyzed for work function values. Both covered and bare levels were calculated, and they are plotted in Figure V-15. These points show a maximum change of about 0.3 eV. The arrival rate for these tests was 0.3 $\mu a/cm^2$ and was evaluated by measuring the cesium ion current produced by the dissociation of the CsF on the hot filament. It is assumed that at these surface temperatures virtually all the incident fluoride molecules are dissociated and form cesium ions which are in turn emitted.*[16, 17] The corresponding particle arrival rate and pressure must then have been 1.9×10^{12} particle/cm^2-sec and 2×10^{-8} torr. At these low values, the question arises whether traces of oxygen contamination could be responsible for these results.

There are several factors which reinforce the conclusion that it was actually fluoride effects that were observed. A calculation of desorption energy, to be described below, indicates much too low a value for oxygen. The work

*This assumption had also been verified in these experiments by showing that there was no increase in ion current when emitter temperature was increased above a threshold value. See Figure V-11 also.

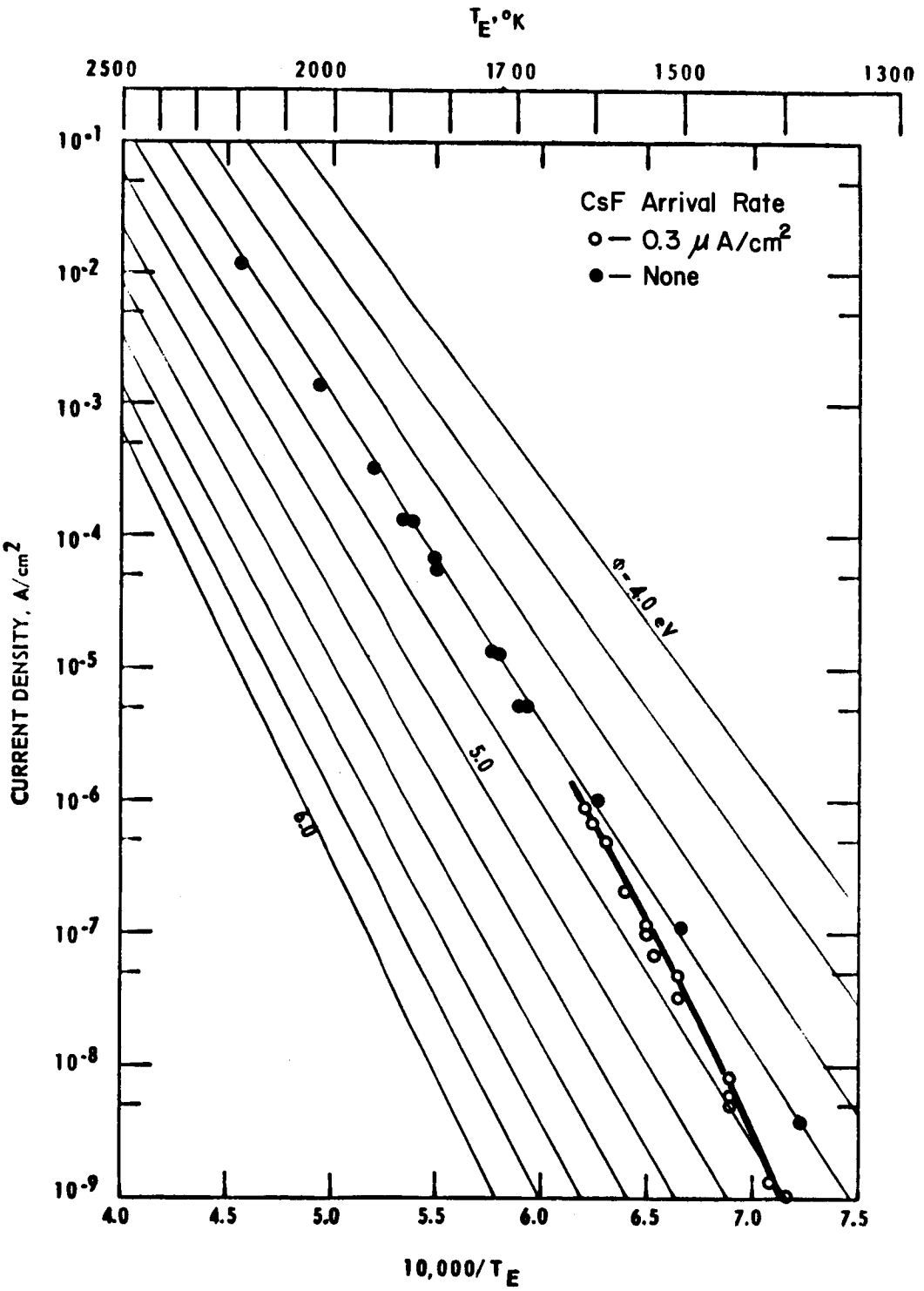

Figure V-15. Surface Work Function of a Tungsten Filament in the Presence of CsF Vapor.

function shifts are also much less than those usually found with oxygen. Finally, in the first group of experiments, where the filament was maintained at a low temperature while the additive was allowed to cover the surface, if any oxygen had been present a pronounced decrease in work function of about 0.7 eV would have been observed. In addition, this change would have remained evident for the long period of time required for the oxygen to desorb from the surface. At 1850°K, Langmuir found lifetimes of the order of 30 minutes for this desorption. In our experiments at these temperatures, no work function change at all was observed. These factors indicate that the cesium fluoride was responsible for the observed phenomena.

f. Desorption Energy. The relations developed in the theoretical discussion may now be used to evaluate the desorption energy. Figure V-16 shows typical plots of normalized coverage versus time and was obtained through the use of equation (14). The logarithm of the time constants τ obtained from this chart are plotted as a function of $1/kT$ for use in equation (16). Figure V-17 shows this plot. The desorption energy from the slope of this curve is about 3.3 eV. This slope has been weighted more heavily toward the low-coverage (high-temperature) points because of the decrease in energy which would be expected as the surface becomes more fully covered.

g. Coverage Relations. Using the measured arrival rate at the start of the desorption experiment, together with the time constants obtained from plots similar to Figure V-16, the actual initial coverage can be determined from equation (18). Combining these results with the work function change indicated in Figure V-15 allows the plot of Figure V-18 to be made. This figure defines work function change in terms of surface coverage and successfully completes one of the main objectives of this study.

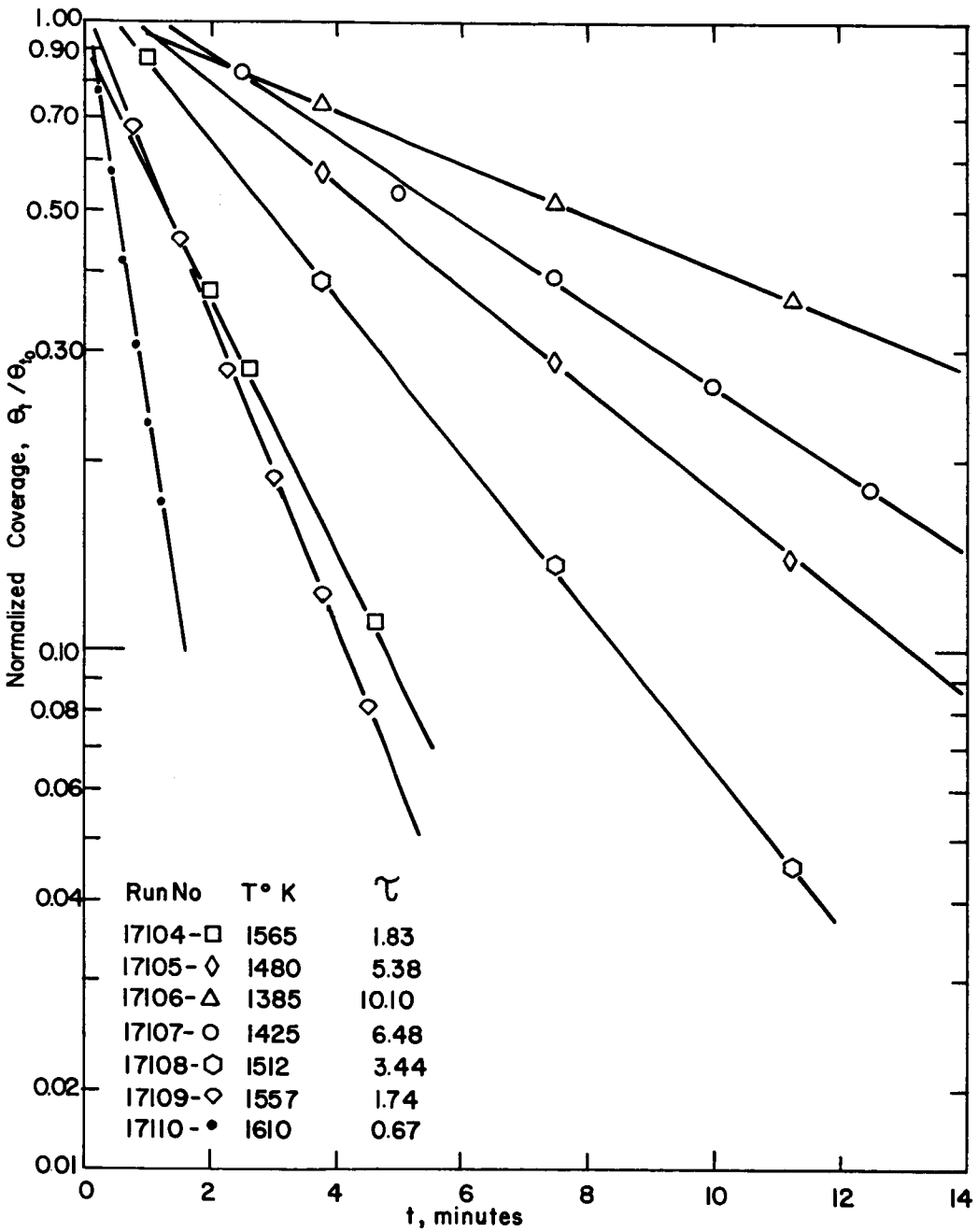

Figure V-16. Characteristic Decay of CsF Coverage for Several Filament Temperatures.

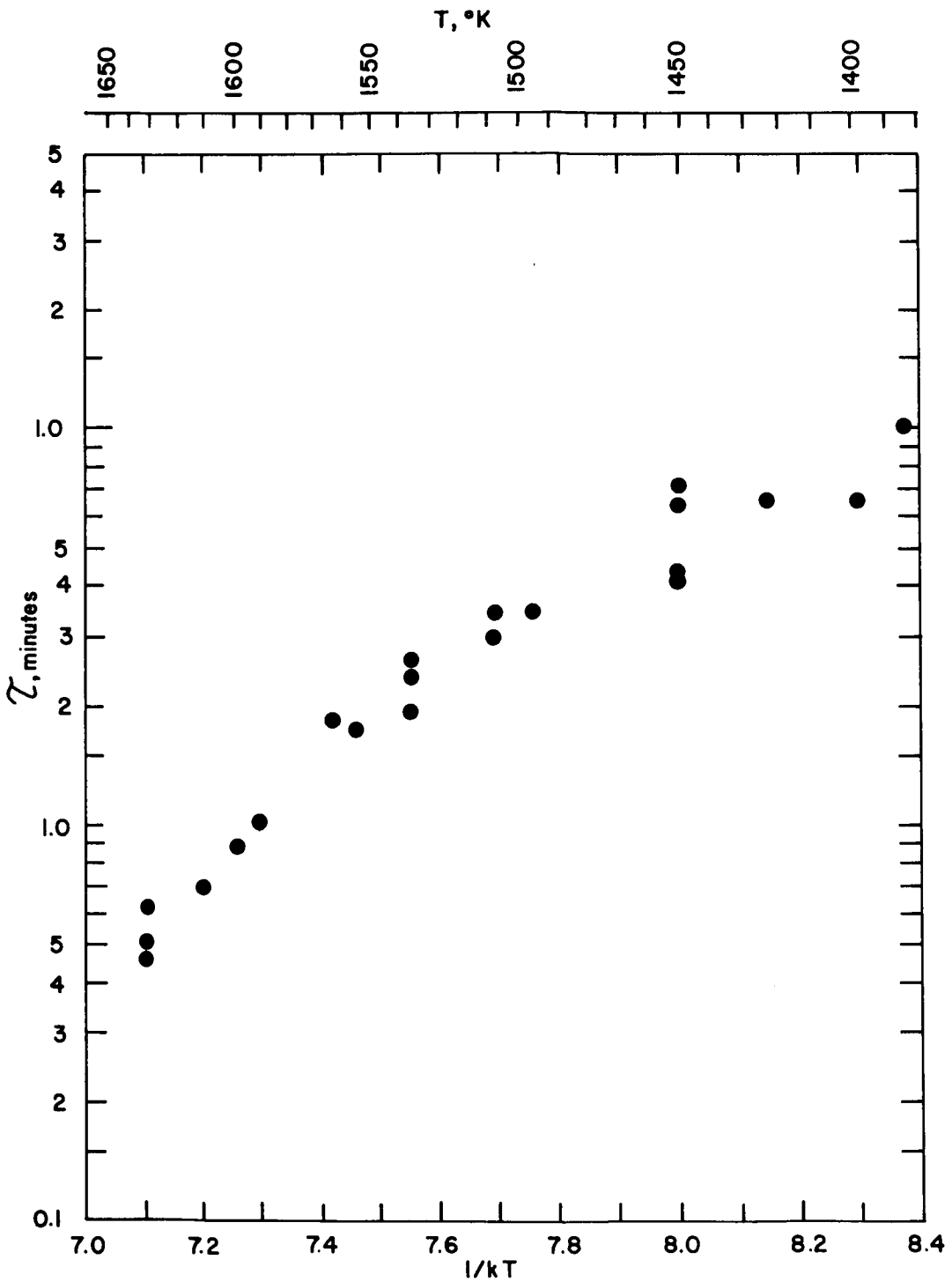

Figure V-17. Decay-Time Constant for CsF Coverage as a Function of Filament Temperature.

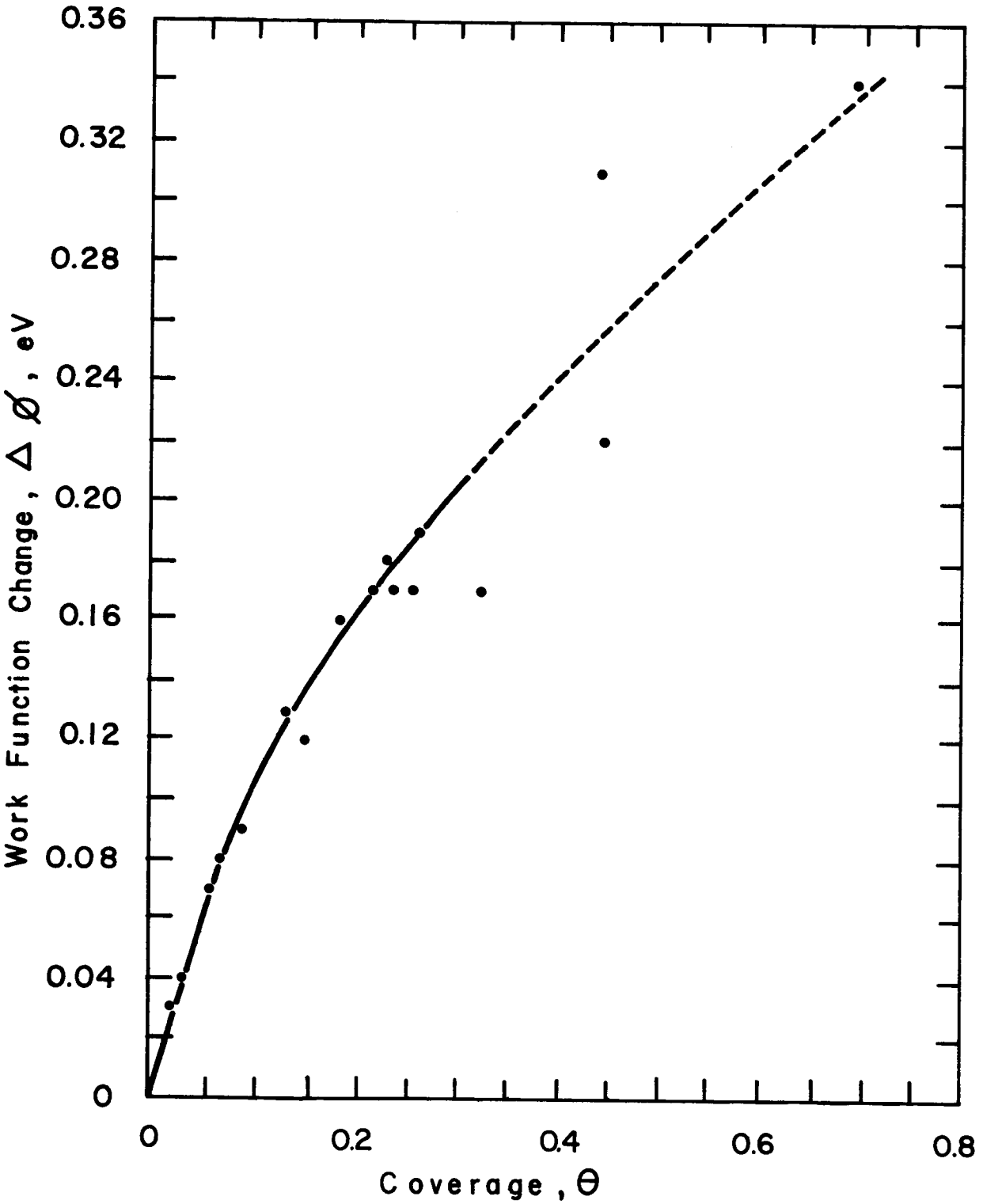

Figure V-18. Surface Work Function Change Produced by CsF Coverage.

These results show that, even where there is significant coverage, the work function is only slightly raised. As the coverage increases, the slope of the curve decreases, indicating that the adsorbate becomes less effective as the surface becomes more covered. A similar behavior has been observed with cesium and is due to the occurrence of depolarization when the adsorbed atoms become closely packed. At the higher coverages, the assumption that the decay is described by a single time constant is no longer valid, and the actual coverage is probably somewhat less than the calculated value. For the low coverages the curve may be used to predict the work function at higher temperatures and can serve as the basis for the development of a surface additive theory.

The coverages shown in Figure V-18 assume that a monolayer consists of one fluorine atom for each tungsten atom, as discussed in the theoretical section. While the initial slope of this curve appears to give characteristics similar to those for oxygen, the curvature of the higher portions seems to indicate that the equivalent changes will not be obtained. In addition, the 3.3-eV desorption constant, as compared with 6.3 eV for oxygen, implies that the fluorine will desorb much more rapidly than oxygen, and therefore much higher arrival rates will be required.

The curve of Figure V-19 indicates the CsF arrival rate required to maintain significant coverage at various surface temperatures and also shows the reservoir temperature required to establish this pressure. This curve is similar to that calculated in Figure V-3 for oxygen and can be used to evaluate the coverage resulting from the reservoir temperatures examined in equilibrium fluoride experiments. Note that the fluoride arrival rate must be 5 to 6 orders of magnitude greater than that for oxygen for equivalent coverages.

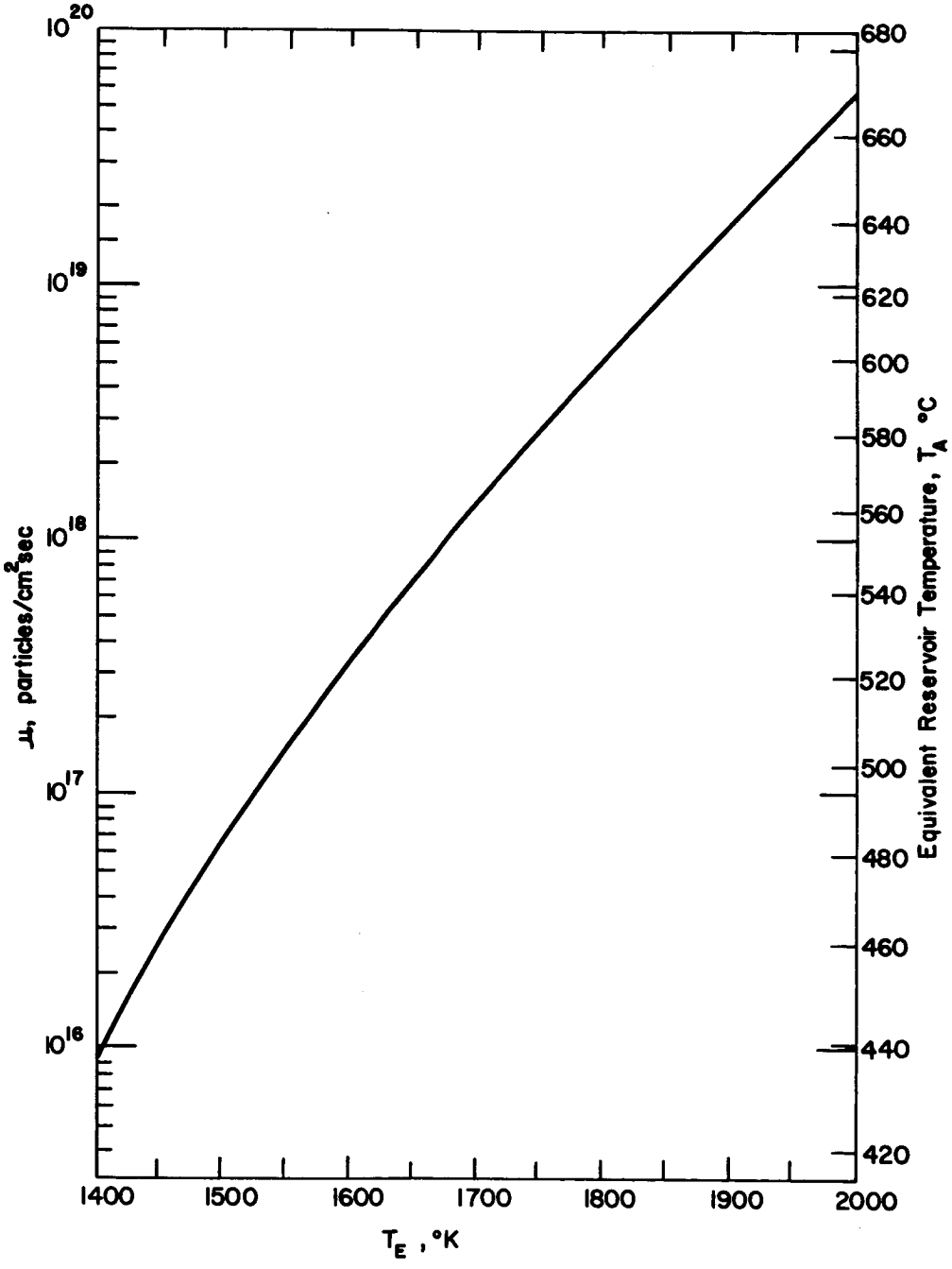

Figure V-19. CsF Arrival Rate Required to Maintain Half a Monolayer Coverage at a given Surface Temperature

3. Converter Studies. This study originated during the previous year and was continued into this year in the hope of performing more controlled experiments and finally extending the greatly enhanced short-term performance of CsF-additive converters to usefully long periods of operation. Initial tests examined the uncesiated work function characteristics of the tungsten emitter. These results were then correlated with the performance obtained when the device was cesiated. Our hopes were not realized in this test vehicle, but enough useful data were obtained to direct additional experiments which finally achieved the desired results.

a. Experimental Procedure. The test vehicle used in these runs was the research parametric converter described in Chapter III and incorporated a tungsten emitter opposite a molybdenum collector and guard. The metallurgical treatment of the emitter is described in Chapter IV. An additional reservoir similar to that for cesium was used to control the CsF vapor pressure in the device.

To minimize water absorption while the CsF pellets were being added, the test vehicle was flushed with dry argon through the cesium reservoir tubulation. Twelve CsF pellets totaling approximately 0.6 g were dropped into the reservoir, the sealed metal Cs capsule was inserted into its reservoir tubulation, and the tube was pinched off. Outgassing was accomplished through the additive tubulation in a manner similar to that used in other test vehicles. A one-liter-per-second ion pump was connected to the additive tubing and left pumping after preliminary outgassing.

In order to avoid any significant loss of CsF during outgassing, the reservoir was maintained at or below 200°C for most of the 24-hour period. For a total of three hours, the CsF was outgassed at 300°C. By following this

schedule we expected to achieve sufficient outgassing with a minimum loss of additive. A final pressure of about 3×10^{-7} torr was attained before leak-checking and pinching-off. The device was then mounted and set up for testing.

Emitter work function values are determined from saturated emission measurements, using the Richardson equation. The experimental task, then, consisted of obtaining current-voltage characteristics at known emitter temperatures. The instrumentation used for this task and described in Chapter III allows tracing of the current-voltage characteristic and plots the characteristic with an X-Y recorder. The saturation currents are then taken from these plots, and, together with the surface temperature, they furnish the data for calculations.

For emitter work function measurements, the collector and guard ring are kept quite cold, around 300°C for vacuum measurements and about 50°C above the additive reservoir temperature for additive work function measurements. The spacing is kept at a low value, 0.5-7 mils, and therefore it is necessary for the collector and emitter surfaces to have been parallelized prior to testing. The purpose of this is to avoid the presence of a negative space charge, which would result in an erroneous saturation current measurement. Procedures for parallelizing are described in Chapter III. The absence of space charge is ascertained by varying the spacing and observing that the saturation current remains virtually constant; that is:

$$\left.\frac{\partial J_s}{\partial d}\right| T_E = 0 \text{ as } d \to 0 \qquad (19)$$

where J_s is the saturation current, d, the spacing, and T_E the emitter temperature. Note that condition (19) does not necessarily hold true when Cs vapor is present, because of scattering. Once all the above conditions are fulfilled, J-V characteristics are traced at selected emitter temperatures.

b. Experimental Results. The saturation current values obtained from these tests have been plotted as a function of reciprocal emitter temperature. On such a plot work functions are associated with a set of roughly parallel diagonal straight lines. Any variation in work function with emitter temperature is shown when the data points cross these lines.

Before raising the additive reservoir temperature, the emitter was tested for bare work function. The values obtained are shown as +'s in Figure V-20. Initial readings were taken starting at a temperature of 1900°K and increasing to 2140°K. As the emitter was then cooled to 1830°K, additional readings were taken. For these runs the spacing was about 7 mils. From the plot it is seen that the initial values (4.85) were somewhat higher than would be expected for bare tungsten, but, as the above cycle was carried out, the values centered on 4.75 eV and remained there after cooling. It was believed that additive probably coated the emitter somewhat during outgassing and was finally driven off at the higher temperatures. The bare surface value then remained, even during the cooler portion of the test.

To verify that space-charge effects were not influencing the results, a variable-spacing run was taken at a T_E of 2090°K, the region where these effects become significant. Figure V-21 shows the J-V characteristics obtained. At less than 7 mils the effect becomes negligible, as shown by the fact that the saturation current does not vary with spacing.

To provide a better overall picture of the history of this diode (#5000), the time and temperature chart shown in Figures V-22 and V-23 was prepared. On this chart, electrode and reservoir temperatures and emitter operating hours are indicated. Cold time was not recorded, but its occurrence is indicated by arrows on the temperature lines. At the top of the figure, the measured work

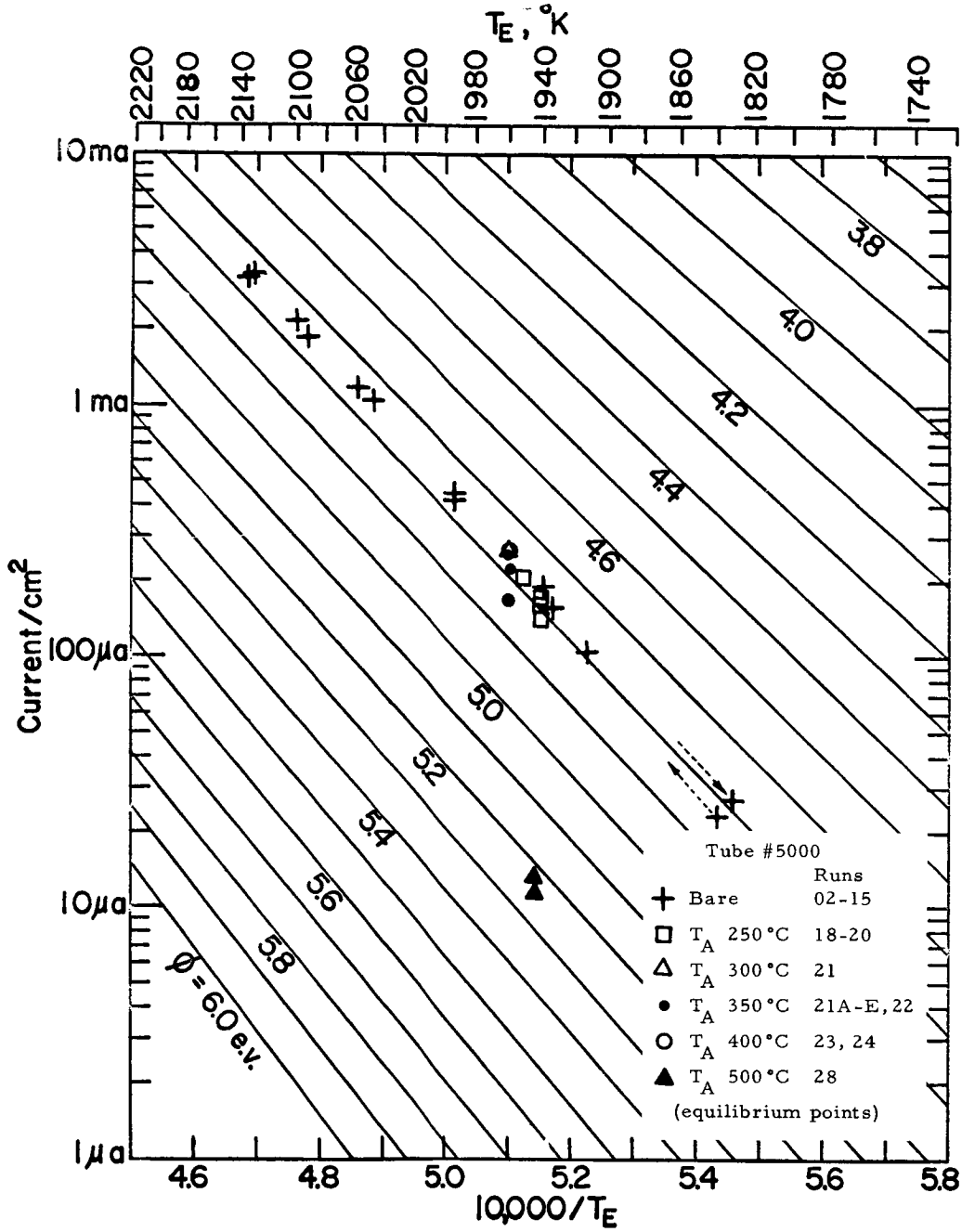

Figure V-20. Saturation Current vs Reciprocal Emitter Temperature for Bare Surface.

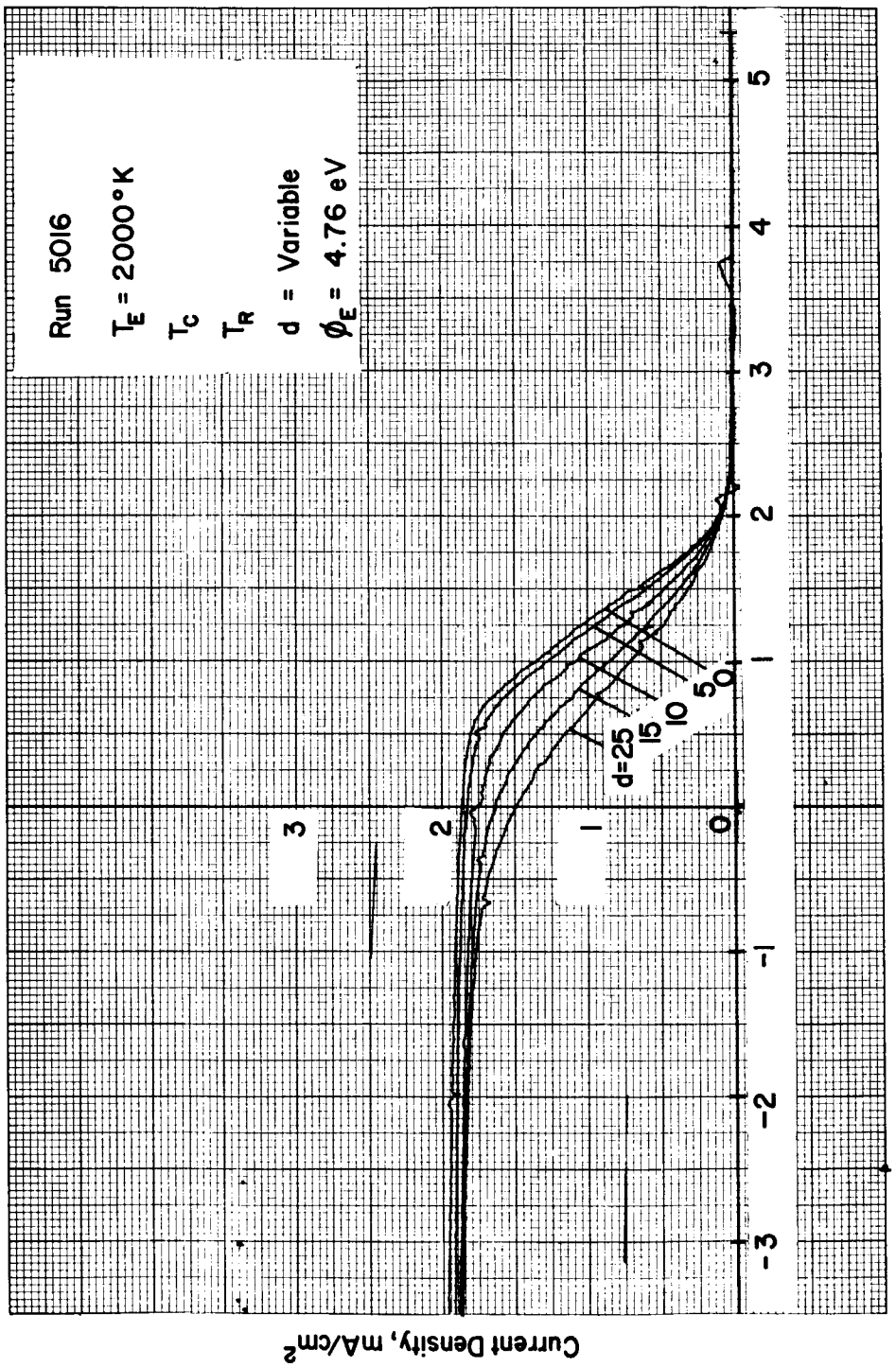

Figure V-21. Variable-Spacing, Current-Voltage Family.

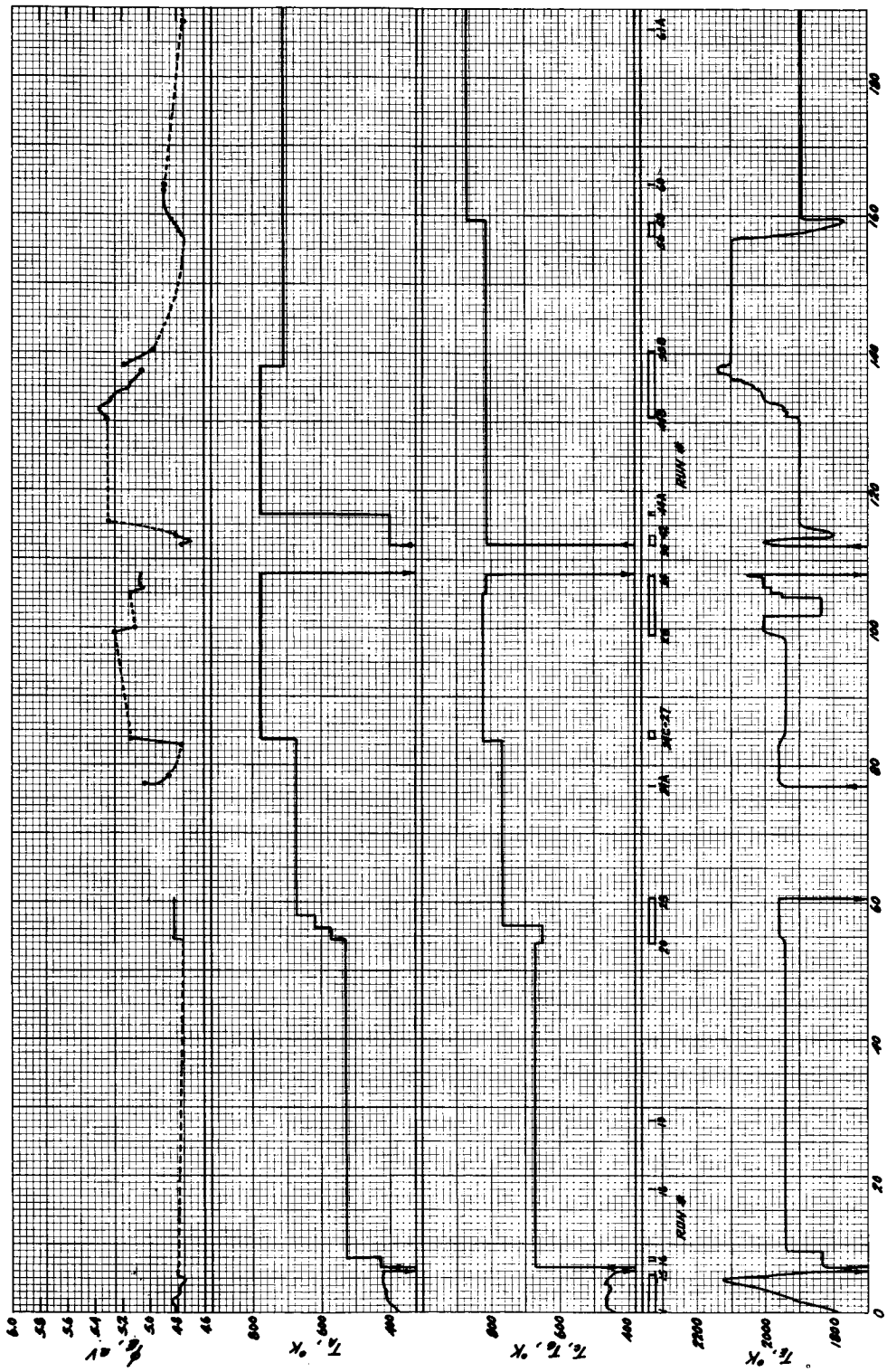

Figure V-22. Time and Temperature History of CsF Converter (500).

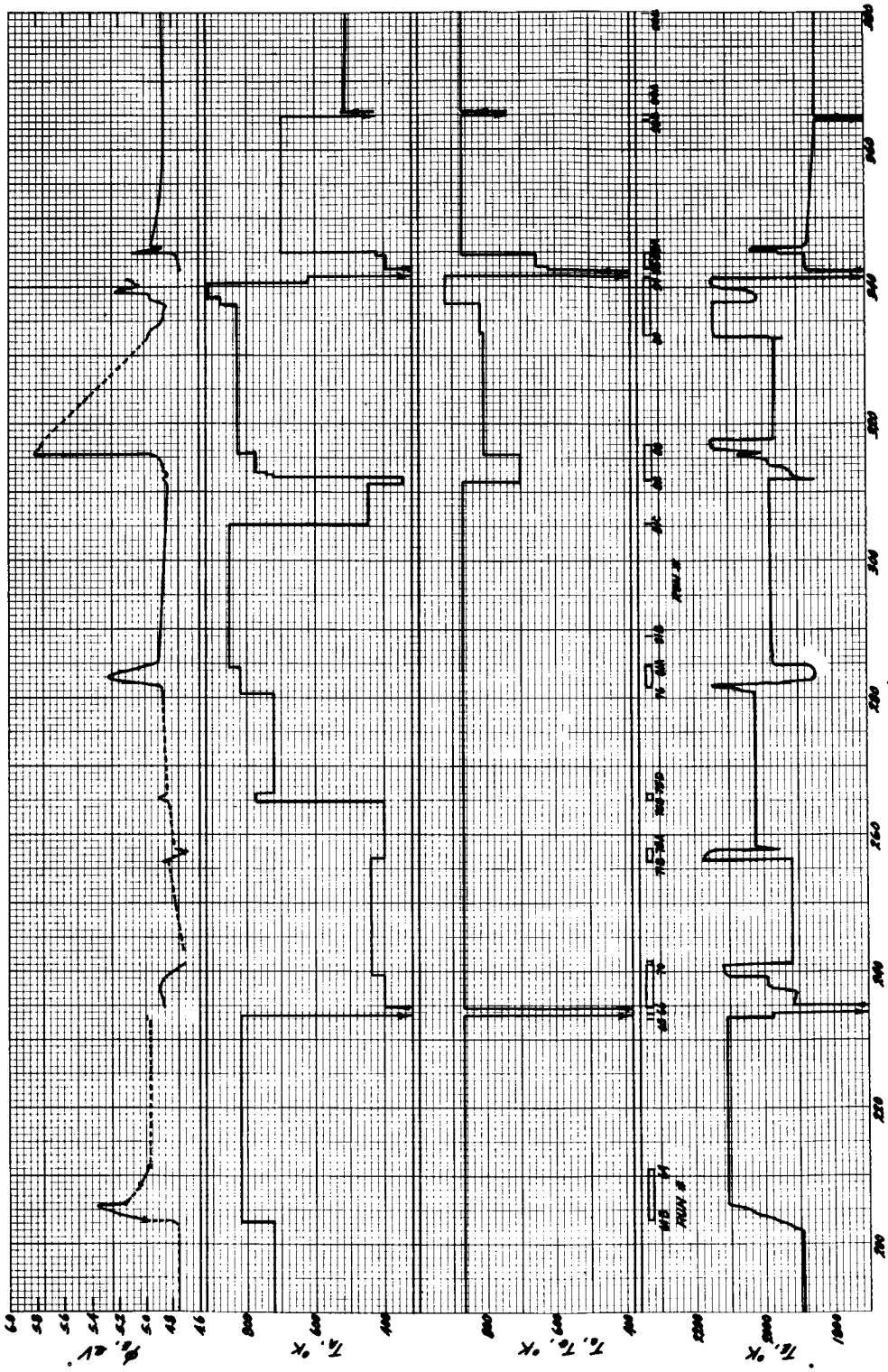

Figure V-23. Time and Temperature History of CsF Converter (500).

function is indicated by solid lines, and values at other times are approximated by the dotted lines.

The initial tests with low additive reservoir temperature, T_A, produced approximately bare tungsten work function values, as indicated, up to hour 6. The additive temperature was then increased in steps, allowing many hours of soaking at each level. Until hour 77, with a T_A of 670°K, the surface remained essentially at the bare value. At this time, a short-term effect was observed when the emitter temperature was rapidly increased. However, the bare value quickly returned, and it was not until a reservoir temperature of 770°K was reached that a long-term stable effect was obtained. It was then possible to cycle reproducibly between the bare value of about 4.75 eV at a T_A of less than 730°K and the somewhat T_E - dependent higher values of 5.2 to 5.4 eV at a T_A of 770°K. This cycling covered the period from hour 83 to hour 158. In preparation for the next step increase in additive temperature, the collectors were heated. An increased work function, which decayed back to the bare value after 25 hours, accompanied the T_C increase.

Upon raising T_A, a temporary work function increase was observed. However, after six hours the bare level was again approached, and this level remained stable until the tube was cooled down at hour 233. Figure V-24 shows the bare, high, and transient work functions observed. After the decay, at hour 210, the surface remained stable at near the bare work function value and only short transient effects could be obtained by raising T_A, by soaking with T_C lower than T_A and then raising T_C, or by raising T_A still further to 910°K. However, the original stable values which occurred at a T_A of 770°K could not be reproduced.

During the tests, a large back current, varying with additive reservoir temperature, was observed, and it is believed to be due to Cs^+ ions produced by

the dissociation of the CsF on the hot emitter surface. Using this current, the presence of CsF pressure may be inferred and compared with the expected arrival rate. A chart of reservoir temperature, arrival rate, pressure, and flow for CsF was prepared to facilitate these calculations, and it is shown in Figure V-25 and V-26. For many runs, however, the current was so large and the ions so massive that it was not possible to reach saturation. The current was thus space-charge-limited except at additive temperatures below 750°K. Figure V-27 shows an ion J-V characteristic with a saturation current of about 3 mA/cm^2, which corresponds to a T_A of 700°K. These observations confirmed the presence of CsF vapor in the converter even after the additive effect had disappeared.

One implication of the presence of the ion current is that the CsF is being broken down on the emitter surface and cesium is continuously being formed in the test vehicle. Cooling the emitter allows any such cesium to cover the surface, and the emitted current will then follow the characteristic Langmuir S-curve as the surface is heated. From the maximum and minimum points on the curve an effective reservoir temperature can be calculated. Figure V-28 shows one such curve with emitter temperature represented by time on the X axis. The calculated reservoir temperature for this plot was 340 to 360°K and corresponds to a pressure of 10^{-4} to 10^{-5} torr. Some cesium was evidently being consumed in the tube, since higher pressures were obtained immediately after heating the emitter, and lower ones after a cold period. Because of the high T_E/T_R ratio of about 6, the small amount of cesium should not significantly cover the emitter surface and could not account for the loss of CsF effect. Attempts were made to drive the cesium into its reservoir, but no change in behavior was observed.

Cesium was finally admitted to the test vehicle by cracking the metal capsule in its reservoir. Since the cesium pressure could then be controlled

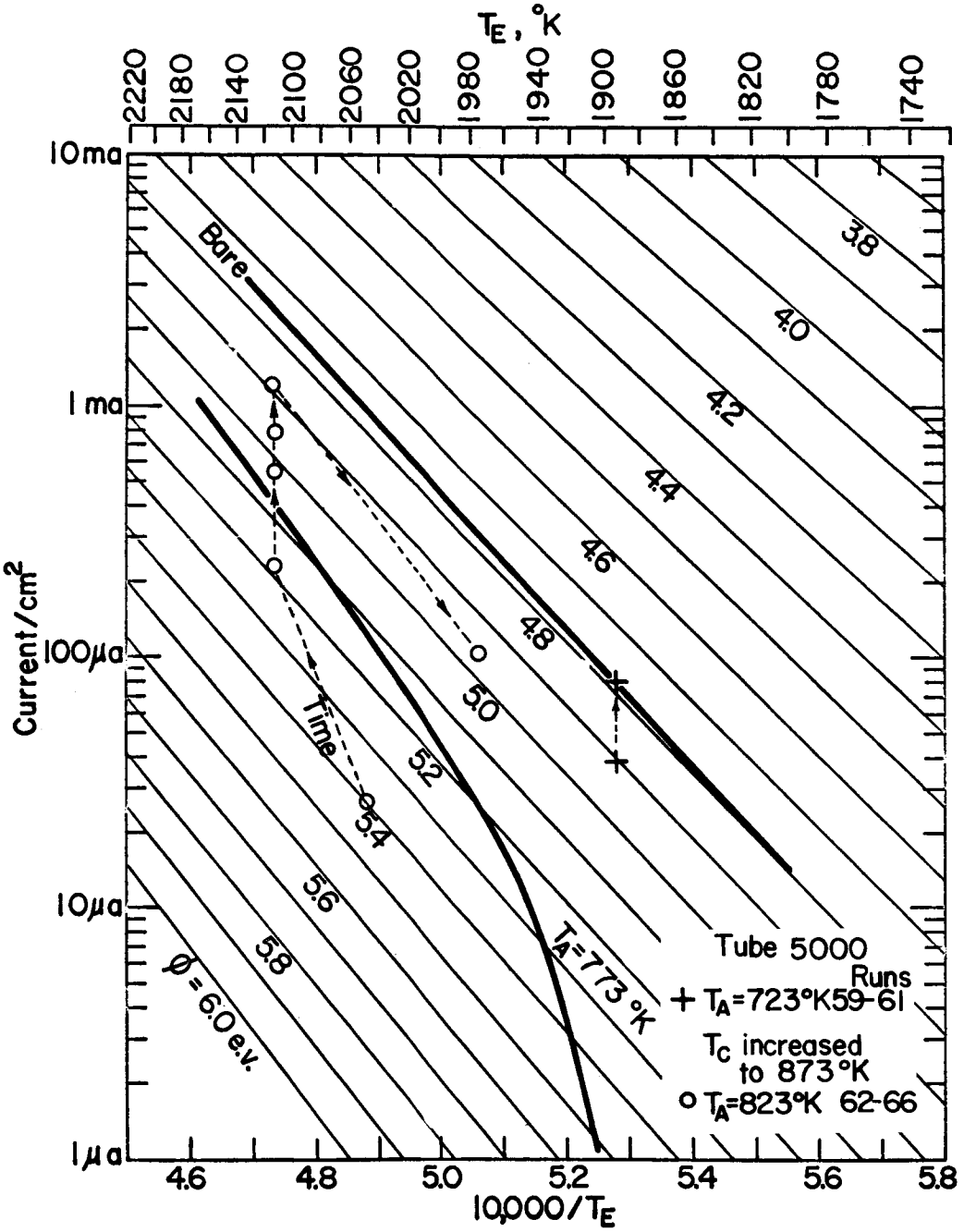

Figure V-24. CsF-Only Work Functions in Converter 5000.

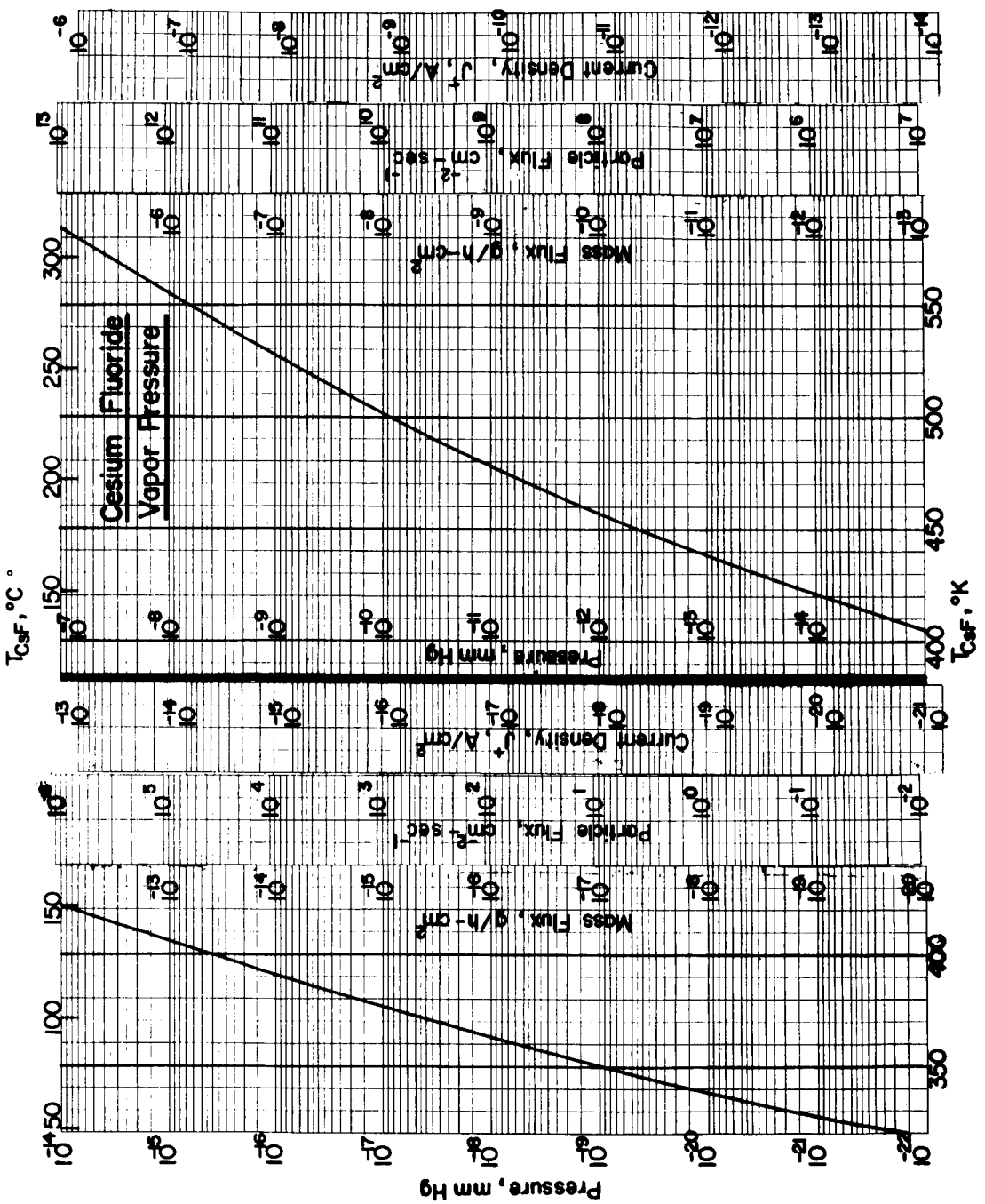

Figure V-25. CsF Arrival Rate as a Function of Temperature, Low Pressure Range.

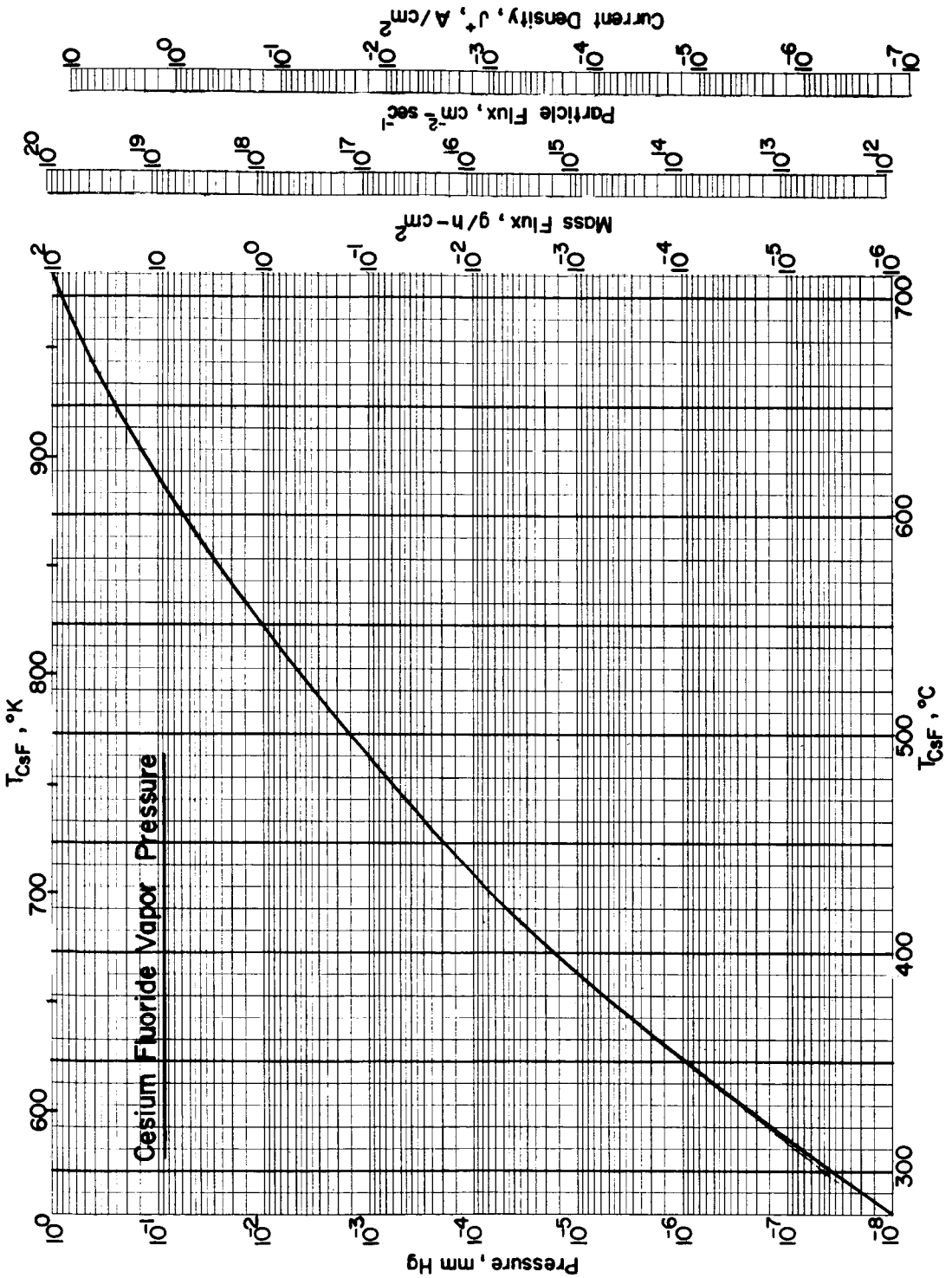

Figure V-26. CsF Arrival Rate as a Function of Temperature, High Pressure Range.

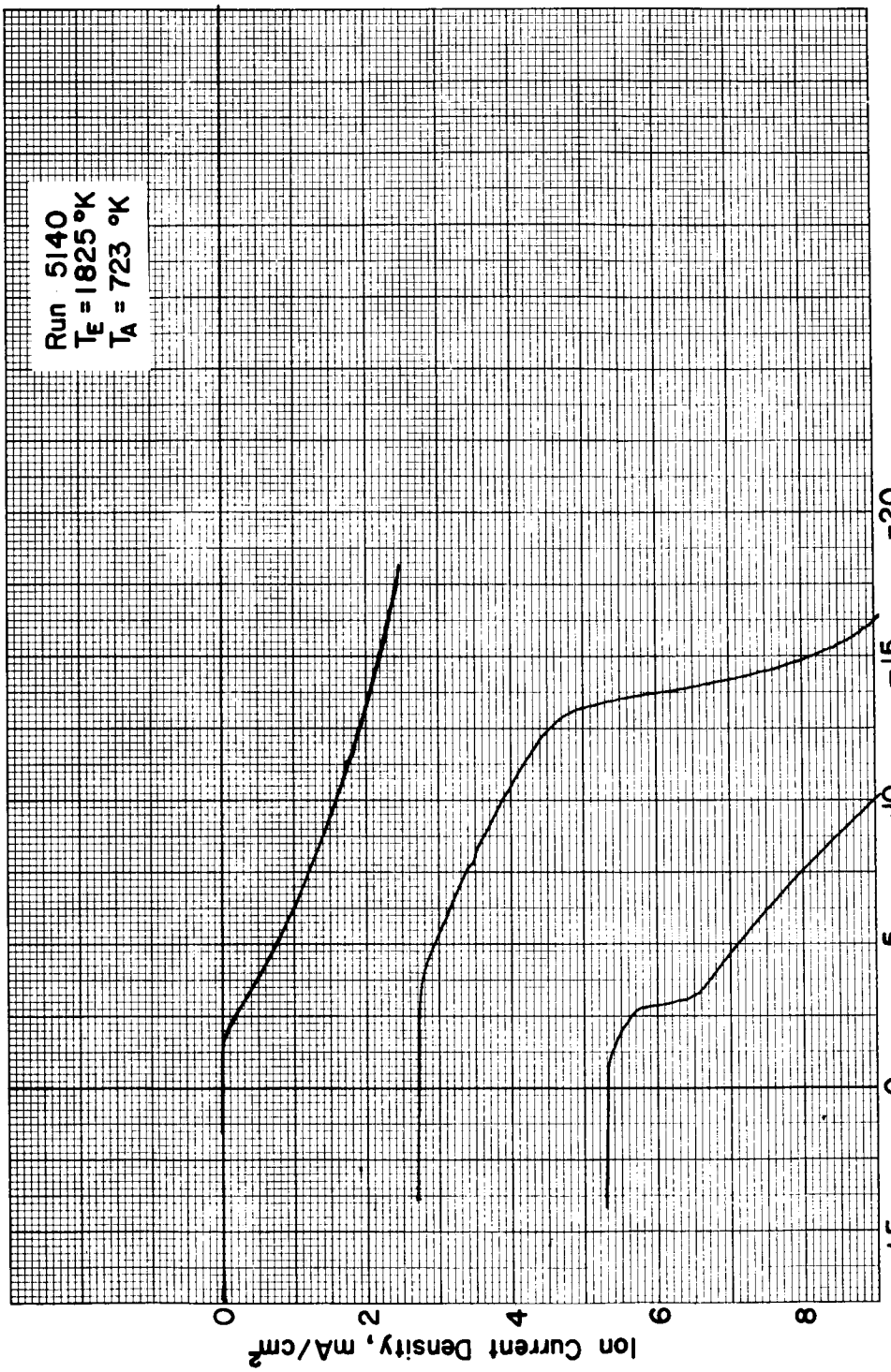

Figure V-27. Cs^+ Ion Current, Showing Space-Charge Limiting.

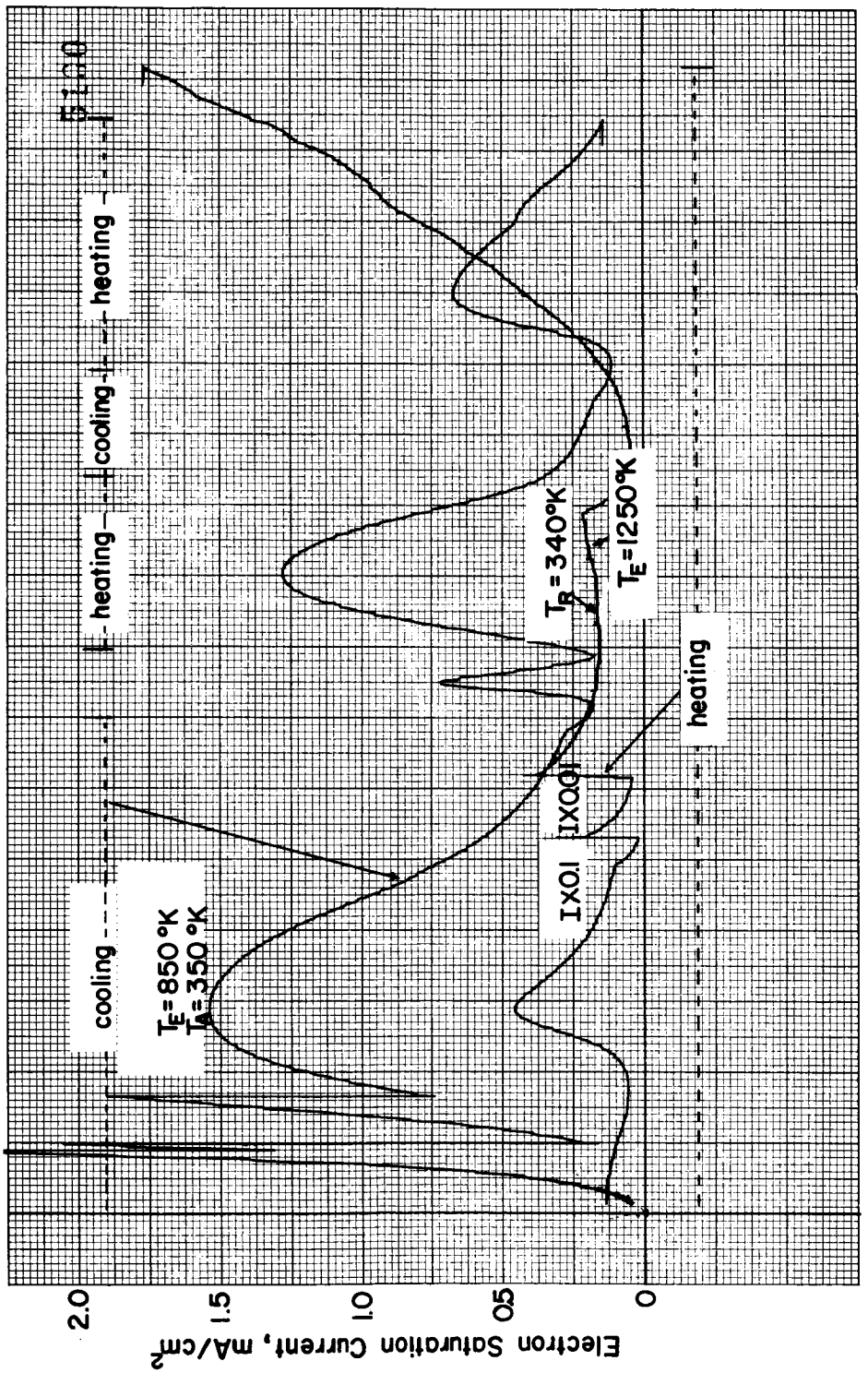

Figure V-28. Electron Current Peaks Due to Cs Coverage Changes with Heating and Cooling of the Emitter.

from its reservoir, any unexpected changes produced by the small amount of free Cs previously present could be eliminated. Work function values obtained are plotted versus T_E/T_R in Figure V-29 and show the "untreated tungsten" characteristic obtained in earlier work[2] with tube #1000 and tube #3000 after a period of testing. Loss of additive effect with CsF only in the converter directly corresponds to loss of additive effect when Cs is also present.

Autopsy and analysis of additive converters have shown on several occasions that, even after the additive has become inactive, the CsF is still present in the devices. In one case the pellets were still in their original form.

The results obtained from these converter studies can be summarized as follows:

1. There is an apparent threshold in additive effect; stable effects do not appear until a certain additive reservoir temperature is reached, usually about 700°K.
2. Only two stable work function levels have been observed, a "bare" one at about 4.8 eV and an "additive" one at about 5.3 to 5.5 eV.
3. When a high CsF reservoir temperature is used, the work function values soon decay to the bare level and a permanent degradation occurs.

After degradation:

1. CsF is still present in the device with a pressure responsive to its reservoir temperature
2. Conditions favoring abnormally high additive coverage, such as low emitter temperature or a sudden increase in collector temperature, produce a short transient increase in work function.

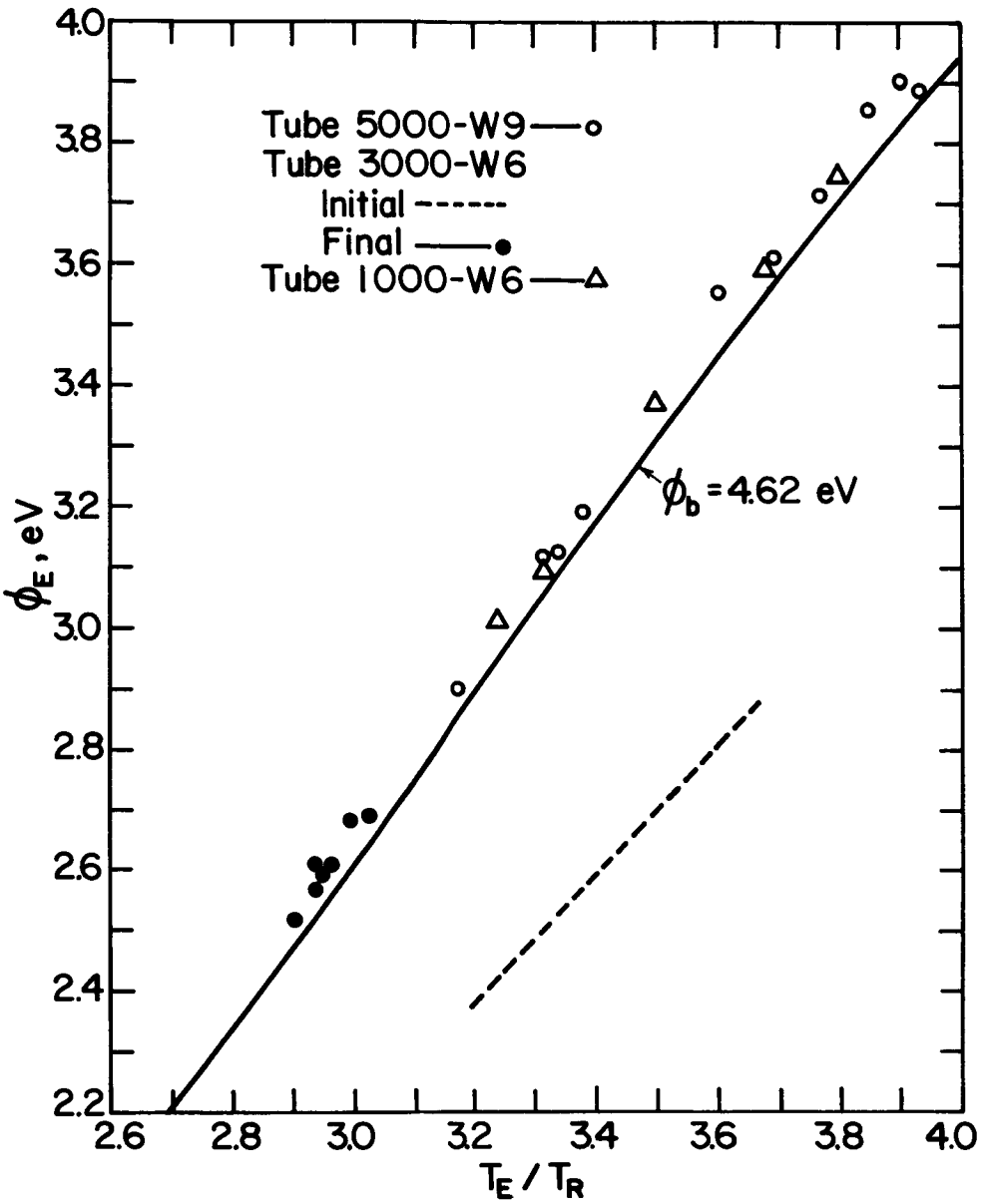

Figure V-29. Comparison of Cesiated ϕ for Various CsF Converters.

3. Very high additive reservoir temperatures do not produce significant changes in work function beyond a short transient.

Two possibilities for the loss of additive effect were proposed at this point: either a contaminating substance had been introduced along with the CsF pellets or else the test vehicle emitter had become "poisoned" and unresponsive to CsF vapor. As is now known, it was the water contamination contained in the fluoride which was responsible for the observed results. The effects to be expected from such water may be summarized as follows and compared with these actually observed:

1. Depending upon the fluoride outgassing time and temperature schedule, there will be a certain minimum reservoir temperature above which additional water will be given off.
2. Such water will act similarly to oxygen, and, since there is only a relatively narrow range of oxygen pressure (about an order of magnitude) between no effect and maximum change, the observed values should cluster about the bare level and a level 0.7 eV higher.
3. Because of the outgassing characteristics of the fluoride, even after the water has been gettered at a specific reservoir temperature, a further increase in temperature can cause additional outgassing of water, which will finally be consumed.
4. CsF vapor itself is relatively ineffective on the emitter surface and causes only a slight increase (0.3 eV) in work function even at close to a monolayer coverage.

Comparing the reservoir temperatures indicated in Figure V-19 with those actually used in the converter, it is found that, for the uncesiated runs where the emitter temperature had to be relatively high, there was insufficient additive pressure to maintain high coverages. When the devices were cesiated, however, the tests were performed at the lower emitter temperatures, where high coverages could occur. In Figure V-29, those work functions obtained after long periods of operation must have had significant coverage. The increased cesiated values obtained are apparently due to the effects of the CsF in the devices, but the actual mechanism responsible for the increase is not understood at this time.

4. Glass Tube Studies. At the time the converter experiments were completed the phenomena occurring were not understood. A series of glass-tube filament-emitter devices were constructed which facilitated testing of the various hypotheses. A brief description of the devices and the experiments performed is given below.

The glass tube design adopted consisted of an 0.005" tungsten-filament emitter mounted opposite a molybdenum-ribbon collector. CsF or other additives were placed in the glass envelope, and the pressure was regulated by controlling the envelope temperature. In effect, the tungsten "emitter" was located within the additive reservoir. The glass tube experiment was expected to eliminate the possibility of poor communication of the reservoir with the emitter surface and allos direct investigation of the possibilities of impurities and of chemical reactions of additives with the converter components. Figure V-30 shows a picture of a typical filament and collector assembly mounted on a glass press before being sealed into the envelope.

a. Experimental Procedure. The tube was outgassed by baking at 200 - 400°C in an oven and flashing the tungsten-filament emitter to 2400°K. After 5 to 6 hours of outgassing, the tube was pinched off and J-V curves generated at various emitter and wall or "reservoir" temperatures. The emitter temperature was measured with an optical pyrometer. A typical J-V curve is shown in Figure V-31. It should be noted that, due to the large spacing (about 0.060") and the fact that the filament was directly heated by dc current, about 10 volts had to be applied before the emitter current saturated. This type of heating resulted in a variation in potential along the filament length, and, since the voltage drop was about two volts, the exponential portion of the J-V curve was broadened by 2 volts. Neither of the above effects has any influence on the saturation current which is of interest here.

From the measured saturation currents, work function values were computed using the Richardson equation. The emitting area is a possible source of error. It was estimated by observing the filament pyrometrically and determining the length at high temperature. The area thus obtained was consistent with the emission current for bare tungsten. At any rate, an error of as much as 0.15 to 0.2 V was possible, and the absolute value of work function obtained should not be considered any more accurate than that. On the other hand, the relative values are self-consistent within much narrower limits.

b. Experimental Results. The first tests on tube #9000 were performed with a CsF additive at emitter temperatures from 2100°K to 2400°K and envelope temperatures from 310°K to 710°K. Figure V-32 is a plot of computed work function versus envelope temperature with an emitter temperature of 2140°K. A pronounced work function maximum is evident at about 450°K, in spite of the scatter of ± 0.1 eV in these measurements. The CsF

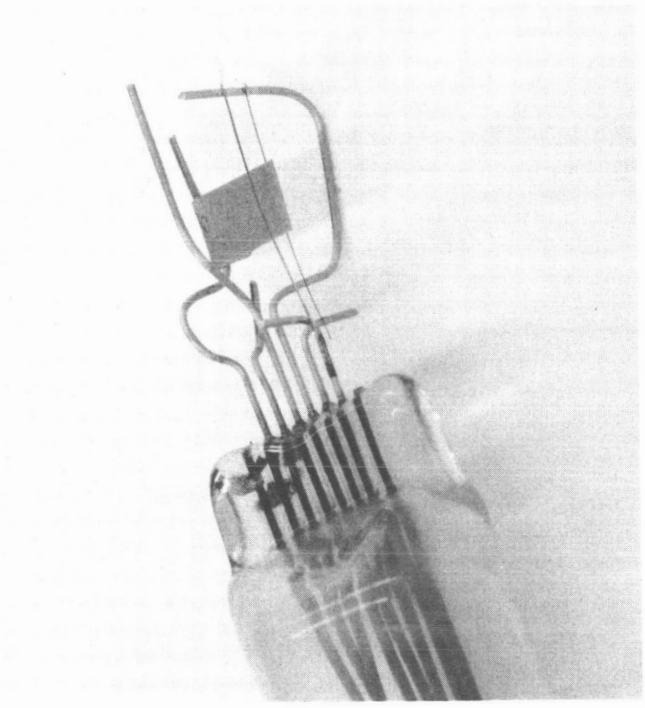

Figure V-30. Typical Glass-Tube Press with Electrodes.

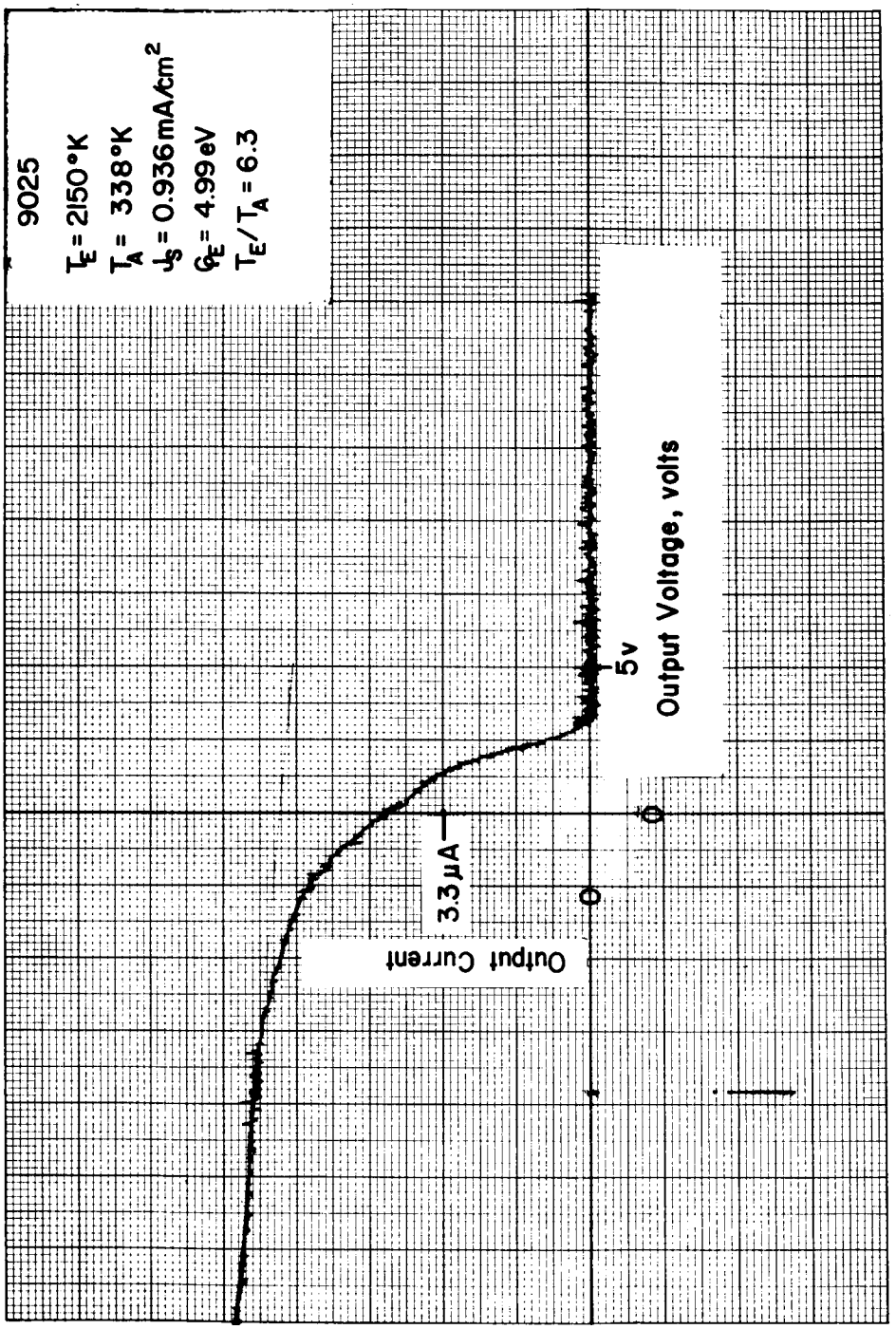

Figure V-31. Typical Glass-Tube J-V Characteristic.

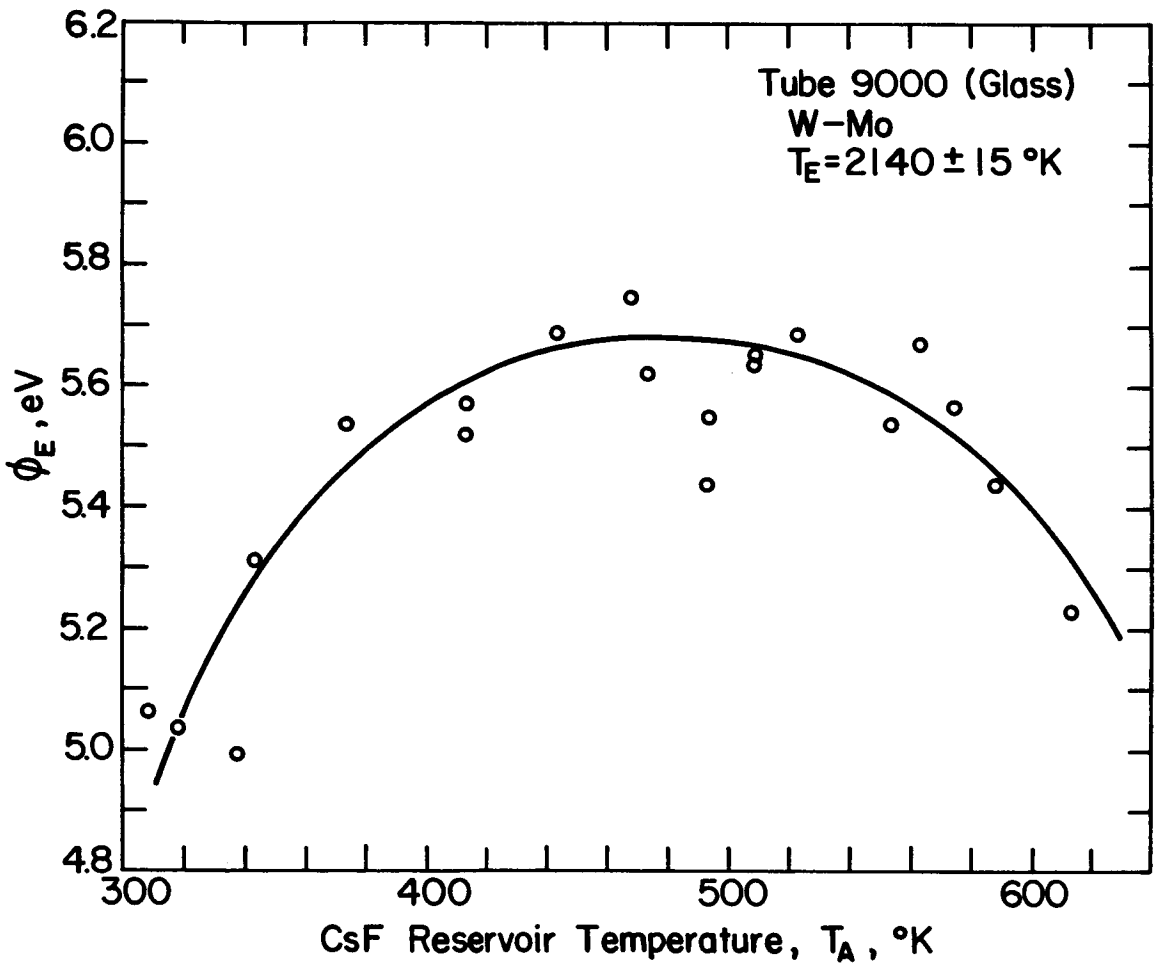

Figure V-32. Work Function Change Produced in CsF Glass Tube.

pressure corresponding to this temperature (obtained from Figure V-25) is less than 10^{-10} torr. This is a surprisingly low envelope temperature for an additive effect. Furthermore, the indication of an optimum temperature for maximum effect was unexpected.

At the higher envelope temperatures the filaments began to be attacked chemically and finally failed. The second tube (11000) produced similar results, and at the conclusion of these runs the glass envelope near the filament region was coated with a metallic deposit, apparently tungsten from the filaments. Considering the low filament temperatures (1800-2100°K) used, evaporation could not be a reasonable explanation, and some sort of chemical mass transport must have been taking place. Figure V-33 shows comparison micrographs of the filament from tube 9000 and of a filament evaporated at 2800°K in a vacuum. The definite pitting observed on the tube filament, as compared with the control in Figure V-33, shows that there must be processes other than evaporation taking place. The arrival rate curve of Figure V-25 shows that at the low temperatures (80 - 300°C) used, it is highly unlikely that the CsF could cause either the observed chemical attack or the pronounced work function shift.

The maximum possible rate of chemical attack on the filament is limited to the rate of formation of a monolayer; in the case of CsF at 300°C, the filament could lose a maximum of 15 monolayers per hour and it would take about 15×10^4 hours to eat through the filament, assuming a monolayer is of the order of 3Å thick. Furthermore, tungsten fluoride compounds break down at high temperatures to leave plain tungsten, and this system is, in fact, customarily used in the chemical vapor-deposition of tungsten.

It is reasonable to assume that a coverage which is at least 10% of a monolayer would be required to cause any work function change, and therefore

66-R-1-3

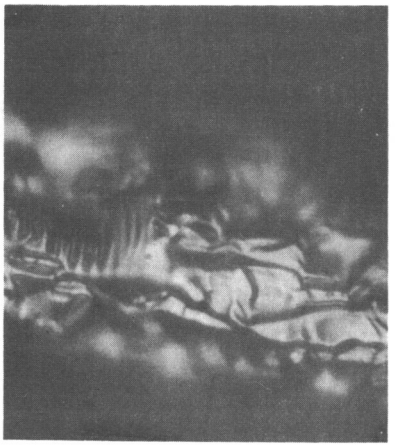

Figure V-33A. Micro-Photograph of Tungsten Filament Eroded in a Glass Tube.

66-R-1-4

Figure V-33B. Micro-Photograph of Tungsten Filament Eroded in a Glass Tube.

66-R-1-5

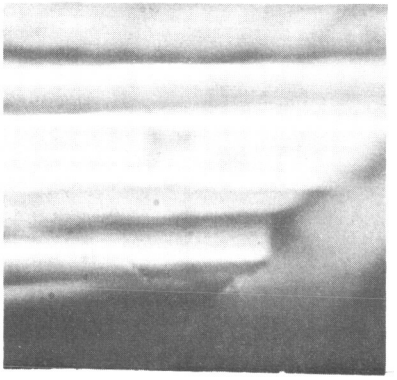

Figure V-33C. Micro-Photograph of Tungsten Filament Operated at High Temperature in Vacuum.

the CsF cannot be responsible for the observed work function change occurring at low envelope temperature. For example, at 300°C the CsF arrival rate is about 4×10^{12} particles/cm^2 sec, and at this rate it would take 2.5×10^2 sec to form a monolayer consisting of 10^{15} atoms/cm^2. At 80°C, with the arrival rate of 10 particles/cm^2 sec, a monolayer would never form during the experiment. In view of the above considerations, the thinning of the filament and the low-envelope-temperature work function changes are almost certainly due to impurities present either in the glass bulbs or the CsF crystals.

Table V-1 summarizes the glass tube results. In the first column are shown the tube number, filament material and relative length, and type of additive. Outgassing temperature and time for the envelope and additive are indicated, in some cases with the ultimate pressure at the pump. Note that this is not the tube pressure because of the tubulation conductance. The bare ϕ values are indicated where data could be taken; in several devices a stable bare value could not be obtained until after the envelope temperature (T_A) was raised. Apparently a layer of impurities was being stripped from the filaments. In each of the normally outgassed devices the maximum work function change observed was of the order of 0.7 eV. The specially dried fluoride sample showed a smaller $\Delta\phi_{max}$.

All the devices failed due to tungsten deposits on the walls, making observation of the filament temperatures impossible. Rapid chemical attack also prevented testing with the rhenium filaments.

These results are again consistent with the presence of large amounts of water vapor in the devices. Dissociation of the water at the hot filament to form tungsten oxide and hydrogen is thermodynamically favorable, and the volatile oxide will then reach the cold walls, where it will be reduced by the hydrogen. In this way, a small amount of water can transport a large quantity

TABLE V-1

GLASS TUBE EXPERIMENTS AT TEECO

Tube # Emitter Material Charge	Outgassing Glass T, t Charge T, t	Experimental Work Function Results	Maximum Work Function Change Observed	Mode of Failure Remarks
9000 W, short filament CsF	400°C 3 hrs 400°C 3 hrs (in envelope)	ϕ bare $\approx$ 5.0 eV ϕ max $\approx$ 5.7 eV at 195°C ϕ vs T_A shows max.	~ 0.7 eV	Fil. disappeared rapidly at 300°C. Visible W deposits on glass. Photo of fil. Fig. V-33 A, B
11,000 W, long filament CsF	400°C 3 hrs	ϕ bare $\approx$ 4.8 eV $\phi_{max} \approx$ 5.4 eV at T_A 80 - 200°C	~ 0.7 eV	Fil. disappeared rapidly at 300°C. W deposit on glass.
12,000 Re, W, long filament CsI	300°C 3 hrs. 300°C 3 hrs (in tubulation) 3×10^{-6} ultimate	Bare difficult to obtain $\approx$ 5.2 eV at start. Later 4.7 eV $\phi_{max} \approx$ 5.4 at T_A 150°C	~ 0.7 eV	Fil. disappeared at 350°C. Re not used. Highly contaminated. Bare ϕ_e stabilized only after envelope was cycled to 200°C with 1600°C T_E.
13,000 Re, W, long filament Control	300°C 3 hrs 3×10^{-6} ultimate	Like 12,000, $\phi_{bare} \approx$ 4.7eV $\phi_{max} \approx$ 5.4 eV at T_A 100°C	~ 0.7 eV	Stopped for re-outgas. Fil. started to disappear.
14,000 Re, W, long filament CsF Special Drying	400°C 100 hrs 1×10^{-6} ultimate 500°C 1 hr 600°C min.	$\phi_{bare} \approx$ 4.75 eV $\phi_{max} \approx$ 5.0 eV at 240°C T_A With $T_A \approx$ 240°C Re filament was heated	~ 0.25 eV	W glass deposit. Best control, slow coating of glass. Least effect on ϕ. Re fil. rapidly attacked
15,000 Re, W, long filament Control	400°C 100 hrs. 5×10^{-7} 300°C 50 hrs. 5×10^{-7}	Unstable		W fil. attacked Unstable ϕ_E with slow drifting.

THERMO ELECTRON ENGINEERING CORPORATION

of tungsten. This is the water cycle described by Langmuir.[18] The same oxygen is also available as an additive and fully accounts for all of the effects observed. For instance, the $\Delta\phi_{max}$ of 0.7 eV is typical of data obtained with oxygen under these conditions, while at these low envelope temperatures, fluoride or iodide cannot be expected to have any effect.

This evidence, together with that from the outgassing study, leads to the conclusion that all of the CsF results obtained were in fact due to contaminants introduced along with the fluoride. It was then obvious that the best approach would be to initiate a new investigation which could take advantage of the very persistent effects of oxygen. This program is described in the next section. Simultaneously the CsF study previously described was begun and finally carried to a successful conclusion.

D. Oxygen Surface Additive

1. General. The preceding discussion has presented experimental evidense that the short-lived high converter performance previously attributed to cesium fluoride was, in fact, due to oxygen contained in the form of water in the CsF crystals. Pure CsF has been shown to be much less effective than O_2 in altering the work function of tungsten and holds little promise as a surface additive. These considerations prompted a re-evaluation of oxygen as an electronegative surface additive, with the objective of exploiting its desirable characteristics for indefinite periods of time, avoiding, of course, any deleterious effects.

2. Oxygen Adsorption Constants. The ability of adsorbed oxygen films to raise the work function of tungsten and also render cesium more effective in subsequently lowering it, was first reported by Kingdon[19] in 1924. Since then several communications have appeared in the literature regarding experiments

in which the work-function change and adsorption constants for oxygen on tungsten were measured. By 1935, two new methods of experimental study of oxygen films had been reported. Roberts[13] used the accommodation coefficient of neon on tungsten filaments to detect the presence of oxygen, and Johnson and Vick[20] used an oscillograph to measure the time constants of O_2 desorption. Langmuir and Villars,[3] in 1931, also published their results with O_2 and Cs, which they regarded as a method of detecting oxygen at extremely low partial pressures. The phenomenon was the subject of considerable controversy at the time, as is evident in A. L. Reimann's[21] communication presenting his own work and attacking Kingdon's inclusion of the temperature dependence of work function in the pre-exponential constant. Progressively more sophisticated studies of the adsorption and diffusion of oxygen on tungsten were performed using the accommodation coefficient technique, developed by Roberts, and field emission, first applied by Müller[22]. Both approaches have been very effective in defining the physics of the system in the temperature range of 4.2 to 700°K. The first significant experimental advance at thermionic emitter temperatures (above 500°K) since the work of Langmuir, Johnson and Vick, and Reimann, however, is that reported by Engelmaier and Stickney.[11] These investigators have measured adsorption energy values and work-function changes under various conditions of coverage. A summary of their data is shown in Table V-2. Inspection of Table V-2 shows that the maximum reported work function change caused by adsorbed oxygen varies between 0.7 and 0.95 eV. Larger differences, as much as 1.8 eV, have been reported by Reimann and Gomer and Hulm.[23] Reimann used contact-potential measurements, while Gomer used field emission; in both cases, the emitter temperatures were very low, less than 700°K. It is doubtful that these low-temperature measurements are applicable to emission at thermionic temperatures because there is reason to believe that the character of the adsorbed oxygen film is greatly altered when the temperature is increased.

The desorption energy values listed in Table V-2 vary from 140 to 160 k cal/gram-atom of O_2 and are in good agreement with one another. The most extensive and well-controlled study is that of Engelmaier, who measured both work function and desorption energy as a function of oxygen pressure and surface temperature. For the remainder of this discussion the 140 k cal/gram-atom value of desorption energy will be used. Figure V-3 is a plot of the oxygen pressure required to maintain full coverage at different emitter temperatures and is based on this value of desorption energy.

3. Chemical Equilibrium. In the preceding sections experimental and theoretical evidence was used to estimate an upper limit for the oxygen pressure required to achieve an "additive effect" on a tungsten emitter. It is the objective of this section to examine whether this oxygen pressure can be compatible with the materials and operating conditions of the converter.

In general, metals react with oxygen to form oxides in accordance with the following reaction:

$$x\ O_2 + yM \rightarrow M_y\ O_{2x}\ . \tag{20}$$

A free energy change is associated with the reaction usually referred to as the free energy of formation of the metal oxide. The free energy of formation, ΔF, is a function of temperature and is related to the equilibrium constant, K, of the reaction by:

$$-\Delta F = RT\ \ell n K, \tag{21}$$

where R is the gas constant and T is the temperature of the system. Assuming that the oxygen pressure is low enough so that the perfect gas laws apply and that the metal and its oxide are solids, the equilibrium constant can be expressed

TABLE V-2

SUMMARY OF DATA ON OXYGEN ADSORPTION

Reference	$\Delta\phi_{max}$	E_o	Type of Measurement
Langmuir, Kingdon Phys. Rev. 34, 129 (1929)	0.8 eV (at T > 1500°K)	–	Emission and Contact Potential
Langmuir Ind. & Eng. Chem. 22, 4, 390 (1930)	–	160 $\frac{k\ cal}{gr\ atom}$	Emission transient
M. C. Johnson F. A. Vick J. Am. Ch. S. 53, 486 (1931)	–	147 $\frac{k\ cal}{gr\ atom}$	Emission transient
J. K. Roberts Proc. Roy. Soc. A154, 464 (1935)	–	140 $\frac{k\ cal}{gr\ atom}$	Accommodation coefficient of Neon
A. L. Reimann Phil. Mag. 20, 594 (1935)	0.7 eV (at T > 1500)	–	Contact Potential
Engelmaier & Stickney Phys. El. Conf. Proceedings, 1966, Mass. Inst. Tech.	0.95 eV (at T > 1500)	140 $\frac{k\ cal}{gr\ atom}$	Emission

in terms of the oxygen pressure and the activities, α, of the solid phases.

$$K = \frac{\alpha_{MyO_{2x}}}{\alpha_M^y \cdot P_{O_2}^x} \tag{22}$$

Since the activity coefficients are equal to unity for the system considered here, we may write

$$K = \frac{1}{P_{O_2}^x} \quad . \tag{23}$$

In the case of the cesium-oxygen equilibrium where the metal exists in the gaseous state, the reaction is:

$$4\,Cs + O_2 \rightarrow 2\,Cs_2O \tag{24}$$

and

$$K = \frac{1}{P_{Cs}^4 \, P_{O_2}} \tag{25}$$

It follows, then, that the equilibrium pressure of oxygen above a metal oxide is fixed, at any given temperature. If the oxygen pressure is increased above this equilibrium value, the chemical reaction (20) will proceed to the right, i. e., more oxide will be formed until one of two things happen: either the oxygen pressure is reduced to the equilibrium value, or all the free metal is consumed in the formation of oxide. If the oxygen pressure is maintained below the equilibrium value all the oxide will decompose. It is possible, then, to maintain a metal in an oxygen atmosphere at any temperature without any oxidation taking place if the oxygen pressure is less than the equilibrium pressure above the oxide.

The equilibrium pressure of oxygen above Cs_2O, Cu_2O, MoO_3, MoO_2, and WO_3 was computed as a function temperature using the relations outlined above and free energy of formation data from Ref. 24. In the case of Cs_2O a cesium reservoir temperature of 400°C was assumed. The results are plotted in Figure V-34 in terms of pressure versus temperature. A line labeled "oxygen pressure" is also shown in this figure. This line is a plot of the oxygen pressure required for substantial coverage on the emitter surface, shown in Figure V-3. For example, at an emitter temperature of 1900°K the oxygen pressure required is 5×10^{-8} torr, which is well below the pressure of O_2 in equilibrium with WO_3, so no tungsten oxide will form. MoO_3 will not form at temperatures higher than 1200°K, Cu_2O at temperatures higher than 980°K, and Cs_2O at temperatures higher than 900°K. The 1200°K limit is higher than the ordinary operating temperatures of molybdenum collectors. It is, however, close enough to normal collector operating temperature so that it is not at all clear that it can be considered a limiting factor on the basis of this rough calculation. A more significant oxide is MoO_2 which has a pressure several orders of magnitude below that of MoO_3. This reaction may easily take place at these temperatures and will be limited only by the reaction rates. Protection of the collector surfaces may be necessary to preserve the thermionic character of the surfaces. Actual corrosion of the material is not expected because of the low oxygen arrival rate.

The cesium reservoir and other cold areas of the converter will certainly constitute sinks for oxygen. To use oxygen as an additive, it is therefore necessary to introduce it directly into the interelectrode space continuously and thus provide for the sustained loss through the gap at the emitter and collector edges. The amount of oxygen lost in this manner can be estimated by

$$G = 5.83 \times 10^{-2} P \sqrt{\frac{M}{T}} A t, \qquad (26)$$

where G is the total mass in grams that flows through area A at pressure P and temperature T in time t, and M is the molecular weight of oxygen. Assuming:

$P = 10^{-6}$ torr

$A = 7.83 \times 10^{-2}$ cm^2 (2 cm diameter emitter - 0.005" gap)

$T = 1000°K$

$t = 3.6 \times 10^{7}$ sec (10,000 hours)

we find that 32 mg of oxygen will be consumed, a very small quantity indeed.

4. Critical Experiment. On the basis of the above discussion, an experiment was devised to determine whether this reasoning was correct. For the results of such an experiment to be conclusive, a true steady-state condition had to be established; i.e., the addition of oxygen could not be a batch addition, the effect of which would then decay over a period of time.* To provide the necessary oxygen in the range of 10^{-8} to 10^{-6} torr continuously and in a controllable fashion, it was decided to use an oxygen compound which would release oxygen at the proper pressure by reversible decomposition when heated to the appropriate temperature. Cesium oxide was selected because it satisfies these requirements, but, in addition, it permitted the use of an existing converter by oxidizing part of its cesium. A converter equipped with a connection to a gas injection system was selected. The cesium was first condensed in the vicinity of the collector and, with the converter at room temperature, 50 mg of oxygen was introduced and was consumed immediately in oxidizing the cesium. The Cs_2O formed served as the source of O_2. Emitter work function measurements were made with Cs and Cs_2O, and the values obtained duplicated previous "CsF" results (see Figure V-35). Performance data were generated subsequently, and a summary

*All previous work cited above, as well as power production experiments by Wilson[25] and Levine[26], used a time transient approach, although the time constant was long in some experiments.

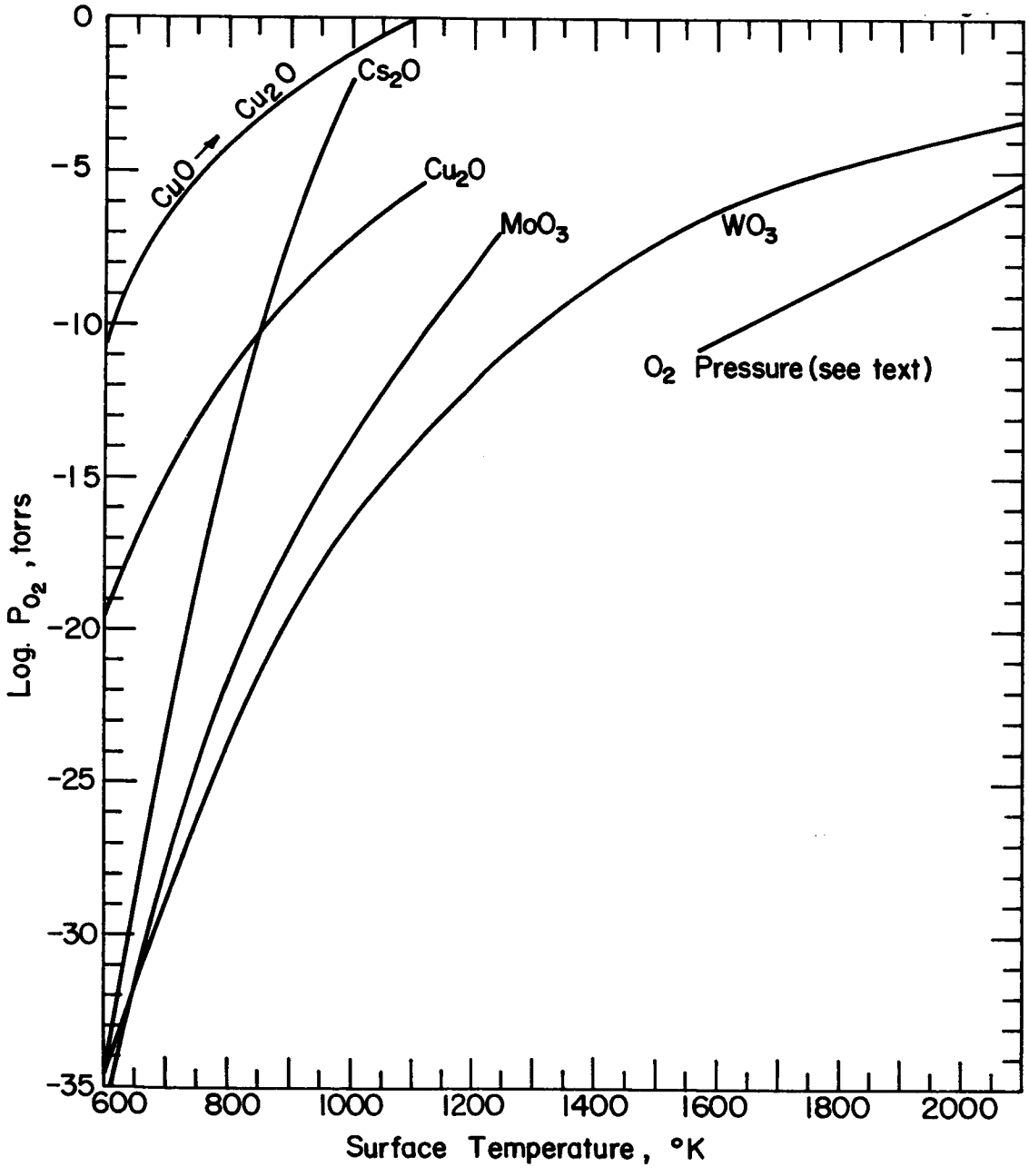

Figure V-34. Oxygen Pressure in Equilibrium with Various Metal Oxides as a Function of Temperature.

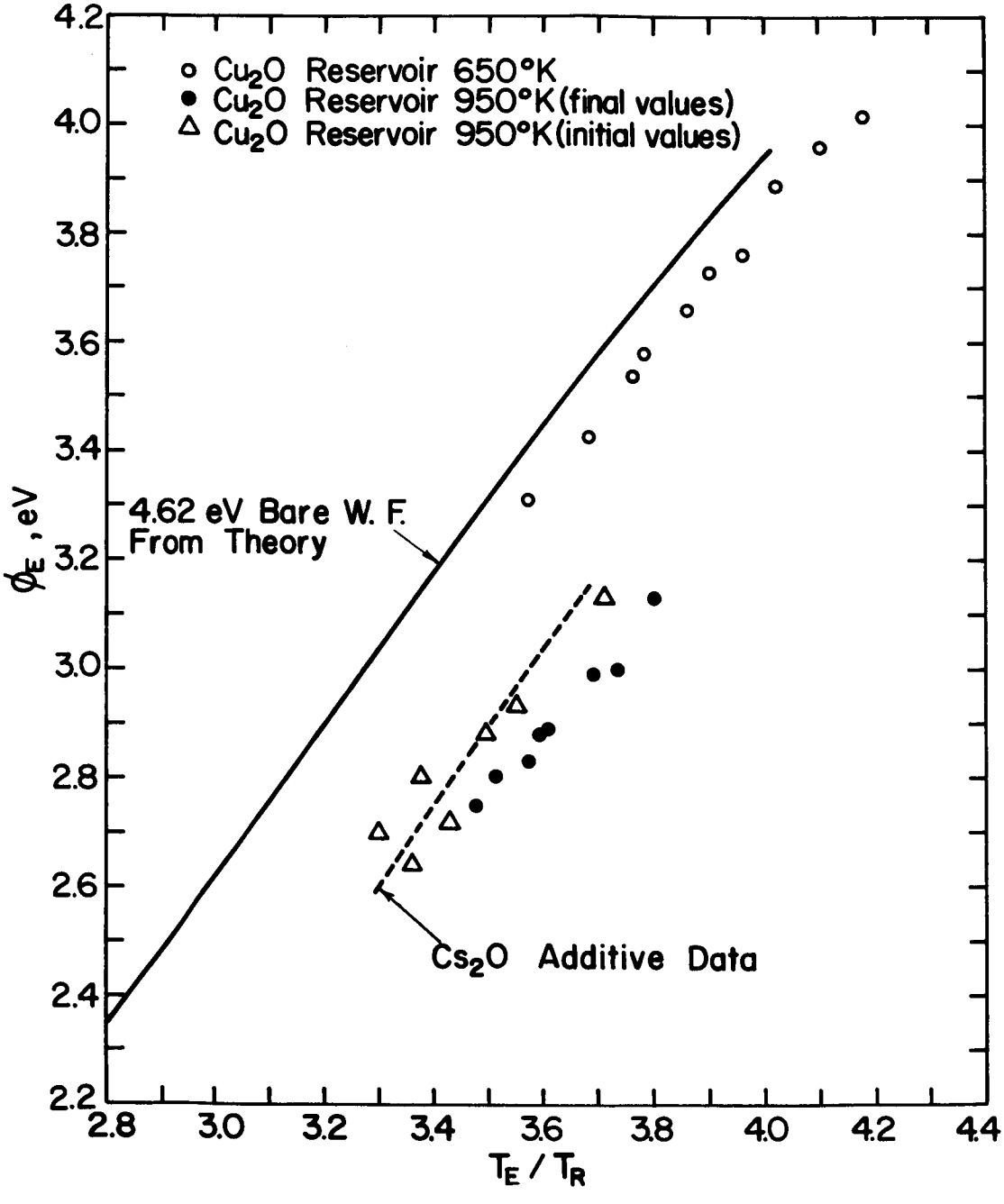

Figure V-35. Cesiated-Surface Work Function vs T/T_R in the Presence of Cs_2O and Cu_2O.

of these results is shown in Figure V-36. The two envelopes in this figure, for Cs and for Cs plus Cs_2O, show the typical increase in power output caused by the additive. Once the performance superiority of the converter was established, the device was placed on a short life test for 130 hours as a check of stability. No changes in the output of the converter were observed except for apparently random fluctuations of ±5%. After one week of life test, the converter was dismantled and examined for evidence of chemical attack on the electrode surfaces; none was found.

Almost all the hypotheses regarding the use of oxygen advanced above were confirmed by these results, giving strong indications that oxygen could be used as a surface additive on a steady-state basis.

5. Oxygen-Additive Test Vehicle. The success of the critical experiment lead to the construction of a special converter equipped with an additive reservoir located below the collector. A tube through the center of the collector connected the additive reservoir to the interelectrode gap. This arrangement allows oxygen from this reservoir to flow to the interelectrode space without coming in contact with any cold surfaces. Figure V-37 is a sketch of the device.

Oxygen was supplied by the decomposition of Cs_2O in the critical experiment. In that instance this approach proved satisfactory, but it does suffer from the limitation that the vapor pressure of O_2 in equilibrium with Cs_2O is a very strong function of temperature. Inspection of Figure V-34 will show that the pressure curve for Cs_2O is the steepest in the group. Cu_2O, on the other hand, shows a much less steep slope; O_2 pressure increases an order of magnitude every 60°K. Cu_2O is therefore a much more suitable compound for our purpose. It does not evaporate as a molecule at useful temperatures, but

decomposes instead, which is, of course, a basic requirement of any O_2 source.

The copper, cupric oxide, cuprous oxide, oxygen system is fairly complex, involving equilibriums between the various components. The reactions were extensively studied by Roberts and Smyth[27] who found two fundamental equations important for the system:

$$2\ CuO(s) \rightleftarrows Cu_2O(s) + \tfrac{1}{2}\ O_2(g) - 2\ \Delta H\ CuO \qquad (27)$$

$$Cu_2O(s) \rightleftarrows Cu(s) + \tfrac{1}{2}\ O_2(g) - \Delta H\ Cu_2O \qquad (28)$$

where ΔH is positive for dissociation.

The dissociation pressures for these reactions were calculated as described earlier and were plotted as a function of temperature in Figure V-34. Oxygen resulting from dissociation according to relation (27) will be at too high a pressure to be compatible with diode operation. Any cupric oxide (CuO) present in the converter must be broken down to cuprous oxide before the electrode surfaces are heated. This may be accomplished during outgassing by raising the additive reservoir temperature while maintaining the partial pressure of O_2 low enough to allow the CuO to dissociate.

At temperatures below 375°C there is some evidence that the cuprous oxide slowly breaks up according to the equation:

$$Cu_2O \rightleftarrows CuO + Cu \qquad (29)$$

If appreciable CuO is formed, difficulties with excessive O_2 pressure will arise when the reservoir is again heated and the CuO breaks down. This reaction may be limited by moving through the temperature range from 25°C to 400°C rapidly.

The new converter was charged with a Cu_2O pellet and cesium. Testing was started with a series of emitter work function determinations. Emitter work

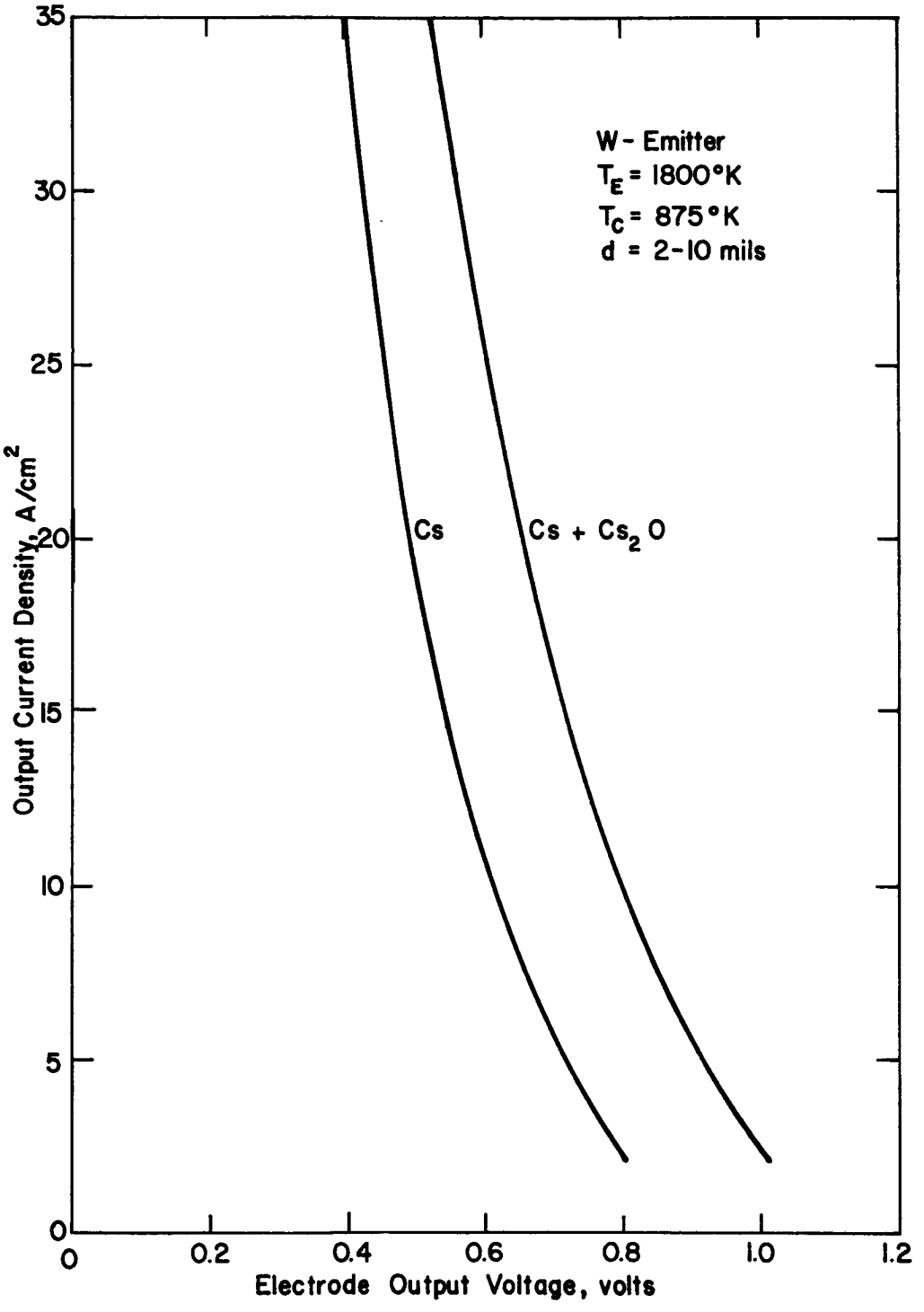

Figure V-36. Performance Envelope with Cs_2O and Cesium.

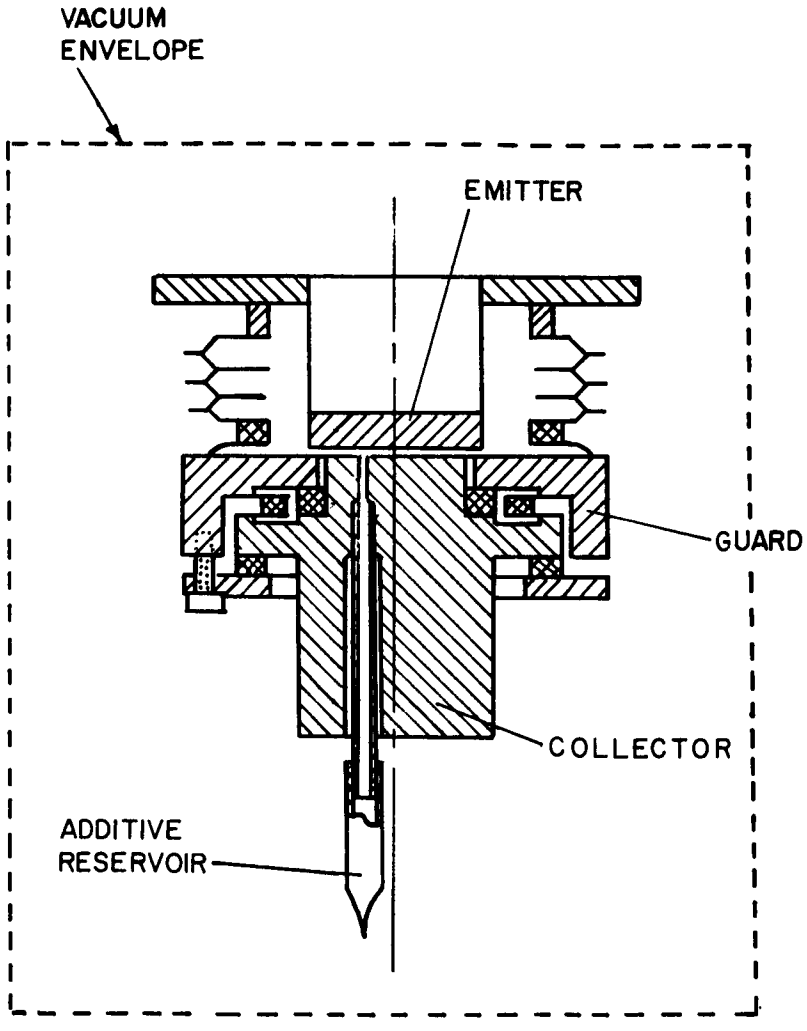

Figure V-37. Schematic of Parametric Converter Showing Additive Reservoir.

function values were determined by measuring the emitter saturation current under ion-rich conditions (ϕ_E > 2.7 eV), using small interelectrode spacings (d< 1 mil) to avoid electron space charge and scattering. A series of runs were made with the additive reservoir at 675°K, corresponding to an oxygen pressure below 10^{-14} torr. The work function values obtained, shown in Figure V-35 as open circles, are typical of treated polycrystalline tungsten. The solid line shown corresponds to a bare work function value of 4.62 as computed from Rasor's theory and has been included for reference purposes.

The next series of runs were taken after heating the additive reservoir to 950°K, resulting in an oxygen pressure of 10^{-8} torr. The first work function measurements made, a few hours after the additive temperature was raised, are shown as triangles in Figure V-38. As time went on, the work function continued to decrease for a given value of T/T_R; i.e., the additive became more active for approximately 20 hours. At the end of this period of time, it stabilized along a line defined by the solid-circle points. This terminal value is somewhat lower than the data obtained with CsF reported in Ref. 2 and shown as a dashed line in Figure V-35. Comparison of the cesium-only data (open circles) with the equilibrium additive data (full circles) shows that the addition of oxygen has resulted in a reduction of approximately 0.45 eV in the emitter work function, for the same T/T_R ratio.

The effect of the additive on collector work function was also investigated. Retarding plots were used to measure collector work function in accordance with the precedure described in Ref. 2. The results of these measurements are shown in Figure V-38, which is a plot of collector work function versus the ratio of the collector temperature to the cesium reservoir temperature. Also shown in this figure is the work function of a molydenum collector without additive from Ref. 2. The effect of the additive has been to shift the minimum collector

work function value from a temperature ratio of 1.8 to 1.45, while the minimum value itself has remained 1.45 eV.

At the time of completion of the electrode work function measurements, 55 hours of testing had passed since the additive reservoir was first heated to 950°K, and 35 hours since a stable, equilibrium work function value was obtained.

The next series of experiments consisted of performance parametric data mapping. Figures V-39 and V-40 show data obtained at 1760°K emitter temperature with 5- and 10-mil spacing. Similar data from a polycrystalline tungsten emitter[28] is shown in Figures V-41 and V-42. Two significant features of the oxygen converter characteristics when compared to the Cs-only data are the greatly decreased Cs temperatures for a given saturation current, as much as 60°C in some cases, and the steeper slope of the envelopes in the oxygen device.

Experiments were continued for about 300 hours of operation. Parametric data in the form of Cs families were obtained over the range of emitter temperature from 1760°K to 1960°K. The electrode J-V envelopes are shown in Figures V-43, V-44, and V-45 and may be compared with the similar data from a Cs-only device shown on the same figures. Electrode power density curves for the two devices are shown in Figures V-46, V-47 and V-48.

On the J-V envelopes in Figures V-43, V-44, and V-45, the contact point of each J-V curve with its envelope is identified with the reservoir temperature, and the significantly lower Cs temperatures associated with the additive device are evident. The reduced scattering at these lower pressures again results in improved performance of the additive converter. Wide spacing with the oxygen additives may thus be expected to produce similar performance to small spacing in Cs-only devices.

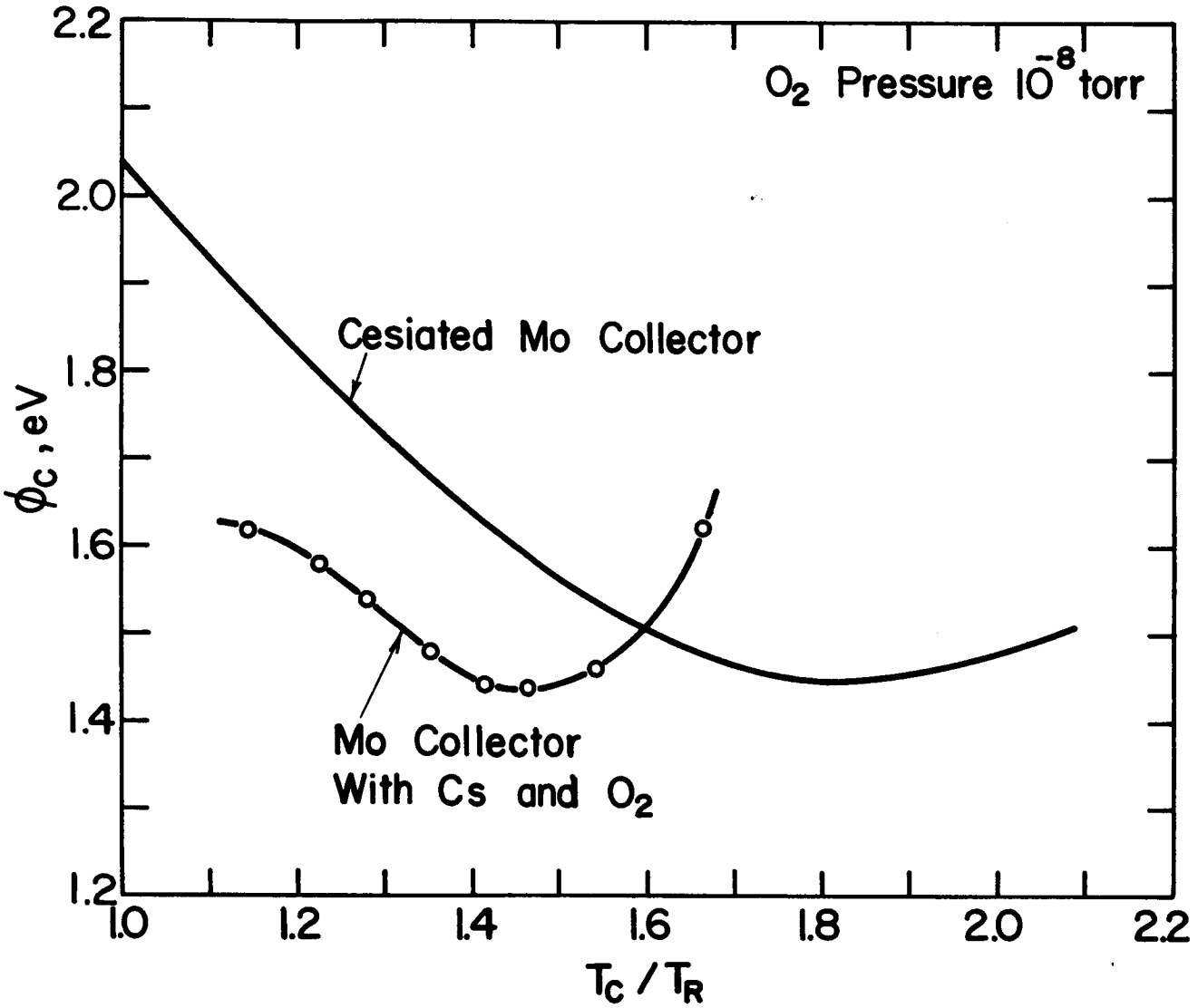

Figure V-38. Cesiated Collector Work Function Comparison With and Without Oxygen.

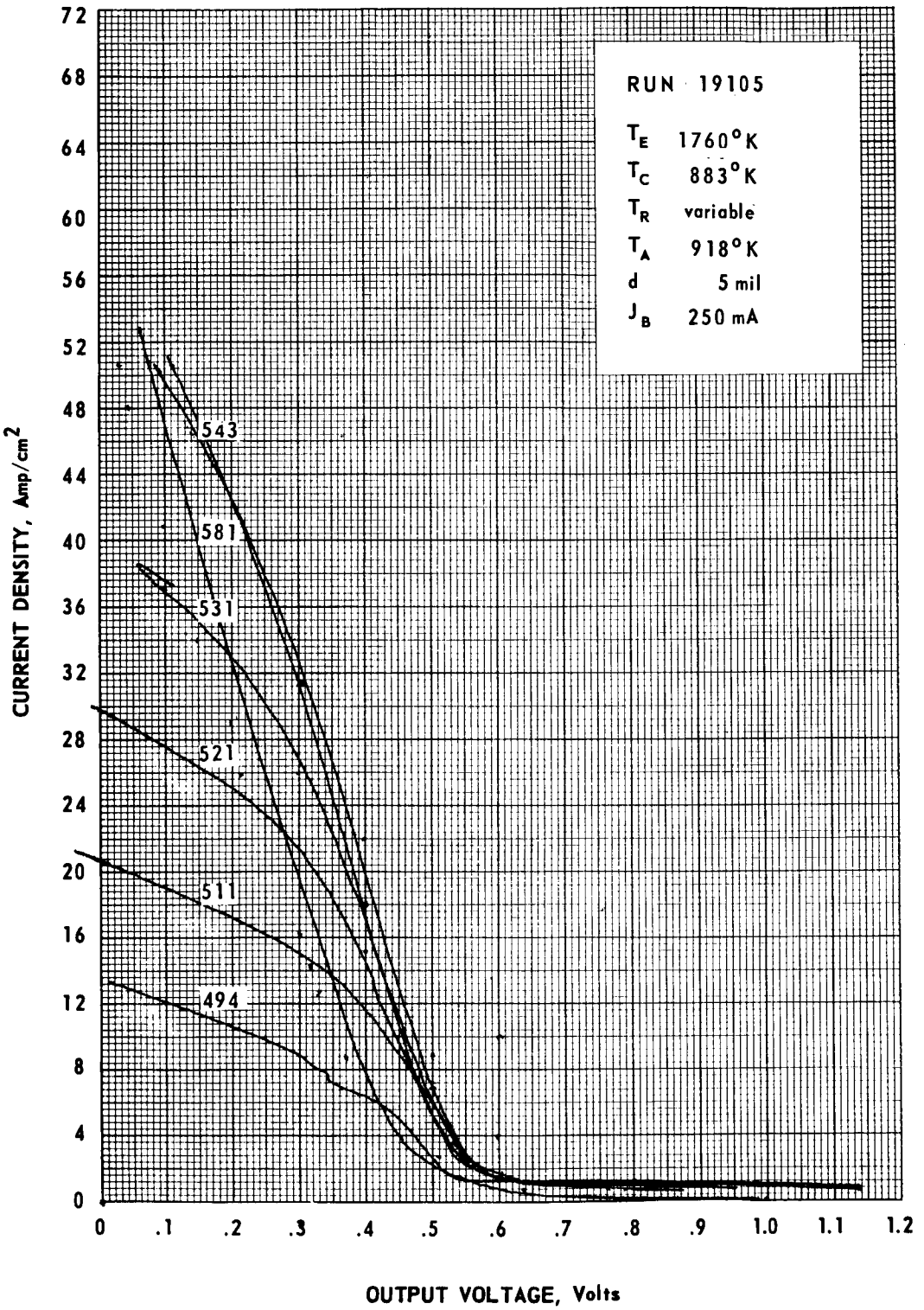

Figure V-39. J-V Family with Cu_2O Additive, T_E 1760°K.

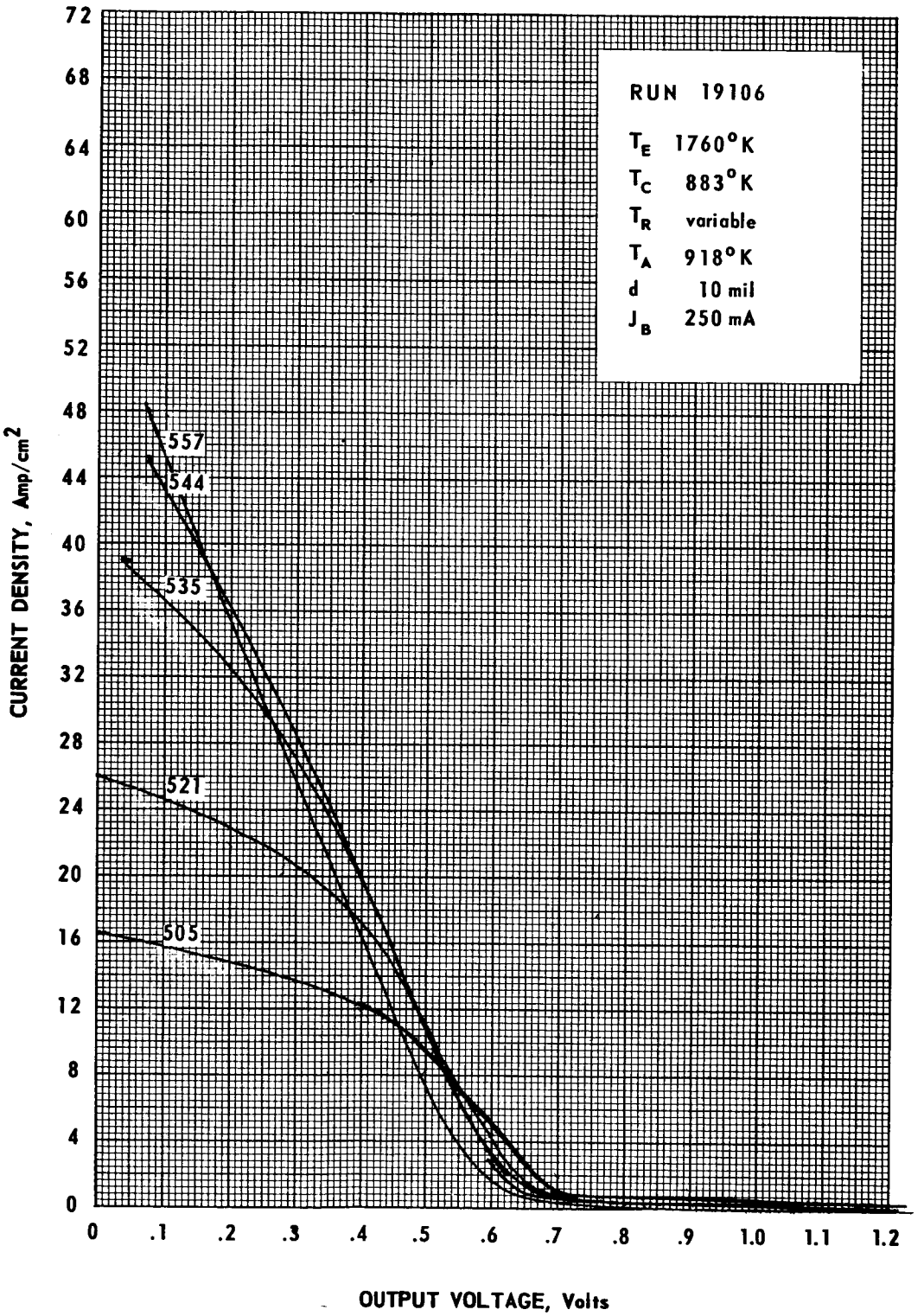

Figure V-40. J-V Family with Cu_2O Additive, T_E 1760°K.

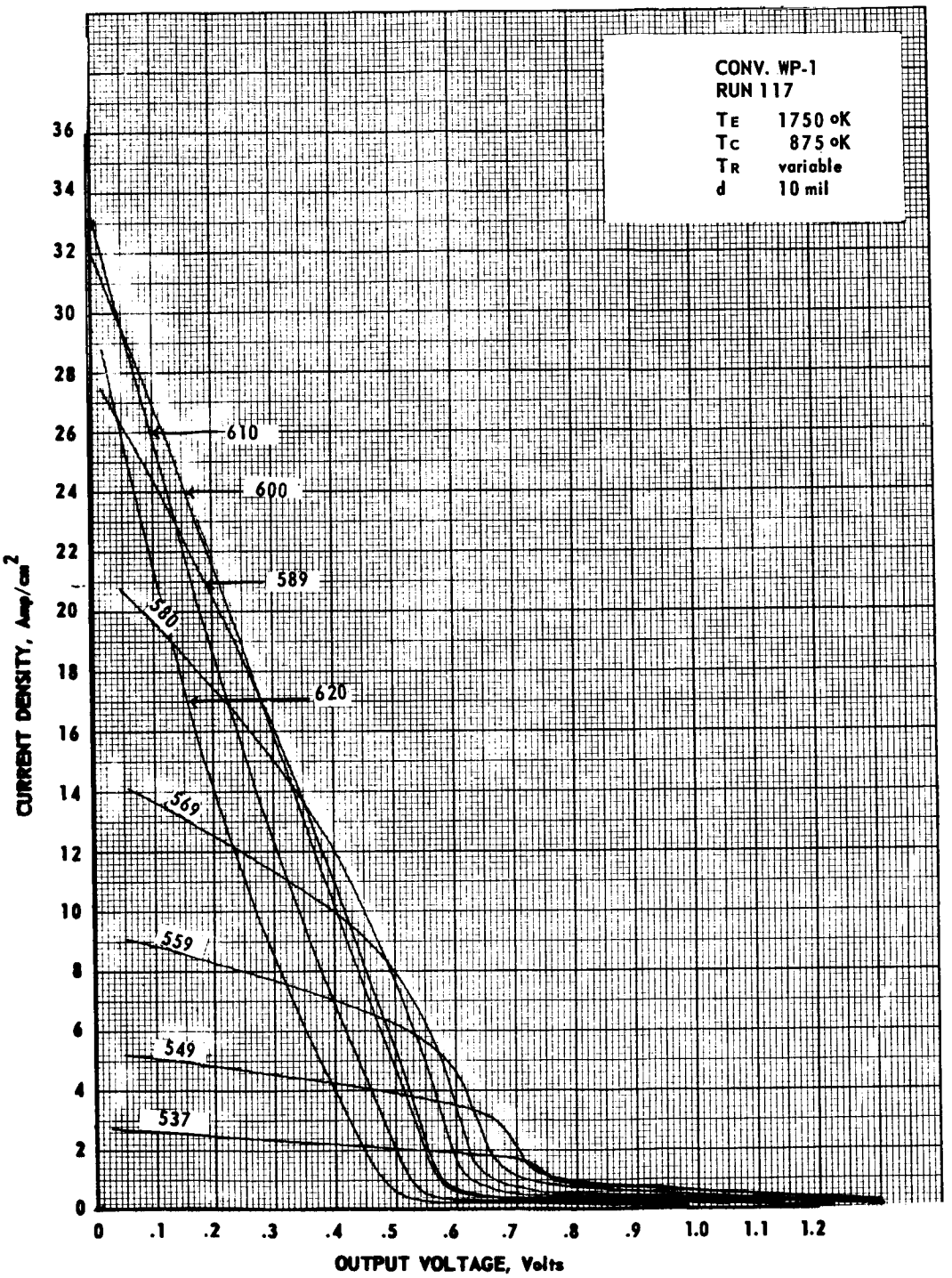

Figure V-41. J-V Family With Cesium Only, T_E 1750°K.

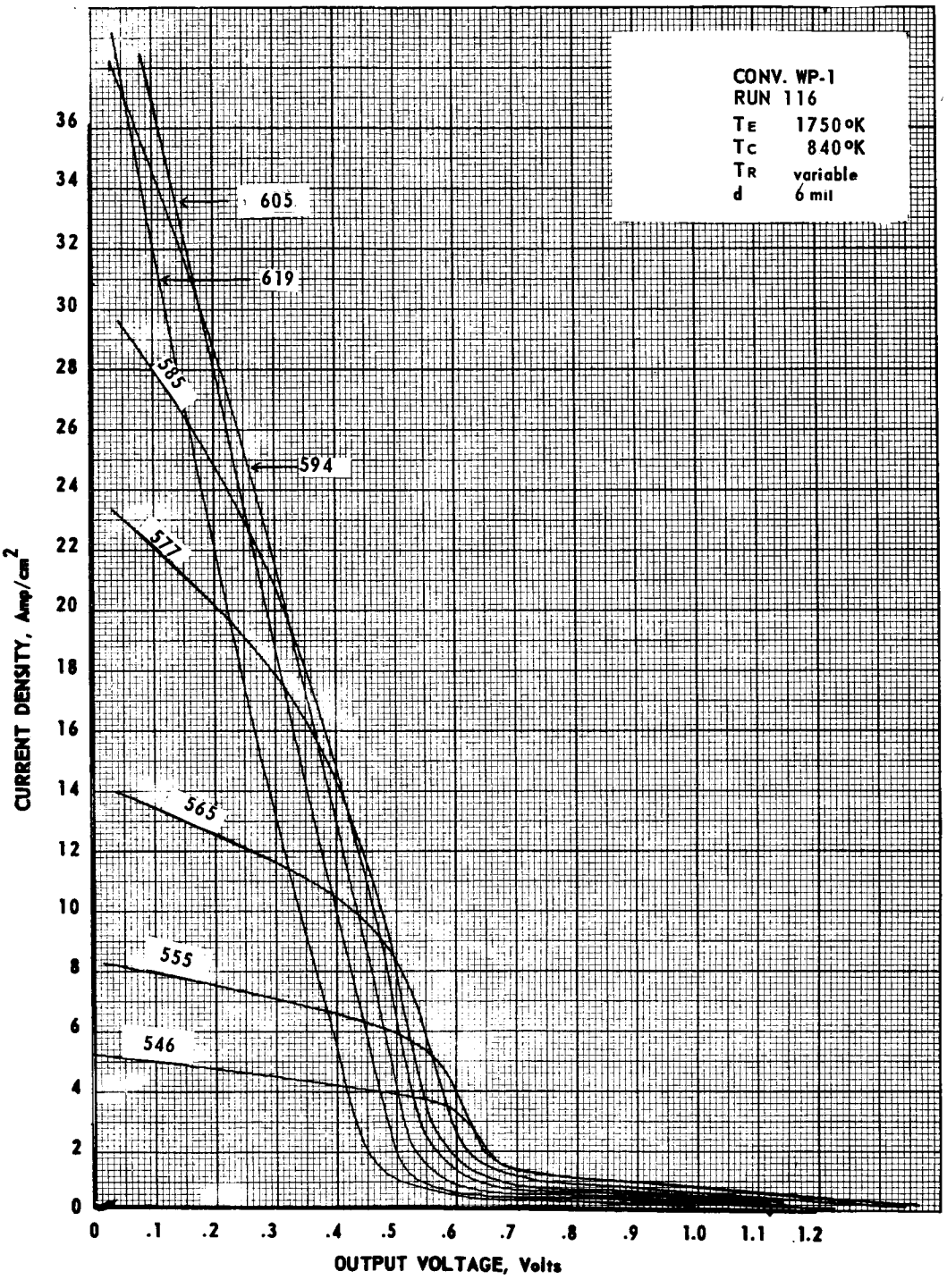

Figure V-42. J-V Family With Cesium Only, T_E 1750°K.

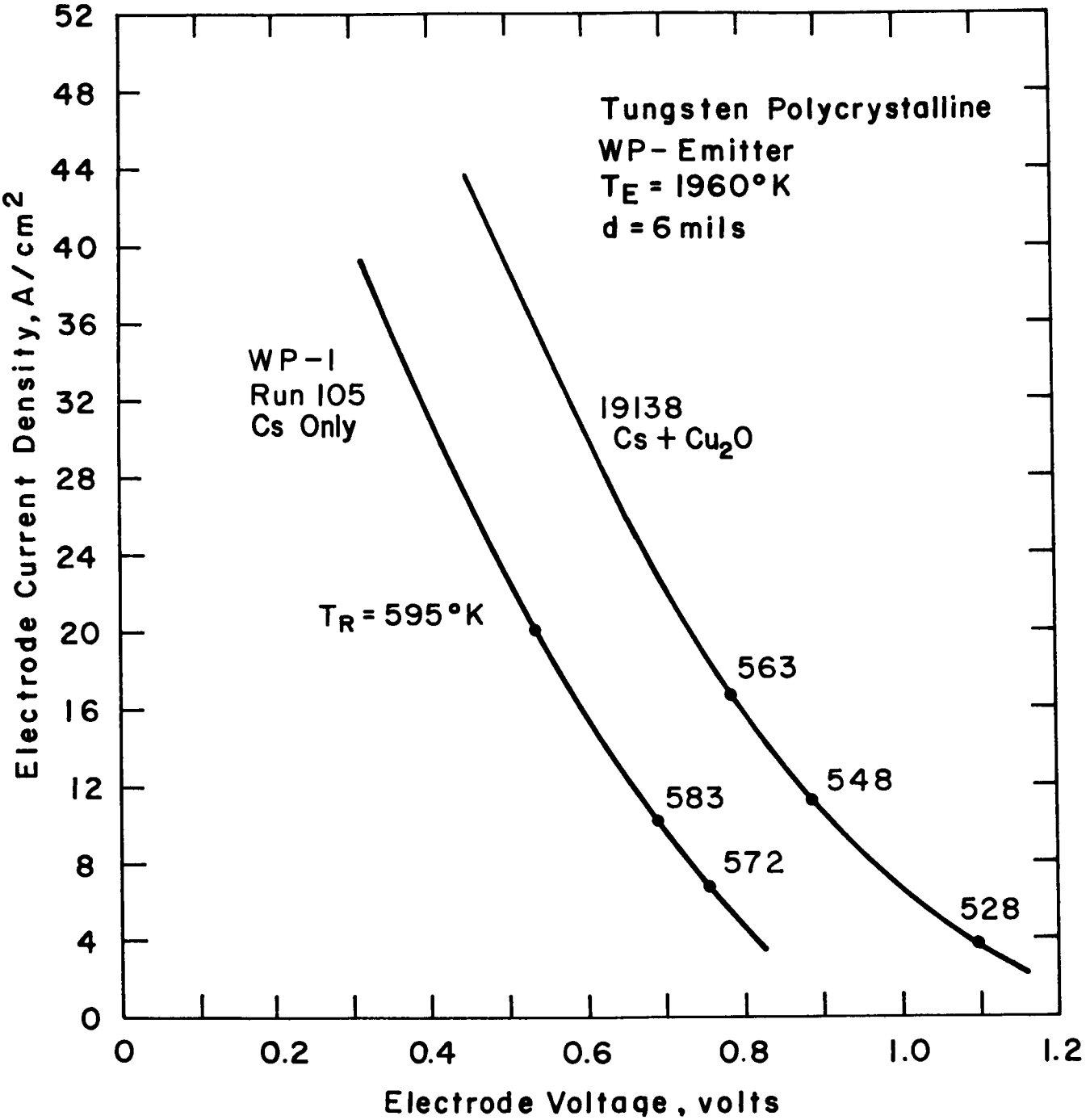

Figure V-43. Performance Envelope Comparison Cs Only and Cs plus Cu_2O, T_E 1960°K.

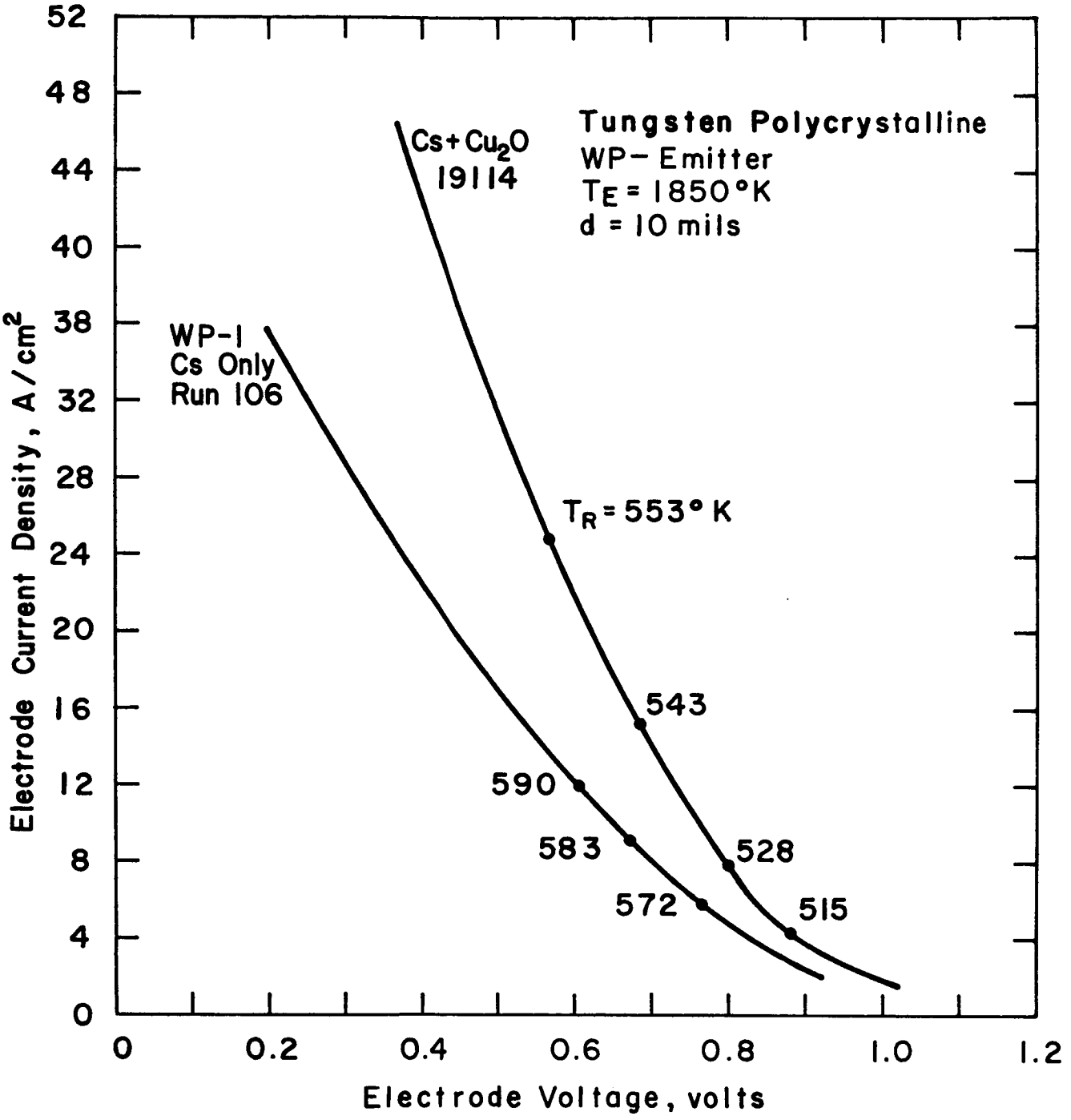

Figure V-44. Performance Envelope Comparison Cs Only and Cs plus Cu_2O, T_E 1850°K.

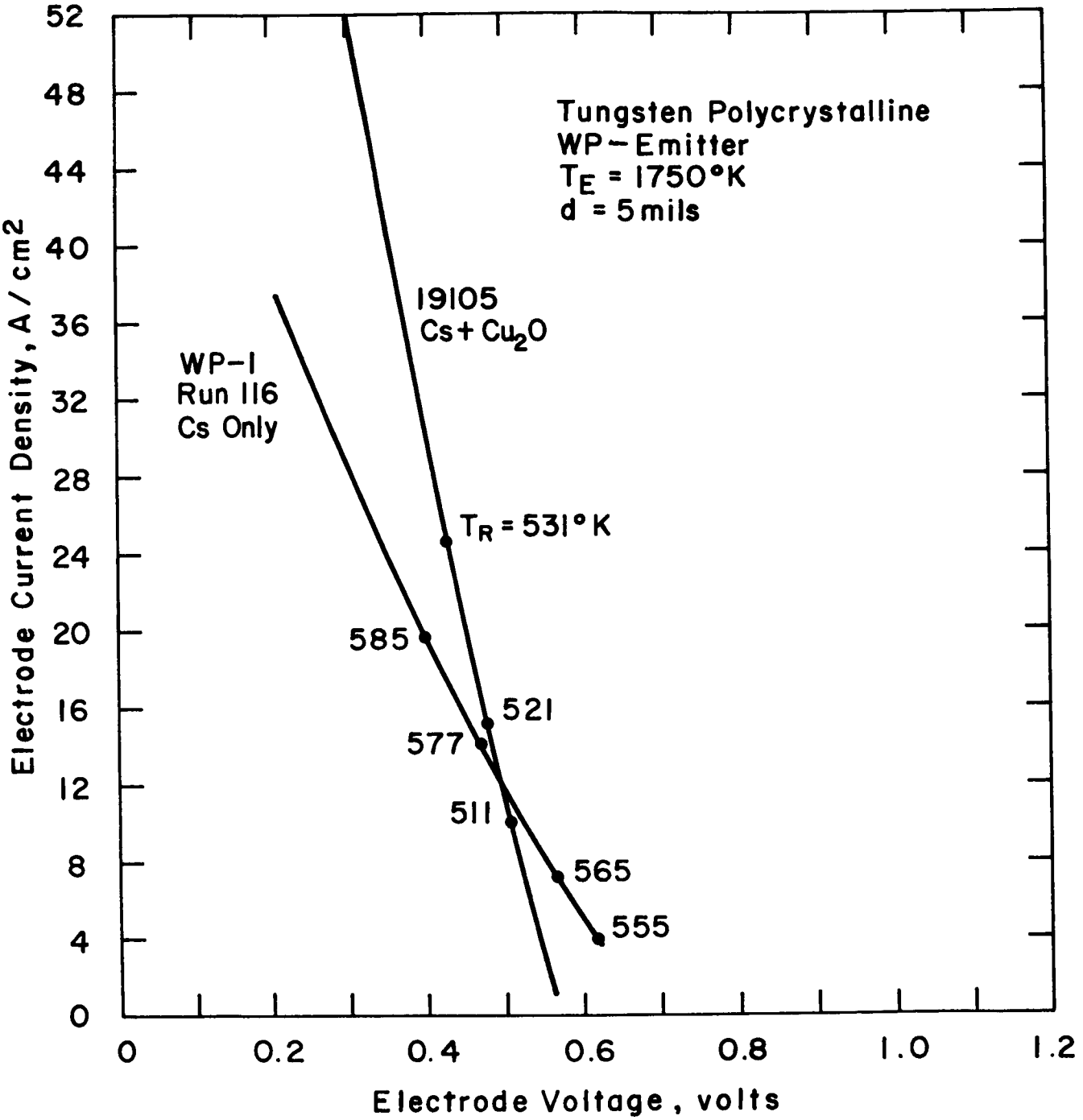

Figure V-45. Performance Envelope Comparison Cs Only and Cs plus Cu_2O, T_E 1750°K.

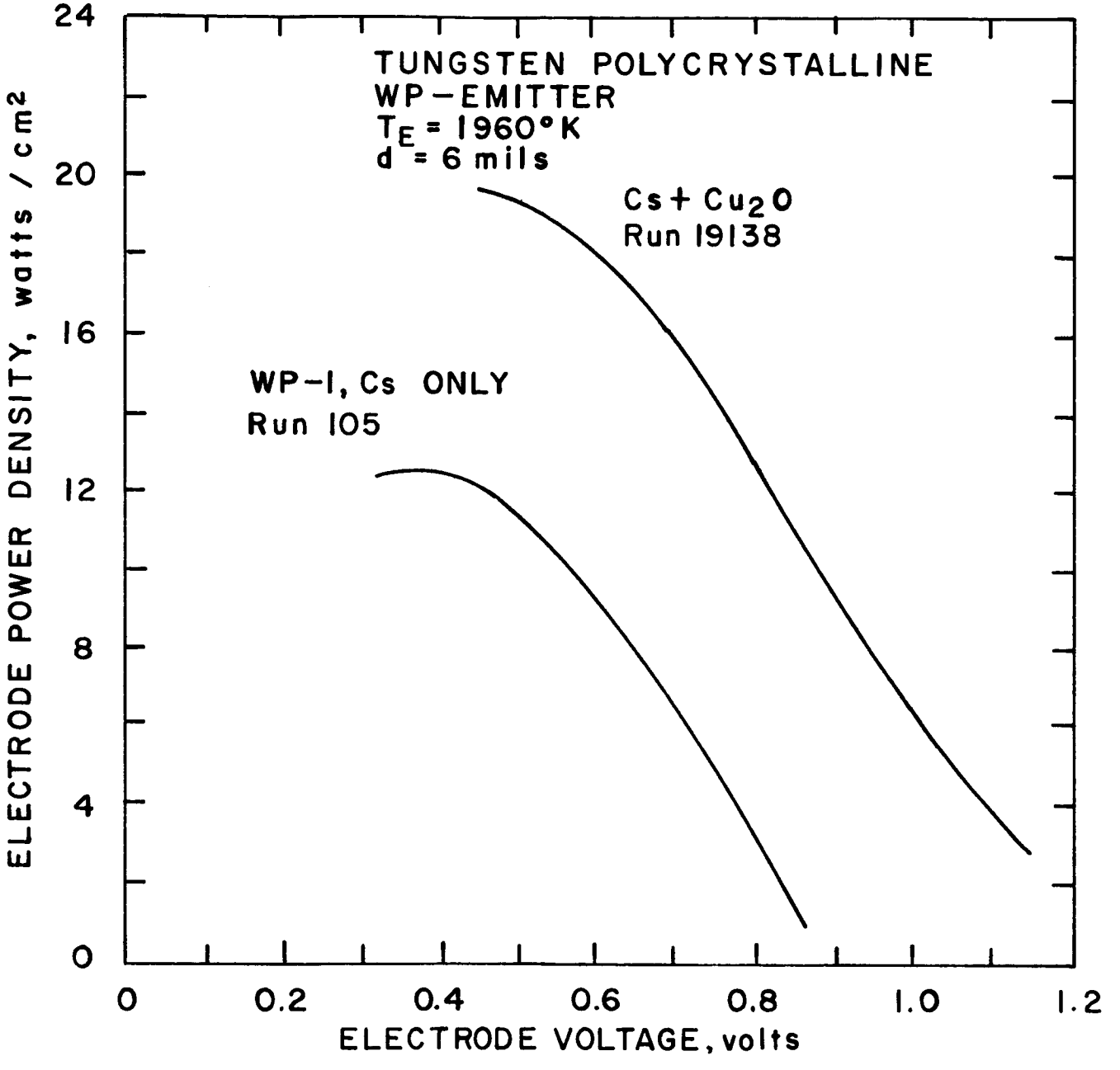

Figure V-46. Power-Density Comparison of Cs Only and Cs plus Cu_2O, T_E 1960°K.

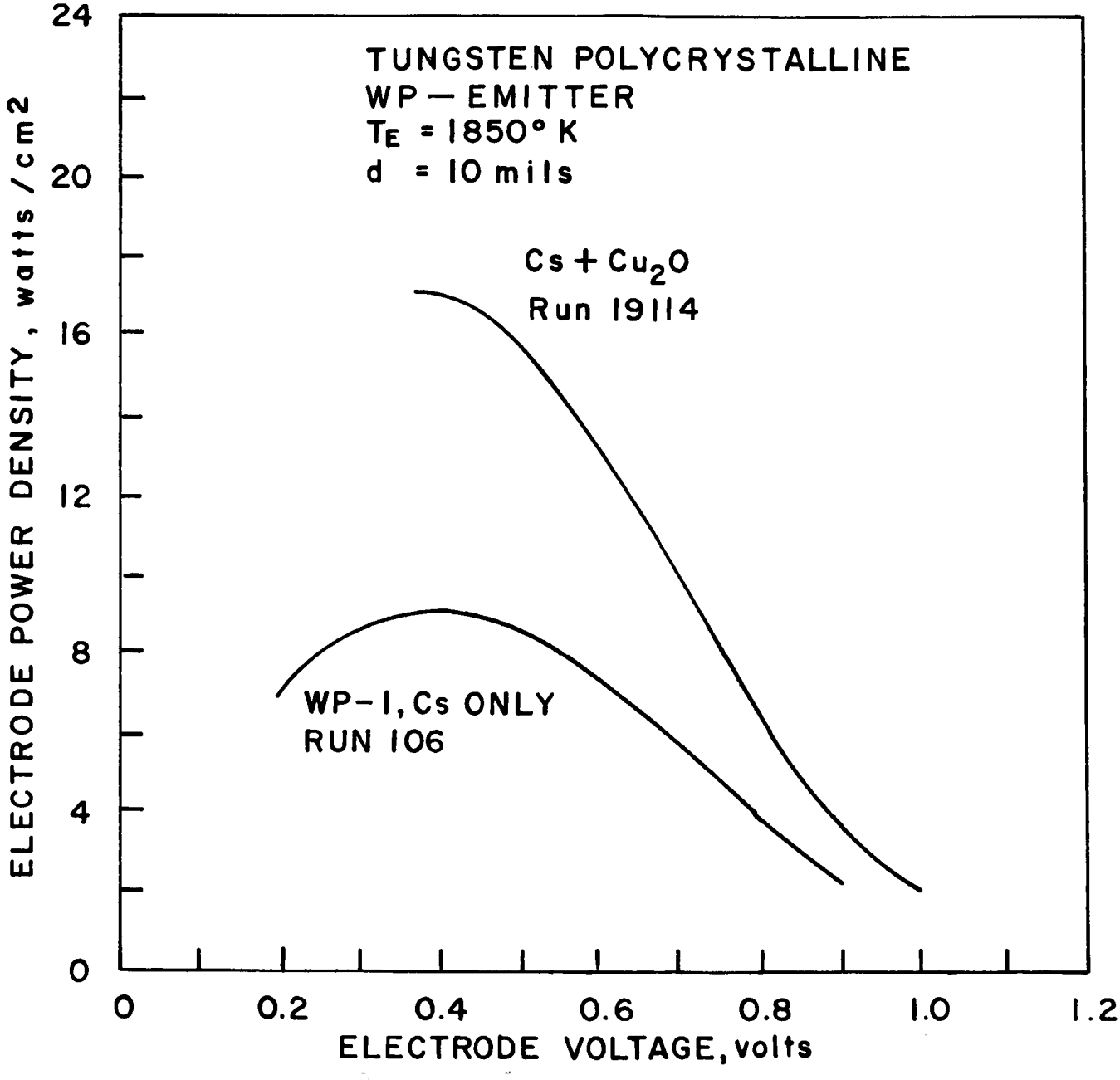

Figure V-47. Power-Density Comparison of Cs Only and Cs plus Cu_2O, T_E 1850°K.

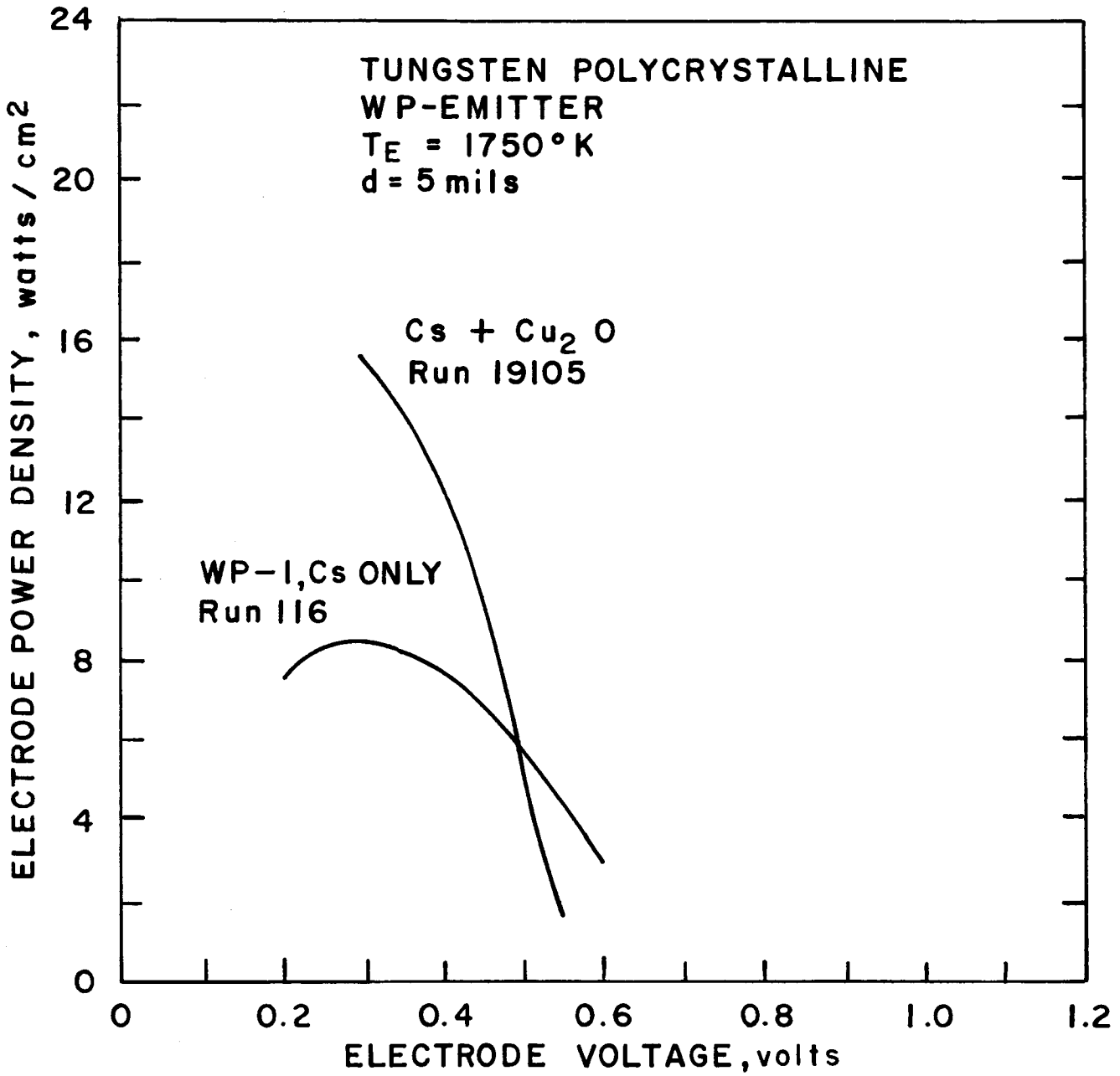

Figure V-48. Power-Density Comparison of Cs Only and Cs plus Cu_2O, T_E 1750°K.

Subsequent to these tests the converter was dismounted and cut apart to determine whether there had been any erosion or excessive oxidation of the electrodes. The emitter surface was found to be clean and shiny except for the small area, about 100 mils in diameter, immediately above the additive-reservoir opening in the collector. In this area some etching of the emitter was evident, a shallow (2 mils) depression having been formed. The tungsten from this region had apparently been oxidized and then evaporated onto the collector. There was a corresponding deposit of this material around the hole in the collector. Spectrographic analysis confirmed the presence of tungsten in the deposit. A slight oxidation of the collector was also observed, but there was no visible erosion of this surface. No traces of copper deposits from the additive were found in the device, either by visual observation or by spectrographic analysis.

In the oxygen pressure range necessary for work function modification, no corrosion of the emitter surface can take place. The fact that some corrosion was evident indicates that there was excessive pressure in the converter during testing. The most likely source was probably the reaction (29) which could take place during the tests attempted with Cs only. Later increases in temperature to introduce O_2 onto the surfaces were based on reaction (28) and any CuO in the reservoir would then dissociate according to (27), producing the excessively high pressure shown in Figure V-34 for this reaction. A further cause for excessive pressure may have been the transport delay at low pressures. This would result in the choice of too high a reservoir temperature because of the lack of response at lower temperatures. Calculations show that the desired pressures must have been exceeded by at least three orders of magnitude for the observed effects to have taken place. With this experience as a guide, it should be possible to obtain satisfactory pressure control in future devices.

E. Conclusions

1. Cesium Fluoride. The studies conducted under this task have determined the true effects of CsF under thermionic conditions and have shown that many of the changes in characteristics previously attributed to the fluorine were actually due to contaminants introduced with the additive. Water was found to be the principal contaminant and was shown to be capable of producing the observed effects.

Extended outgassing of the CsF, combined with the construction of a specially designed surface-studies device, made it possible to determine the behavior of the pure fluoride. It was found that, at coverages approaching a complete monolayer, only about 0.3 eV change in work function could be obtained. The energy for desorption was derived from the same experiments and was about 3.3 eV. With the relatively small change in work function and the high arrival rates required, it appears that the fluorine additives hold little promise for improving converter performance.

The relative inactivity of CsF as a surface additive, in spite of its similarities to oxygen, indicates the need for further theoretical studies in this field. These data, together with those for oxygen, define boundaries for the investigations.

2. Oxygen. The Cu_2O converter experiments have successfully achieved the objectives of the program and have demonstrated that the enhanced power output first associated with CsF can be maintained through the use of oxygen for at least 300 hours of operation with no degradation. The results obtained agree with the theoretical predictions of lowered Cs pressure and wider allowable spacing. The feasibility of a continuous oxygen source consisting of the equilibrium dissociation of a metal oxide has been demonstrated and successfully applied to a functioning thermionic converter.

Several areas for future work have become apparent. While oxygen may be used satisfactorily as an additive, further studies are desirable to define the mechanism of operation and to predict the behavior of other materials which might be more effective or more easily controlled. More complete documentation of the converter performance, and extension to longer periods of operation with better control of the oxygen pressure, would further the utilization of this additive in hardware devices. The effect of the oxygen on the Mo collector material has not been fully explored, and it is not clear whether some other material might produce better performance under these conditions.

CHAPTER V

REFERENCES

1. N. S. Rasor and C. Warner, J. Appl. Phys., 35, 2589 (1964).

2. S. S. Kitrilakis et al., "Final Report, Task IV," JPL Contract No. 950671, Thermo Electron Report No. TE 7-66 (1965).

3. I. Langmuir and D. S. Villars, "Oxygen Films on Tungsten - I. A Study of Stability by Means of Electron Emission in Presence of Cesium Vapor," J. Am. Chem. Soc. 53, 486 (1931).

4. R. L. Aamodt et al., "Thermionic Emission from Molybdenum in Vapors of Cesium and Cesium Fluoride," J. Appl. Phys. 33, 6, 2080 (1962).

5. W. A. Ranken et al., Advanced Energy Conversion 3, 235 (1963).

6. R. Langpape and A. Minor, "Influence of CsF and Cs + CsF on the Work Function of Refractory Metals," Therm. Conv. Spec. Conf., Cleveland (1964).

7. S. S. Kitrilakis and J. H. Weinstein, "Second Annual Technical Summary Report," Contract No. Nonr-3563(00), Thermo Electron Report No. TE 27-64 (1963).

8. S. S. Kitrilakis et al., "Final Report, NASA-Lewis Research Center Contract No. NAS 3-2539," Thermo Electron Report No. TE 19-65 (1964).

9. A. Jester and A. Minor, "Electron Emission of Tungsten in a CsF Atmosphere," Therm. Conv. Spec. Conf., Cleveland (1964).

10. L. Pauling, Nature of the Chemical Bond, Cornell U. Press, 228 (1960).

11. W. Engelmaier and R. Stickney, "Thermionic and Adsorption Characteristics of a Single-Crystal Tungsten Filament Exposed to Oxygen," Proc. Phys. El. Conf. M.I.T. (1966).

12. I. Langmuir, "Electrochemical Interactions of Tungsten, Thorium, Cesium, and Oxygen," Ind. and Engrg. Chem. 22, 390 (1930).

13. J.K. Roberts, "Some Properties of Adsorbed Films of Oxygen on Tungsten," Proc. Roy. Soc. A152, 464 (1935).

14. I. Langmuir and H.A. Jones, "The Characteristics of Tungsten Filaments as Functions of Temperature," G.E. Rev. 30, 408; 310; 354 (1927).

15. I. Langmuir et al., "Effect of End Losses on the Characteristics of Filaments of Tungsten and Other Materials," Phys. Rev. 35, 478 (1930).

16. E. Ya. Zandberg and A. Ya. Tontegode, "Surface Ionization of Li, Na, K and Cs Atoms and Li Cl, K Cl and Cs Cl Molecules on Polycrystalline Rhenium," Soviet Physics - Tech. Physics 10, 858 (1965).

17. S. Datz and E.H. Taylor, "Ionization on Platinum and Tungsten Surfaces - II. The Potassium Halides," J. of Chem. Phys. 25, 395 (1956).

18. I. Langmuir, "Tungsten Lamps of High Efficiency - I. Blackening of Tungsten Lamps and Methods of Preventing it," Trans. Am. Inst. Elec. Eng. 32, 1921 (1913).

19 K.H. Kingdon, Phys. Rev. 24, 510 (1924).

20. M.C. Johnson and F.A. Vick, "Cathode Ray Oscillography of Gas Adsorption Phenomena - II. Durations of an Adsorbed State of Oxygen on Tungsten," Proc. Roy. Soc. A151, 308 (1935).

21. A. L. Reimann, Phil. Mag. 20, 594 (1935).

22. E. W. Müller, Ergelo. exakt. Naturw. 27, 290 (1953).

23. R. Gomer and J. K. Hulm, J. Chem. Phys. 27, 1363 (1957).

24. C. E. Wicks and F. E. Block, "Thermodynamic Properties of 65 Elements - Their Oxides, Halides, Carbides, and Nitrides," Bulletin 605, Bureau of Mines, U. S. Dept. of Interior (1963).

25. V. C. Wilson, "Operation and Analysis of a Plane Parallel Cesium Thermionic Converter with an Oxygen Treated Tantalum Emitter," Proc. Ther. Conv. Spec. Conf , IEEE, Gatlinburg, Tenn., 121 (1963).

26. J. D. Levine et al., "Oxygen as a Controllable, Reversible and Beneficial Additive in the Cesium Converter," Proc. Therm. Conv. Spec. Conf., IEEE, San Diego, Calif., 276 (1965).

27. Roberts and Smyth, J. Am. Chem. Soc., 42 (1921).

28. Miskolczy et al., "Final Report, NASA-JPL Contract No. 950228," Thermo Electron Report No. TE 63-64 (1964).

CHAPTER VI

THE OUTPUT CHARACTERISTICS OF AN ELECTROETCHED RHENIUM SURFACE

A. Introduction

The parametric diode used in inert gas studies uses an electroetched rhenium emitter. Its preparation and metallurgical examinations were discussed in Chapter IV. The surface and performance characteristics of this diode must be established for reference in the inert gas experiments. These characteristics are also important in the evaluation of this new method of surface preparation and its overall effect on the output power and efficiency of the converter. For these reasons, the bare work function and the cesiated work function of electroetched rhenium were determined. The volt-ampere characteristics of the diode were recorded for a wide range of emitter temperature, cesium temperature and interelectrode spacing. The complete performance map is summarized in this chapter.

B. Bare Work Function

The experimental procedure for determination of emitter work function is described in Chapter III. The saturation electron current is measured experimentally, and the surface work function is obtained from Richardson's equation and the known values of saturation current and surface temperature. Typical volt-ampere characteristics are shown in Figures VI-1 and VI-2. In both plots, a well-defined saturation current is evident. The observed reverse current, however, is unusually high for this type of data. This is explained by the fact that one of the cesium capsules, contained in an appendage below the cesium reservoir, cracked during the outgassing of the diode. This

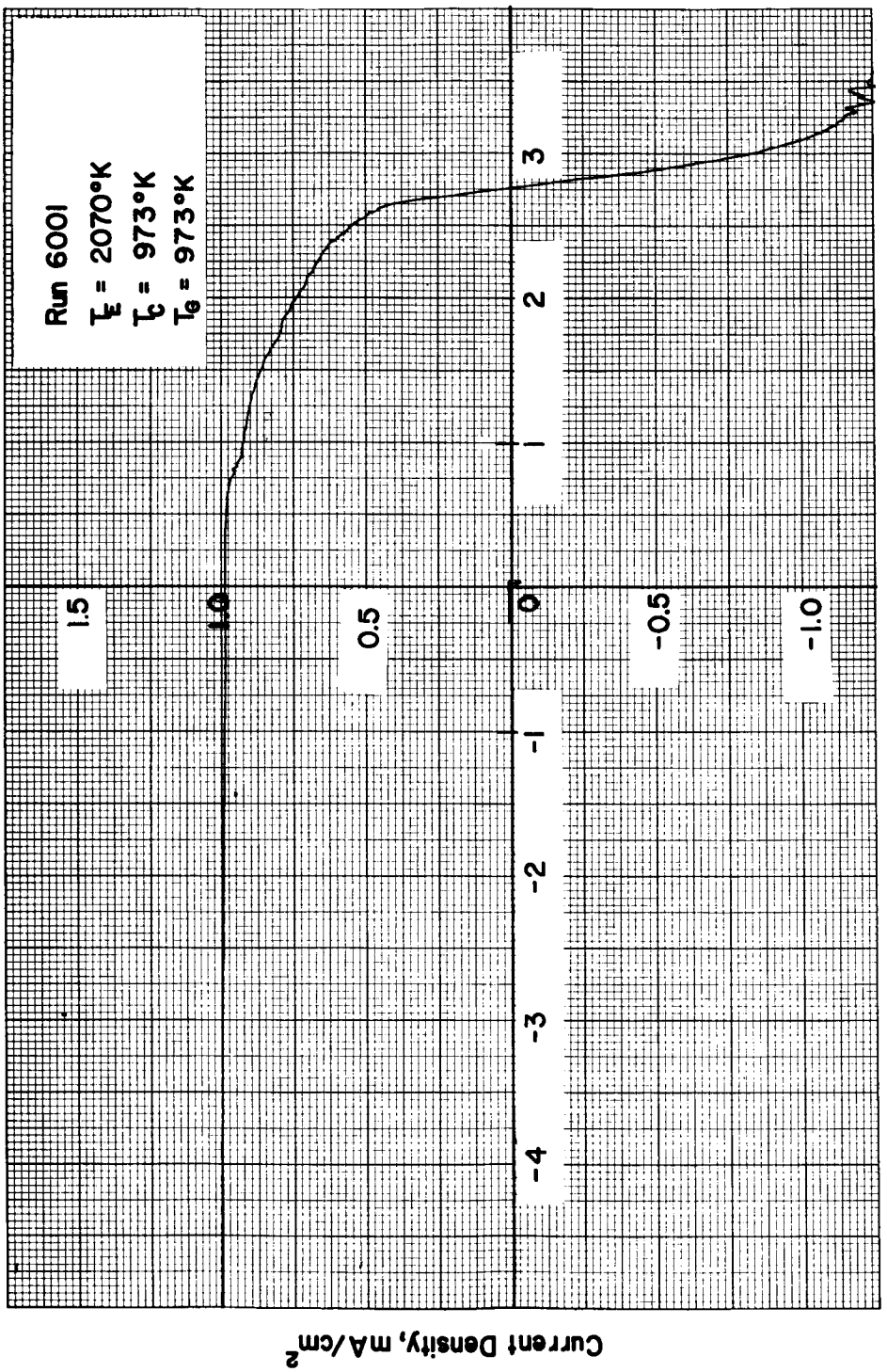

Figure VI-1. Typical J-V Characteristic used for "Bare" Work Function Determination.

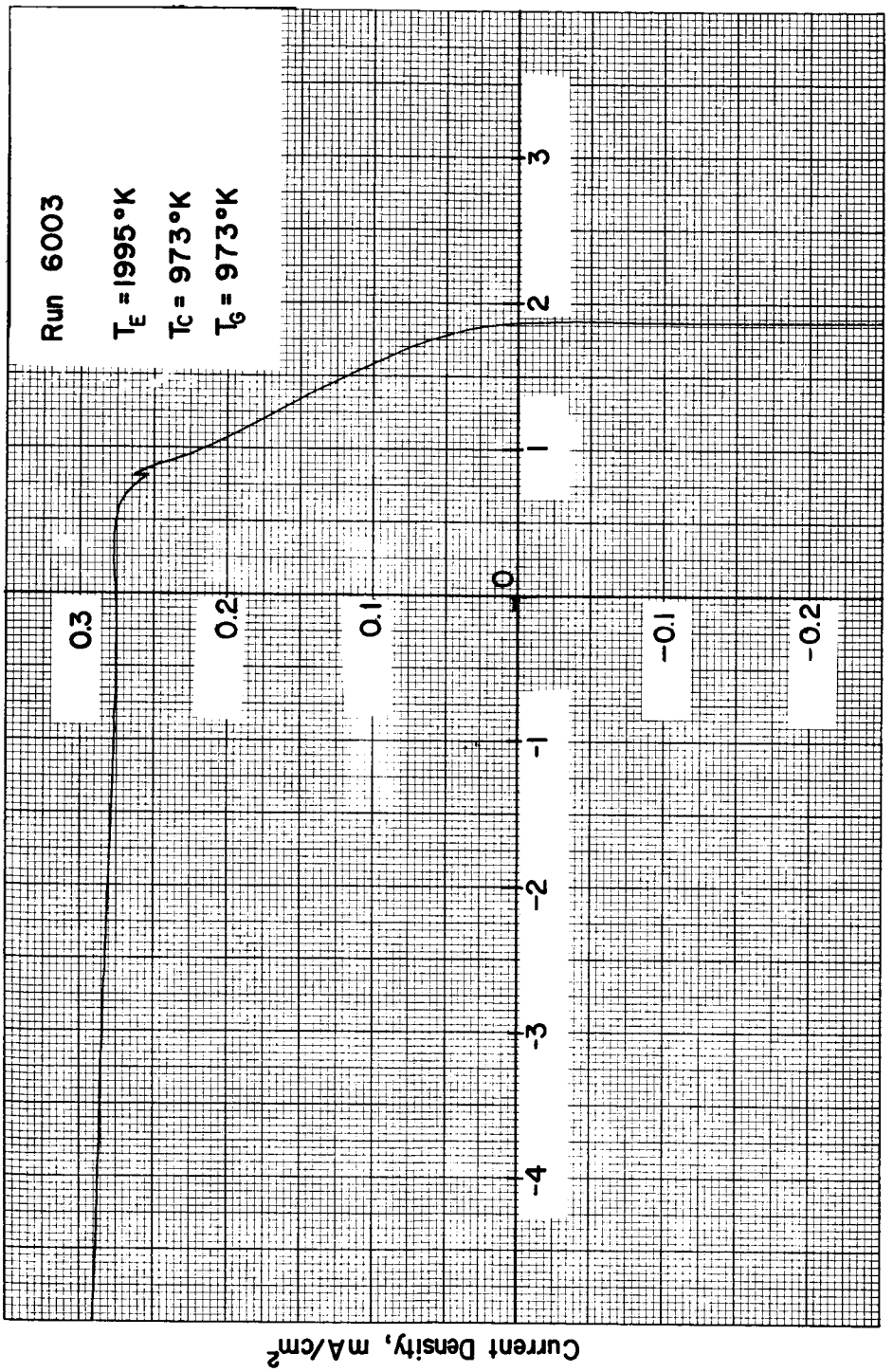

Figure VI-2. Typical J-V Characteristic used for "Bare" Work Function Determination.

resulted in the injection of a small amount of cesium into the converter. This quantity of cesium is responsible for the observed ion current, although it is not enough to reduce the surface work function. To make sure that the measured values of work function are actually those of the bare surface and are not affected by the low vapor pressure of cesium, the results are plotted as in Figure VI-3. This is a plot of Richardson's equation in terms of current and inverse surface temperature. The diagonal lines represent constant values of surface work function. At high surface temperatures, the data points follow a constant work function line at 0.88 eV. At lower temperatures, however, the data points deviate from the constant-work-function lines and tend to give lower values of work function. In this temperature range, apparently, the temperature of the surface is low enough so that cesium starts to adhere to the surface. The data points corresponding to emitter temperatures above 2000°K are therefore considered to be valid measurements of the bare work function of this surface.

C. Cesiated Work Function

Figures VI-4 and VI-5 are typical characteristics used for determining the rhenium work function in the presence of cesium. Again, the well-defined saturation-current values from such plots are substituted in the Richardson equation, along with the emitter temperature, and the Richardson work function values are obtained. With these measurements a plot is made of work function versus the ratio of surface to reservoir temperature, as shown in Figure VI-6. Here the cesiated and bare work functions are plotted versus the ratio of surface to reservoir temperature. The curve defined by these measurements in the presence of cesium smoothly approaches the bare-work-function asymptote at ϕ_o = 4.88 eV. This, of course, was to be expected. The scatter in these

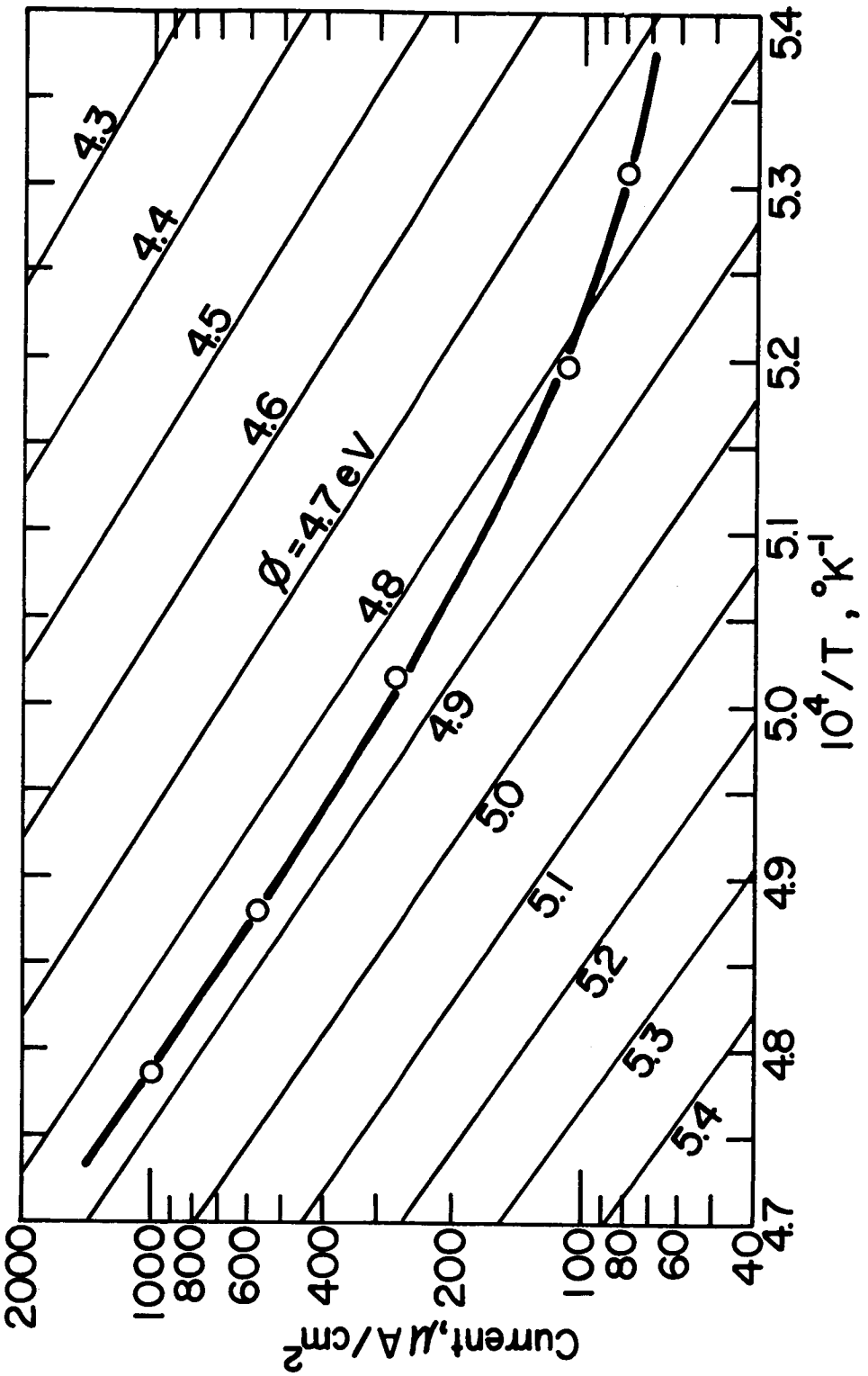

Figure VI-3. Plot of Richardson Equation.

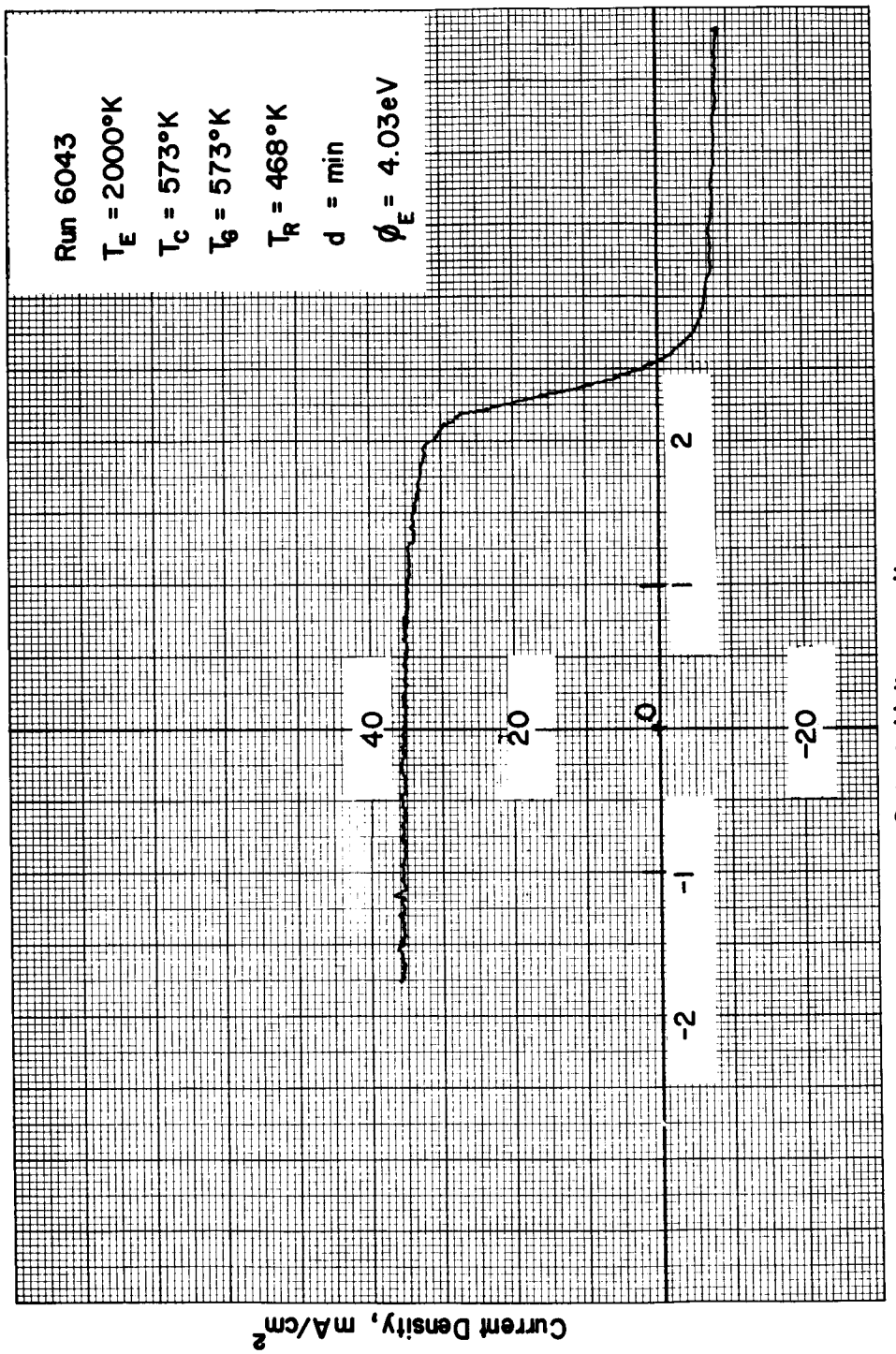

Figure VI-4. Typical J-V Characteristic used for Cesiated Work Function Determination.

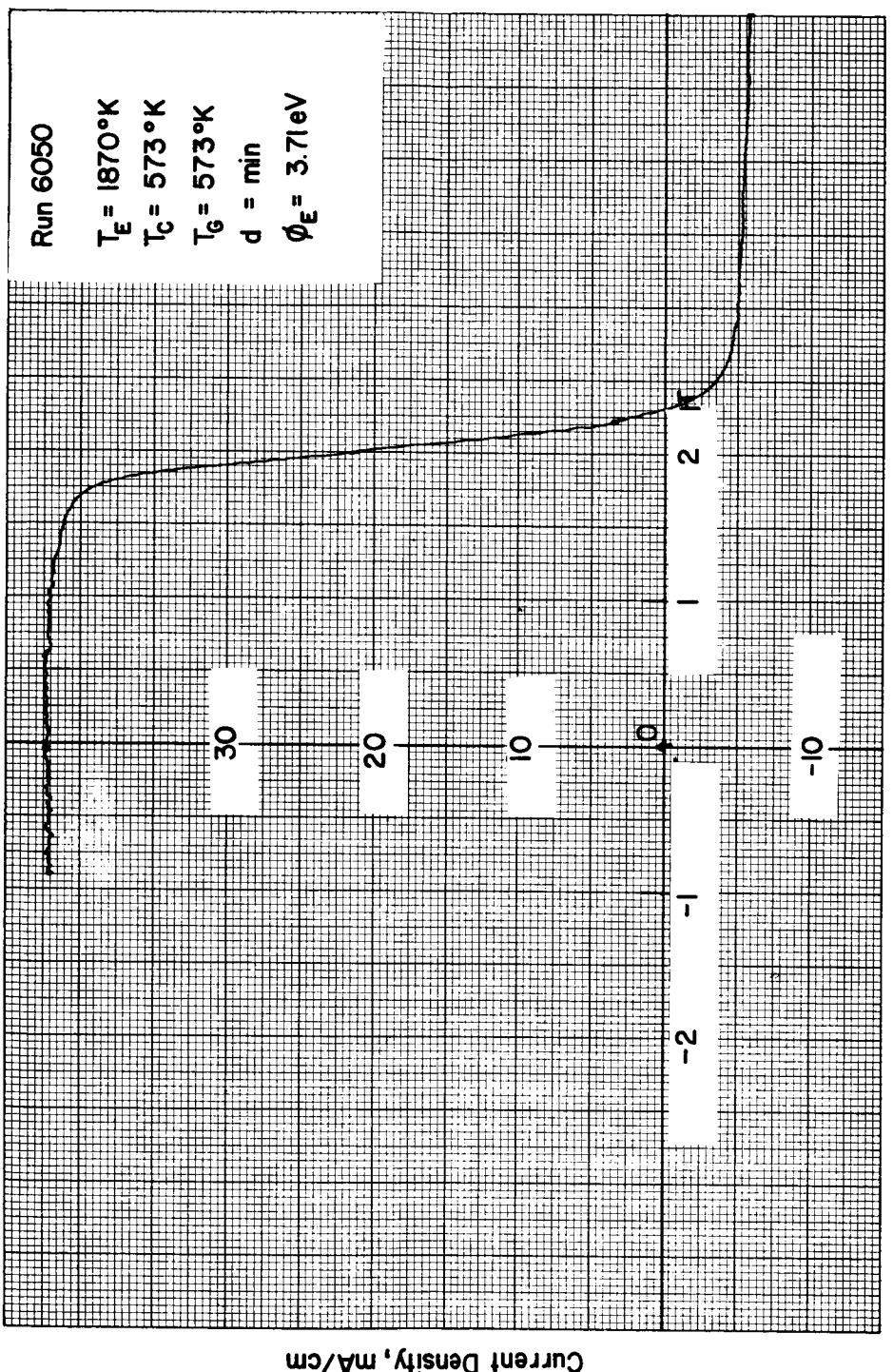

Figure VI-5. Typical J-V Characteristic used for Cesiated Work Function Determination.

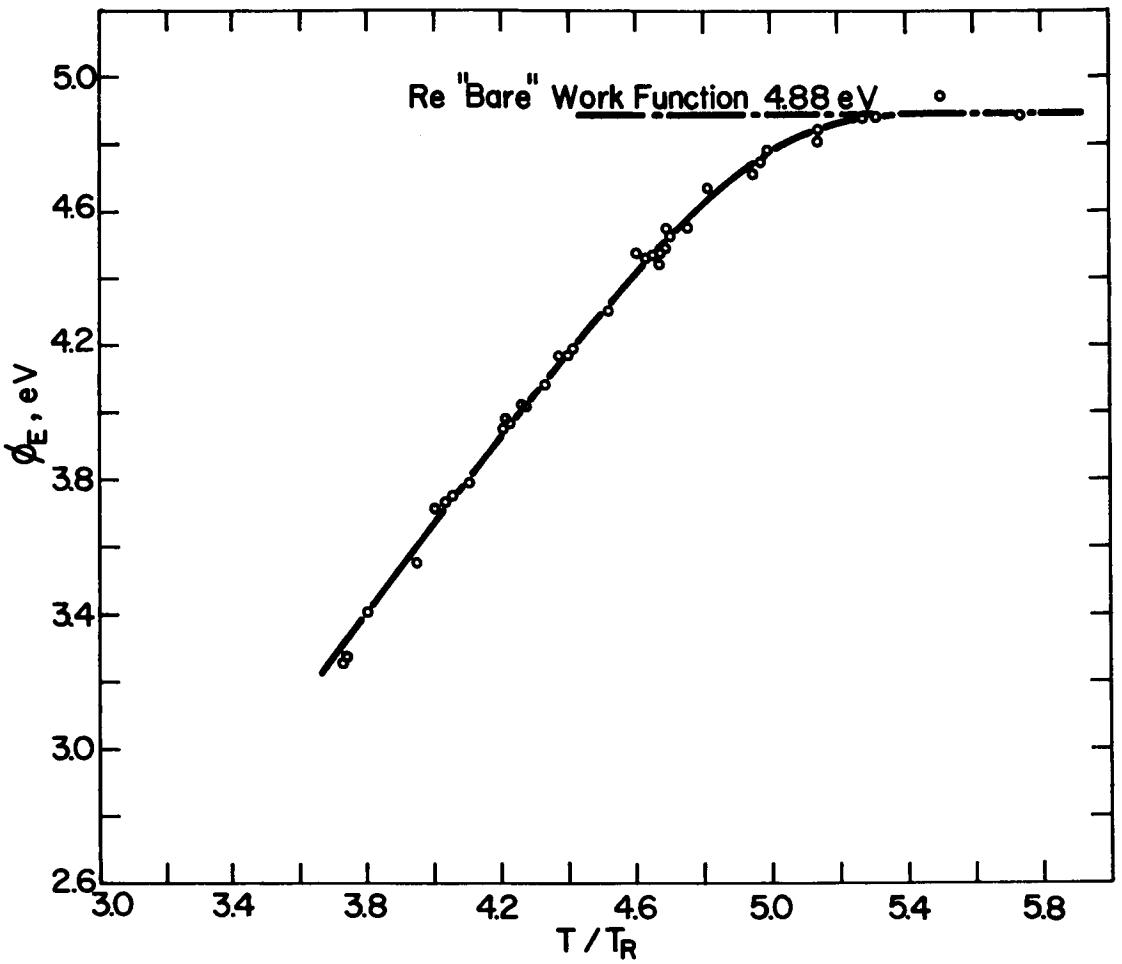

Figure VI-6. Work Function vs Surface-to-Reservoir Temperature Ratio Plot of Cesiated Work Function Measurements.

data is surprisingly low. To compare the present results with the data obtained from electropolished rhenium in the previous year,[1] Figure VI-7 was prepared. This, again, is a plot of work function versus the ratio of surface to reservoir temperature. The present data are shown as a solid line together with the corresponding bare-work-function asymptote. The data of Reference 1 are shown as the dashed line, again with the corresponding asymptote. These two sets of data are probably the best illustration of the Rasor-Warner theory obtained to date. Their bare-work-function asymptotes differ by about 130 mV (the bare work function for electropolished rhenium is 4.75 eV), and they behave very much as predicted by the theory in that they cross soon after a small amount of cesium coverage occurs at a T/T_R value of 4.7, and the higher bare-work-function line falls lower than the other.

D. Parametric Performance Data

The results of the previous section indicate that the bare work function of etched rhenium is higher than that of electropolished rhenium. The cesiated work function of the etched rhenium is about 0.13 eV lower than the electropolished rhenium work function at a given T/T_R. Or, conversely, in the case of an etched rhenium emitter, a lower cesium pressure is required to achieve the same cesiated work function. A significant part of the current in the ignited mode is attenuated by interactions with cesium atoms. Therefore, the output characteristics corresponding to the electroetched rhenium emitter must be substantially higher than for electropolished rhenium.

Parametric performance data was obtained on the converter employing an etched rhenium emitter, covering a wide range of converter variables. Families of current-voltage characteristics were generated by varying the cesium

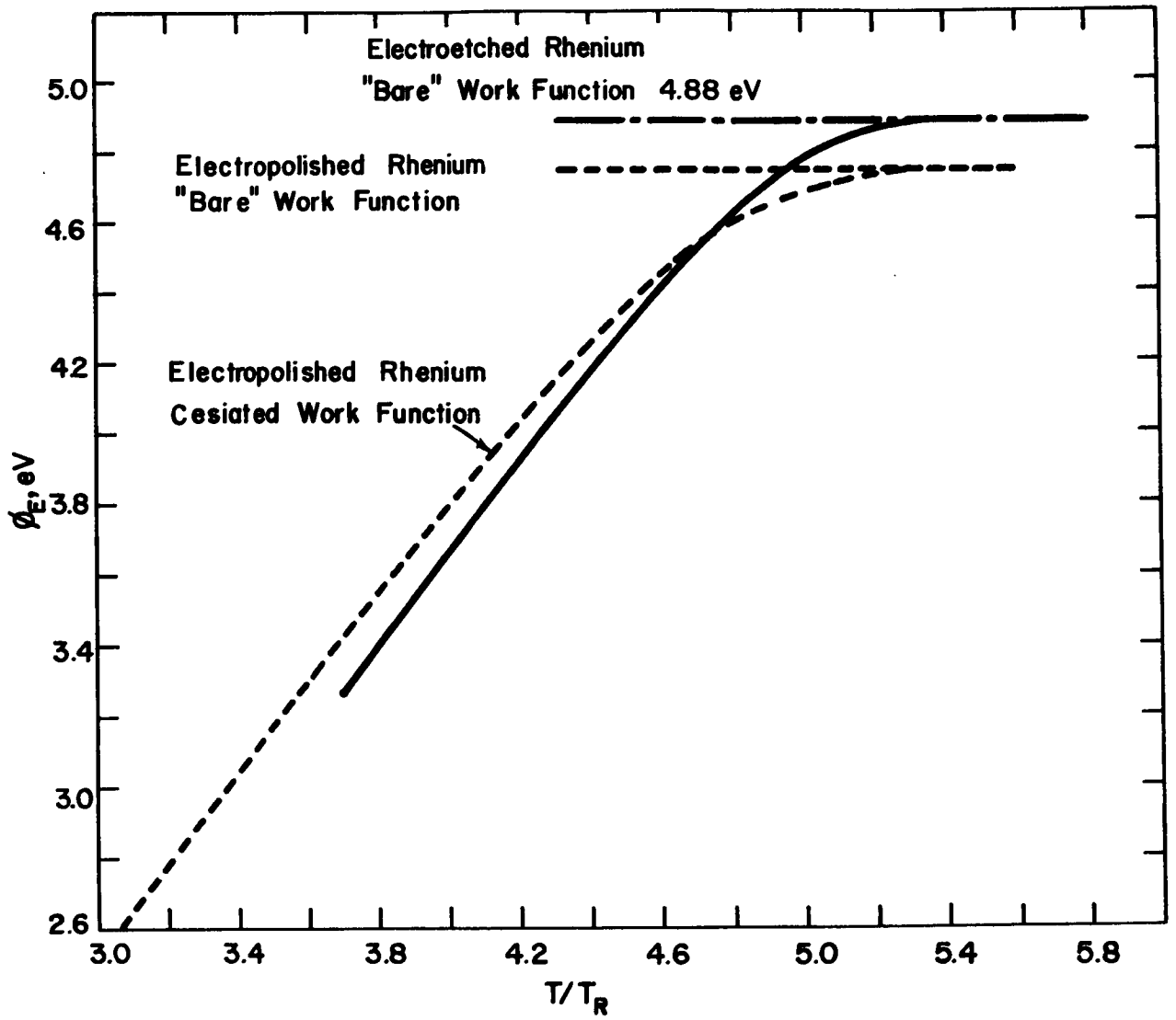

Figure VI-7. Comparison of the Work Functions of Electroetched and Electropolished Rhenium.

reservoir temperature, collector temperature, emitter temperature and interelectrode spacing. A total of 125 families, representing about 1000 individual J-V curves, were required to complete the study.

The performance of the device has been summarized using the envelopes of the variable-cesium-reservoir-temperature families. Figures VI-8 through VI-12 show this summary. Each figure shows the envelopes of several families taken at different interelectrode spacings but the same emitter and collector temperature. The collector temperature indicated was selected near the optimum value corresponding to the emitter temperature used. The dashed line in these figures represents the envelope of the spacing envelopes corrected for the emitter lead voltage loss. It corresponds to the output at the electrodes under fully optimized conditions for the emitter temperature indicated.

The fully optimized performance has been summarized in Figure VI-13, and the fully optimized electrode power output is shown in Figure VI-14. Comparison of Figure VI-14 with the corresponding figure for electropolished rhenium of Ref. 1 indicates that the etched rhenium has shown substantial improvement. This performance improvement is equivalent to an increase in spacing by a factor of 2.

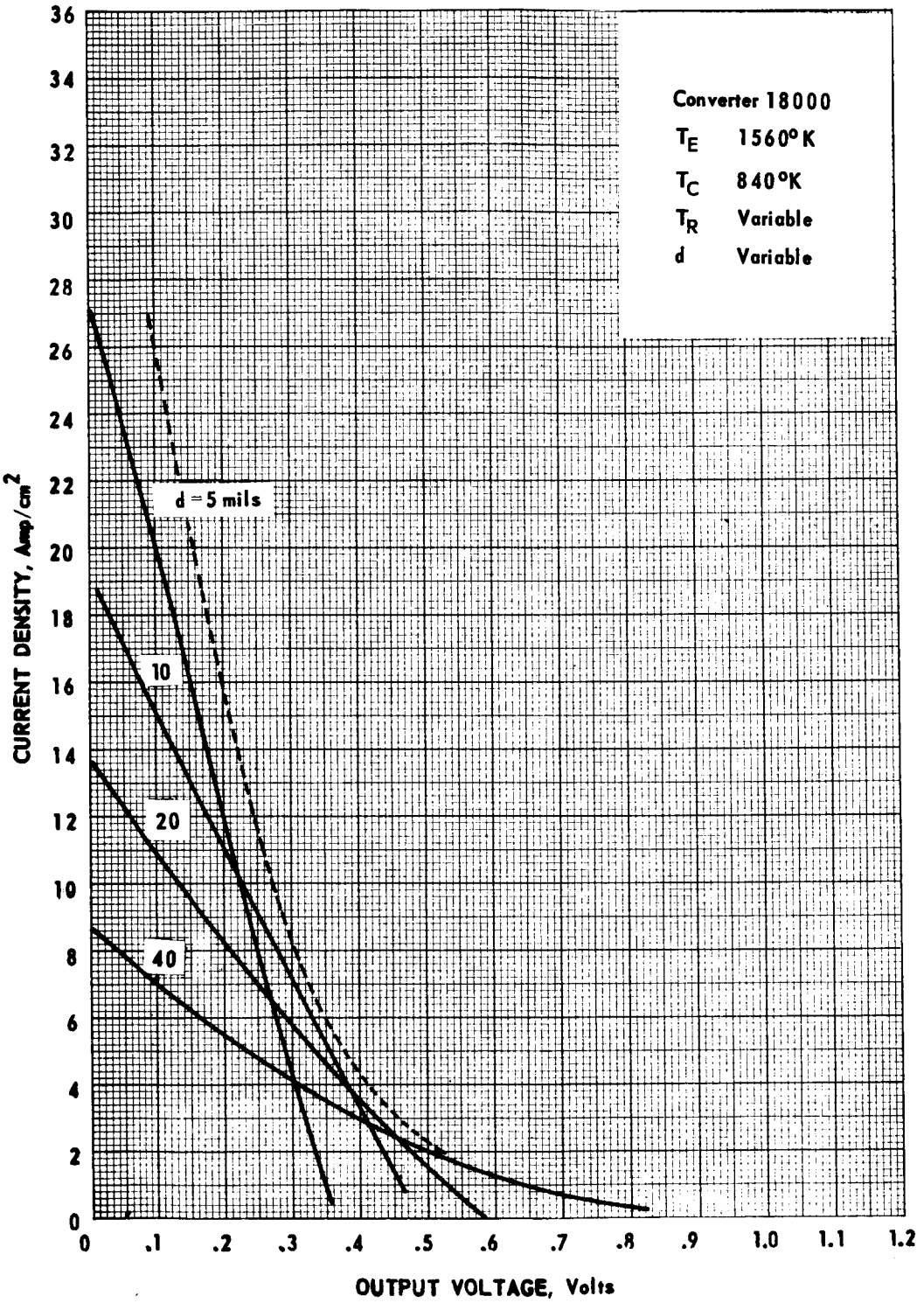

Figure VI-8. Summary of J-V Families at 1560°K.

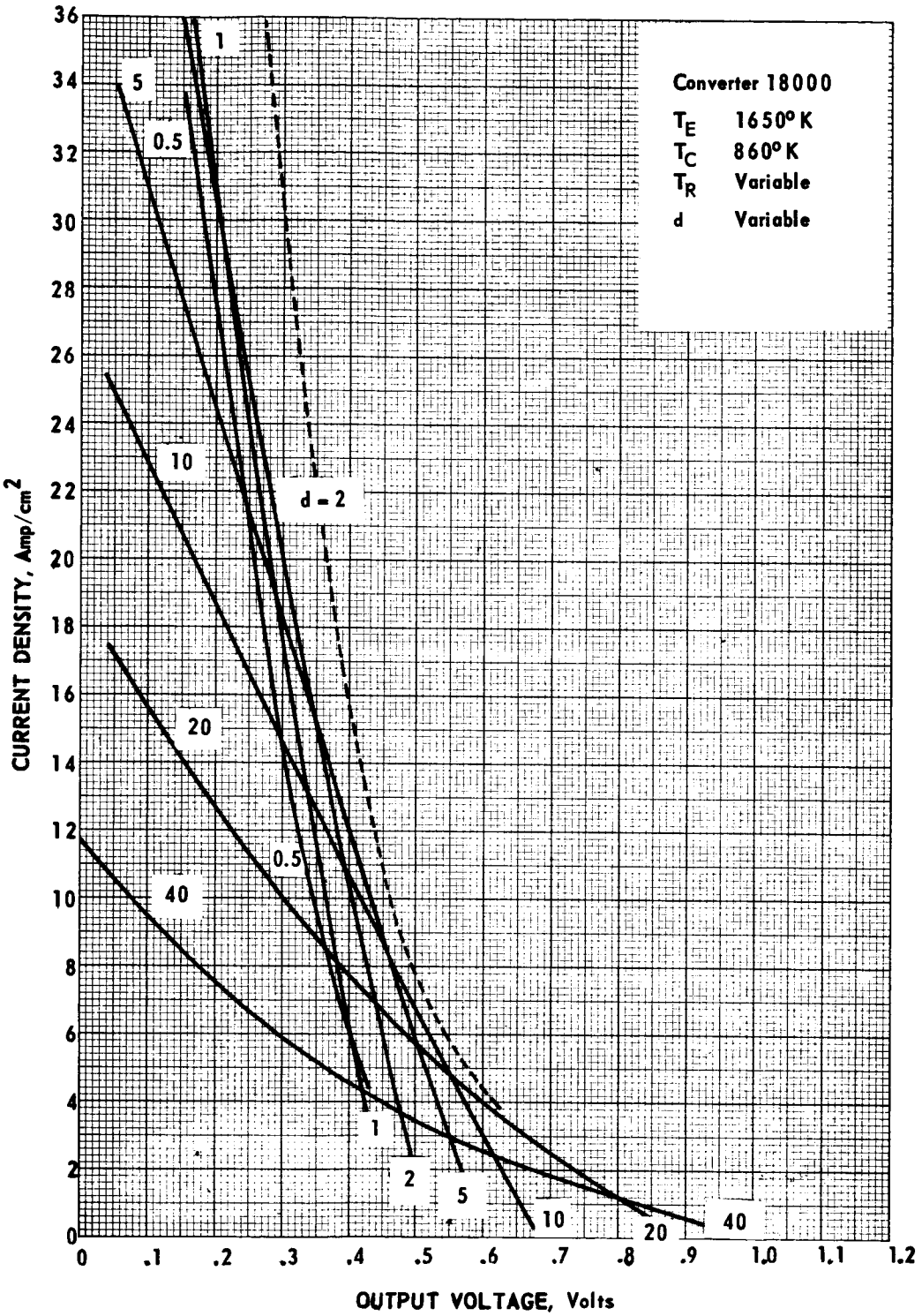

Figure VI-9. Summary of J-V Families at 1650°K.

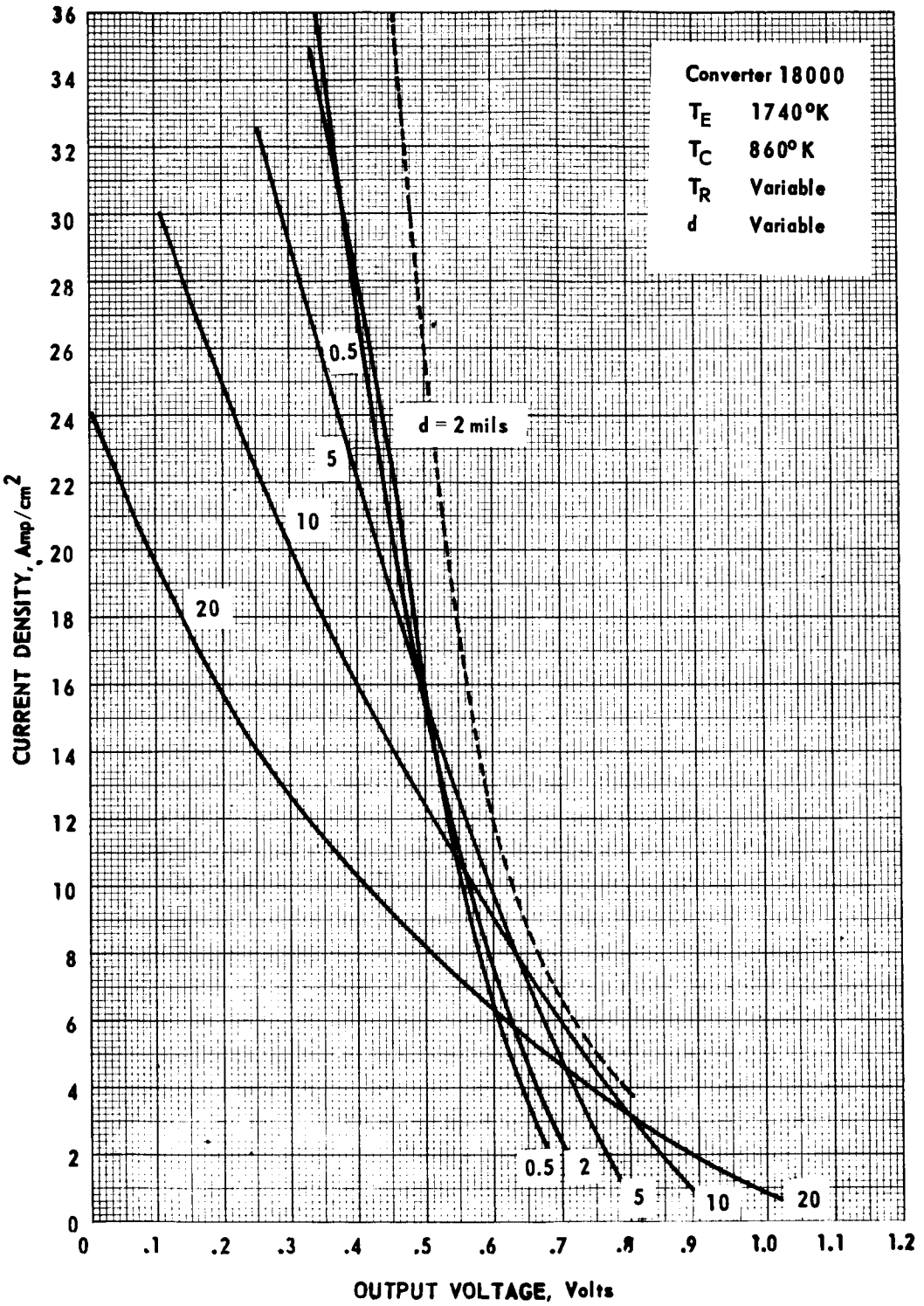

Figure VI-10. Summary of J-V Families at 1740 °K.

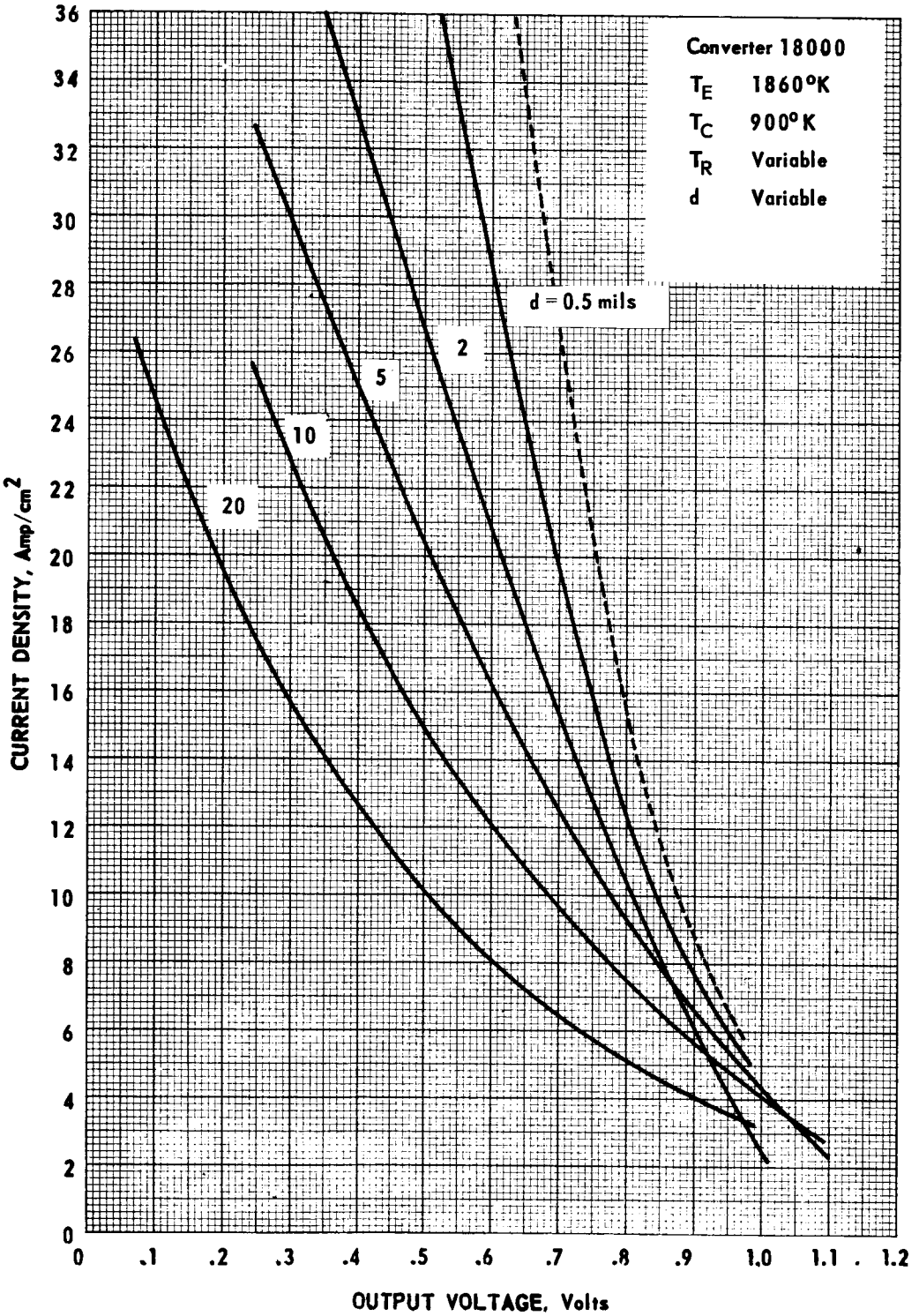

Figure VI-11. Summary of J-V Families at 1860°K.

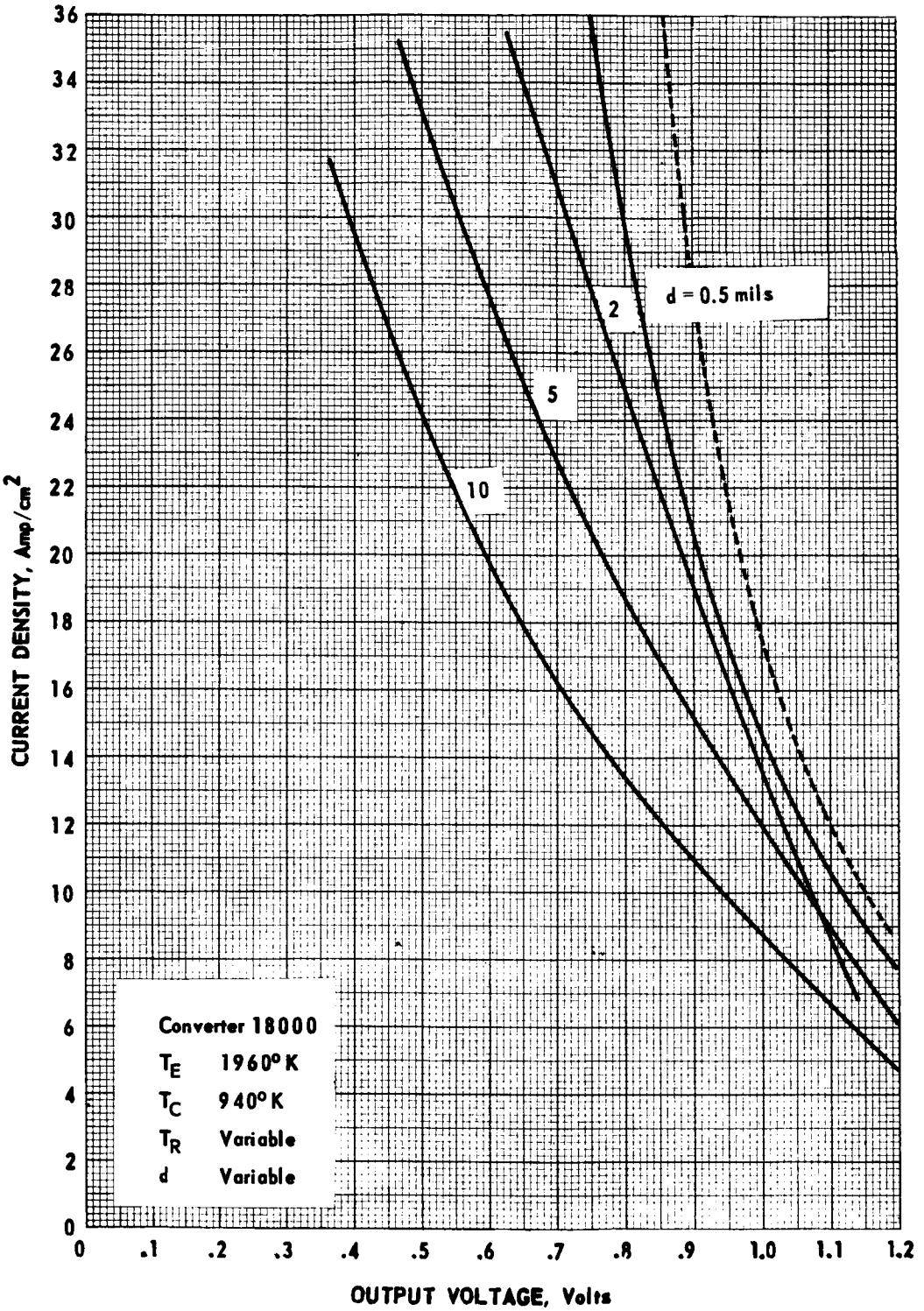

Figure VI-12. Summary of J-V Families at 1960°K.

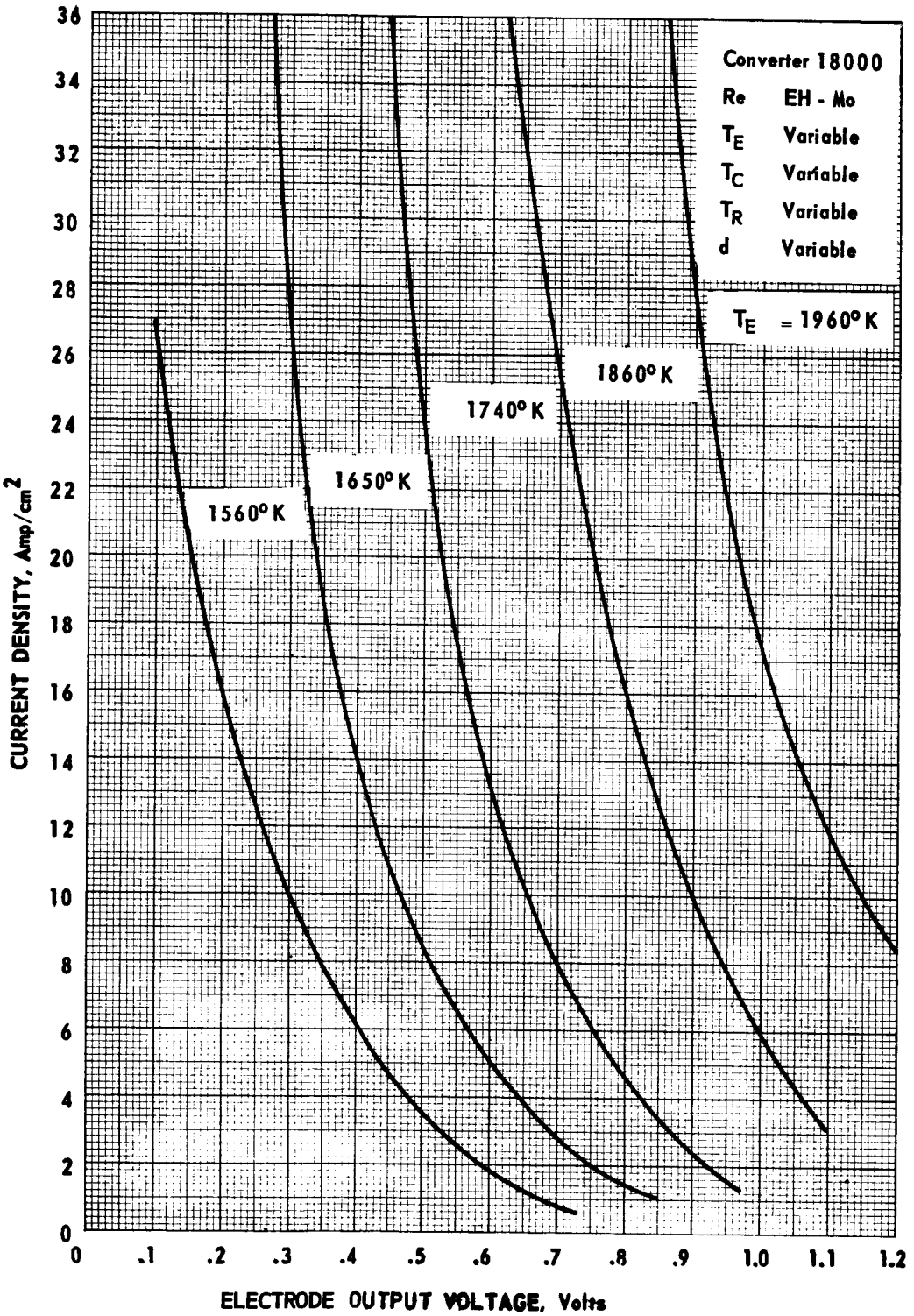

Figure VI-13. Fully Optimized Performance Map.

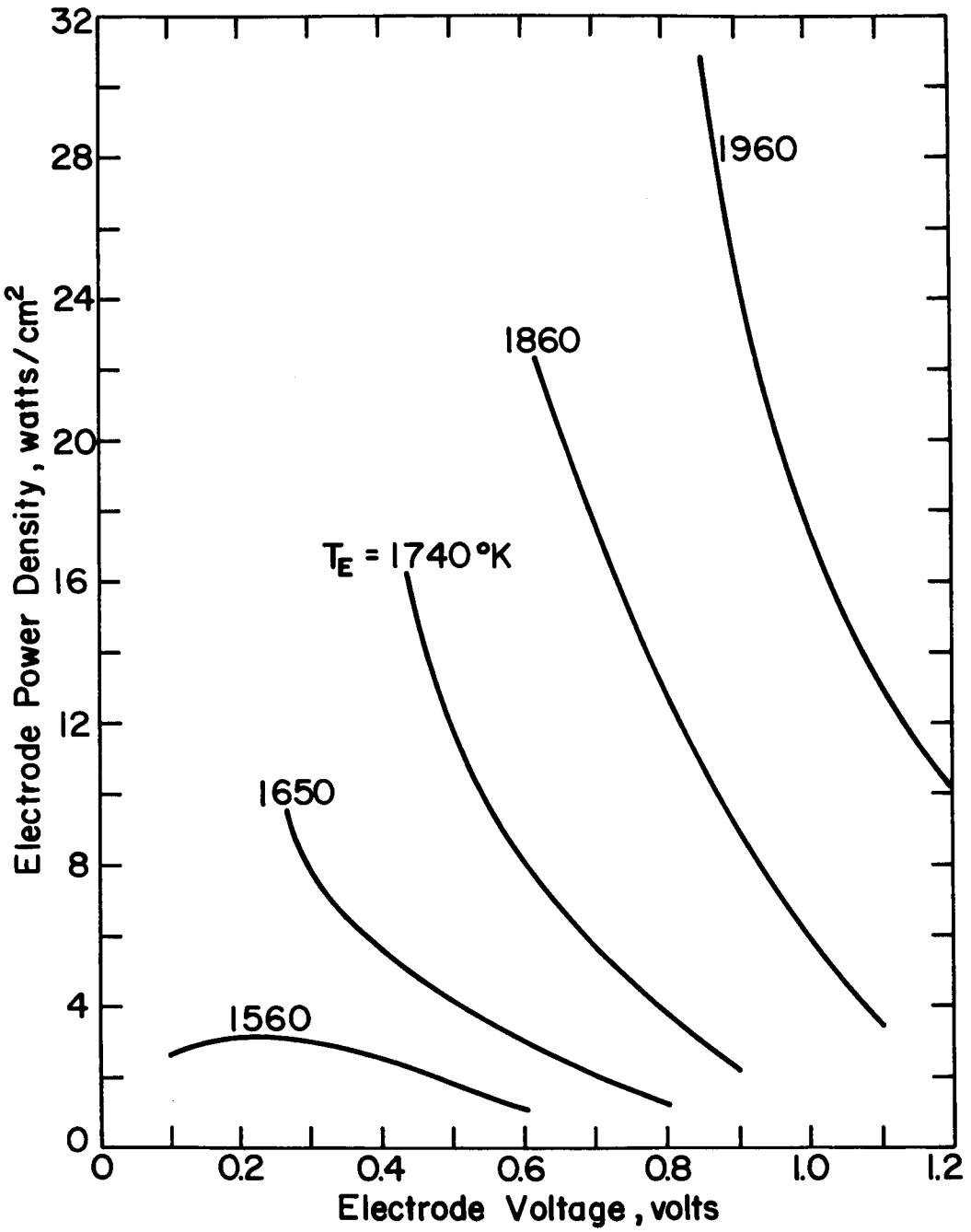

Figure VI-14. Fully Optimized Electrode Power Output Map.

REFERENCE

CHAPTER VI

1. Kitrilakis et al., "Final Report for the Thermionic Research Program, Task IV, Contract No. 950671," Thermo Electron Report No. TE 7-66, Prepared for Jet Propulsion Laboratory, Pasadena, California (1965).

CHAPTER VII

INERT GAS STUDIES

A. Introduction

Previous studies of volt-ampere characteristics in the presence of inert gases have been limited to several scattered operating points, and a very narrow range of converter variables was examined.[1,2] Moreover, in the earlier experiments the effect of inert gases was usually overshadowed by the interaction of gaseous impurities with the electrode surfaces.[3] Therefore, a more comprehensive investigation of the effect of inert gases on the output characteristics of converters is important for several reasons:

First, the addition of inert gases to the interelectrode plasma provides a new experimental technique to aid in the analysis of volt-ampere characteristics in the ignited mode. For example, the collision probability of electrons with cesium atoms may be compared with the known values for inert gases.

Second, the ionization of cesium atoms by electron impact results in an internal voltage drop which is observed as a decrease in the output voltage. There is a possibility that conservation of cesium ions in the interelectrode space may reduce the voltage drop. The possible ion loss mechanisms include diffusion to the electrodes, and recombination with electrons, but there is not yet enough data available to determine which mechanism is dominant. If diffusion is the major cause, the loss rate may be decreased by reducing the diffusion coefficient of the ions in the plasma through the addition of another gas. Most of the gases that act as a diffusion barrier for ions will cause an appreciable reduction in the flow of electrons. Inert gases, however, are possible exceptions to this rule, and therefore would be excellent additives for experiments of this type.

Third, inert gases comprise a significant portion of the gaseous fission products in nuclear reactors. Therefore, the possibility exists that these gases will be present in the interelectrode space of converters in nuclear thermionic reactors. Since a high pressure of inert gases causes an attenuation in electron current, it is important to know the functional dependence of electron current attenuation on inert gas pressure.

In the past, an inherent difficulty in this type of experiment has been the presence of impurities in the inert gases. Even the highest-purity research-grade gases available contain a high enough percentage of extraneous gases to prevent the achievement of any meaningful results. It was shown in Chapter V that the presence of oxygen at a pressure of about 10^{-8} torr changes the emitter work function, and therefore the emission characteristics, appreciably. If 100 torr of argon is injected into the diode, a pressure of 10^{-8} torr of oxygen will be present in the interelectrode space if this impurity is present in a concentration of only one part per million. The highest-purity inert gases available contain at least 5 parts per million of impurities.

Another major difficulty in inert-gas studies has been the design of a successful method of control over the inert gas pressure while the diode is operating. If the pressure of the inert gas can be varied without changing the diode parameters, this will eliminate any experimental errors that would result from resetting the parameters. Comparison of the data at various inert-gas pressures would therefore be more meaningful.

A thorough literature survey was carried out to select the most appropriate gas for these experiments. The results of this survey are summarized in Section B of this chapter. The experimental problems of impurities and pressure control discussed above were solved (Section C and D-3). An apparatus consisting of

a parametric diode and a gas injection system was designed and constructed (Section C). The use of inert gases as a research tool is introduced in Section D, and their overall effects are discussed in Section E. The conclusions of these investigations are summarized in Section F.

B. Selection of Plasma Additives

Selection of the gas additives was made on the basis of their use as diffusion barriers for cesium ions. The gases appropriate for this purpose usually have a high scattering cross section for electrons. Therefore, although these gases form good diffusion barriers for ions, they also attenuate electron current. Inert gases, however, are an exception to this rule. Ramsauer and Kolath[4] investigated the dependence of the collision probability of inert gases on electron energy. They discovered that the collision probability has a minimum value in the electron energy range of 0.2 - 0.7 eV. Electron energies encountered in the operation of thermionic diodes are well within this range. Inert gases, therefore, can be used as diffusion barriers for ions without causing an appreciable attenuation of electron current.

An extensive literature survey was carried out to select the most appropriate inert gas for this experiment. A list of the important references is included in this report.[1-18] The values of the transport parameters reported by these authors were used in a simplified calculation to estimate the relative effects of Ar, Kr and Xe on the scattering of electrons and cesium ions.

The attenuation of electron or ion current due to scattering by the inert gases is calculated for the short- and long-mean-free-path cases.†

† See Chapter VIII for the derivations.

$$\frac{J}{J^*} = \exp(-d/\lambda) \qquad \text{for } (d/\lambda) << 1$$

$$\frac{J}{J^*} = \frac{1}{1 + \frac{3}{4}\frac{d}{\lambda}} \qquad \text{for } (d/\lambda) << 1$$

J = attenuated current of ions or electrons

J^* = incident current of ions or electrons

d = interelectrode spacing

λ = electron or ion mean free path

The values of electron mean free path in Ar, Kr and Xe were calculated from the values of the collision probability reported by Ramsauer and Kollath.[4] The mean free path of cesium ions in Kr and Xe was obtained from the values of mobility reported by Powell and Brada[6] and for argon from those reported by Chanin and Biondi.[7] The approximate values of collision probability for electrons in inert gases are:

	Collision Probability cm^2/cm^3 of vapor at 0°C and 1 torr
Ar	1
Kr	2
Xe	5

These values correspond to an electron energy of about 0.4 eV. The absorption coefficient is given by

$$P_c = n_o \sigma$$

where n_o is the particle density at 0°C and 1 torr and is equal to 3.5×10^{16} particles/cm^3, and σ is the collision cross section in cm^2.

In general, the mean free path, λ, is calculated from the equation

$$\lambda = \frac{n_o}{n} \frac{1}{P_c}$$

where n is the particle density. Mobility and diffusion coefficients are related by Einstein's relation

$$\mu = \frac{eD}{kT}$$

where μ = mobility of ions

D = diffusion coefficient

T = average gas temperature

k = Boltzmann constant

Diffusion coefficient, in turn, is related to mean free path by

$$D = \frac{v\lambda}{3}$$

where v is the velocity of the particles in cm/sec.

The mobility of Cs ions in Kr and Xe, as given by Powell and Brada[6] at one atmosphere of pressure, is:

	μ $cm^2/sec\ volt$
Kr	1.4
Xe	1.0

The value for argon is given by Chanin and Brondi at one atmosphere:

$$\mu = 2\ cm^2/sec\ volt$$

By converting these values to mean free path and calculating the attenuation of electrons and cesium ions at 1 torr pressure and 1000°K average gas temperature for a 10-mil interelectrode spacing, Table VII-1 is obtained. From examination of this table, it is evident that argon is the most appropriate inert gas to serve as an ion diffusion barrier. Although the effectiveness of all three gases as diffusion barriers is similar, argon was chosen for the plasma experiments because it produces much less electron attenuation.

C. Experimental Apparatus

The experimental apparatus consists of a variable-parameter diode and a gas injection system. The diode was discussed in detail in Chapter III. A modification in the cesium reservoir was necessary to allow the inert gas to be introduced and its pressure to be changed while the diode is operating.

The principle of operation of the reservoir is illustrated in Figure VII-1. Pressure equilibrium is maintained between the reservoir and the diode by a tubulation which is kept at about 500°C. Argon is introduced into the diode through a series of baffles and a 60-mil orifice. The cesium pressure in the diode is still determined by the temperature of the liquid in the reservoir, since the liquid-gas interface area is much larger than the orifice area. Any cesium that passes through the orifice is condensed by the baffles and flows back to the reservoir.

The gas injection system is shown schematically in Figure VII-2. The high-purity standard gas is stored in a cylinder equipped with a two-stage regulator. The gas is introduced into a 75-cc stainless-steel cylinder at a pressure of about 2 atmospheres. A micro-flow valve allows the rest of the system to be filled to the desired pressure in the range of 0.2 - 200 torr. The inert gas passes through a cold trap and a hot zirconium trap to minimize the impurities. The gas pressure in the converter is monitored by a diaphragm pressure gauge. The pumping system

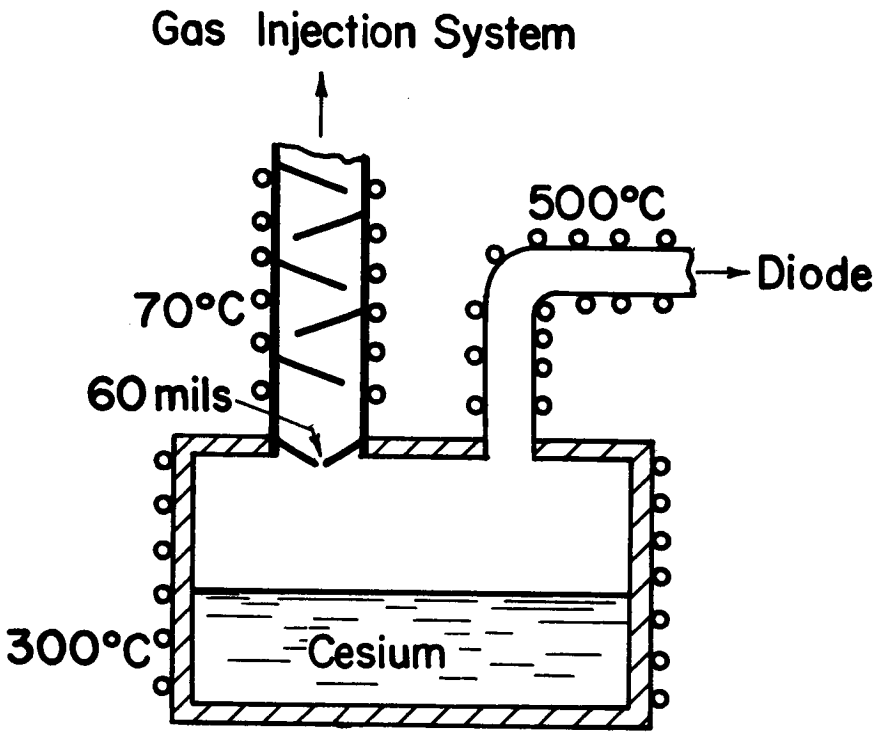

Figure VII-1. The Modified Cesium Reservoir.

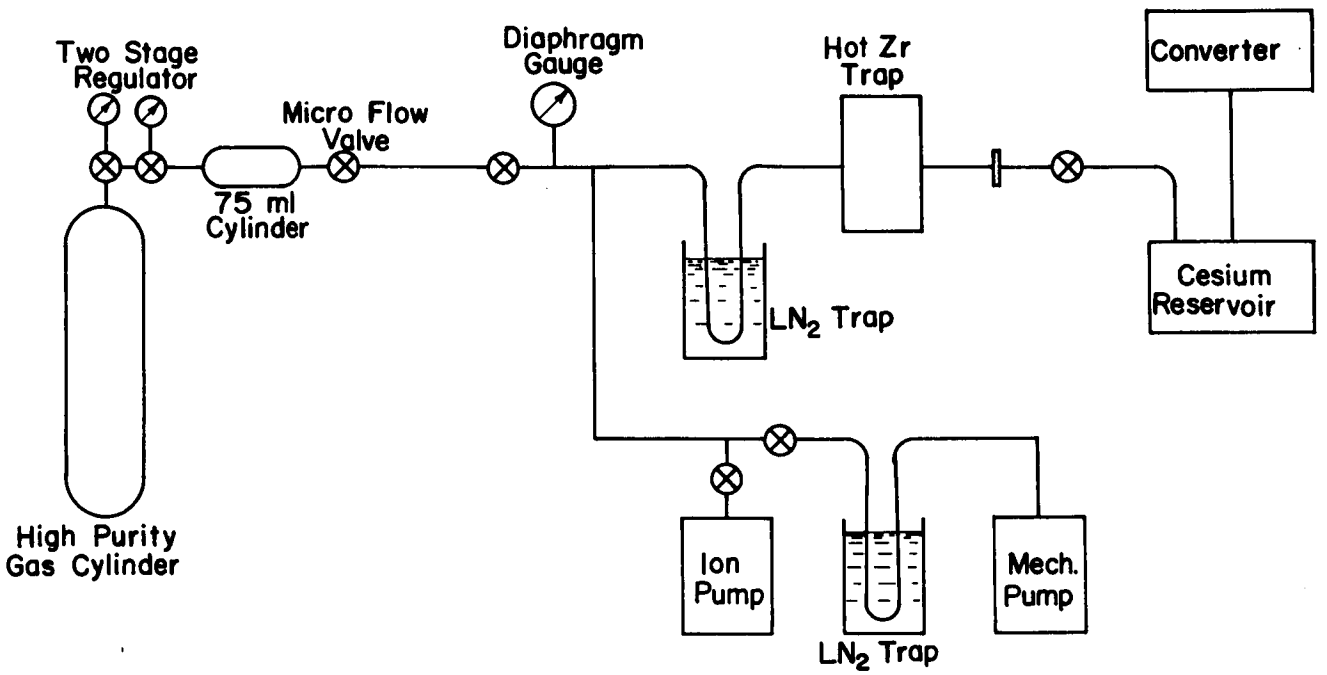

Figure VII-2. Schematic of the Standard Gas Injection System.

TABLE VII-1

EFFECT OF ADDITION OF 1 TORR OF INERT GAS
IN A 10-MIL WIDE PLASMA AT 1000°K

Inert Gas	λ_i, mils	λ_e, mils	$\frac{J_i}{J_i^*} = \frac{1}{1+\frac{3}{4}\frac{d}{\lambda_i}}$	$\frac{J_e}{J_e^*} = e^{-d/\lambda_e}$	Ion Current Attenuation	Electron Current Attenuation
A	4.2	1400	0.36	0.993	64%	0.7%
Kr	2.9	700	0.28	0.986	72%	1.4%
Xe	1	280	0.22	0.968	78%	3.2%

THERMO ELECTRON
ENGINEERING CORPORATION

consists of an ion pump, which can be isolated by an all-metal on-off valve, and a mechanical pump used for roughing the entire system.

D. The Ignited Mode in Presence of Inert Gases

1. Introduction. Electron scattering is a major phenomenon occurring in the interelectrode space of thermionic diodes This process is especially important in the ignited mode of operation because of the high particle concentration. In this section, inert gases are used to introduce an extra degree of freedom in the analysis of the ignited mode.

2. Theory. In this analysis, use is made of the motive diagram postulated by Rasor[22] for the ignited mode, shown in Figure VII-3. The electron current J_s leaves the emitter surface, and the current J arrives at the collector. The difference between J_s and J is back-scattered to the emitter. The assumption is made that the interelectrode space is composed of a neutral plasma of width d, much larger than the electron mean free path, bounded by the emitter and collector sheaths, V_e and V_c, of negligible thickness. In the quasi-saturation mode, as the output voltage V is increased, V_e is decreased. The transition from the quasi-saturation mode to the obstructed mode takes place when the emitter sheath height is equal to V'_e. This analysis is mainly concerned with the quasi-saturation mode.

Since there are no appreciable sources or sinks in the neutral plasma, the diffusion equation is

$$\nabla^2 n = 0 \tag{1}$$

At the emitter side of the plasma (x = 0), the current entering the plasma is

$$\left[\frac{vn}{4} - \frac{1}{6}\frac{1}{\rho_1\Psi_1 + \rho_2\Psi_2}\frac{dn}{dx}\right] = J_s + \left[\frac{vn}{4} + \frac{1}{6}\frac{1}{\rho_1\Psi_1 + \rho_2\Psi_2}\frac{dn}{dx}\right]\left[1 - \exp\left(-V_E/kT_{\epsilon E}\right)\right] \tag{2}$$

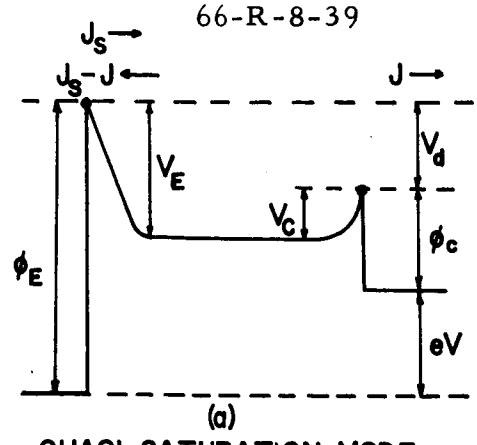

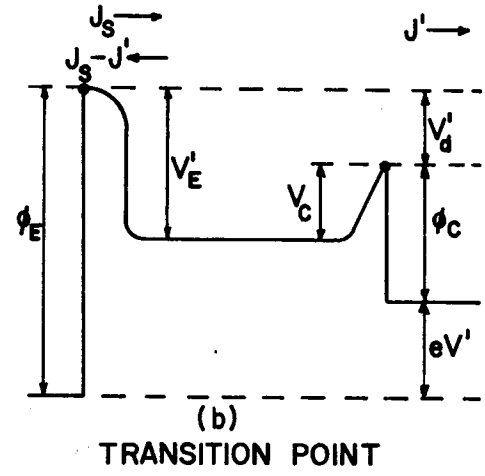

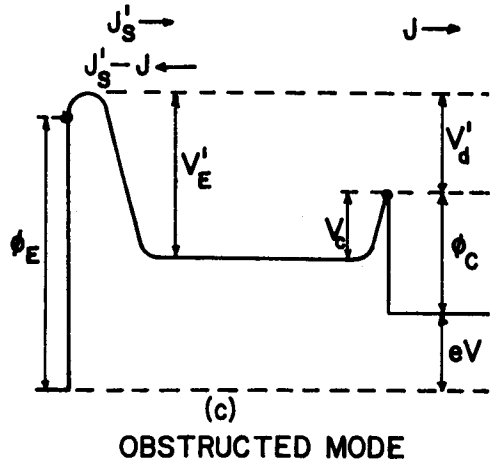

Figure VII-3. Modes of Discharge.

Similarly, at the collector side (x = d),

$$\frac{vn}{4} + \frac{1}{6}\frac{1}{\wp_1\Psi_1 + \wp_2\Psi_2}\frac{dn}{dx} = J_{cs} + \left[\frac{nv}{4} - \frac{1}{6}\frac{1}{\wp_1\Psi_1 + \wp_2\Psi_2}\frac{dn}{dx}\right]\left[1 - \exp(-V_c/kT_{\epsilon c})\right] \quad (3)$$

where v is the average electron velocity, n is the electron density, J_s and J_{cs} are the emitter and collector saturation currents, $T_{\epsilon E}$ and $T_{\epsilon C}$ are the electron temperatures at the emitter and collector edges of the plasma, $\wp$ is the pressure and Ψ is the effective collision probability, defined by

$$\Psi = \int_0^\infty P_c(E)\, f(E)\, dE \quad (4)$$

where P_c is the collision probability at 0°C and 1 torr, f(E) is the Maxwell distribution of electrons and E is the electron energy. The subscripts 1 and 2 refer to cesium and argon. The solution to the differential equation is:

$$n(x) = C_1 x + C_2 \quad (5)$$

where

$$C_1 = \frac{J_{cs}\exp[V_c/kT_{\epsilon c}] - J_s\exp[T_E/kT_{\epsilon E}]}{\frac{1}{3\wp_1\Psi_1 + \wp_2\Psi_2}[\exp(V_c/kT_{\epsilon c}) + \exp(V_E/kT_{\epsilon E}) - 1] + \frac{d}{4}} \quad (6)$$

$$C_2 = 4J_s\exp(V_E/kT_{\epsilon E}) +$$

$$[4\exp(V_E/kT_{\epsilon E}) - 2]\frac{J_{cs}\exp(V_c/kT_{\epsilon E}) - J_s\exp(V_E/kT_{\epsilon E})}{\exp(V_c/kT_{\epsilon c}) + \frac{3d}{4}(\wp_1\Psi_1 + \wp_2\Psi_2) - 1 + \exp(V_E/kT_{\epsilon E})} \quad (7)$$

and $T_{\epsilon E}$ and $T_{\epsilon C}$ are the electron temperatures at the emitter and collector ends

of the plasma. The net current through the plasma is required by Fick's law to be

$$J = \frac{1}{3(\wp_1 \Psi_1 + \wp_2 \Psi_2)} \frac{dn}{dx} \tag{8}$$

Combining equations (4), (5) and (7), we get

$$J = \frac{J_s \exp\left[V_E/kT_{\epsilon E}\right] - J_{cs} \exp\left[V_c/kT_{\epsilon c}\right]}{\frac{3d}{4}(\wp_1 \Psi_1 + \wp_2 \Psi_2 + \exp\left[V_c/kT_{\epsilon c}\right] + \exp\left[V_E/kT_{\epsilon E}\right] - 1} \tag{9}$$

In equation (9) the net current through the plasma is given in terms of plasma parameters. To facilitate comparison with experimental results, this equation will be simplified. The back emission from the collector is usually small and can be neglected, subject to the following condition:

$$J_{cs} \ll J_s \exp\left[\frac{V_E}{kT_{\epsilon c}}\right] \tag{10}$$

Neglecting back emission, equation (9) becomes:

$$\frac{J_s}{J} = \exp\left[\frac{V_c}{kT_{\epsilon c}} - \frac{V_E}{kT_{\epsilon E}}\right] - \exp\left[\frac{-V_E}{kT_{\epsilon E}}\right] + 1$$

$$+ \frac{3}{4}(\wp_1 \Psi_1 + \wp_2 \Psi_2)\, d \exp\left[-V_E/kT_{\epsilon E}\right] \tag{11}$$

From the motive diagram in Figure VII-4 we get:

$$V_E = \phi_E - \phi_c + V_c - eV \tag{12}$$

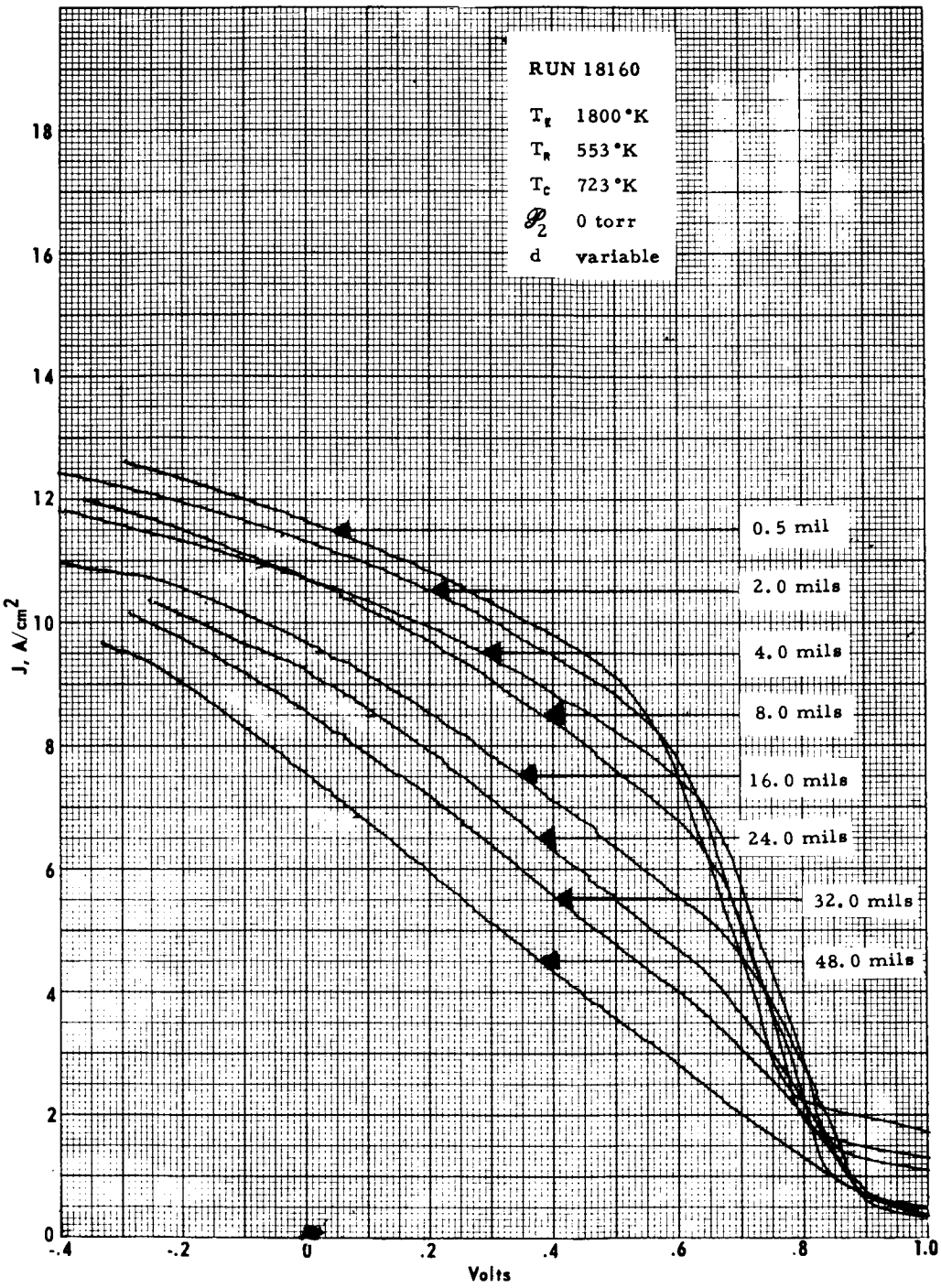

Figure VII-4. Typical Variable-Spacing Electrical Output Characteristic.

Substituting (12) in (11) results in:

$$\frac{1}{J} = \frac{1}{J_s} + K \exp\left[\frac{eV}{kT}\right]\left[L + \frac{3}{4}\wp_1\Psi_1 d + \frac{3}{4}\wp_2\Psi_2 d\right] \tag{13}$$

where

$$K = \frac{1}{J_s}\exp\left[-\frac{\phi_\epsilon - \phi_c + V_c}{kT_{\epsilon\epsilon}}\right] \tag{14}$$

$$L = \exp\left[\frac{V_c}{kT_{\epsilon c}}\right] - 1 \tag{15}$$

According to equation (13), a plot of inverse current as a function of interelectrode spacing yields a straight line for each output voltage V.

3. Experimental Approach. The gas injection system has been described in detail in Section C. It consists of several bakable expansion chambers and pressure-regulating valves. The argon used in these experiments is the highest-purity research grade commercially available. Before injection into the diode, the gas is passed through a liquid-nitrogen trap to remove condensable impurities. During these experiments it was noticed, however, that in spite of all these precautions, the electron emission was increased by several orders of magnitude when argon was introduced into the system. This was traced to the presence of a residual oxygen pressure of the order of 10^{-8} torr. It is clear that this pressure of oxygen will result if the oxygen impurity in the argon is more than one part per billion at 100 torr of argon pressure.

To minimize its oxygen content, the argon was kept in a trap containing a mixture of zirconium and titanium chips at 400°C for about one hour. This technique was successful, as indicated by work function measurements. Several sets of variable-spacing families were obtained after the incorporation of these improvements.

4. Experimental Results and Conclusions. Several variable-spacing families of volt-ampere characteristics were obtained. The data covers the cesium temperature range of 533 to 563°K at emitter temperatures of 1675 and 1800°K, and the argon pressure range of 0 to 100 torr. Typical samples of variable-spacing families are shown in Figure VII-4. The variable-spacing families are plotted according to equation (15) in Figures VII-5 to VII-7. As predicted by the theory, the inverse current at constant voltage is a linear function of the interelectrode spacing. Furthermore, the constant-voltage lines converge to a single focal point whose coordinates, according to equation (15), are given by

$$\left[\frac{1}{J}\right]_o = \frac{1}{J_s} \tag{16}$$

and

$$[d_o] = \frac{-4L}{3(P_1 \Psi_1 + P_2 \Psi_2)} \tag{17}$$

Equation (17) is rearranged to give

$$\frac{-1}{[d]_o} = \frac{3}{4L} P_1 \Psi_1 + \frac{3}{4L} P_2 \Psi_2 \tag{18}$$

In the absence of inert gases, equation (18) shows that a plot of $\frac{1}{[d]_o}$ versus the cesium pressure P_1 is a straight line passing through the origin. At high argon pressures, however, there is an intercept which is proportional to the pressure and collision probability of argon. The coordinates of the focal points obtained from plots similar to Figures VII-5 to VII-7 are shown as a function of cesium pressure in Figure VII-8. This data was obtained at the argon pressures of 0, 48 and 100 torr. There is no significant difference between the data points

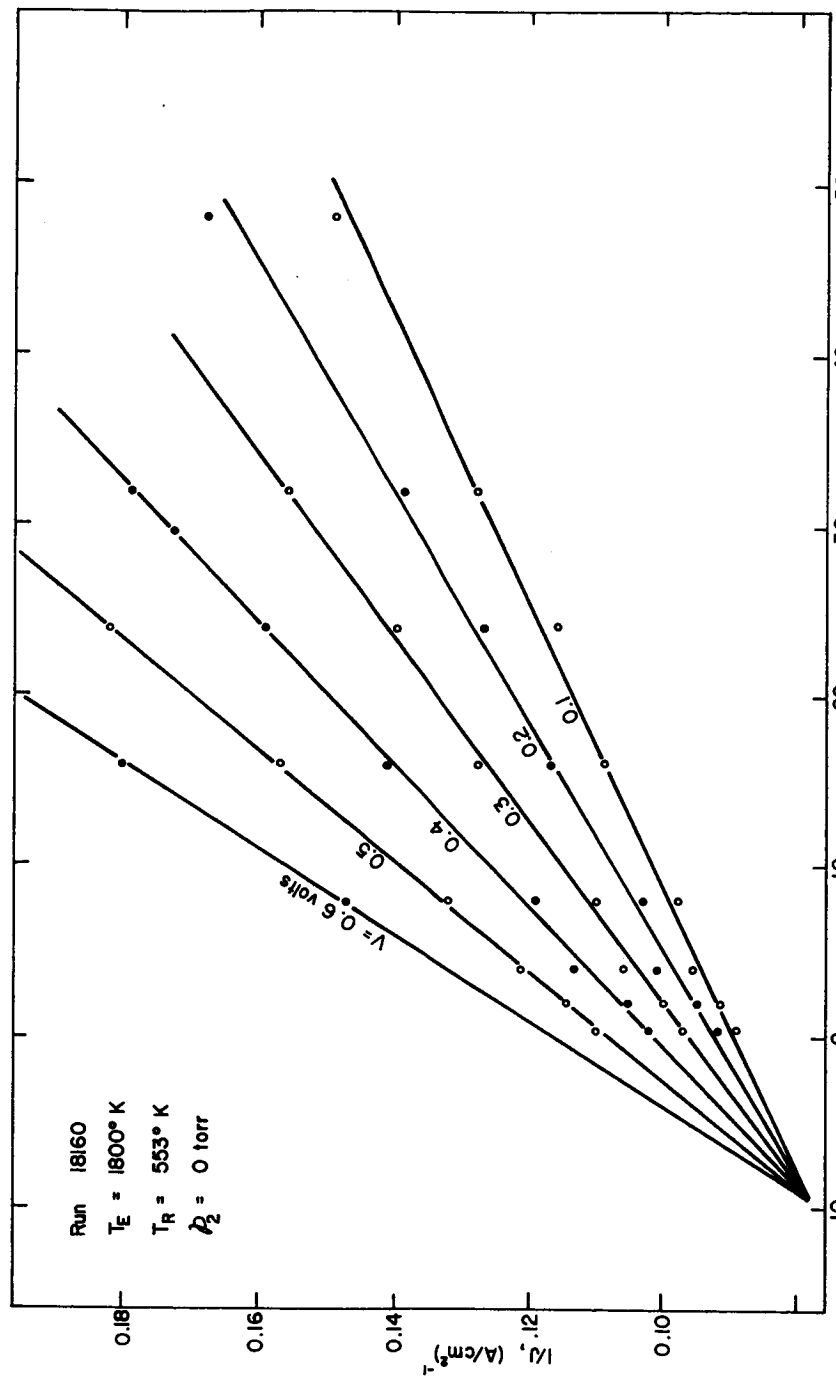

Figure VII-5. Plot of Variable-Spacing Families According to Equation (15).

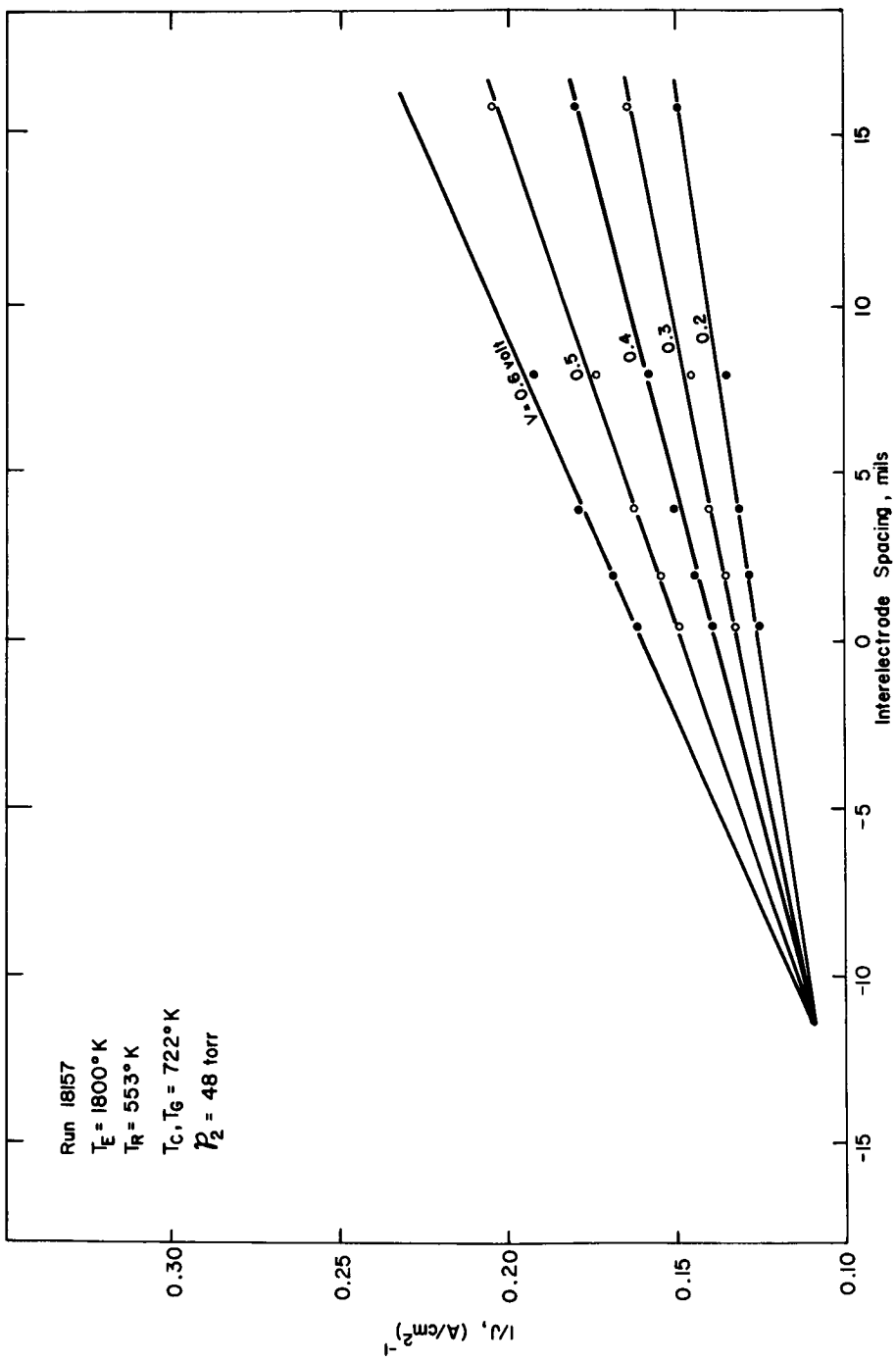

Figure VII-6. Variable-Spacing Families According to Equation (15).

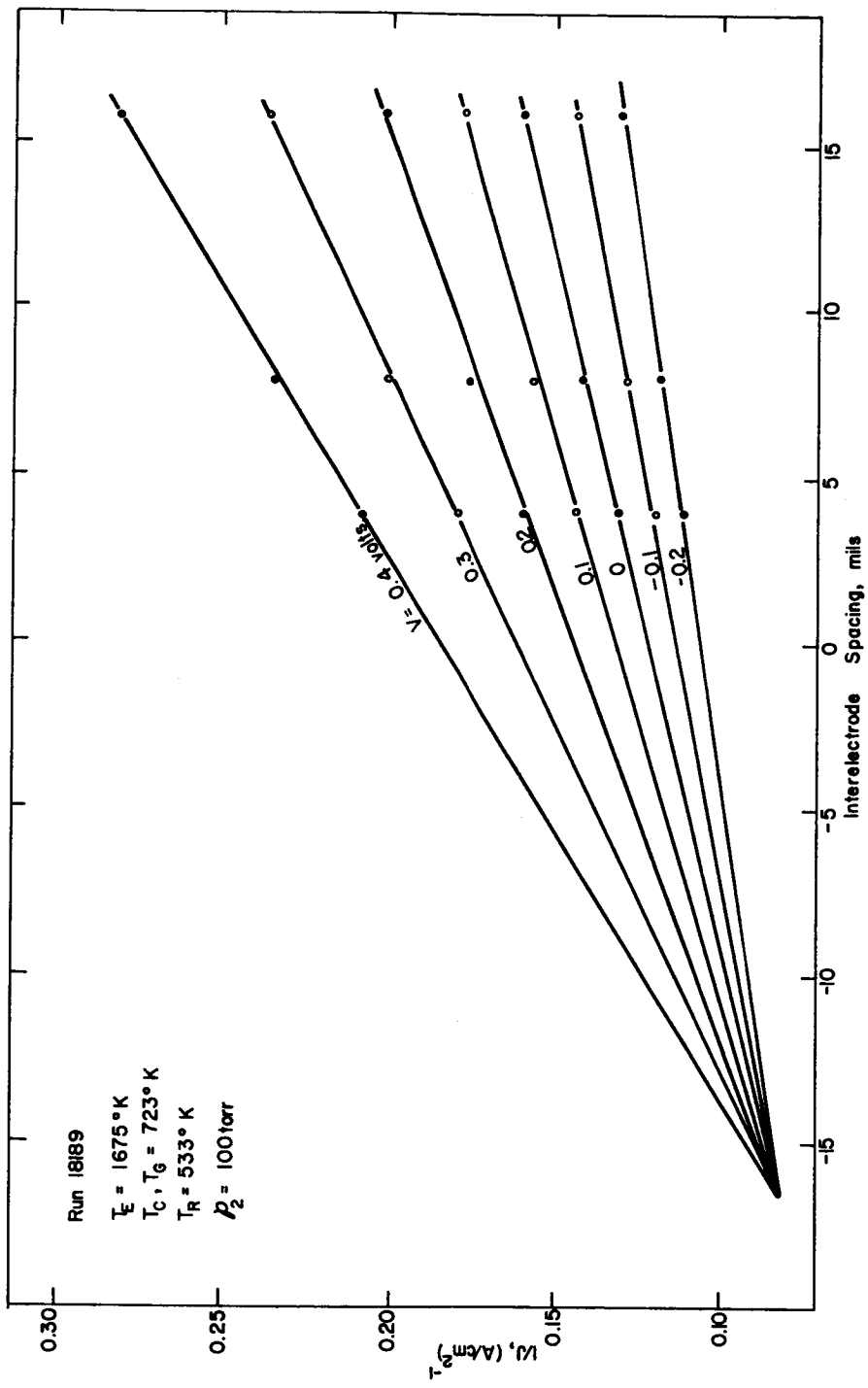

Figure VII-7. Plot of Variable-Spacing Families According to Equation (15).

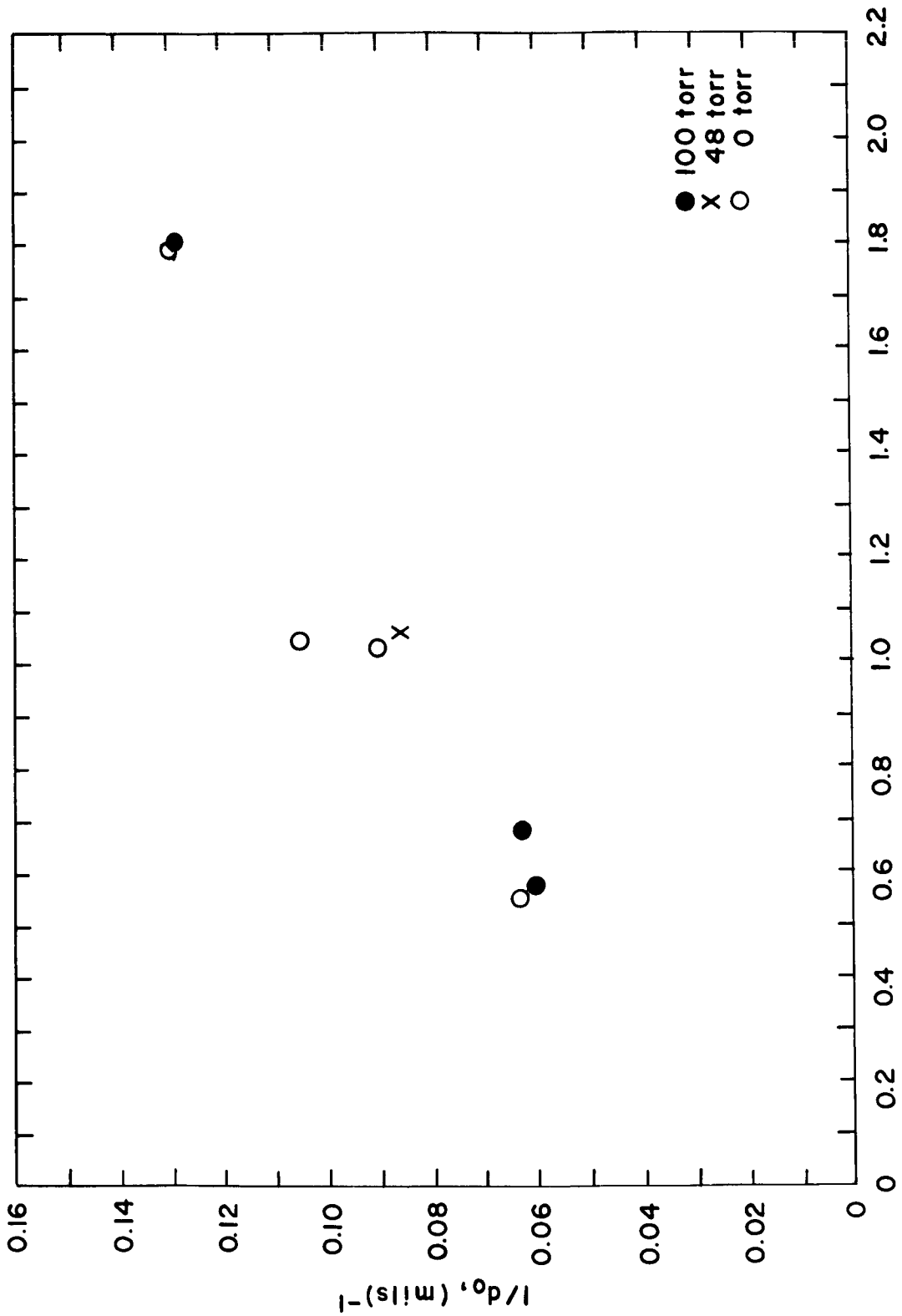

Figure VII-8. Plot of the Focal Points According to Equation (18).

at various argon pressures, whereas the dependence of $\frac{1}{d_o}$ on cesium pressure is observed clearly. This result indicates that even at 100 torr of argon, the electron scattering by argon is much less than the scattering by the lowest cesium pressure investigated (p_1 = 0.6 torr), or

$$p_2 \Psi_2 \ll p_1 \Psi_1 \tag{19}$$

The lower bound of the collision probability of cesium is therefore given by the equation

$$\Psi_1 \gg \frac{100}{0.6} \Psi_2 \tag{20}$$

The collision probability of argon has been measured by Ramsauer and Kolath[4] as a function of electron energy and is shown in Figure VII-9. The values shown are for monoenergetic electrons. In the ignited mode, however, there is a distribution of electron energy. The effective collision probability Ψ_2, which takes the electron energy distribution into account, is calculated from equation (4) and Figure VII-9. The effective collision probability for argon is plotted in Figure VII-10. The extrapolation of collision probability to zero energy reported by Pack et al.[25] was also used in this calculation.

For electron energy in the range of 0.3 - 0.4 eV, the effective collision probability for argon is about 4 cm^{-1}. The lower bound for the collision probability of cesium is calculated from equation (20) and is equal to 700 cm^{-1}.

From the results of this section, it may be concluded that: (a) the quasi-saturation region of the ignited mode is diffusion-dominated, (b) argon atoms are essentially transparent to electrons of energies encountered in the ignited mode of thermionic diodes, and (c) the lower bound of the collision probability of cesium atoms with electrons in the ignited mode is equal to 700 cm^{-1}.

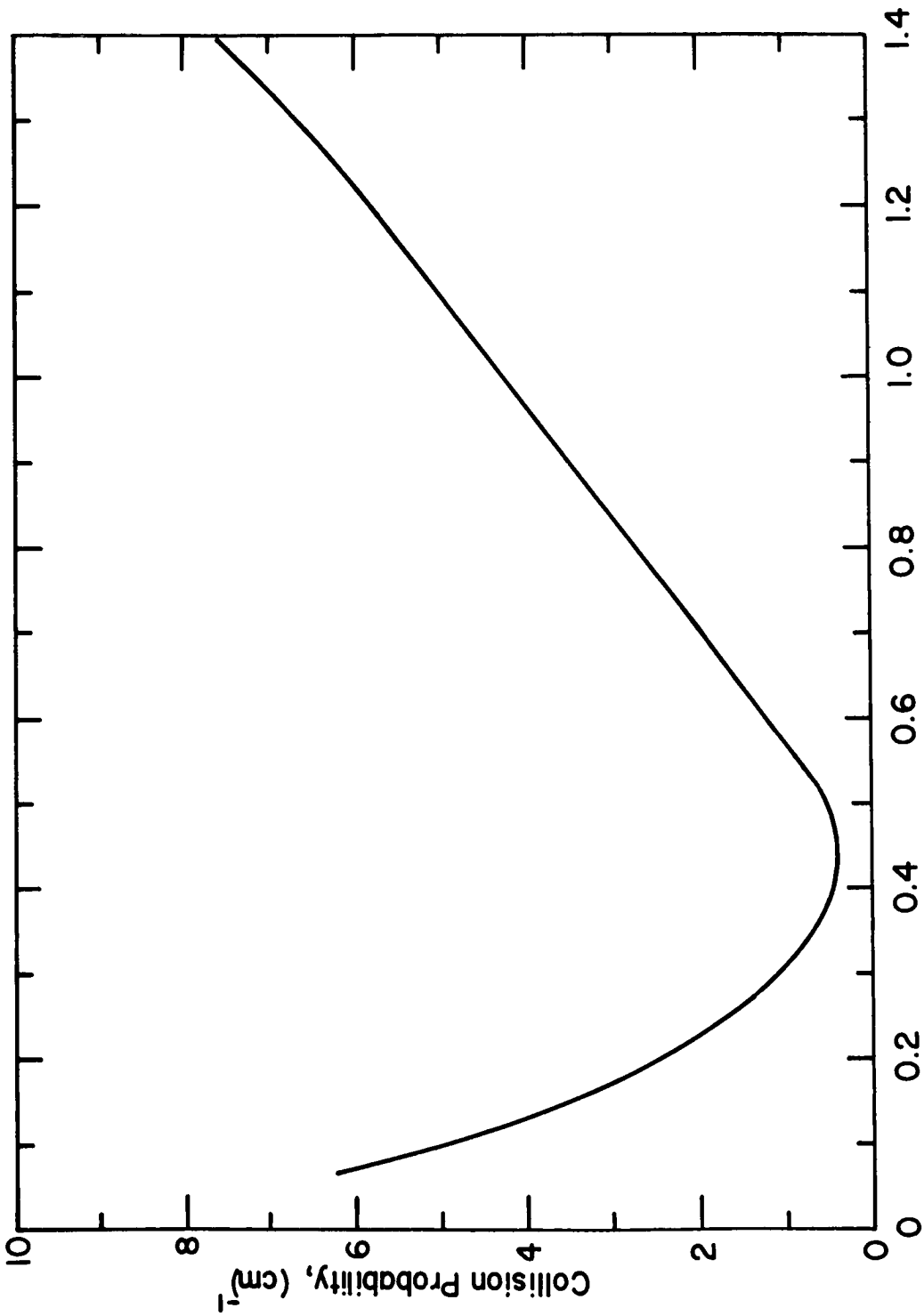

Figure VII-9. Collision Probability of Electrons with Argon.

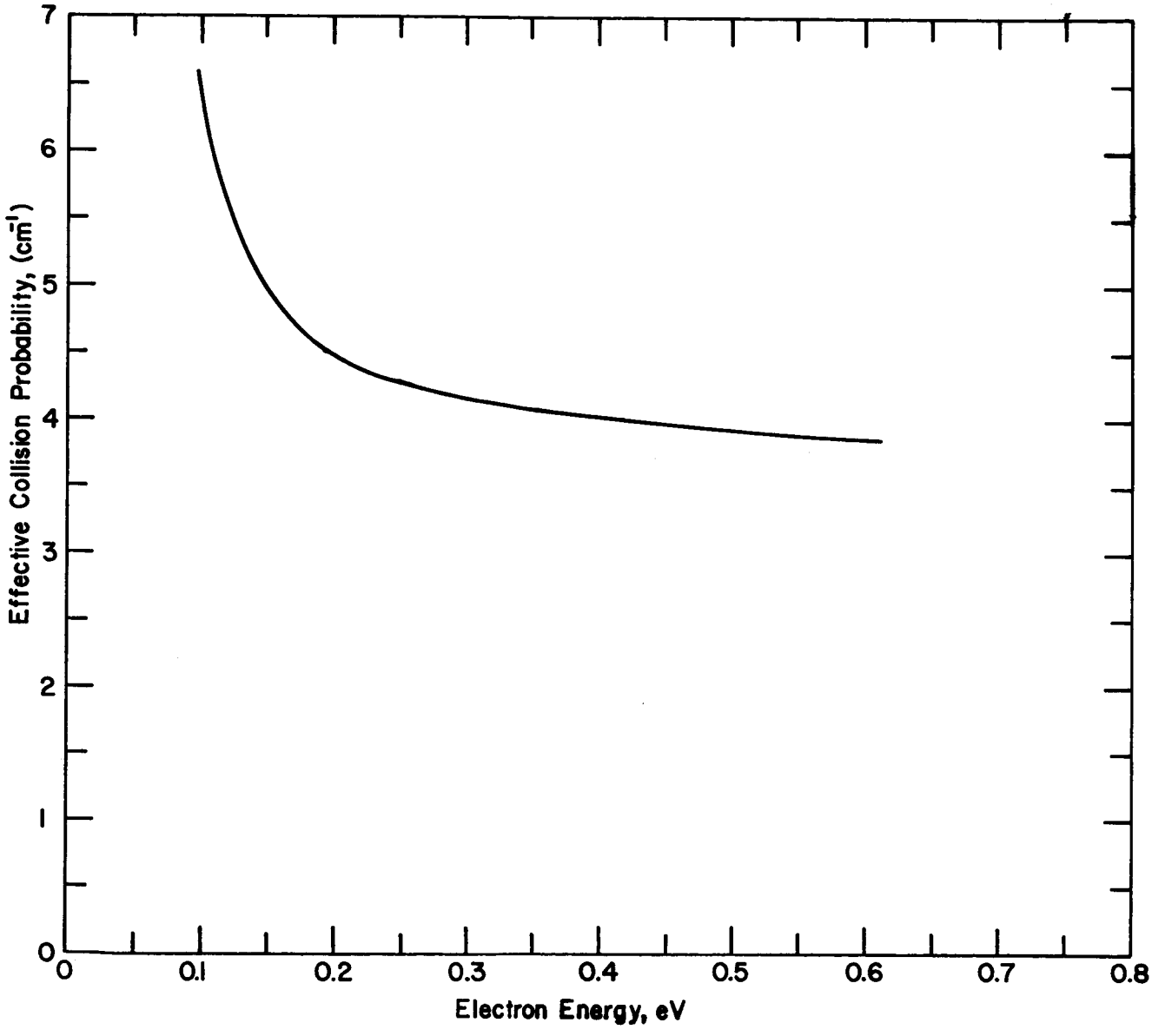

Figure VII-10. Effective Collision Probability of Electrons with Argon.

E. The Overall Effect of the Inert Gases on the Output Characteristics

1. Introduction. The ignited mode of thermionic diodes in the presence of inert gases was discussed in the previous sections. There are two other important interactions of these gases with the plasma in the interelectrode space:

(a) There is the possibility that inert gases may form an effective diffusion barrier for cesium ions, resulting in a decrease of ion loss to the electrodes. Therefore, the internal voltage drop consumed in the generation of cesium ions will be kept to a minimum.

(b) The presence of a high pressure of inert gas in the interelectrode space results in the attenuation of electron current. Therefore, an accurate knowledge of electron scattering as a function of inert gas pressure is important to nuclear thermionics.

A careful and systematic investigation of the dependence of the output characteristics on inert gas pressure is necessary for a complete understanding of the process. The possible increase in power output from the use of inert gases is likely to occur at low argon pressures, less than 20 torr. This pressure range must be covered in steps small enough to ensure the observation of the increase. The electron current attenuation, on the other hand, must be studied in the higher pressure range. Therefore, the dependence must be studied carefully, covering a large range of inert gas pressure in small increments.

The problems concerned with impurities and injection of the inert gas were solved by the methods described in section C of the chapter. The influence of the inert gases on the output characteristics was determined in the range of 0 - 100 torr.

This pressure range was covered in steps small enough to yield the required information. The results were extrapolated to the pressure of 1000 torr by using theoretical expressions developed in this chapter.

2. Experimental Procedure. The first step in the investigation of the overall effect of the inert gases is the choice of the type of data to be used for comparison. One possibility is the use of the volt-ampere characteristics at various inert gas pressures and at constant emitter, collector, and cesium reservoir temperatures, and constant interelectrode spacing. The difficulty in such comparison is that the volt-ampere characteristic is a strong function of cesium reservoir temperature, with the result that a small uncertainty in this parameter can cause a large error in the experimental data. A family of volt-ampere characteristics obtained by varying the reservoir temperature, T_R, has an envelope which is tangent to each member of the family. The experimental error in the measurement of T_R is therefore eliminated, if the envelope is used for comparison.

Before the injection of argon into the interelectrode space, a complete set of parametric data was obtained on the diode to establish its basic performance characteristics and serve as the basis of comparison. Since this diode employed an electroetched and heat-treated rhenium surface, the complete performance map of the emitter was also useful for design calculations. This data was summarized in Chapter VI. A series of more specific data was also obtained for comparison with the characteristics in the presence of argon.

The gas injection system described in section C-2 of this chapter was outgassed thoroughly for several days. The baking temperature was about 800°K for the hot zirconium container and about 500°K for the rest of the system. The diode volume was kept under vacuum and isolated by a valve while the desired

pressure of argon was established in the gas injection system. The inert gas was kept in the hot zirconium trap (at 700°K) and the liquid nitrogen trap for several hours. Then the gas was injected into the operating diode, and the volt-ampere characteristic was monitored. A sudden change in the characteristic was observed, and then equilibrium was reached at the initial conditions after about 30 minutes. A possible cause for the transient behavior is that the sudden injection of the inert gas may force an excess of cesium vapor into the inter-electrode space, causing a transient cesium vapor pressure that does not correspond to the cesium reservoir temperature. Next a complete set of variable-T_R families covering a wide range of diode parameters was obtained. The same procedure was followed covering argon pressures of 0 - 100 torr.

3. Experimental Results and Conclusions. The cesium-temperature envelopes obtained under various conditions are summarized in Figures VII-11 and VII-19. The pressure range of 0 - 100 torr was covered in steps of 0, 2.8, 5.0, 10.5, 20, 29, 40, 75 and 100 torr, to ensure the observation of any possible maxima or minima. For each argon pressure, the cesium reservoir envelopes were obtained at emitter temperatures of 1863, 1740 and 1650°K, in order to resolve possible discrepancies that might arise. Three interelectrode spacings (2, 10 and 20 mils) were studied at each emitter temperature in order to determine the dependencies on spacing. These 81 families correspond to approximately 1200 single volt-ampere characteristics and are summarized in Figures VII-11 to VII-19. Each figure shows the envelopes at a particular emitter temperature and interelectrode spacing, and at several argon pressures. For the sake of brevity, only five of the argon pressures investigated are shown. The behavior of the other pressures may be seen from the cross plots (Figures VII-20 to VII-28). As the above figures show, there is no output power increase due to the presence of argon in the interelectrode space. Since argon is the most appropriate inert gas

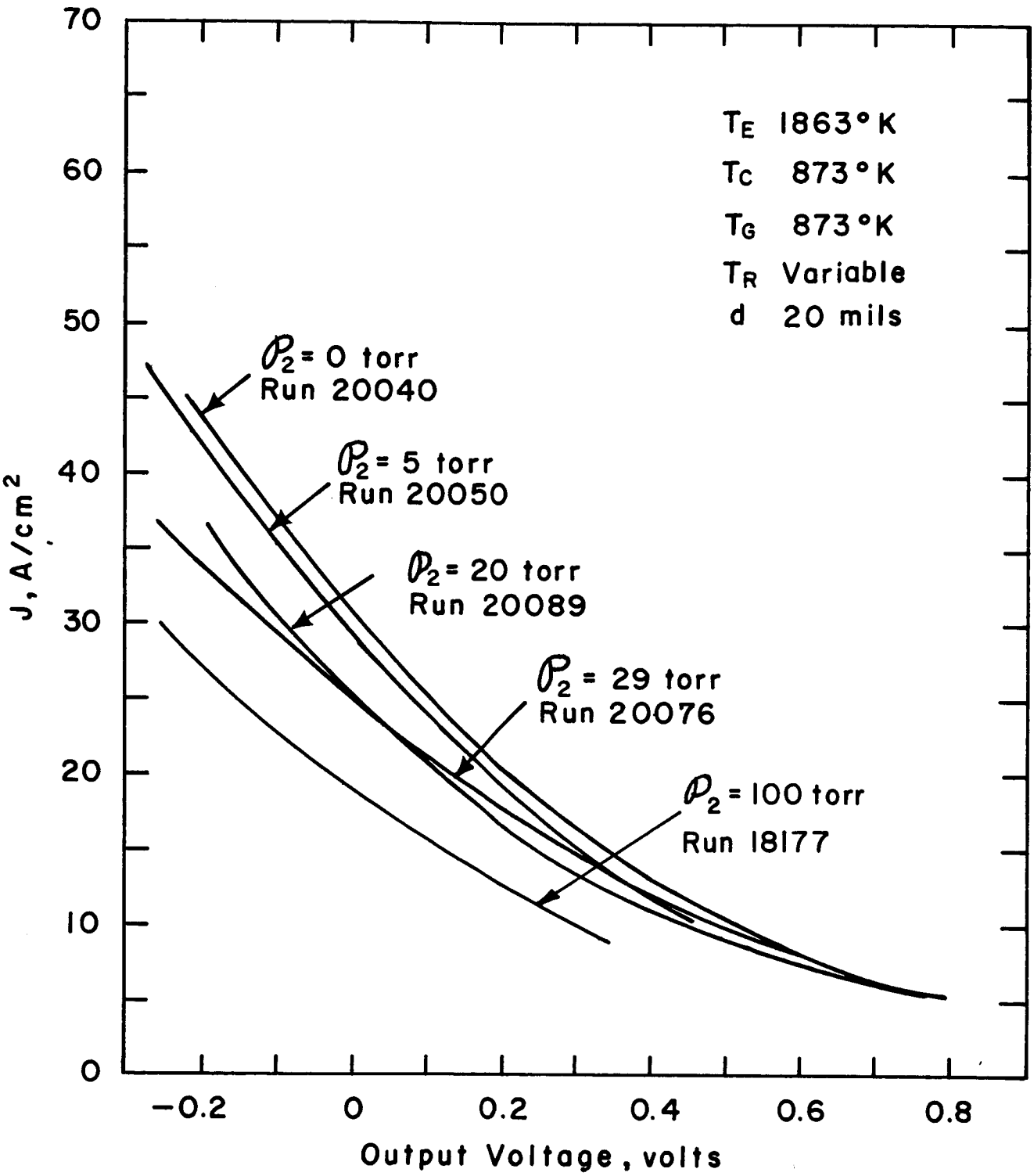

Figure VII-11. Variable-Reservoir-Temperature Envelopes at T_E = 1863°K and d = 20 mils.

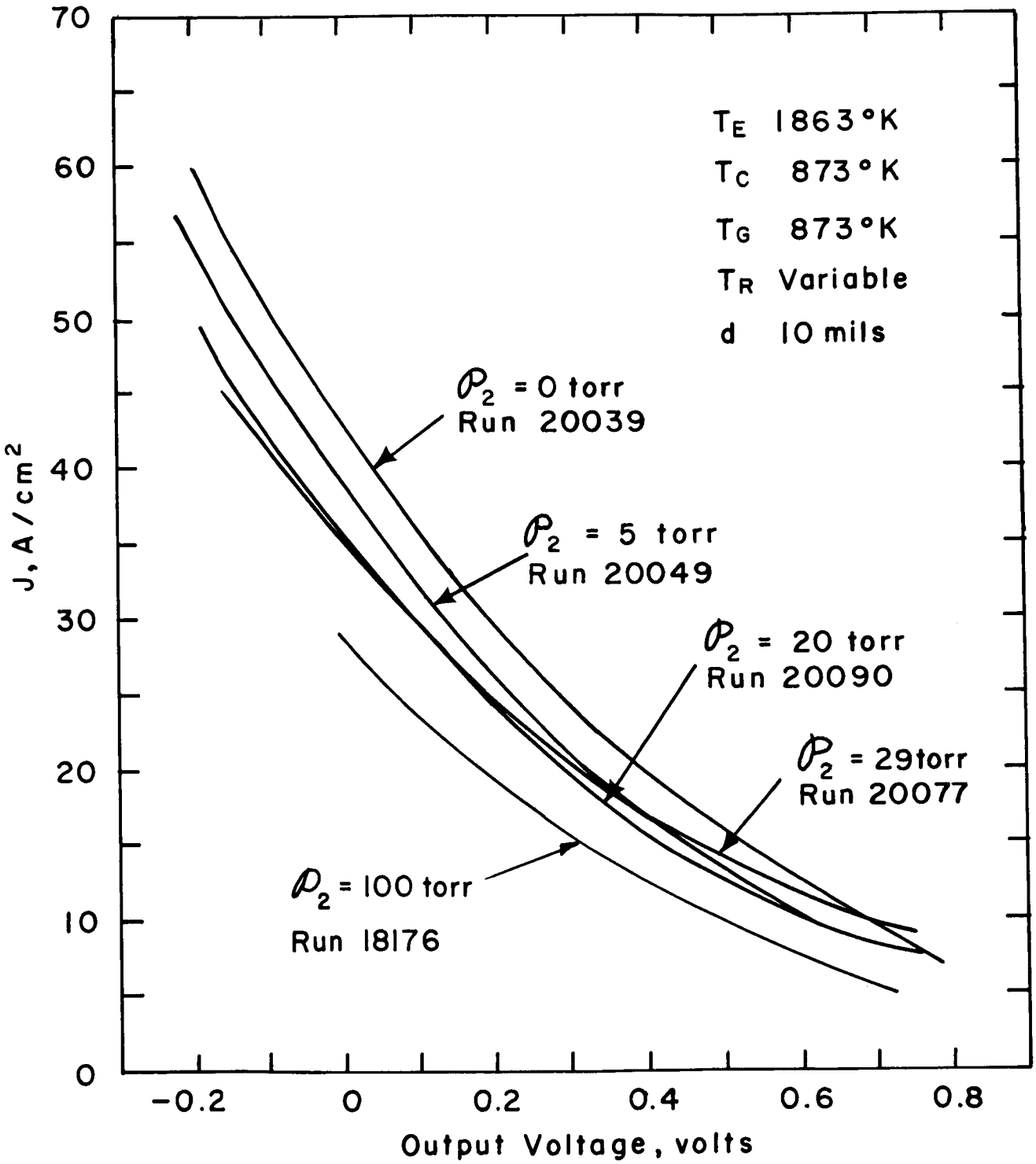

Figure VII-12. Variable-Reservoir-Temperature Envelopes at T_E = 1863°K and d = 10 mils.

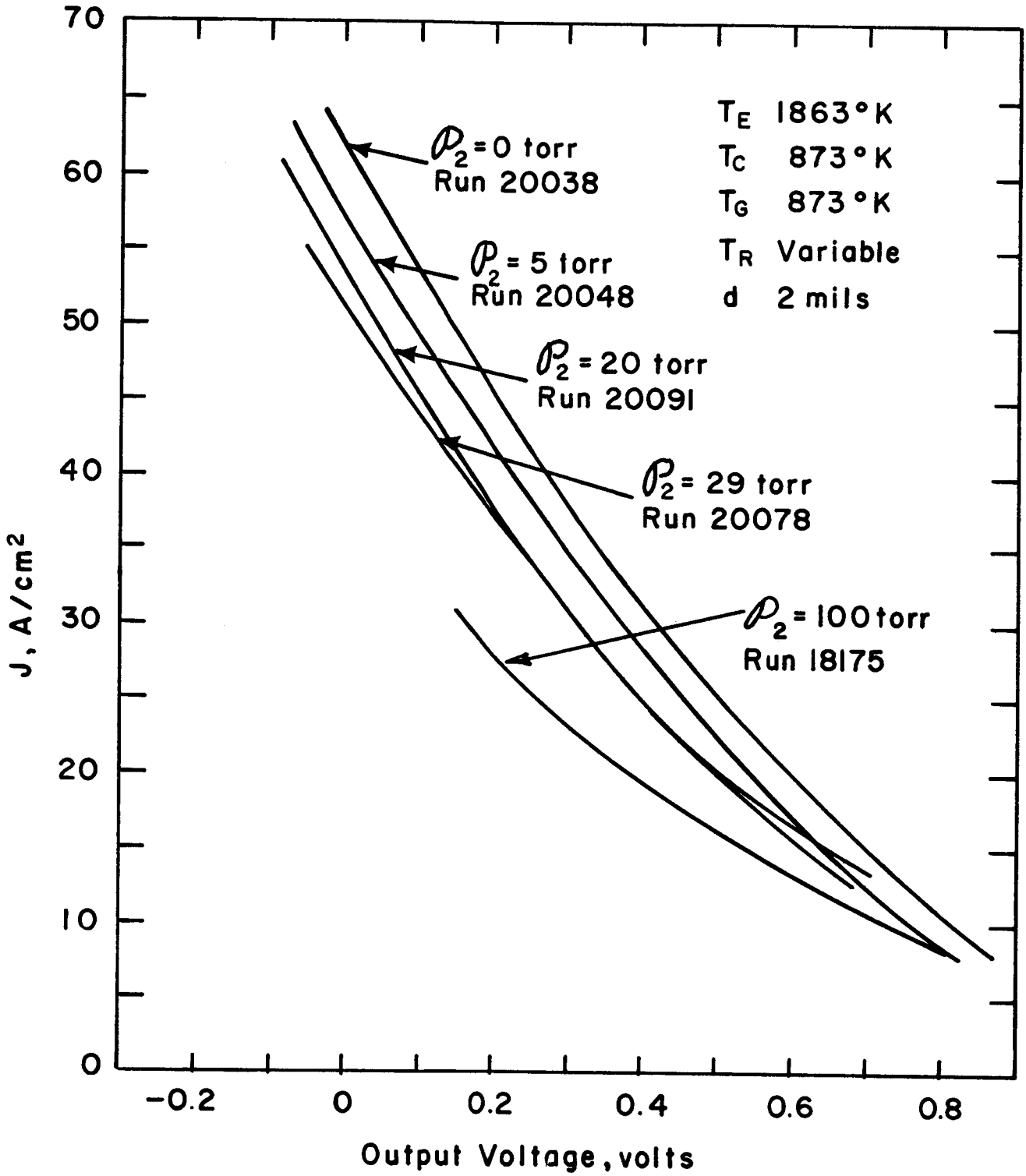

Figure VII-13. Variable-Reservoir-Temperature Envelopes at T_E = 1863°K and d = 2 mils.

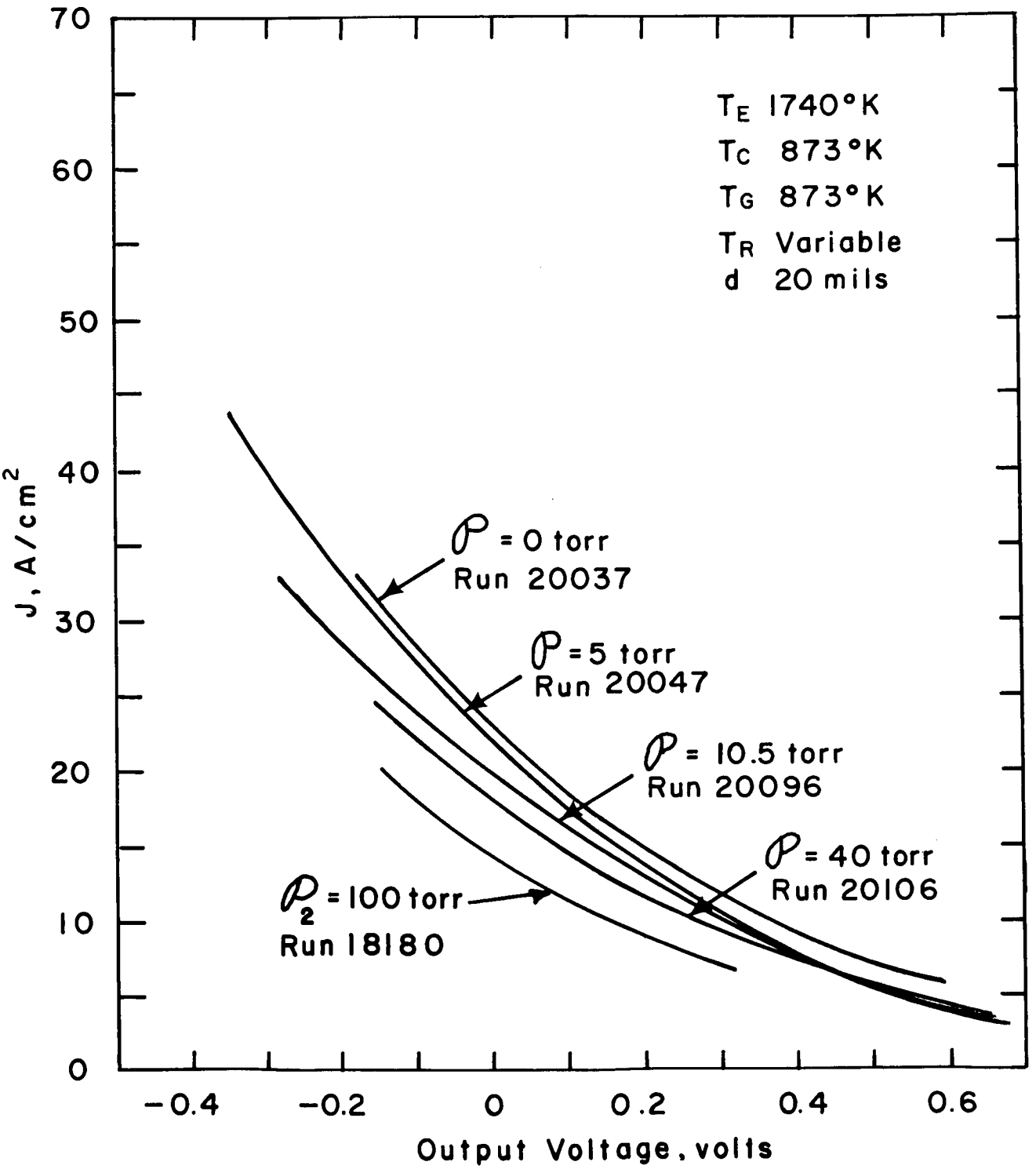

Figure VII-14. Variable-Reservoir-Temperature Envelopes at T_E = 1740°K and d = 20 mils.

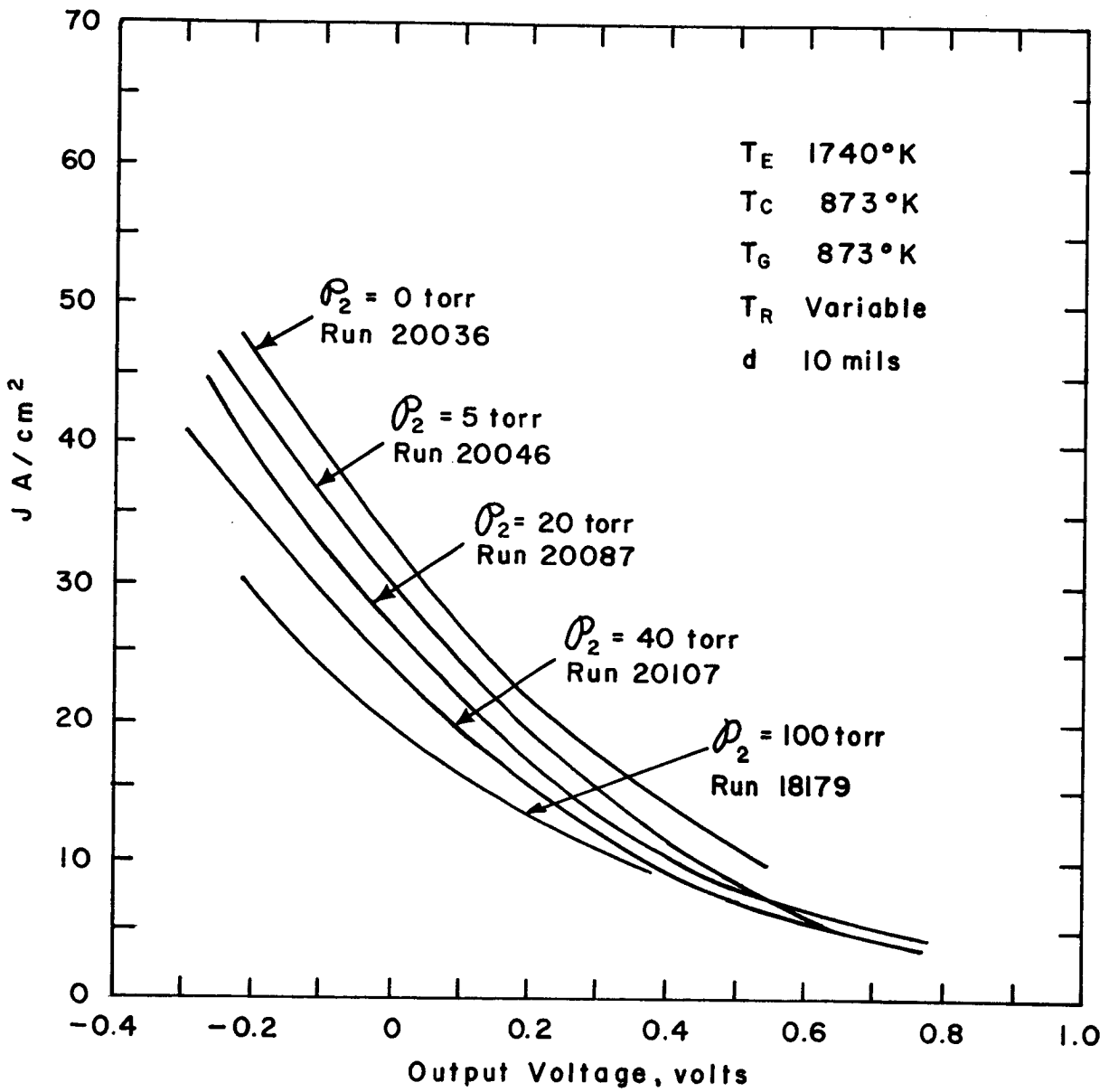

Figure VII-15. Variable-Reservoir-Temperature Envelopes at T_E = 1740°K and d = 10 mils.

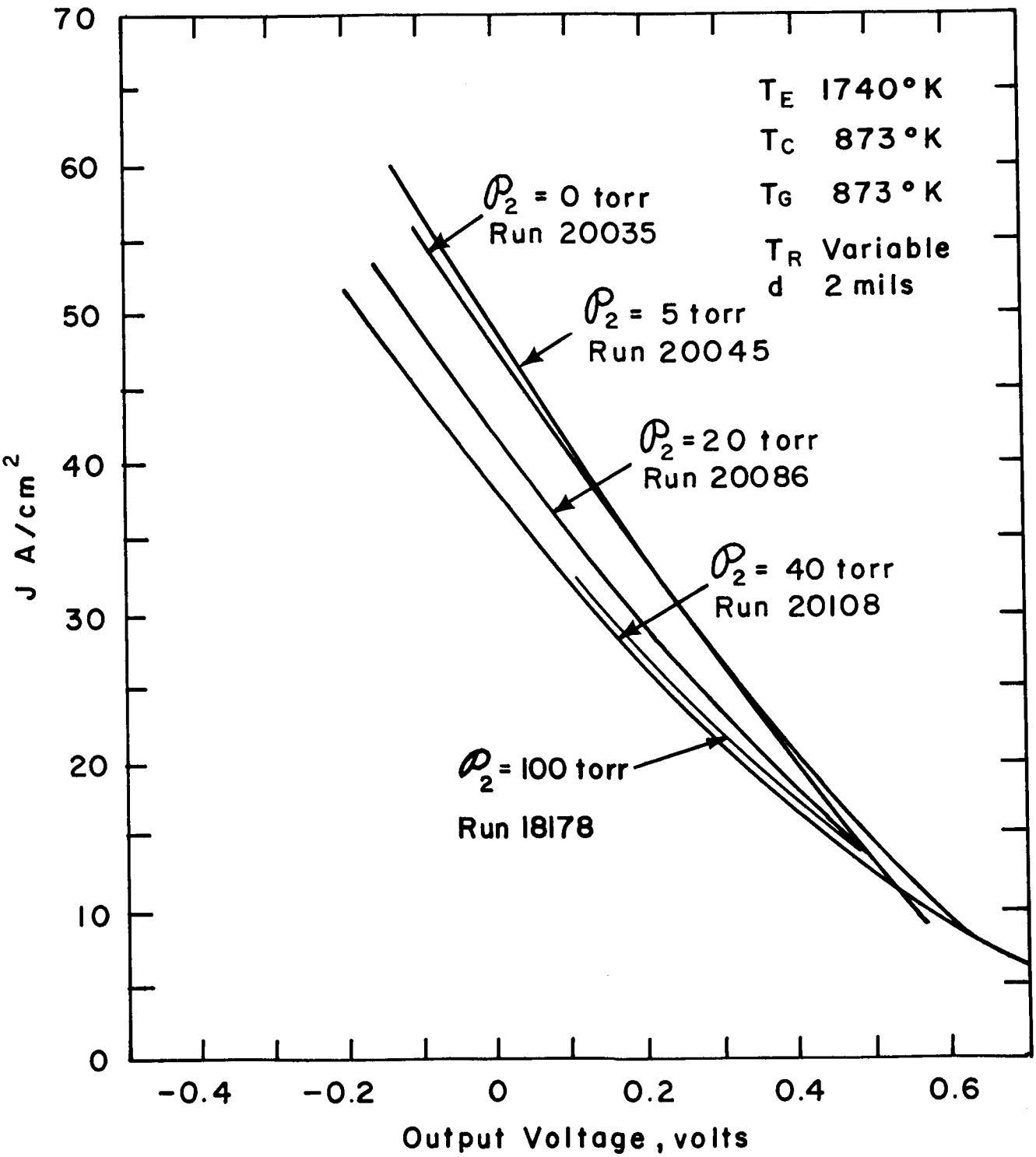

Figure VII-16. Variable-Reservoir-Temperature Envelopes at T_E = 1740°K and d = 2 mils.

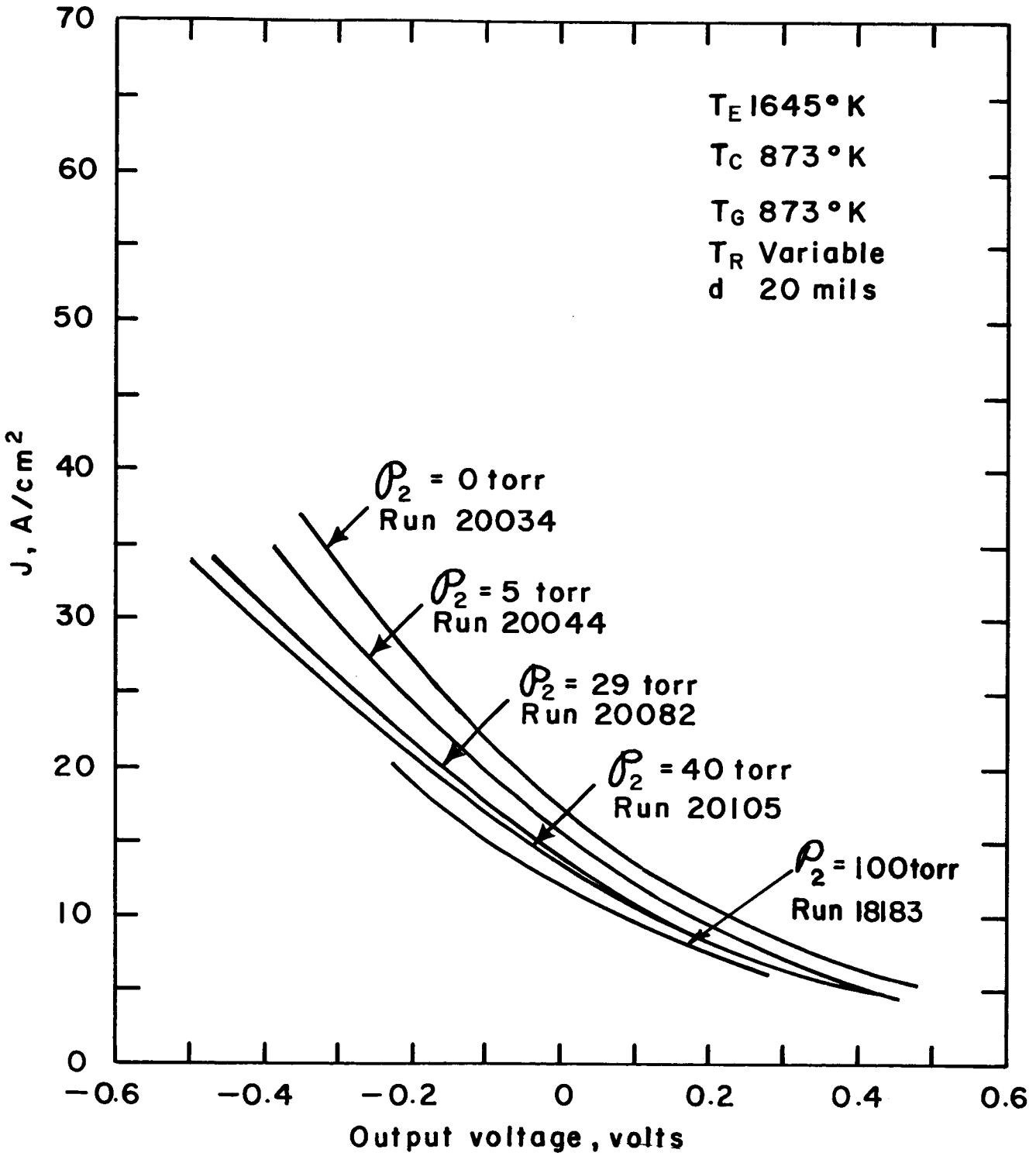

Figure VII-17. Variable-Reservoir-Temperature Envelopes at T_E = 1645°K and d = 20 mils.

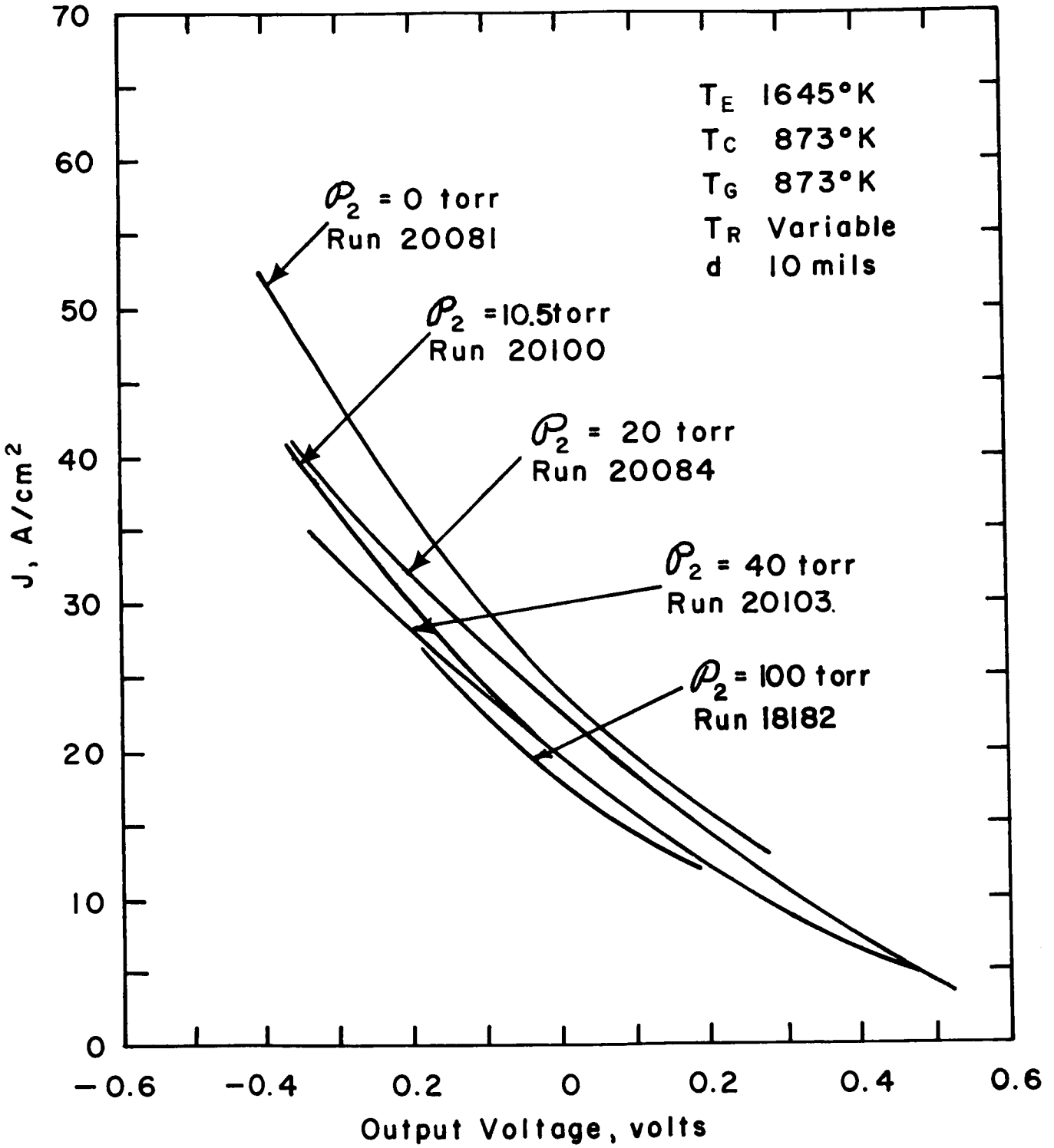

Figure VII-18. Variable-Reservoir-Temperature Envelopes at T_E = 1645°K and d = 10 mils.

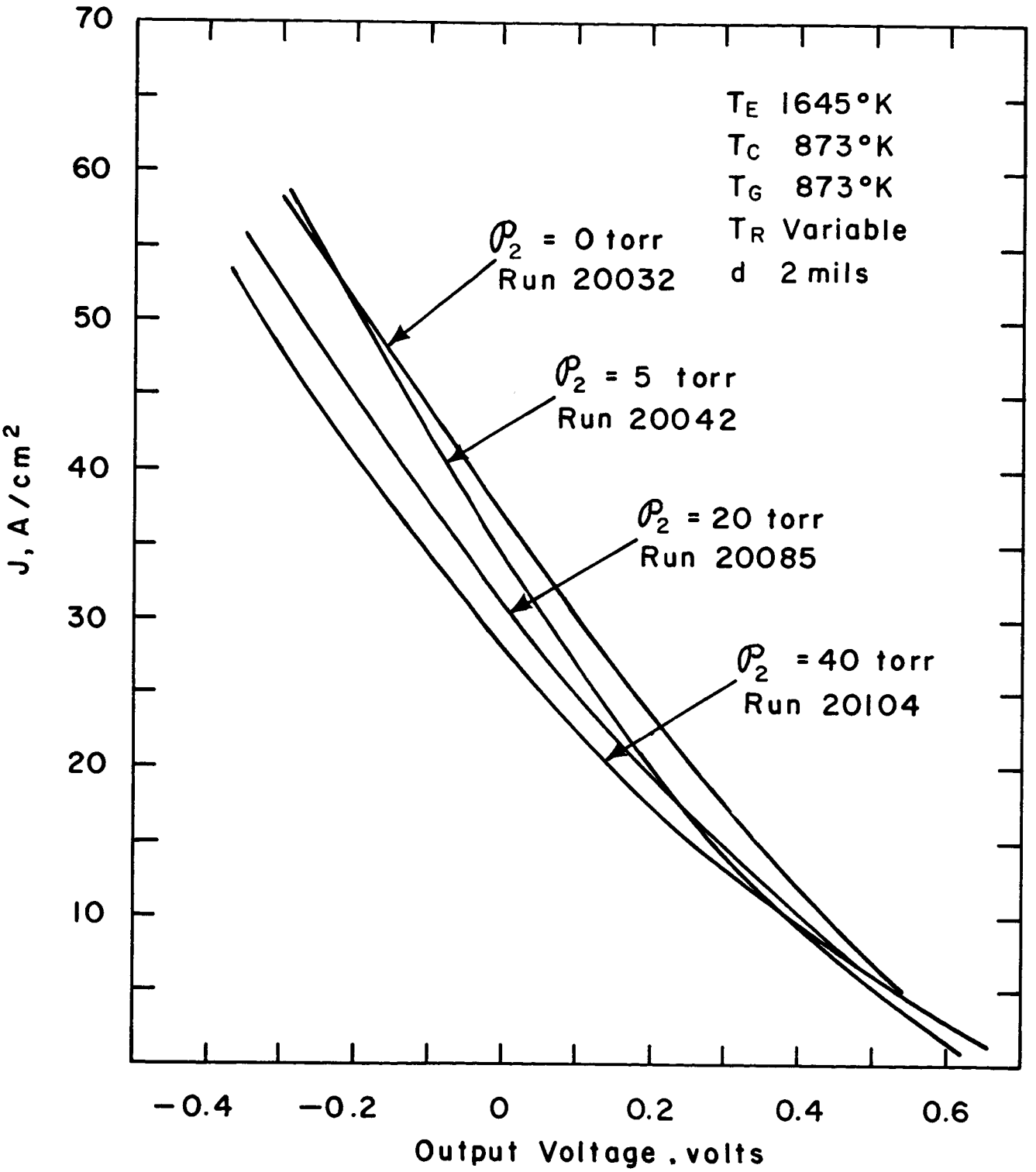

Figure VII-19. Variable-Reservoir-Temperature Envelopes at T_E = 1645°K and d = 2 mils.

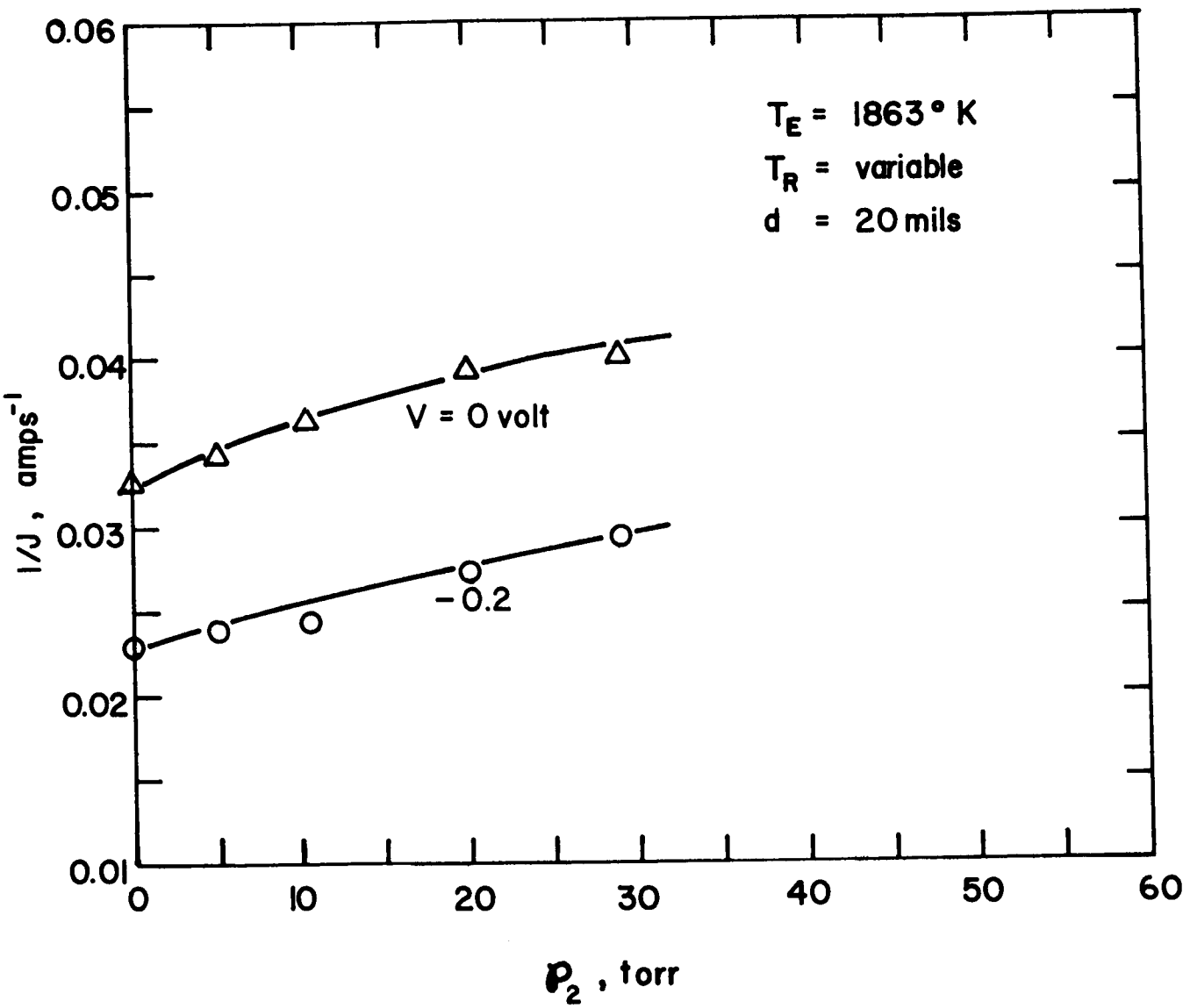

Figure VII-20. Cross Plot Corresponding to Figure VII-11.

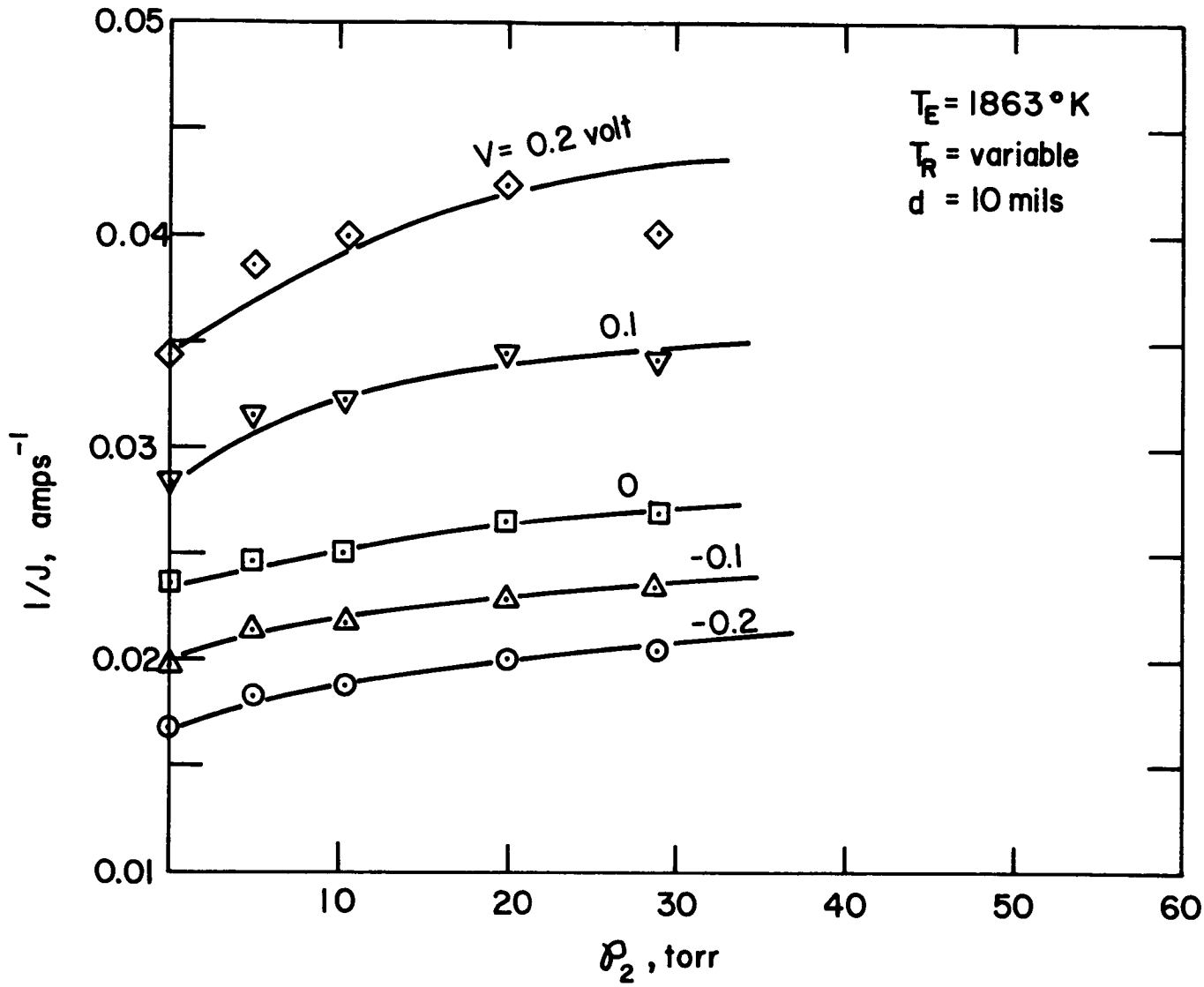

Figure VII-21. Cross Plot Corresponding to Figure VII-12.

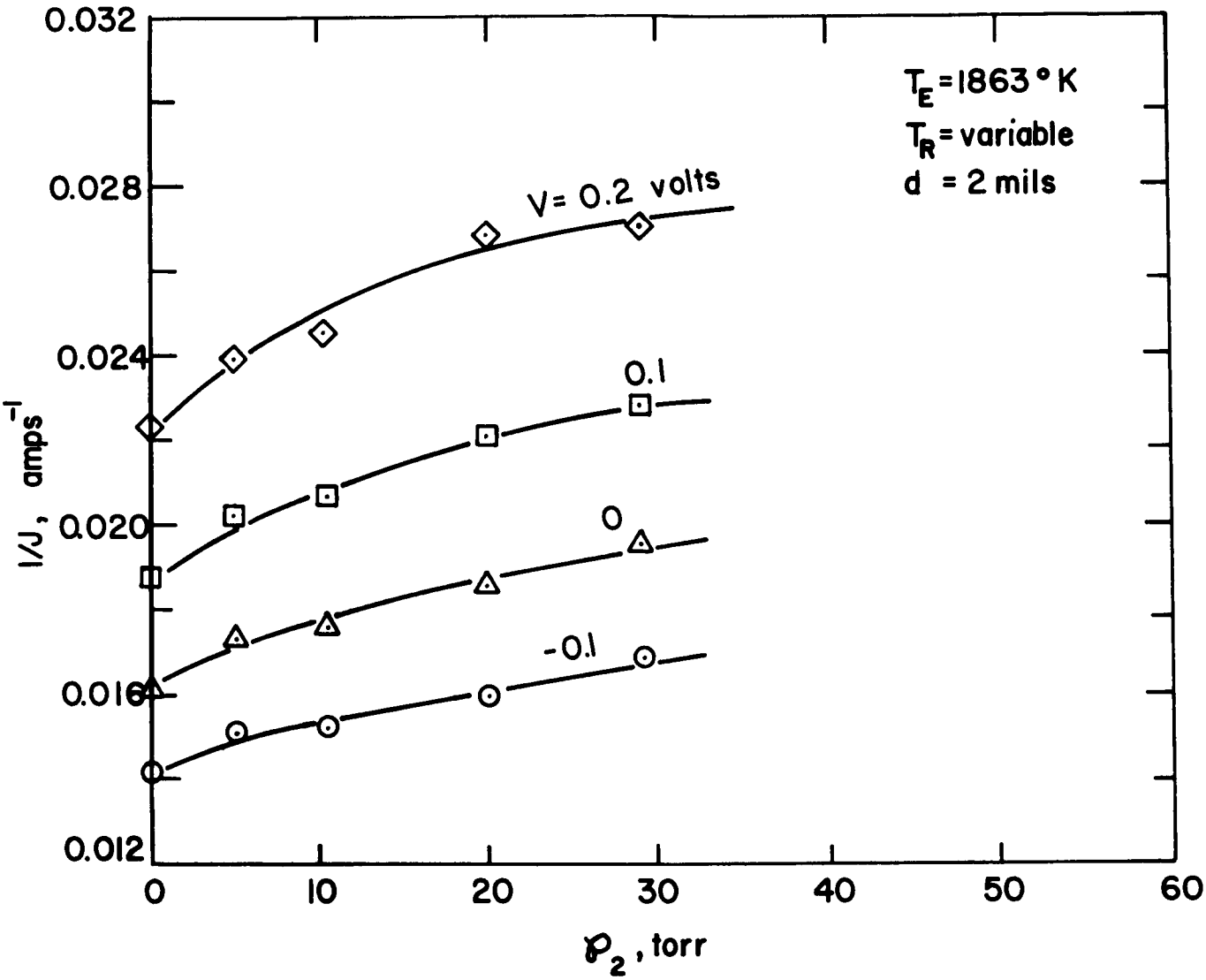

Figure VII-22. Cross Plot Corresponding to Figure VII-13.

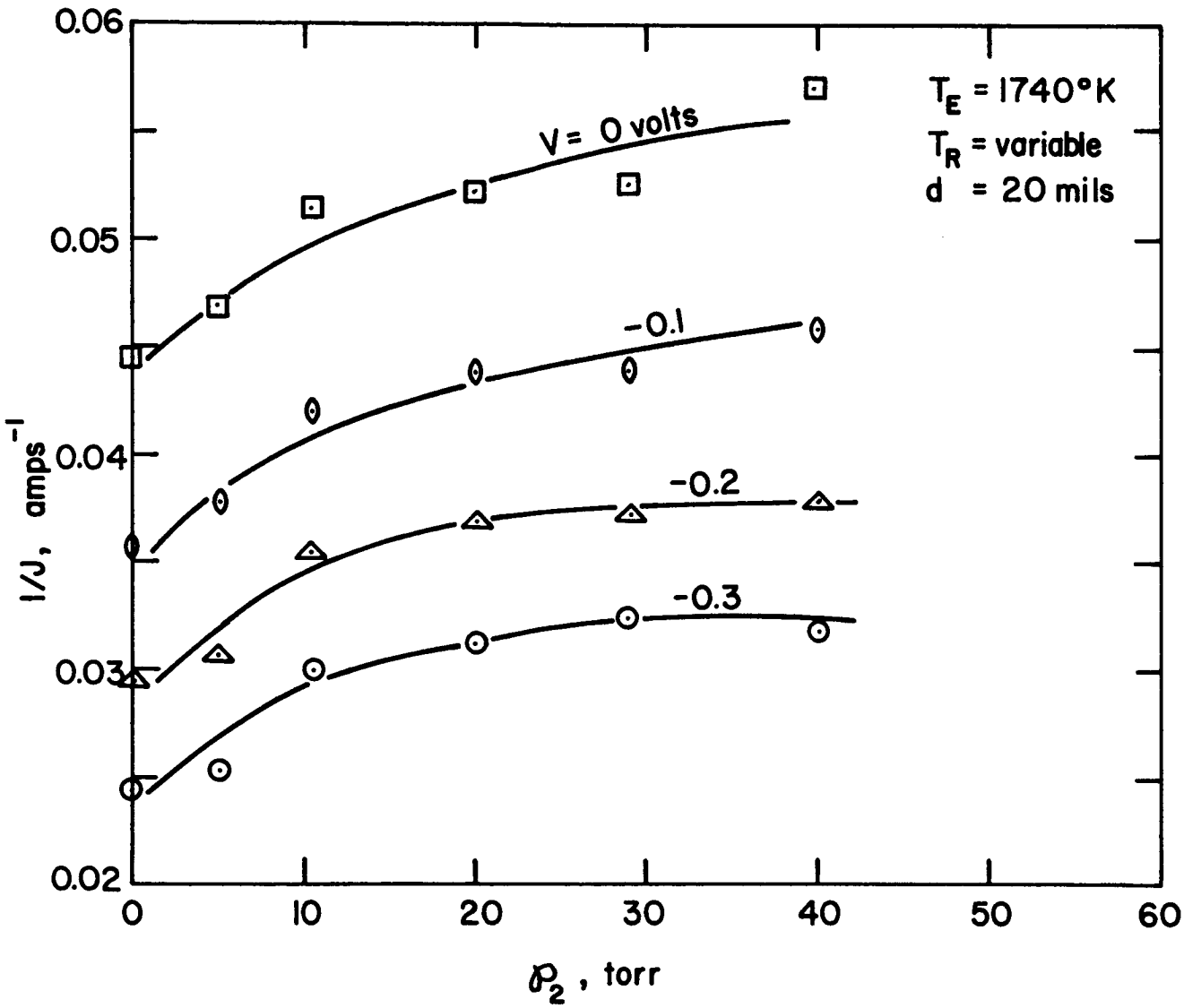

Figure VII-23. Cross Plot Corresponding to Figure VII-14.

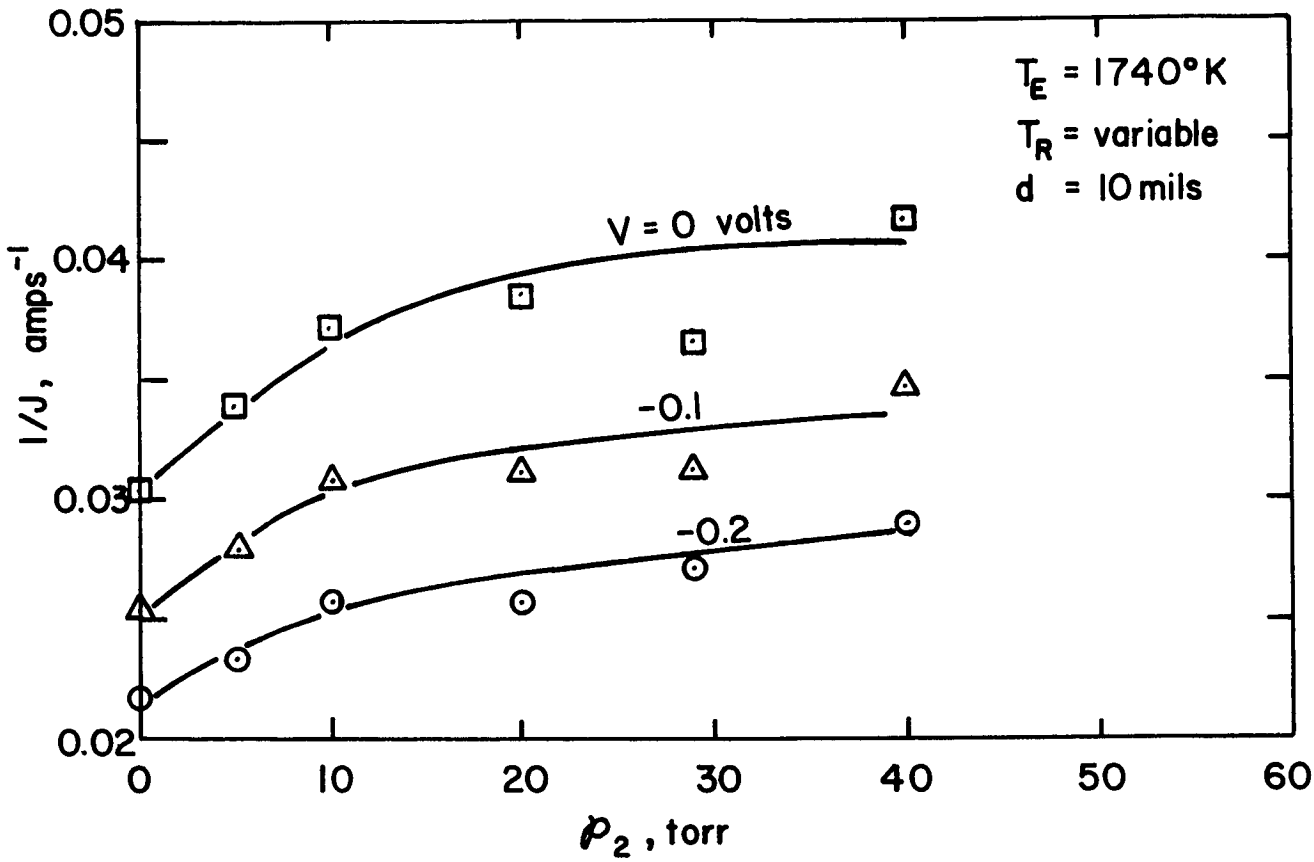

Figure VII-24. Cross Plot Corresponding to Figure VII-15.

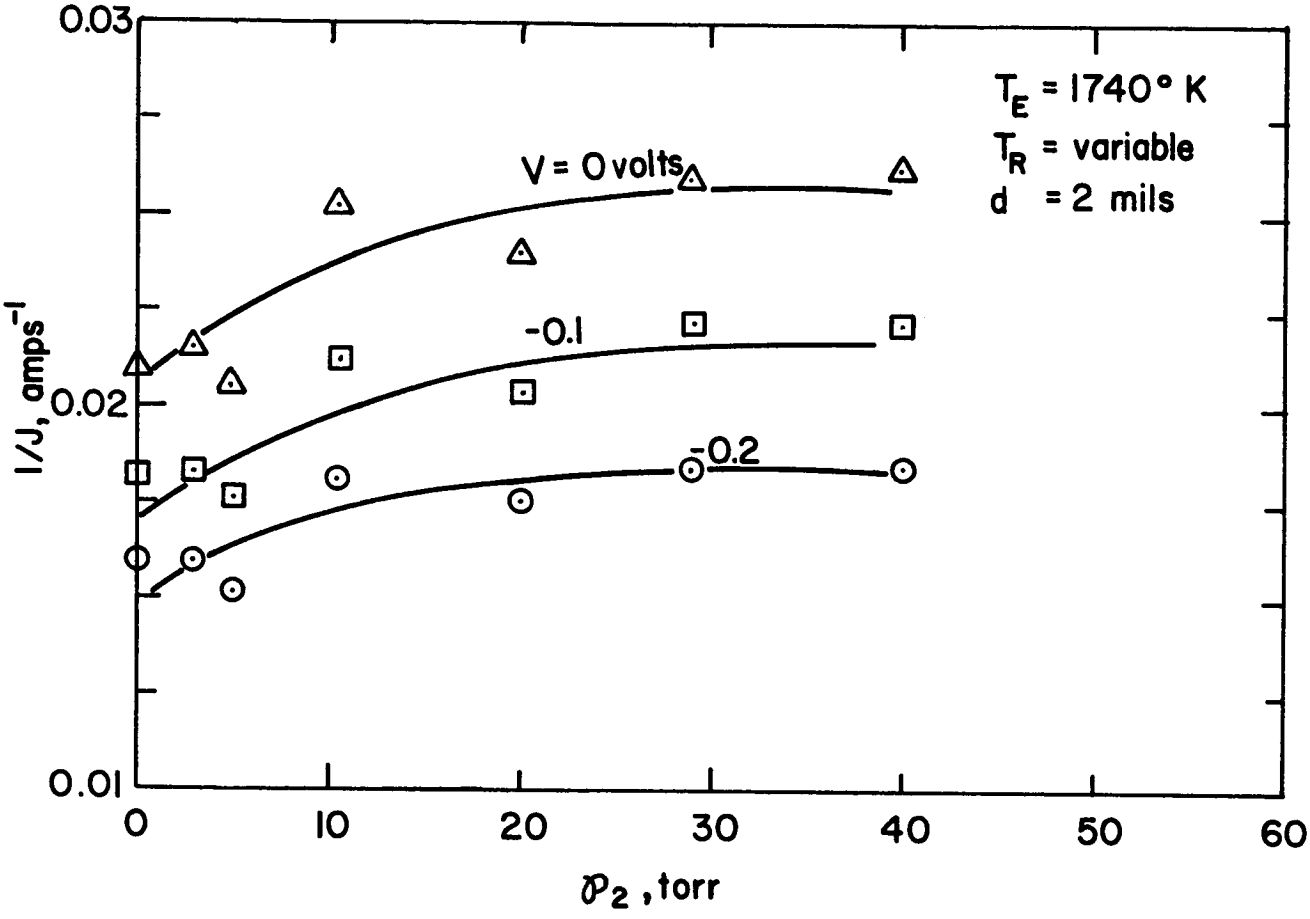

Figure VII-25. Cross Plot Corresponding to Figure VII-16.

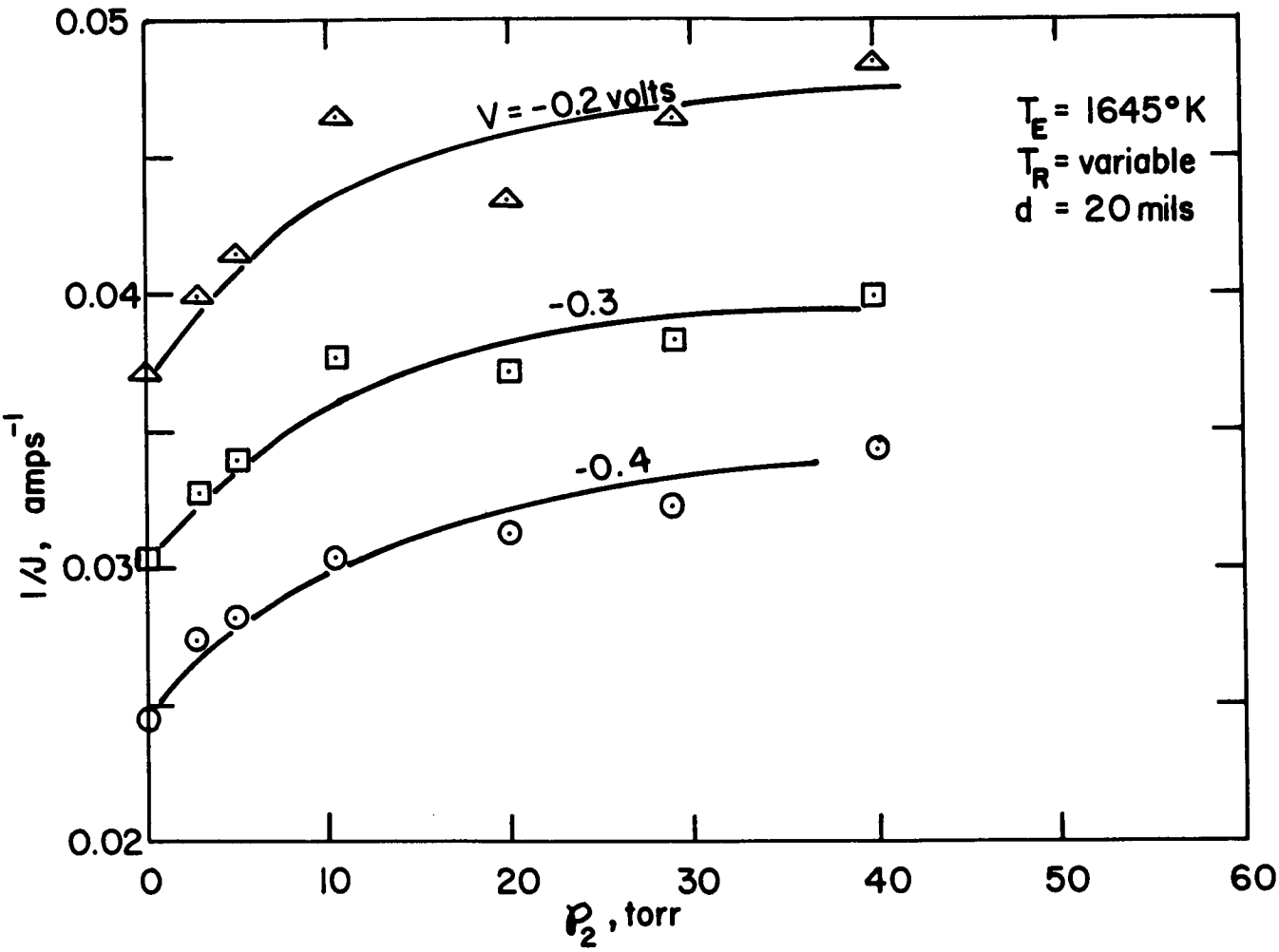

Figure VII-26. Cross Plot Corresponding to Figure VII-17.

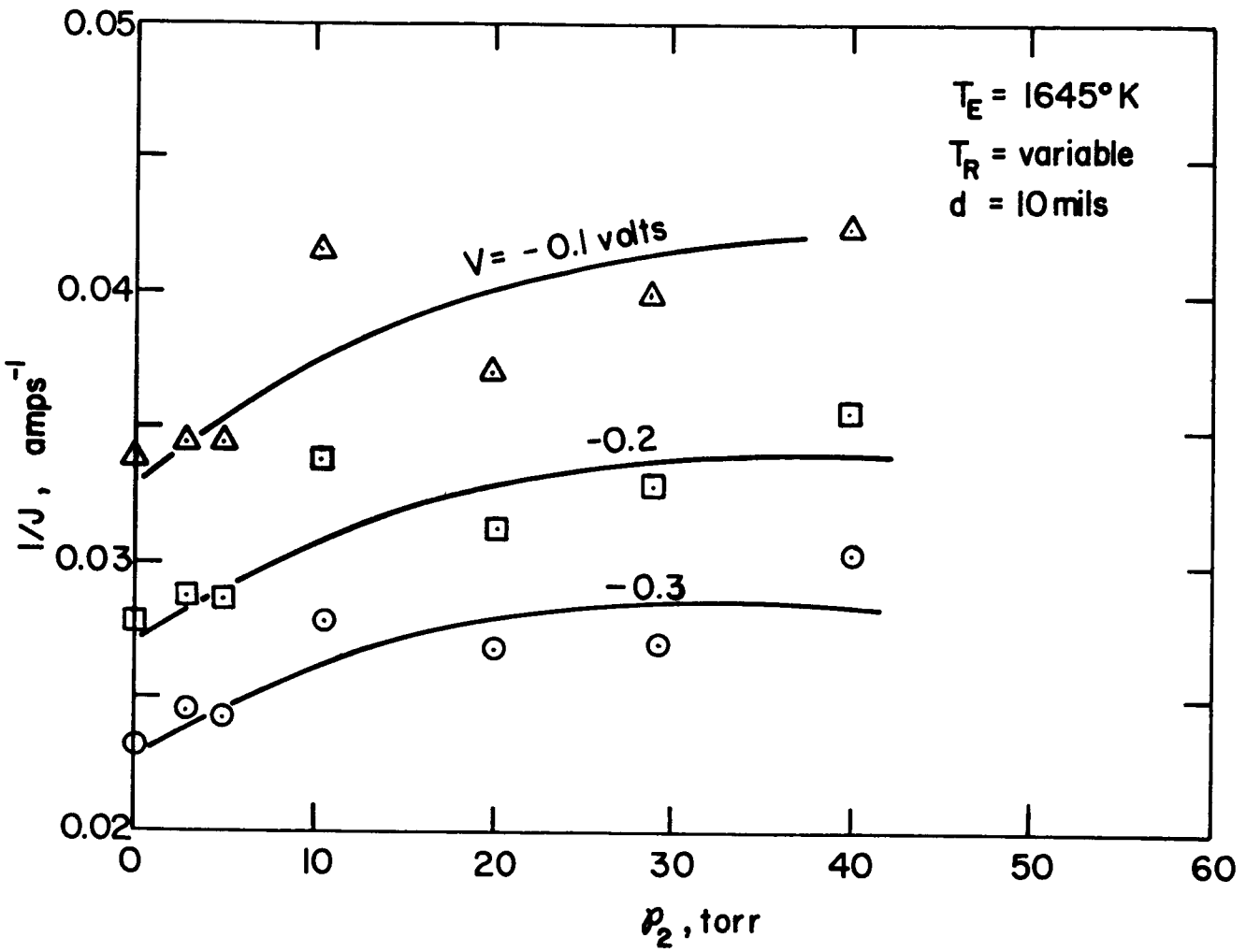

Figure VII-27. Cross Plot Corresponding to Figure VII-18.

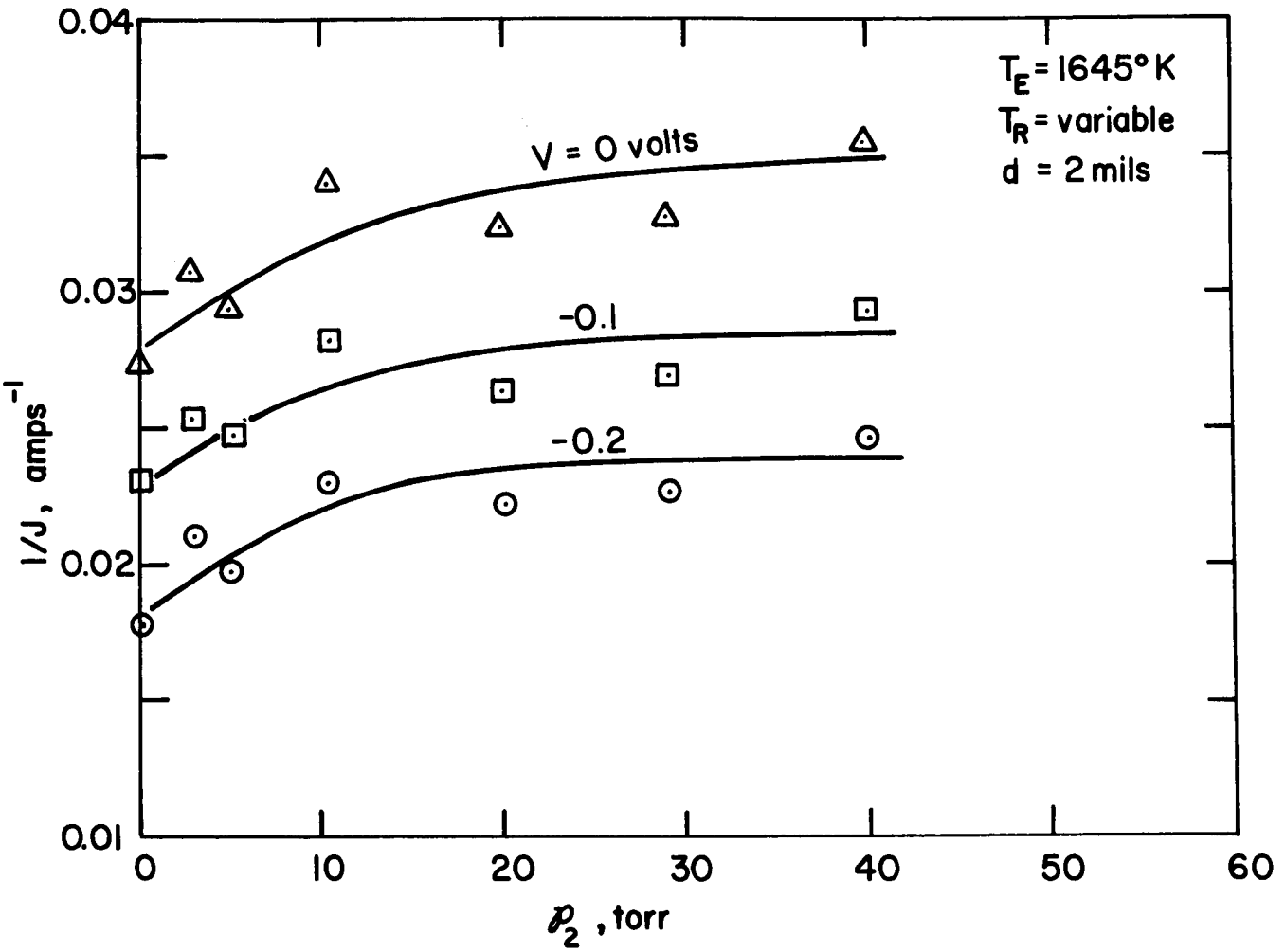

Figure VII-28. Cross Plot Corresponding to Figure VII-19.

for this purpose, it is reasonable to assume that this conclusion applies also to other inert gases such as xenon and krypton.

We may also conclude, from examination of the experimental data, that the output characteristics in the power-producing region are not highly affected by the presence of argon below 20 torr. This conclusion has significance in nuclear thermionics.

Because of the complex dependence of scattering on argon pressure, cesium pressure and interelectrode spacing, it is not possible to present a more general correlation in the experimental data. The complex dependence is as follows: Electron scattering by cesium follows a simple dependence on $P_1 d$, where P_1 is the cesium pressure and d is the interelectrode spacing. Electron scattering is also a function of the internal arc drop, V'_d, since this parameter acts as a reflector for the electrons that are directed to the emitter. The internal arc drop,[20] however, is also a function of $P_1 d$. Therefore, electron scattering by cesium atoms can still be correlated with the product $P_1 d$. It is not possible to find the same type of dependence for argon. Electron scattering by argon is a function of $P_2 d$ and V'_d, where P_2 is the argon pressure. The arc drop V'_d is, in turn, a function of the product $P_1 d$. This complicates the dependence of electron scattering by argon, on the interelectrode spacing, argon pressure and cesium pressure.

The dependence of electron current attenuation on the inert-gas pressure can be calculated from the theory using the parameters determined in section D of this chapter. This dependence for argon was calculated using the plasma properties discussed in Refs. 21 and 22. The experimental data follows the theory for pressures higher than 30 torr. In the lower pressure range, the data indicates that electron scattering is slightly higher than that predicted by

theory. The current attenuation was extrapolated to 1000 torr of argon using the above procedure and is shown in Figures VII-29 through VII-31 for various parameters. These plots should only be used as a rough estimate. More accurate values for specific diode conditions can be obtained from the results of section D and the parameters discussed in Refs. 24 and 25.

Electron current attenuation for krypton and xenon has also been computed in a similar manner, and is shown in Figures VII-32 to VII-37. Electron scattering by krypton is higher than that by argon by about a factor of 6, and the scattering by xenon is approximately twice that by krypton.

In conclusion, the possibility of increasing output power by the use of argon as a diffusion barrier was studied. No increase was observed in the pressure range of 2 - 100 torr. This result indicates either that diffusion is not the dominant ion loss mechanism or that internal voltage drop is not highly dependent on ion concentration. The latter possibility suggests the presence of a surplus of ions in the ignited mode. Volume ionization occurs in this case and a surplus of ions is produced as long as the emitter sheath height is larger than the critical value, V'_E.

The electron current attenuation due to the presence of argon was determined experimentally in the pressure range of 0 - 100 torr. At 10 torr of argon, the attenuation is approximately 5 - 15%, depending on the specific condition. This pressure of argon corresponds to about 2 torr of krypton and 1 torr of xenon. The data are in agreement with the theory for pressures higher than 30 torr. In the pressure range of 0 - 30 torr, however, electron scattering predicted by the theory is slightly lower than the experimental data. The pressure range was extended up to 1000 torr by theoretical equations. Based on the results from argon, the attenuation of electron current by krypton and xenon was also

evaluated. The fractional attenuation increases moderately with increasing argon pressure up to 10 torr. For higher pressures, fractional attenuation increases very slowly with increasing pressure.

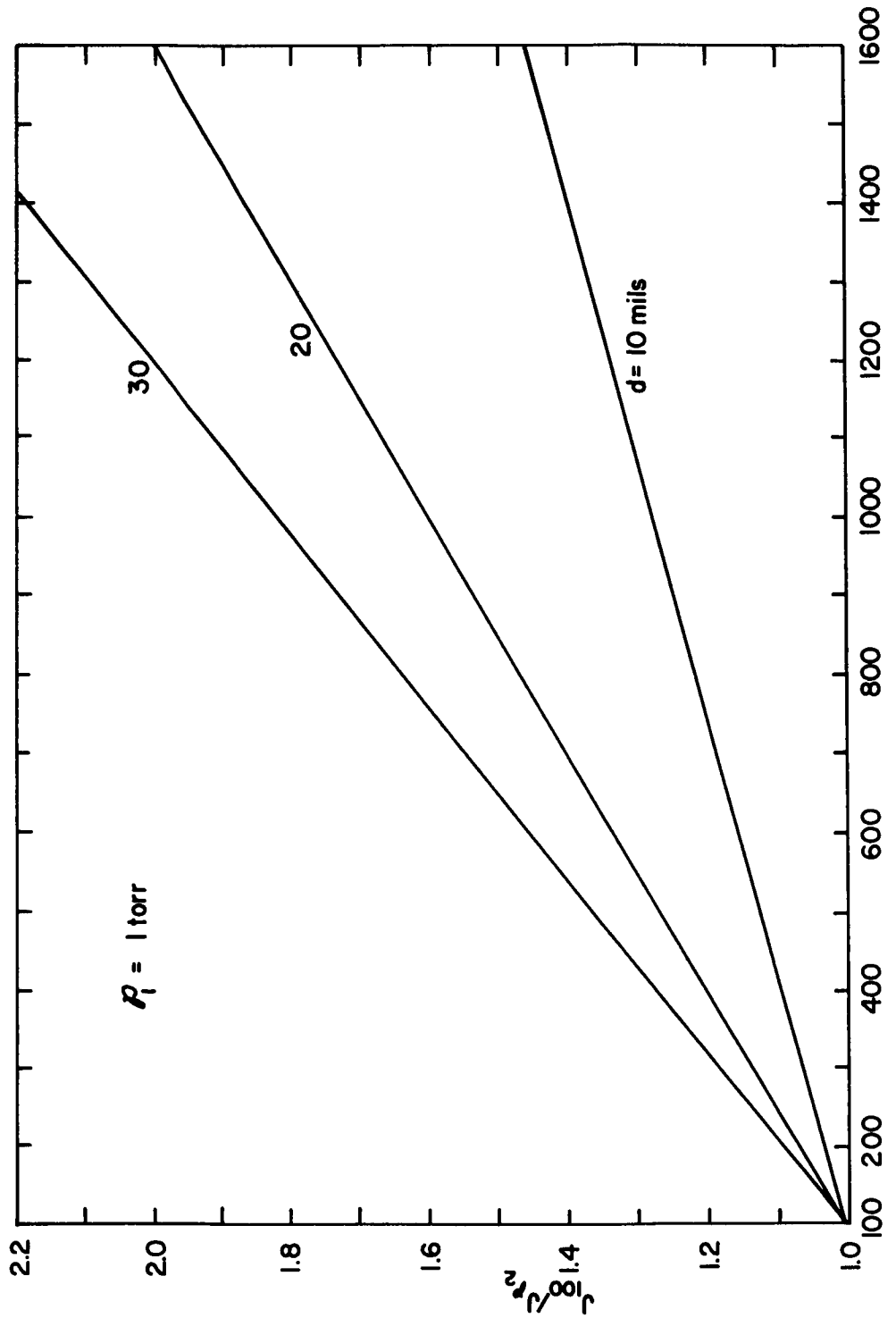

Figure VII-29. Fractional Current Attenuation by Argon for Cesium Pressure of 1 Torr and Several Interelectrode Spacings.

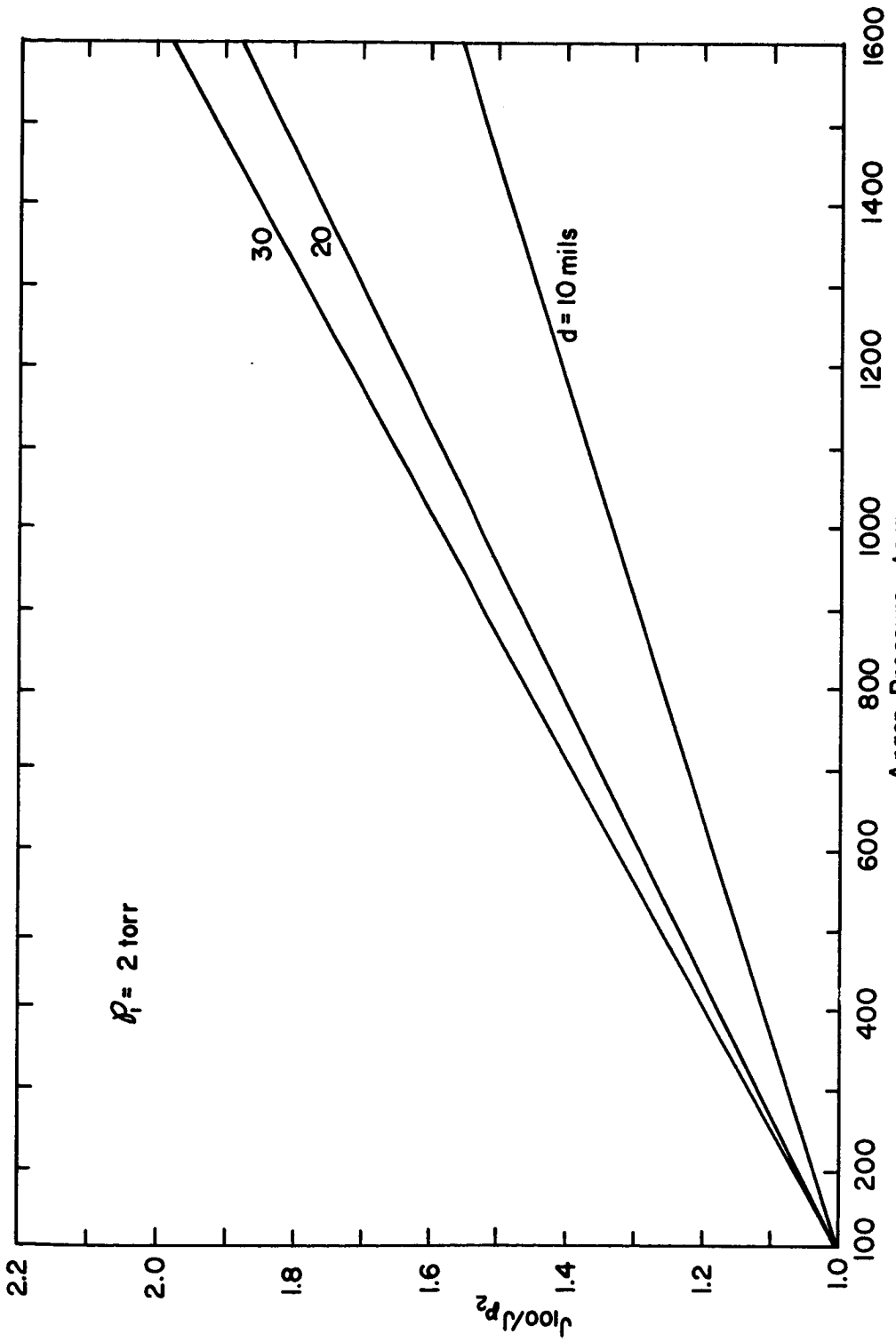

Figure VII-30. Fractional Current Attenuation by Argon for Cesium Pressure of 2 Torr and Several Interelectrode Spacings.

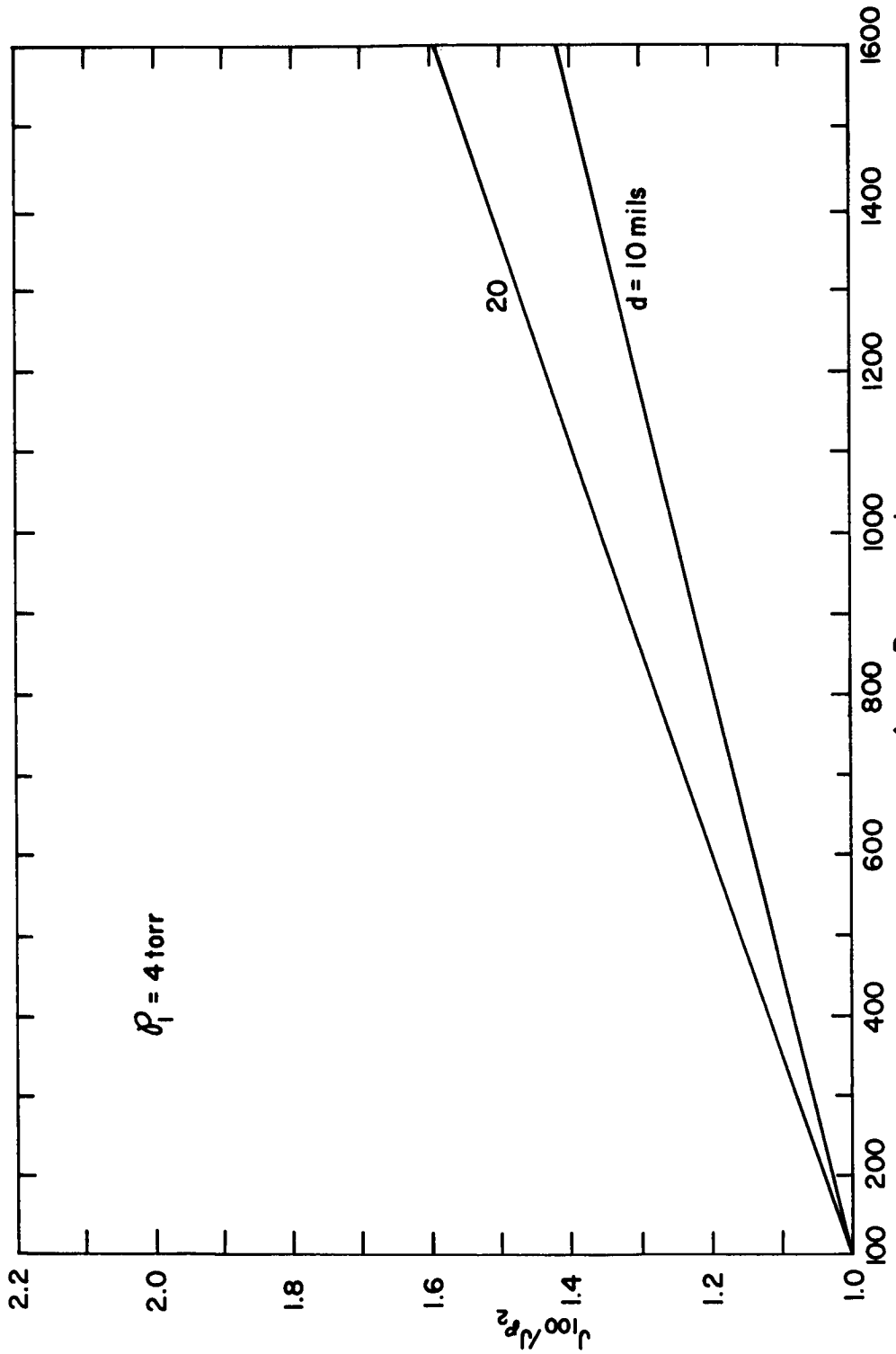

Figure VII-31. Fractional Current Attenuation by Argon for Cesium Pressure of 4 Torr and Several Interelectrode Spacings.

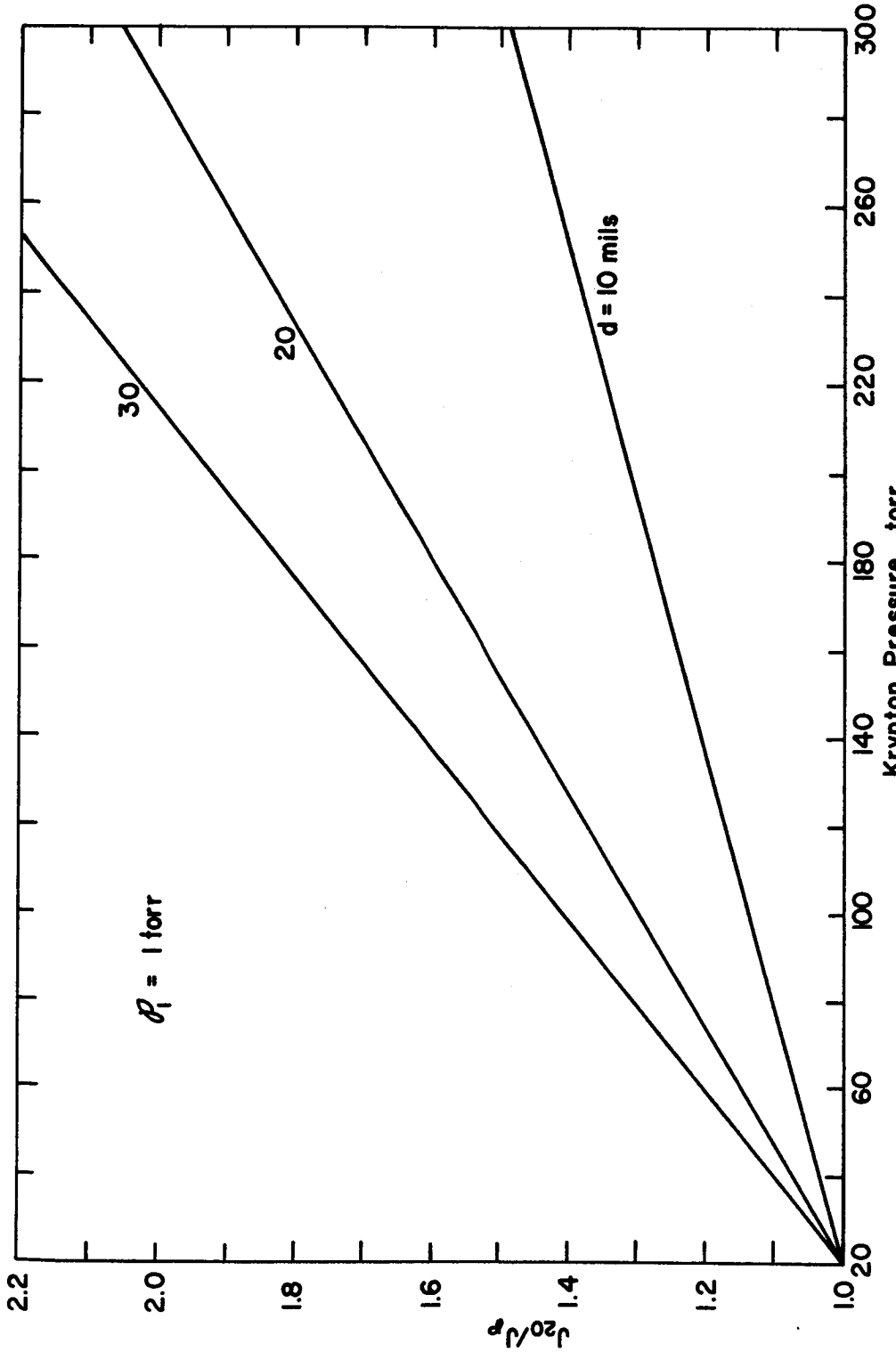

Figure VII-32. Fractional Current Attenuation by Krypton for Cesium Pressure of 1 Torr and Several Interelectrode Spacings.

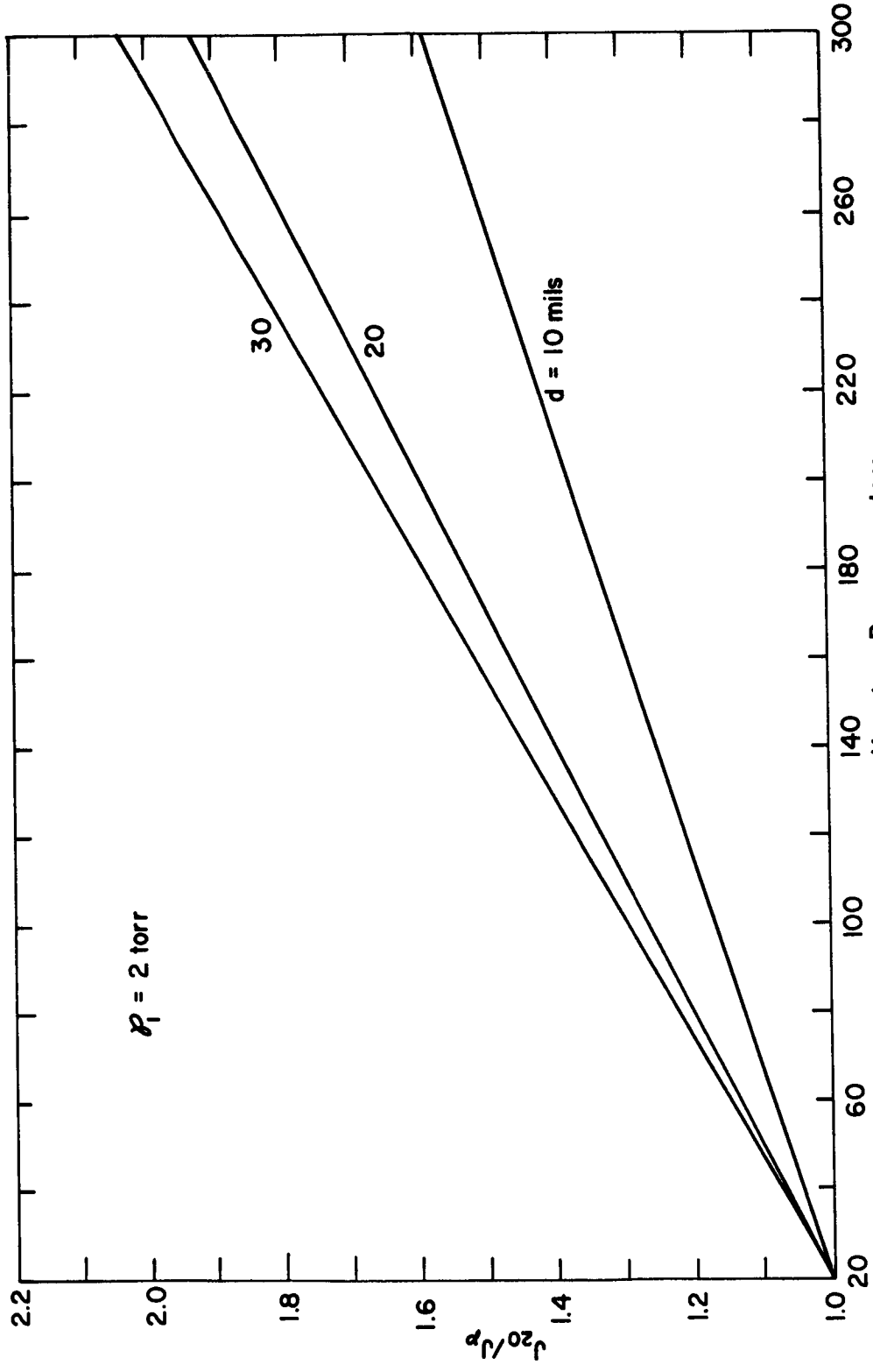

Figure VII-33. Fractional Current Attenuation by Krypton for Cesium Pressure of 2 Torr and Several Interelectrode Spacings.

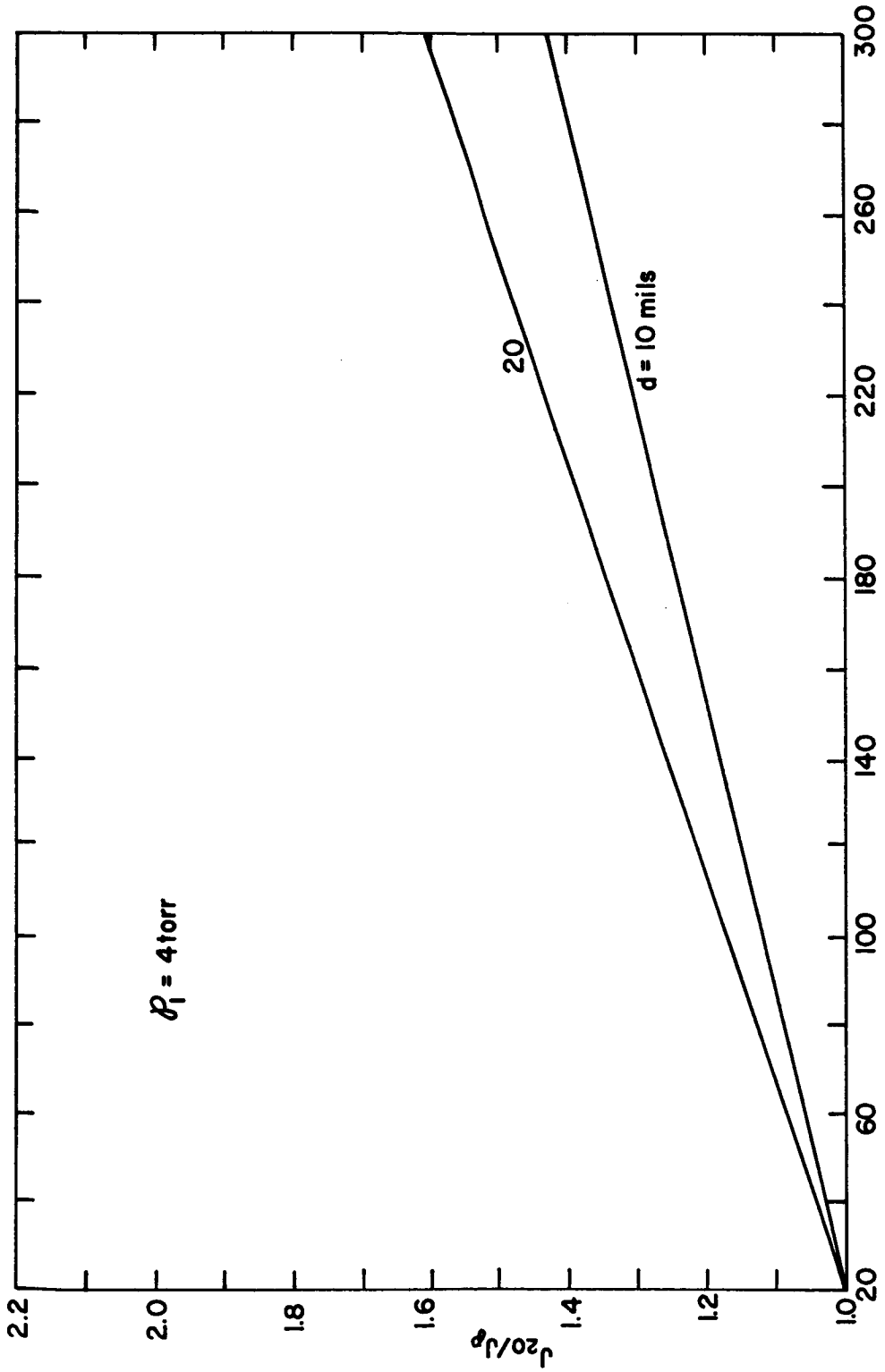

Figure VII-34. Fractional Current Attenuation by Krypton for Cesium Pressure of 4 Torr and Several Interelectrode Spacings.

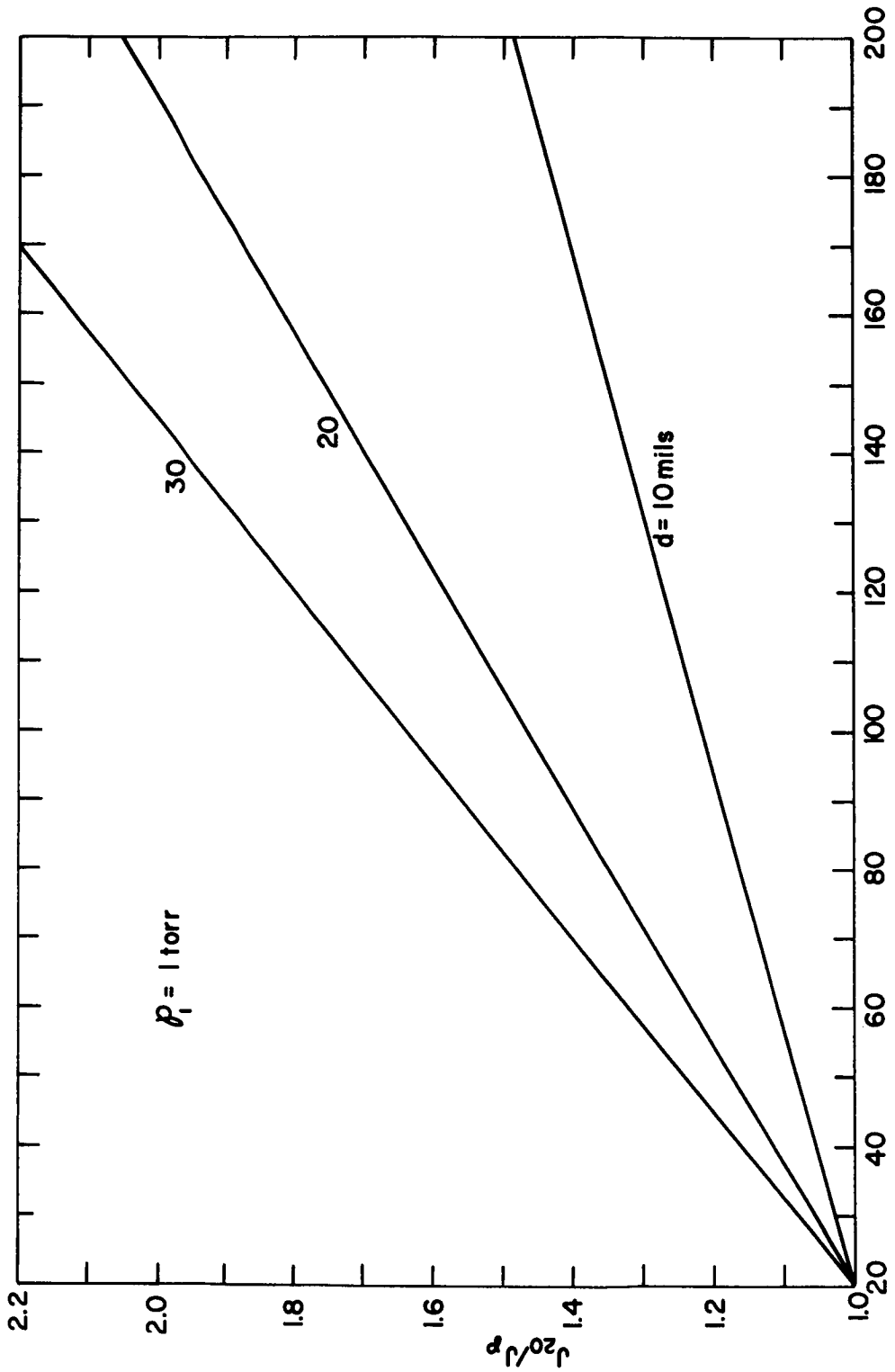

Figure VII-35. Fractional Current Attenuation by Xenon for Cesium Pressure of 1 Torr and Several Interelectrode Spacings.

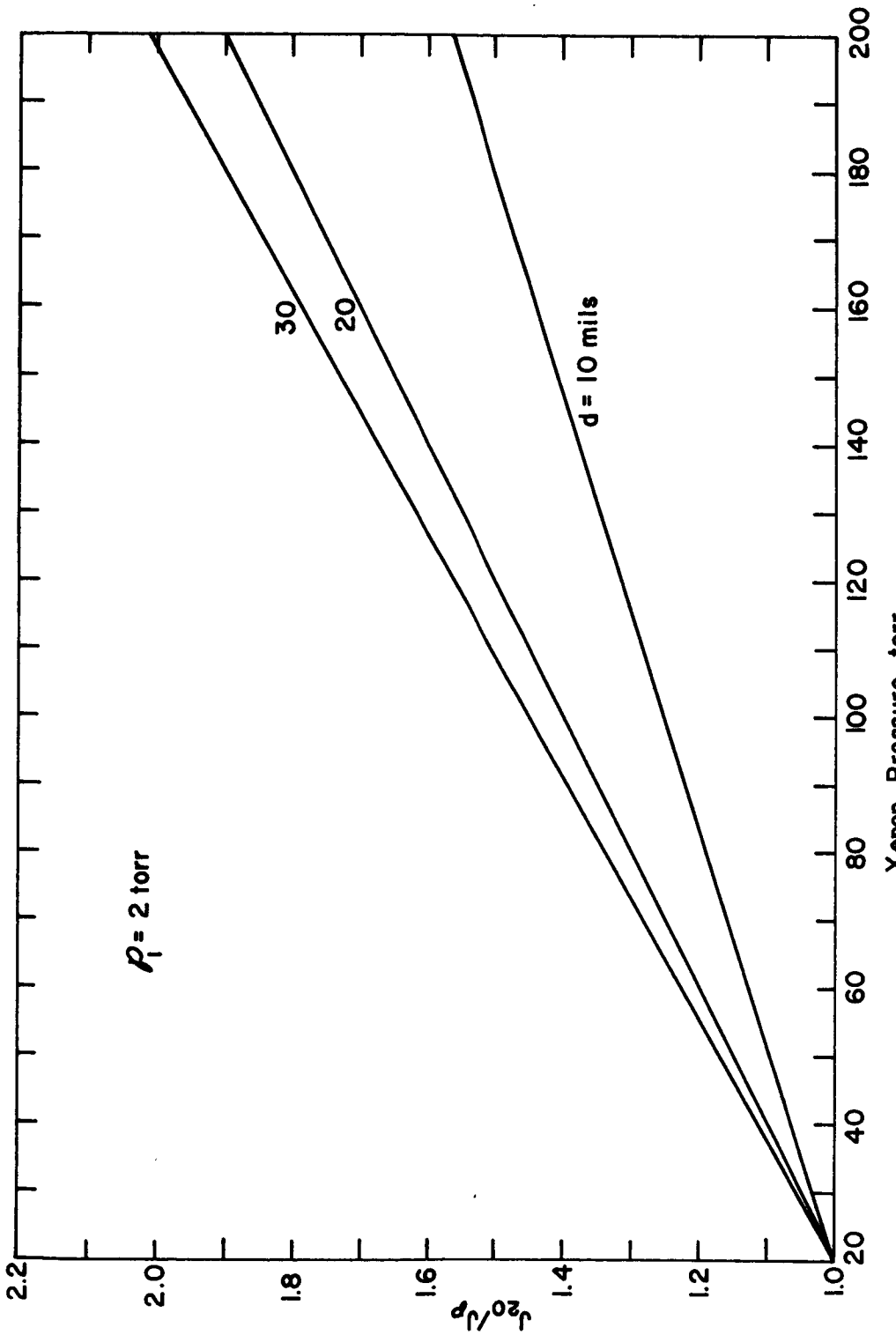

Figure VII-36. Fractional Current Attenuation by Xenon for Cesium Pressure of 2 Torr and Several Interelectrode Spacings.

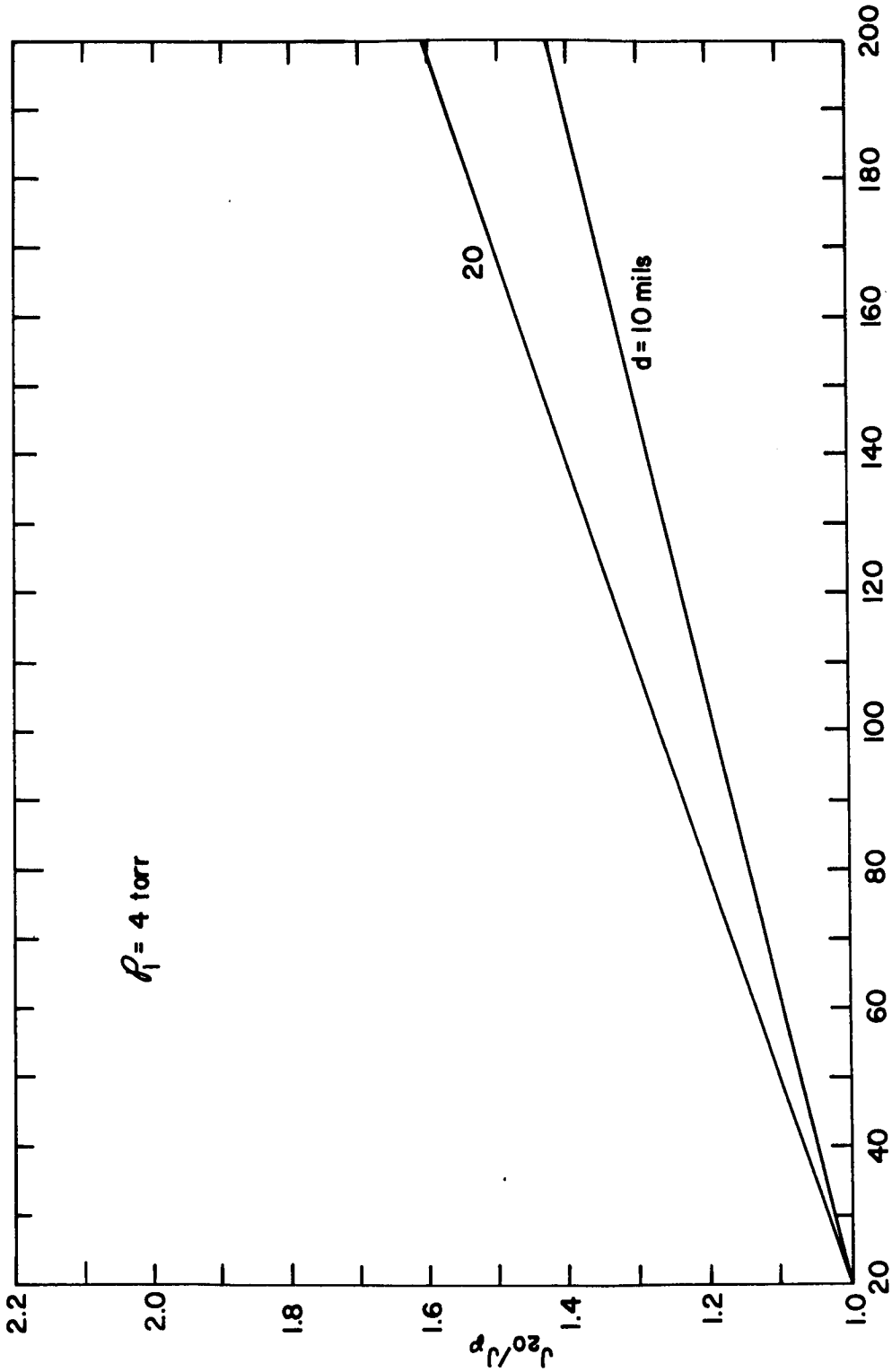

Figure VII-37. Fractional Current Attenuation by Xenon for Cesium Pressure of 4 Torr and Several Interelectrode Spacings.

CHAPTER VII

REFERENCES

1. E. S. Bekmukhambetov et al., "Thermionic Converter Operation in the Presence of Krypton," Sov. Phys.-Tech. Phys. 10, 1318-1319 (1966).

2. E. S. Bekmukhambetov et al., "Cesium Thermionic Converter Operation in the Presence of Xenon," Sov. Phys.-Tech. Phys. 10, 1320-1321 (1966).

3. C. Kaplan and J. B. Merzenich, "Investigation of the Current Density Limitations in a Thermionic Converter," Technical Summary Report, Contract Nonr 3738(00), Task NR 099-366, Marquardt Report No. 25,150 (1964).

4. C. Ramsauer and R. Kollath, "Über den Wirkungsquerschnitt der Nichtedelgasmoleküle gegenübur Elektronen unterhalb 1 Volt," Ann. d. Physik 3, 536 (1929).

5. de Voto, "Argon Plasma Transport Properties, "Institute for Plasma Research, Stanford University, Report No. SUAA 217.

6. C. F. Powell and L. Brada, Proc. Roy. Soc. (London) A138, 117 (1932).

7. L. M. Chanin and M. A. Biondi, Phys. Rev. 107, 1219 (1957).

8. R. B. Brode, "The Absorption Coefficient for Slow Electrons in Alkali Metal Vapors," Phys. Rev. 34, 673 (1929).

9. W. Aberth et al., "Absolute Measurement of Total Cross Sections for the Scattering of Low Energy Electrons by Argon, Nitrogen and Oxygen," Atomic Collision Processes, N. Holland Publishing Co., p. 53.

10. C. E. Normand, "The Absorption Coefficient for Slow Electrons in Gases," Phys. Rev. 35, 1217 (1930).

11. C. L. Chen and M. Raether, Phys. Rev. 125, 2679 (1962).

12. R. G. Meyerand, Jr., and R. K. Flavin, "Measurement of the Elastic Collision Cross Section of Low Energy Electrons with Cesium Atoms Using Electron-Cyclotron Resonance," Atomic Collision Processes, N. Holland Publishing Co., p. 59.

13. E. Bauer and H. N. Browne, "Elastic Scattering of Electrons by the Many-Electron Atom," Atomic Collision Processes, N. Holland Publishing Co., p. 16.

14. Von E. Brüche, "Freie Elektronen als Sonden des Baues der Molekeln," Ergeb. Exact. Naturwiss 8, 185 (1929).

15. H. S. W. Massey, "The Present State of the Study of Atomic Collisions," Atomic Collision Processes, N. Holland Publishing Co., p. 3.

16. K. Jost and J. Kessler, "Die Ortsverteilung Mittelschneller Elektronen bei Mehrfachstreuung," Zeitschrift für Physik 176, 126-142 (1963).

17. R. W. Warren and J. H. Parker, Jr., "Ratio of the Diffusion Coefficient to the Mobility Coefficient for Electrons in He, Ar, N_2, H_2, D_2, CO, and CO_2 at Low Temperatures and Low E/p," Phys. Rev. 128, 2661 (1962).

18. Caren, Phys. Rev. 131, 1904 (1963).

19. R. B. Brode, Phys. Rev. 5, 257 (1933).

20. L. Gould and S. C. Brown, "Microwave Determination of the Probability of Collision of Electrons in Helium," Phys. Rev. 95, 897 (1954).

21. R. T. Brachman and W. L. Fite, "Collisions of Electrons with Hydrogen Atoms, III. Elastic Scattering," Phys. Rev. 112, 1157 (1958).

22. F. Rufeh et al., "Third Quarterly Progress Report for Task IV," JPL Contract No. 950671, Thermo Electron Report No. TE 67-65 (1965).

23. S. S. Kitrilakis and J. H. Weinstein, "Second Annual Technical Summary Report," Contract No. Nonr-3563(00), Thermo Electron Report No. TE 27-64 (1963).

24. S. S. Kitrilakis et al., "Final Report, Task IV," JPL Contract No. 950671, Thermo Electron Report No. TE 7-66 (1965).

25. J. L. Pack, R. E. Voshall, and A. V. Phelps, "Drift Velocities of Slow Electron in Krypton, Xenon, Deuterium, Carbon Monoxide, Carbon Dioxide, Water Vapor, Nitrous Oxide, and Ammonia," Phys. Rev. 127, 2084 (1962).

CHAPTER VIII

ELECTRON SCATTERING IN THE BOLTZMANN REGION

A. Introduction

The first-order analysis of the Boltzmann region was presented in Ref. 1. At that time there was not enough experimental data available to compare with the theory. In this chapter, the analytical relations are refined and compared with the experimental data obtained in this program. The Boltzmann region is defined[2] as "the region where the electrons from the plasma begin to reach the collector." It is characterized by the fact that the electrons encounter a barrier consisting of the sum of the output voltage and collector work function. As a result, the number of electrons that surmount this barrier varies exponentially with output voltage.

The Boltzmann region has received a great deal of attention[3, 4, 5, 6] in experimental and theoretical studies because of its importance in the experimental determination of the collector work function and its key role in unignited-mode operation. However, a number of observations reported in the literature are in apparent conflict. It is the objective of this chapter to show that these observations can be reconciled if all the relevant phenomena are considered. In addition to the physical interpretation given, practical guidelines are furnished for the determination of accurate values of collector work function.

The cesium ion current (generated by ions released from the emitter surface and accelerated toward the collector) makes study of this region particularly difficult because it cannot be distinguished from the electron current. In this study we avoided this complication by conducting all experiments under highly electron-rich conditions. In addition, the electron density was kept small enough so that

electron-electron interactions were negligible. Since the dominant effect under these conditions is the scattering of electrons by cesium atoms, it was possible to study electron-atom collisions and to determine the mean free path of electrons in cesium vapor.

Electron scattering occurs in two different forms, depending on the ratio of electron mean free path, λ, to interelectrode spacing, d. When the electron mean free path is larger than the spacing, an electron which collides with a cesium atom and is reflected toward the emitter will probably reach the emitter without suffering another collision, and therefore it will have a very small chance of reaching the collector. On the other hand, when the mean free path is smaller than the spacing, an electron that is reflected toward the emitter will be very likely to suffer additional collisions, and therefore it will have a greater chance of reaching the collector.

Because of the above considerations, we have treated the two modes separately. However, the scattering cross sections obtained in the two cases must be in agreement if our model is valid.

B. Theoretical Analysis

In the Boltzmann mode of operation the barrier composed of the collector work function and the output voltage is greater than the emitter work function barrier (Figure VIII-1). If, in addition, the electron current emitted by the collector and the emitter ion current are negligible and the emitted electrons suffer no collisions, then the output current is given by the Richardson equation:

$$J_o = AT_E^2 \exp\left[-(\phi_C + eV)/kT_E\right] \qquad (1)$$

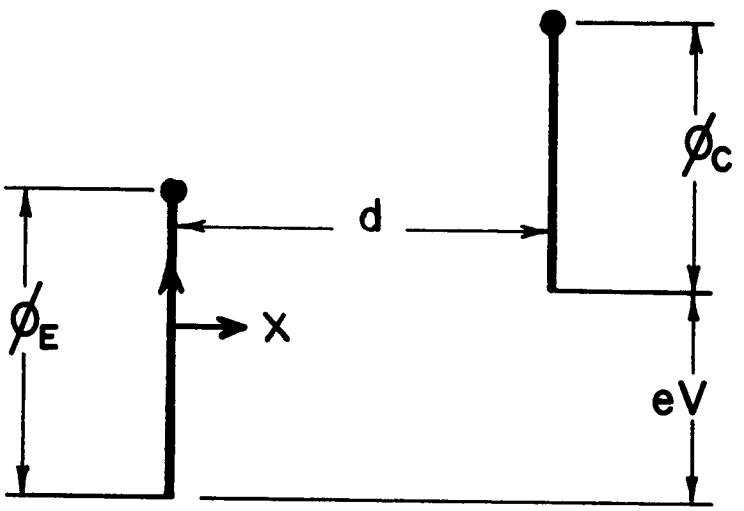

Figure VIII-1. Boltzmann Region.

where:

$A \equiv$ Richardson constant

$T_E \equiv$ Emitter temperature

$\phi_C \equiv$ Collector work function

$V \equiv$ Voltage output

$k \equiv$ Boltzmann constant

$e \equiv$ Electronic charge

The effect of electron scattering by cesium atoms is determined from the deviation of the actual current from that predicted by equation (1). This analysis is based on the following assumptions:

1. Ion current and back-emission are negligible compared with the net electron current.
2. The electrons can be divided into two groups, depending on whether their energies are larger or smaller than $(\phi_C + eV)$, and can be treated separately.

To satisfy the first assumption, the emission must be highly electron-rich and the collector temperature low enough so that back emission is negligible. The second assumption has been suggested by Hansen and Warner[3] and is justified in this analysis since, for $\beta < 1$, the electron density is low enough to render electron-electron interactions negligible.

Only those electrons that possess energies larger than $(\phi_C + eV)$ need be considered, since the others will not be able to surmount this barrier and will return to the emitter without interacting with any part of the system. The number of these more energetic electrons, J_o, is given by equation (1). Of these a smaller number J will reach the collector, and the remainder will be scattered

back to the emitter. J is related to J_o by a probability factor, S

$$J = SJ_o \tag{2}$$

The probability S will be evaluated for the long- and short-mean-free-path cases.

1. Long-Mean-Free-Path Solution, $d/\lambda << 1$. In the region where the inter-electrode spacing is smaller than electron mean free path, the incremental change in the directional electron current, dJ, in the interval x to x + dx is given by:

$$dJ = -J \Sigma \omega \, dx \tag{3}$$

where:

- J ≡ electron current
- Σ ≡ macroscopic cross section = $N\sigma$
- N ≡ cesium atom density
- σ ≡ microscopic collision cross section of electrons with cesium atoms
- x ≡ distance

and ω is the fraction of particles scattered from an elastic sphere that have a component of velocity in the negative x direction, i.e., ω is the fraction of the projected area of the sphere that reflects the incident particles by more than 90°. From geometrical considerations,

$$\omega \equiv [\sin(\pi/4)]^2 = \tfrac{1}{2} \tag{4}$$

Integrating equation (1) from x = 0 to d,

$$J = J_o \exp(-d/2\lambda) \tag{5}$$

where λ is the electron mean free path in cesium vapor and is given by

$$\lambda = \frac{1}{N\Sigma} \tag{6}$$

Comparison of equations (1) and (5) shows that when $d/\lambda < 1$ the effect of electron scattering by cesium atoms is to reduce the output current by a constant fraction, $\exp(-d/2\lambda)$. In a plot of $\ln J$ versus V this amounts to a translation of the J-V characteristic along the voltage axis. If J is used in equation (1) instead of J_o, an apparent collector work function, ϕ_{ca}, is computed as in equation (7):

$$J = AT_E^2 \exp(\phi_{ca} - eV)/kT_E \tag{7}$$

The difference between the actual and apparent collector work functions, $\Delta\phi_c$, is given by:

$$\Delta\phi_c = \phi_{ca} - \phi_c = \frac{kT_E}{2\lambda} d \qquad \text{for } d/\lambda < 1 \tag{8}$$

Equation (8) gives the deviation of the measured collector work function, ϕ_{ca}, from its true value ϕ_c as a function of interelectrode spacing d, electron mean free path λ, and emitter temperature T_E for $d/\lambda < 1$.

2. Short-Mean-Free-Path Solution, $d/\lambda >> 1$. In this region, again, only the more energetic electrons need be considered. Collisions with neutral atoms cause the motion of electrons in the interelectrode space to become random in direction. In effect, their motion is diffusion-dominated. For an absorption-free diffusing medium the diffusion equation is of the form

$$\nabla^2 n = o \tag{9}$$

where n is the electron density. The boundary conditions are:

At the emitter $$\frac{vn}{4} - \frac{1}{2} D \nabla n = J_o \tag{10}$$

At the collector $$\frac{vn}{4} + \frac{1}{2} D \nabla n = o \tag{11}$$

where:

v ≡ average electron velocity

D ≡ electron diffusion coefficient in cesium vapor

The first boundary condition states that, at the emitter boundary of the plasma, the directional current into the plasma is equal to J_o; i. e., J_o fast electrons enter the plasma from the emitter. The second boundary condition states that the directional current into the plasma at the collector boundary is zero. The solution to the differential equation is given by

$$n(x) = C_1 x + C_2 \tag{12}$$

From the two boundary conditions, the constants C_1 and C_2 are found to be

$$C_1 = \frac{-4 J_o}{4D + vd} \tag{13}$$

$$C_2 = \frac{4 J_o}{D} \left[\frac{2D + vd}{4D + vd}\right] \tag{14}$$

or

$$n(x) = \frac{-4 J_o}{4D + vd} x + \frac{4 J_o}{D} \left[\frac{2D + vd}{4D + vd}\right] \tag{15}$$

The net electron current J through the plasma is required by Fick's law to be

$$J = -D \frac{dn}{dx} \tag{16}$$

or

$$J = \frac{4J_o D}{4D + vd} \tag{17}$$

The diffusion coefficient D is related to electron mean free path by

$$D = v\lambda/3 \tag{18}$$

Equations (17) and (18) give

$$\frac{J}{J_o} = \frac{1}{1 + \frac{3d}{4\lambda}} \tag{19}$$

Algebraic manipulation of equations (1) and (19) results in

$$J = A T_E^2 \exp \left[- \frac{\phi_c + V + k T_E \ln\left(1 + \frac{3d}{4\lambda}\right)}{k T_E} \right] \tag{20}$$

It follows from equation (19) that the effect of electron scattering is to translate the J-V curve along the voltage axis by the amount

$$k T_E \ln\left(1 + \frac{3d}{4\lambda}\right) \tag{21}$$

The collector work function can be computed using the actual current J in equation (7) if the apparent collector work function value, ϕ_{ca}, is corrected by $\Delta\phi_c$, as given by equation (22):

$$\Delta\phi_c = \phi_{ca} - \phi_c = k T_E \ln\left(1 + \frac{3d}{4\lambda}\right) \tag{22}$$

C. Experimental Technique and Results

In the preceding section we showed that, in the Boltzmann region, electron current is an exponential function of voltage. The logarithmic plot of current versus voltage is displaced from the "ideal" Boltzmann line by a voltage increment which is a function of d/λ.

To test this hypothesis we measured the change in apparent collector work function as we varied the interelectrode spacing and cesium pressure.

The success of this technique requires that the emitter, collector and cesium reservoir temperature remain constant while the spacing is varied. To accomplish this, an experimental procedure was developed which produces a direct measure of the apparent collector work function as a function of spacing. This technique is based on the fact that, in the Boltzmann region, where ln J is proportional to output voltage, the effect of a spacing change is to translate the J-V characteristic along the voltage axis. Instead of generating a series of volt-ampere characteristics at different spacing settings, with the possibility that changes in the values of other parameters may take place, the output voltage is recorded as a function of spacing at constant output current. Changes in output voltage under these conditions are equal to the changes in the effective collector work function.

Two modifications of the variable-parameter test vehicle[1] were necessary for the present experiment. First, the variable-spacing mechanism was equipped with a reversible electric motor so that the spacing could be varied continuously and at a constant rate from "minimum" to 60 mils. Second, an electric signal proportional to spacing was generated by using a 10-turn potentiometer driven by one of the micrometer screws that adjust the spacing. The emitter temperature was continuously monitored by a thermocouple. The diode and these changes are shown schematically in Figure VIII-2.

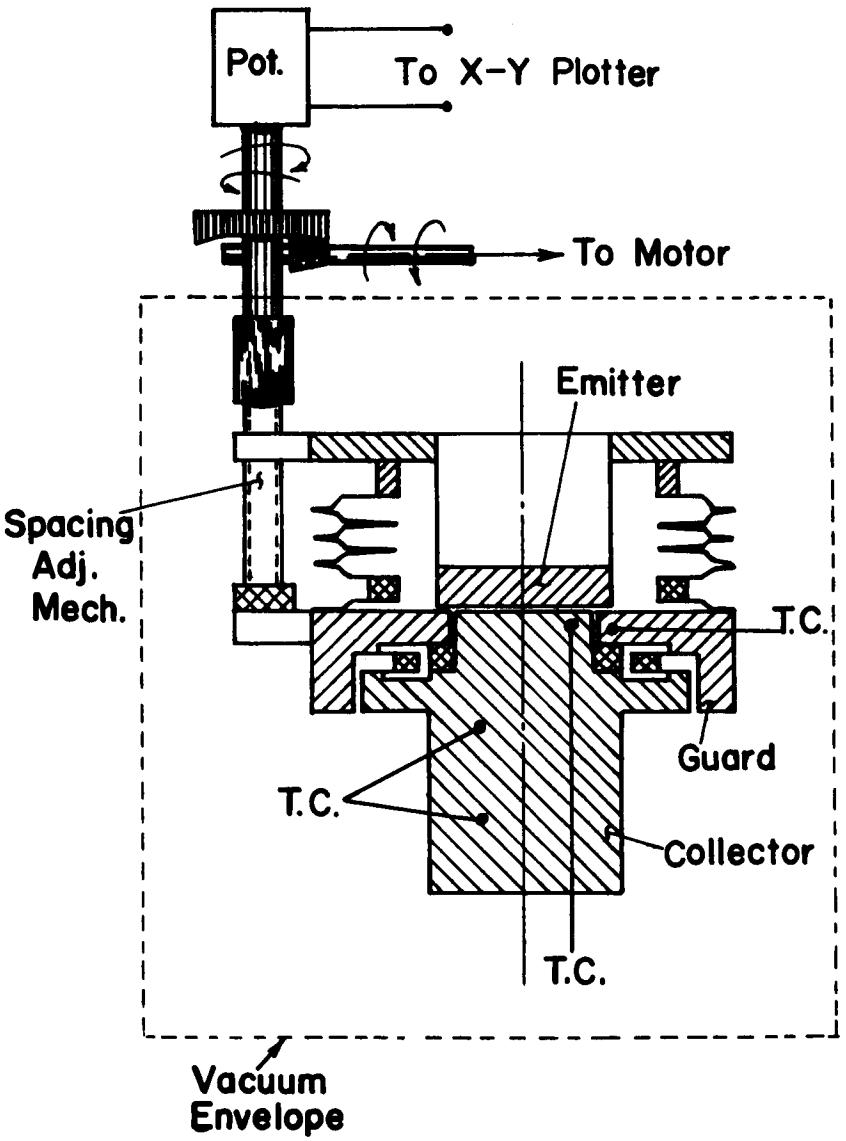

Figure VIII-2. Schematic of the Cesium Diode.

A typical run consists of varying the spacing while the electron current is kept constant at a selected value on the Boltzmann line, usually 1 mA. The output voltage is plotted as a function of spacing by an X-Y recorder, and the entire run is completed within a few seconds.

To investigate the long- and short-mean-free-path cases, two sets of data were taken, both covering a cesium temperature range of 510°-600°K (0.2 - 4.0 torr), at T_E = 1300°K. In the first set, the spacing was increased from minimum to several mils. In the second set, the spacing was decreased from 60 mils to minimum. Several typical runs for the two sets are shown (Figures VIII-3 through VIII-6 and Figure VIII-7). The reason for this procedure is that, for the first set, the spacing range of 0-5 mils was of primary interest, and it was important to minimize the departure from the state of equilibrium established prior to the run, while for the second set the larger spacings were of interest and the procedure was reversed.

D. Comparison of Experimental Results with Theory

According to equation (8), for small spacings $\Delta\phi_c$ is a linear function of the interelectrode spacing. The experimental data (Figures VIII-3 through VIII-6) show such a dependence. The slopes of the dashed lines were used to calculate the electron mean free path, which is plotted as a function of inverse pressure (indicated by the diamonds) in Figure VIII-10.

The data from the high spacing range should fit equation (12), i.e., a plot of $\exp [\Delta\phi_c/k T_E]$ vs spacing should be a straight line with the slope $\frac{3}{4\lambda}$. Such plots are shown in Figures VIII-8 and VIII-9 for two cesium pressures. The lower-pressure run (Figure VIII-8) agrees well with the form of equation (12) for $d > 35$ mils. A small deviation is observed at lower spacings. A case where

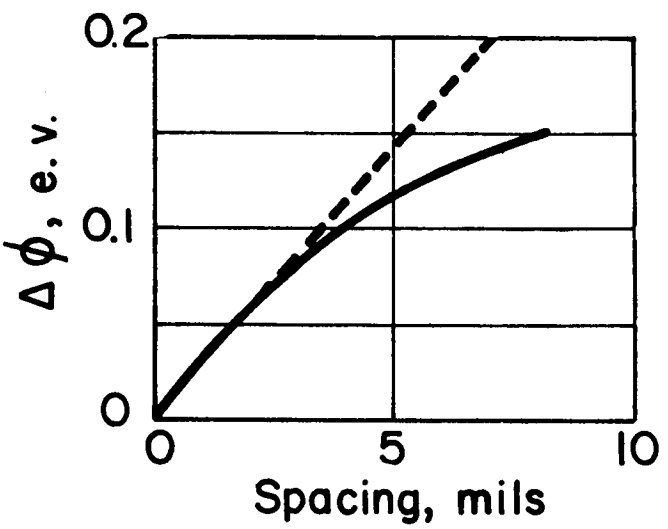

Figure VIII-3. Variation in Collector Work Function with Spacing.
T_E = 1314°K, T_C = 609°K, T_R = 543°K

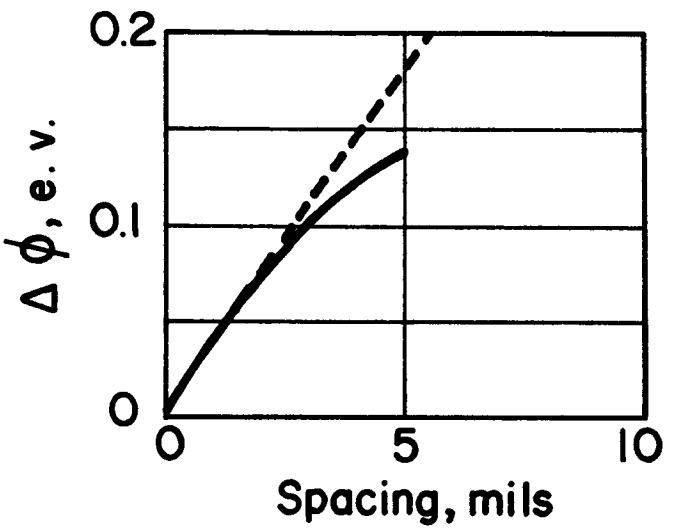

Figure VIII-4. Variation in Collector Work Function with Spacing.
T_E = 1313°K, T_C = 611°K, T_R = 554°K.

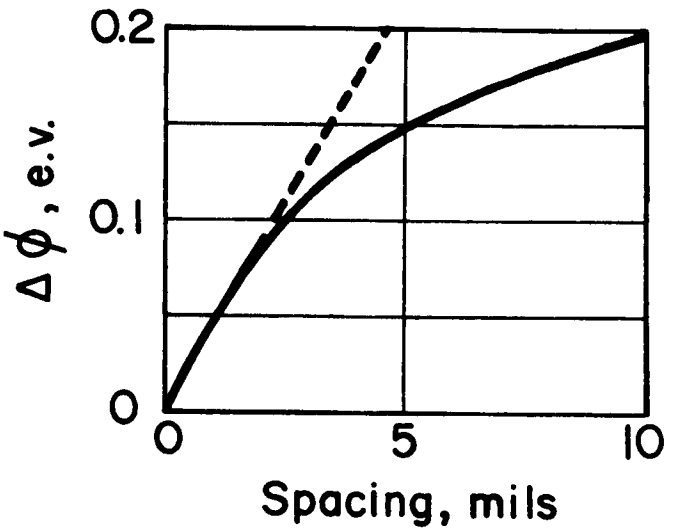

Figure VIII-5. Variation in Collector Work Function with Spacing.
T_E = 1298°K, T_C = 618°K, T_R = 572°K.

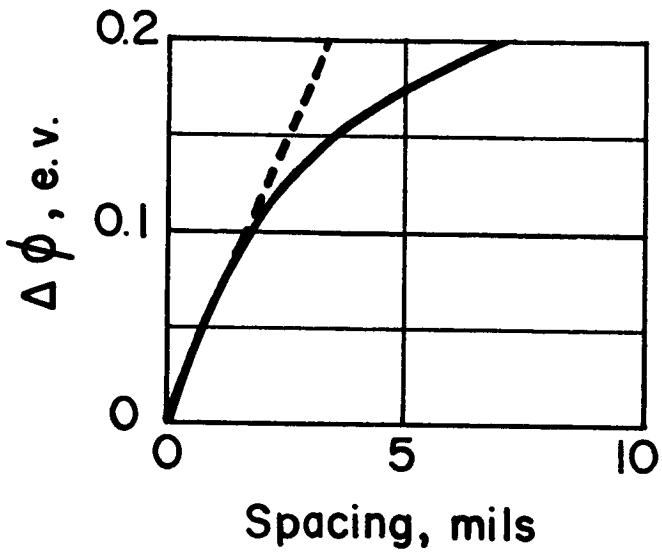

Figure VIII-6. Variation in Collector Work Function with Spacing.
T_E = 1308°K, T_C = 621°K, T_R = 593°K.

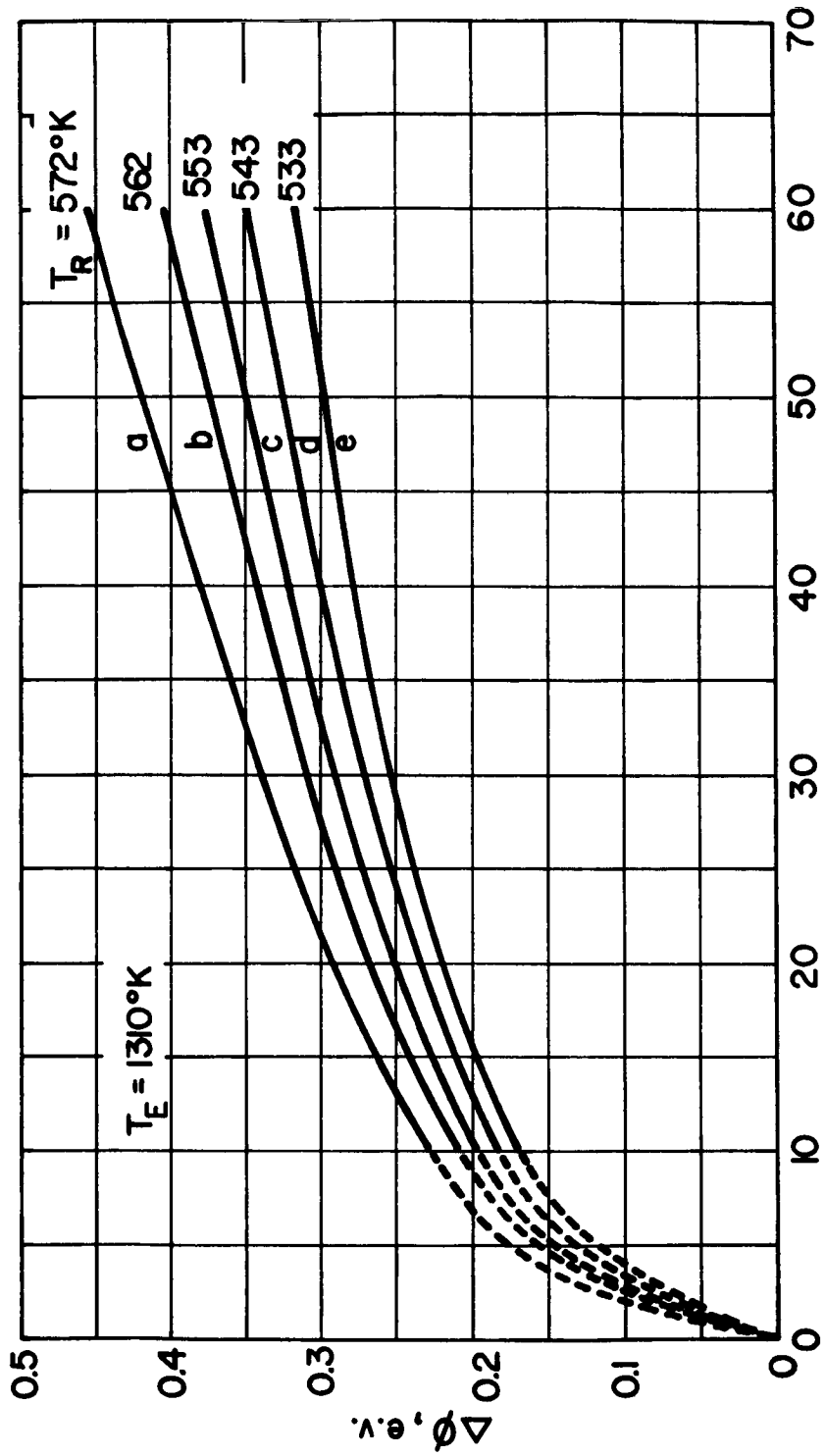

Figure VIII-7. Variation in Collector Work Function with Spacing.
(a) T_c = 628°K, (b) T_c = 628°K, (c) T_c = 627°K
(d) T_c = 827°K, (e) T_c = 623°K.

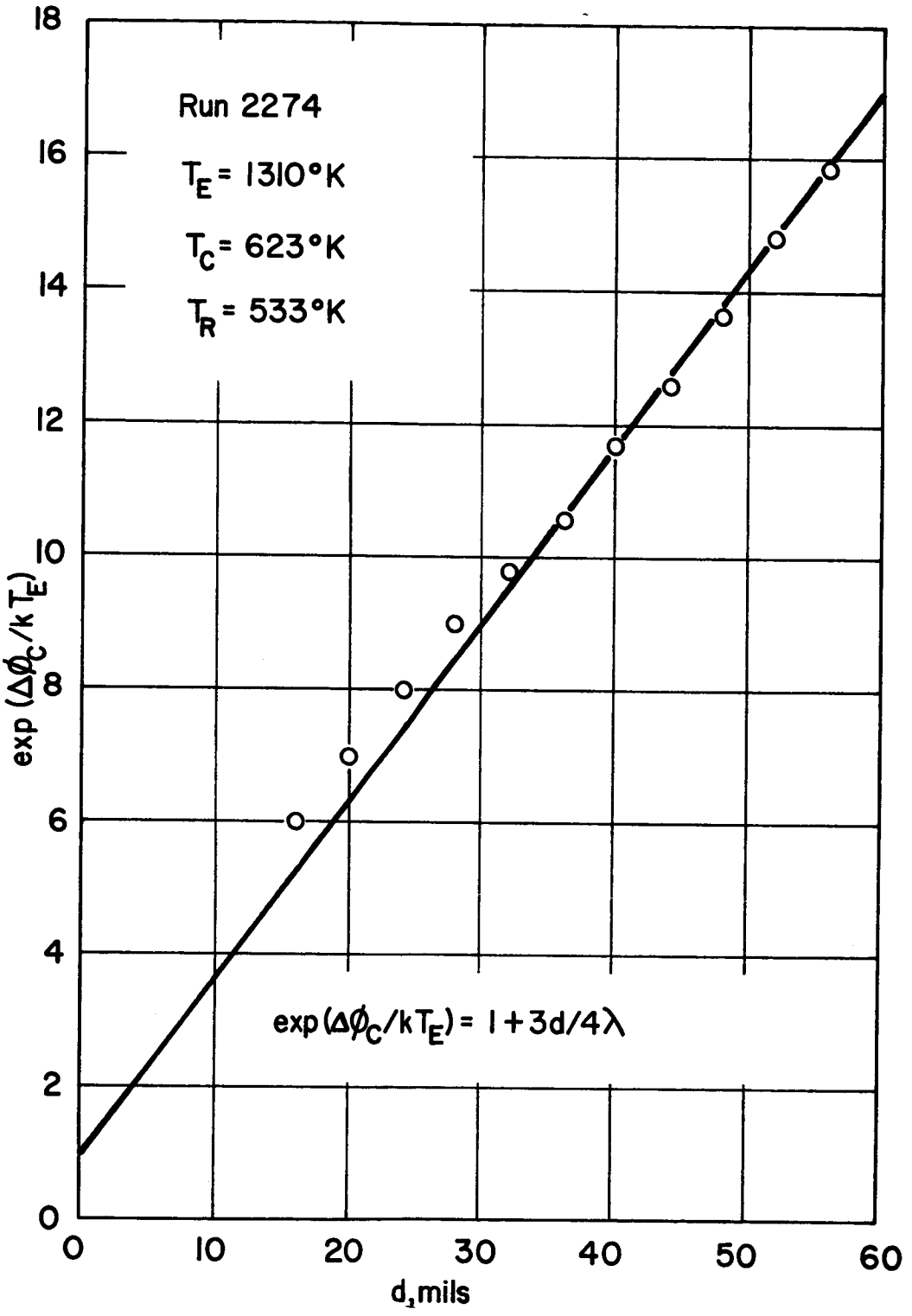

Figure VIII-8. Plot for Obtaining Electron Mean Free Path.

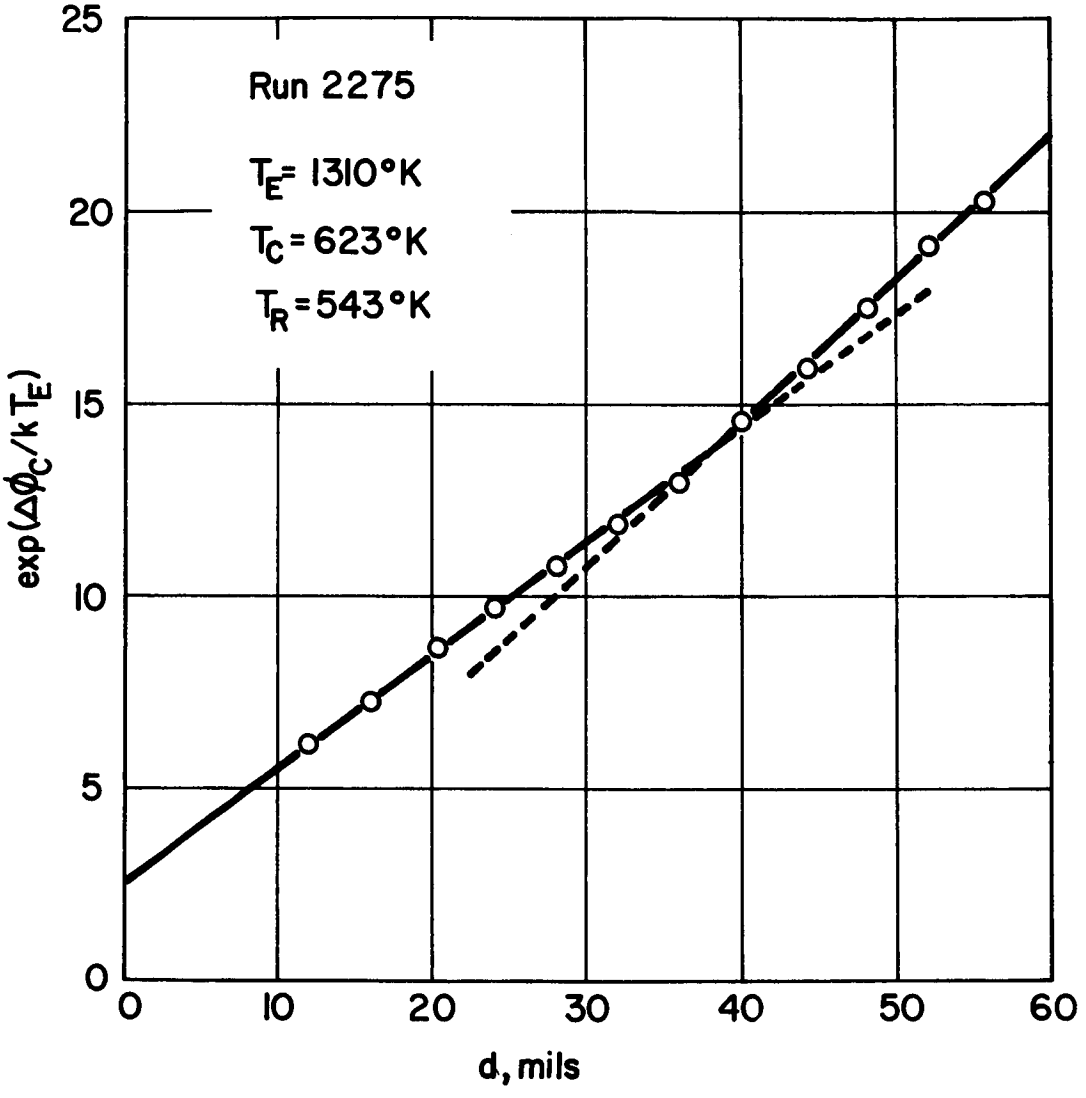

Figure VIII-9. Plot for Obtaining Electron Mean Free Path.

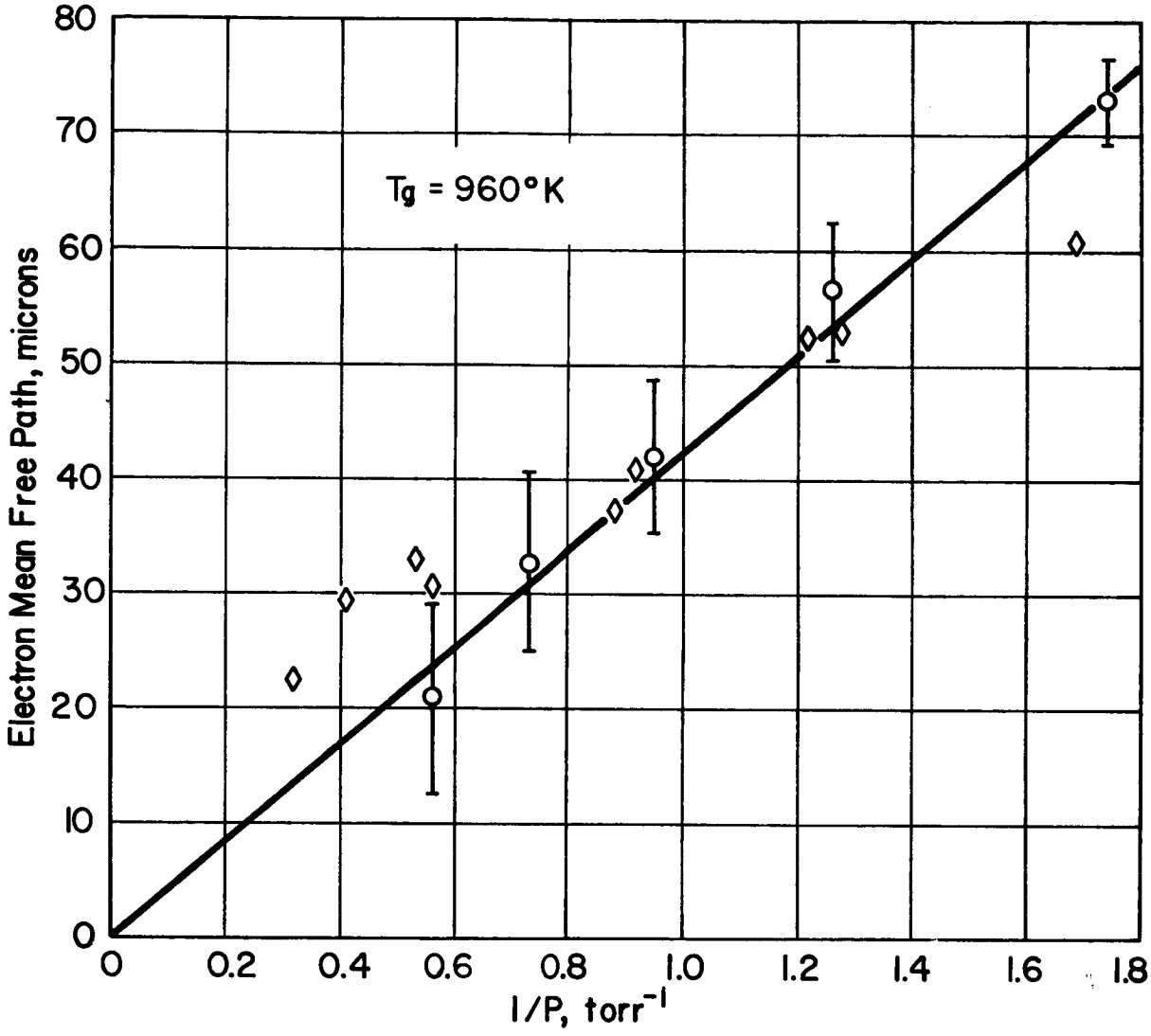

Figure VIII-10. Electron Mean Free Path in Cesium Vapor.

the deviation is larger is shown in Figure VIII-9. This is probably caused by small changes in emitter temperature, since emitter heat loss by cesium conduction becomes more important at higher pressures. Although a curvature is present at high pressures, the maximum variation of the slope of these curves is not large. The electron mean free path calculated from such plots is shown as a function of inverse pressure in Figure VIII-10. Scatter bars indicate the maximum variation in the slope.

The values of the electron mean free path obtained by the two methods are in satisfactory agreement with each other, and show the expected dependence on cesium pressure.

The best fit to the data (Figure VIII-10) corresponds to $P\lambda = \frac{kT_g}{e\sigma} = 1.6$ millitorr for the gas temperature $T_g = 960°K$, or the electron-atom collision cross section $\sigma = 230\ (\mathring{A})^2$. Table VIII-1 compares the value of σ obtained here with values reported or estimated by others for the same region of electron temperature.

TABLE VIII-1[7]

COLLISION CROSS SECTION OF ELECTRONS WITH Cs ATOMS

	$\sigma\ (\mathring{A})^2$
This work[(a)]	230
Warner and Hansen[(a)]	200
Merlin[(a)]	200
Nottingham[(c)]	400
Roehling[(a)]	90
Stone and Reitz[(b)]	160
Zollweg and Gottlieb[(a)]	400
Robinson[(b)]	480
Harris[(a)]	320
Flavin & Meyerand[(a)]	310

a = experimental
b = theoretical
c = estimated

As may be seen, the value of $\sigma = 230(\mathring{A})^2$ is quite close to the most probable value and falls within the range of uncertainty.

E. Conclusions

The experimental evidence we have obtained supports the analytical model presented. This simple model describes adequately the experimental observations, provided extraneous effects are either eliminated or accounted for. Of particular importance is the fact that the short- and long-mean-free-path cases treated have yielded the same value of electron-atom scattering cross section. The $230(\mathring{A})^2$ value obtained is in good agreement with values obtained in other experiments and by theoretical calculation.

This method for the experimental determination of collector work function values has proved reliable. Figure VIII-11 is a plot designed to facilitate the correction of observed apparent collector work function values for the effects of interelectrode spacing and cesium pressure.

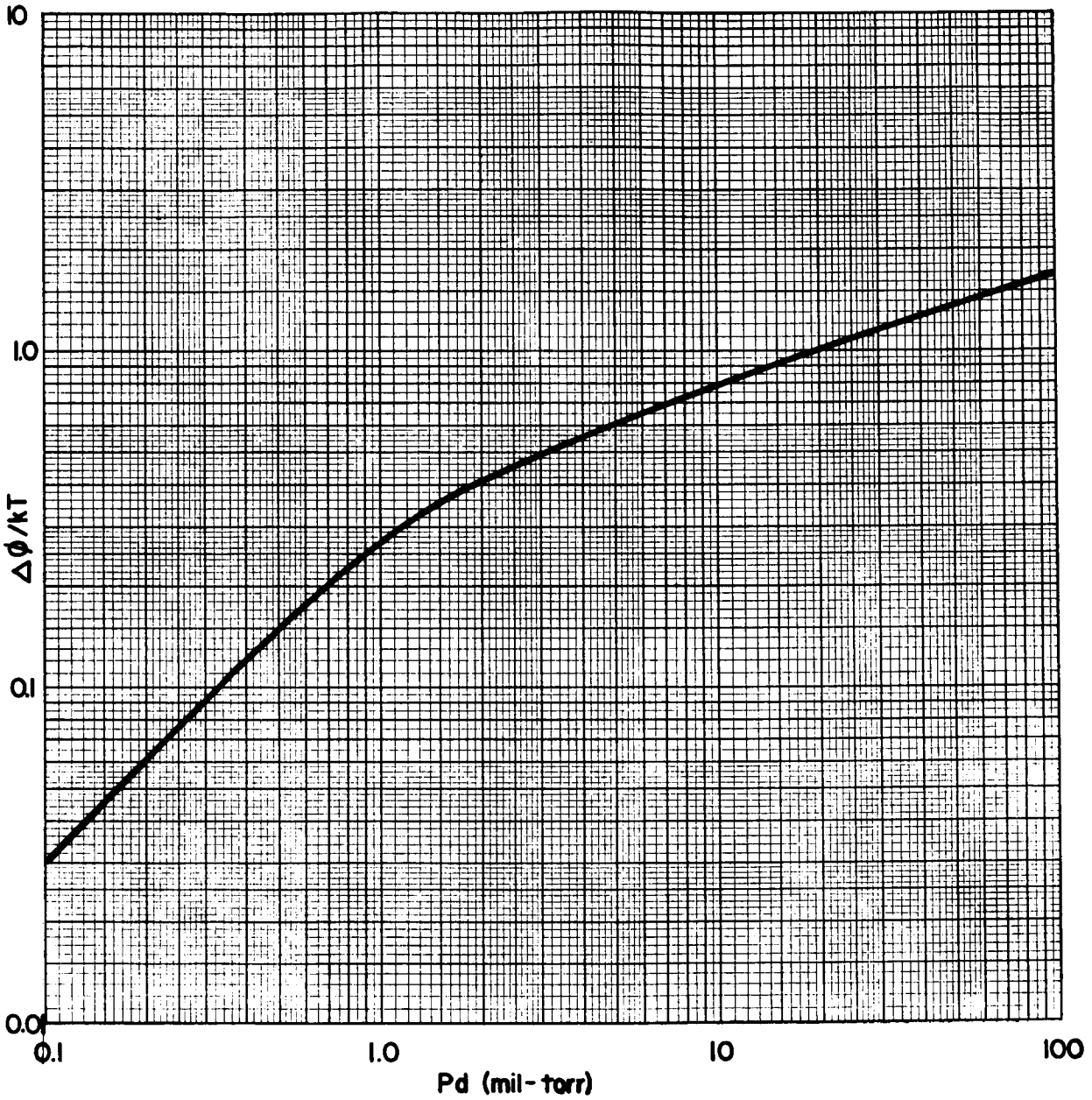

Figure VIII-11. Recommended Correction for Collector Work Function Measured by Retarding Technique.

CHAPTER VIII
REFERENCES

1. S. S. Kitrilakis, F. Rufeh, D. Lieb, L. van Someren and J. Weinstein, "Final Report for the Thermionic Research Program, Task IV," prepared for the Jet Propulsion Laboratory under Contract No. 950671, Thermo Electron Report No. TE 7-66, 1965.

2. R. H. Bullis et al., "The Plasma Physics of Thermionic Converters," Report on the Thermionic Conversion Specialist Conference, San Diego, 1965.

3. C. Warner and L. K. Hansen, "Transport Effects in the Unignited Mode of Thermionic Diodes," Report on the Twenty-Third Annual Conference on Physical Electronics, Cambridge, 1963.

4. J. M. Houston, "Measurement of Emitter Heat Balance in a Cesium Thermionic Converter," Report on the Thermionic Conversion Specialist Conference, Gatlinburg, 1963.

5. J. D. Dunlop II, "Determination of the Collector Work Function in the Retarding Region," Report on the Thermionic Conversion Specialist Conference, Cleveland, 1964.

6. R. Breitwieser, "On the Relation of Ion and Electron Emission to Diode Diagnostics," Report on the Thermionic Conversion Specialist Conference, Gatlinburg, 1963.

7. J. M. Houston, "Cross Section Values to use in Analyzing the Cesium Thermionic Converter," Report on the Thermionic Conversion Specialist Conference, Cleveland, 1964.

APPENDIX A

LITERATURE REFERENCES TO WORK FUNCTION MEASUREMENTS WITH FLUORINE COVERAGE

A literature search uncovered five references to refractory metal work function measurements in the presence of either free fluorine gas or CsF. These references have been abstracted in tabular form in Table A-1 and will be discussed here. The technical aspects of these investigations will be examined in chronological sequence, and the relative influence they appear to have had on each other will be pointed out.

Metlay and Kimball were concerned with the measurement of the electron affinity of fluorine. In this they were not successful, for reasons that are of no interest here, but in the process of measuring the ion and electron emission from a hot tungsten filament they observed an increase in work function which persisted to temperatures of 2600°K. They attributed this change to a tenaciously held adsorbed fluorine layer. They also experienced a rapid loss of tungsten, which they explained by a peculiar dislodging action of fluorine atoms on the array of tungsten atoms, ignoring the fact that tungsten fluoride cannot exist at these temperatures. Furthermore, having stated that this tungsten loss rate was unaffected by filament temperature and fluorine pressure, they ignored completely the possibility that a third agent might be responsible for the reaction taking place on the tungsten.

In general, their technique was not what has come to be referred to as "vacuum technique," but rather one usually associated with chemical reaction vessels. The difficulties experienced by the authors are best explained by 0.2 to 1% of oxygen contamination in the fluorine gas. This corresponds to 10^{-5} torr

partial pressure of O_2. Part of this oxygen may have been contained in fluorine used, but it may very well have been released by the reaction of the pyrex wall of the vessel with the fluorine.

This work, nevertheless, was probably responsible for all subsequent halide investigations except for the work of Morgulis which was published in 1956.

Morgulis measured the work function of tungsten coated with CsCl versus CsCl coverage at 600°C using the contact-potential method. He measured coverage by using Cs tagged with Cs^{134}, which he could count very accurately. The vacuum technique employed in this experiment was carefully controlled, and, as a result, the ultimate pressure in the device was 10^{-9} to 10^{-10} torr. The CsCl was found to lower the work function of tungsten by a maximum amount of 1.8 eV. The authors do not exclude the possibility of a "slight dissociation of the CsCl," but think it improbable. It is therefore questionable that their results are valid at thermionic emitter temperatures, where complete dissociation is expected.

Aamodt and his co-workers, probably encouraged by Metlay's results, used CsF crystals as the source of fluorine. The maximum work function change (0.6 eV) and the desorption rates he observed are very much like those reported for O_2 by many workers, which are discussed elsewhere in this report. Ranken continued this work in a metal-ceramic tube, which, of course, avoids the difficulty of water evolution from the pyrex walls at 300°C, but did not outgas his CsF higher than 220°C.

Chronologically, our program started experiments with CsF next, but that work has been discussed in detail in the August 1965 annual report and, of course, in current reports, so it will not be summarized in this table.

Jester, Langpape and Minor worked at first with glass tubes and later with metal-ceramic tubes. They also observed maximum work function changes of the order of 0.6 eV in tubes which had residual gas pressures exceeding 10^{-7} torr. They made steady-state measurements and observed that the "additive effect" was lost after prolonged testing.

The summary table, A-1, in conjunction with the results of this program, strongly supports the conclusions drawn in the body of this report. Perhaps the single most important factor responsible for the error made by all the investigators of adsorbed halide films, with the exception of Morgulis, is the preconception, shared by all, that fluorine ought to behave like oxygen, only more so.

TABLE A-1

Reference	Tube Type Absorbate(s)	Outgassing of Additive	Outgassing of Tube	Character of Experiment	Maximum Work Function Change and Activation Energy	Remarks
Mellay and Kimball J. Ch. Ph. 16, 8, 779-1948	Glass tube F	None	None	Filament exposed to "microns" of Fluorine gas emission measured after evacuation	$\Delta\phi \approx 1.0$ eV	No awareness of vacuum technique.
Morgulis Sov. Phys. 3, 2, 159-1956	Glass tube Cs Cl	Not given	Several 25-30 hr. outgassings Residual 10^{-9}-10^{-10} torr	Isotope tracer of Cs Cl coverage. Contact potential ϕ measurements tungsten temp. 600°C	$\Delta\phi = -1.8$ eV	Extremely clean system. Results of limited value to thermionic emitters.
Aamodt et al JAP 33, 6, 2080-1961	Glass tube Cs CsF	450°C Several hours	450°C Several hours	Coating of filament by raising CsF to 300°C - Transient w. f. measurements	$\Delta\phi \cong 0.6$ eV $E^* 145 \frac{\text{k cal}}{\text{gr-atom}}$	$E^* = 145$ k cal/mol. very similar to O_2.
Ranken et al AEC 3, 235 1963	Metal tube Cs CsF F	220°C	325°C	Steady state at wall temp 250°-300°C Emission measurement	$\Delta\phi \approx 0.55$ eV	CsF outgassing inadequate.
Jester and Minor Therm. Spec. Conv. Conf. Cleve.-1964	Glass tube CsF	Not given	Residual gas pressure $>10^{-7}$ torr	Work function by emission in CsF steady state	$\Delta\phi = 0.7$ eV	Additive effect observed with "CsF" pressure of 10^{-11} mm Hg.
Langpape and Minor TCSC Clev. 1964	Glass tube Cs CsF	Not given	Residual gas pressure $>10^{-7}$ torr	Work function by emission in CsF and Cs + CsF - Steady State	$\Delta\phi \approx 0.6$ eV	Additive effect observed with "CsF" pressure of 10^{-11} mm Hg.

THERMO ELECTRON ENGINEERING CORPORATION